

1
 2
 3
 4
 5
 6
 7
 8
 9
 10
 11
 12
 13
 14
 15
 16
 17
 18
 19
 20
 21
 22
 23
 24
 25
 26
 27
 28
 29
 30
 31
 32
 33
 34
 35
 36
 37
 38
 39
 40
 41
 42
 43
 44
 45
 46
 47
 48
 49
 50
 51
 52
 53
 54
 55
 56
 57
 58
 59
 60
 61
 62
 63
 64
 65
 66
 67
 68
 69
 70
 71
 72
 73
 74
 75
 76
 77
 78
 79
 80
 81
 82
 83
 84
 85
 86
 87
 88
 89
 90
 91
 92
 93
 94
 95
 96
 97
 98
 99
 100
 101
 102
 103
 104
 105
 106
 107
 108
 109
 110
 111
 112
 113
 114
 115
 116
 117
 118
 119
 120
 121
 122
 123
 124
 125
 126
 127
 128
 129
 130
 131
 132
 133
 134
 135
 136
 137
 138
 139
 140
 141
 142
 143
 144
 145
 146
 147
 148
 149
 150
 151
 152
 153
 154
 155
 156
 157
 158
 159
 160
 161
 162
 163
 164
 165
 166
 167
 168
 169
 170
 171
 172
 173
 174
 175
 176
 177
 178
 179
 180
 181
 182
 183
 184
 185
 186
 187
 188
 189
 190
 191
 192
 193
 194
 195
 196
 197
 198
 199
 200
 201
 202
 203
 204
 205
 206
 207
 208
 209
 210
 211
 212
 213
 214
 215
 216
 217
 218
 219
 220
 221
 222
 223
 224
 225
 226
 227
 228
 229
 230
 231
 232
 233
 234
 235
 236
 237
 238
 239
 240
 241
 242
 243
 244
 245
 246
 247
 248
 249
 250
 251
 252
 253
 254
 255
 256
 257
 258
 259
 260
 261
 262
 263
 264
 265
 266
 267
 268
 269
 270
 271
 272
 273
 274
 275
 276
 277
 278
 279
 280
 281
 282
 283
 284
 285
 286
 287
 288
 289
 290
 291
 292
 293
 294
 295
 296
 297
 298
 299
 300
 301
 302
 303
 304
 305
 306
 307
 308
 309
 310
 311
 312
 313
 314
 315
 316
 317
 318
 319
 320
 321
 322
 323
 324
 325
 326
 327
 328
 329
 330
 331
 332
 333
 334
 335
 336
 337
 338
 339
 340
 341
 342
 343
 344
 345
 346
 347
 348
 349
 350
 351
 352
 353
 354
 355
 356
 357
 358
 359
 360
 361
 362
 363
 364
 365
 366
 367
 368
 369
 370
 371
 372
 373
 374
 375
 376
 377
 378
 379
 380
 381
 382
 383
 384
 385
 386
 387
 388
 389
 390
 391
 392
 393
 394
 395
 396
 397
 398
 399
 400
 401
 402
 403
 404
 405
 406
 407
 408
 409
 410
 411
 412
 413
 414
 415
 416
 417
 418
 419
 420
 421
 422
 423
 424
 425
 426
 427
 428
 429
 430
 431
 432
 433
 434
 435
 436
 437
 438
 439
 440
 441
 442
 443
 444
 445
 446
 447
 448
 449
 450
 451
 452
 453
 454
 455
 456
 457
 458
 459
 460
 461
 462
 463
 464
 465
 466
 467
 468
 469
 470
 471
 472
 473
 474
 475
 476
 477
 478
 479
 480
 481
 482
 483
 484
 485
 486
 487
 488
 489
 490
 491
 492
 493
 494
 495
 496
 497
 498
 499
 500
 501
 502
 503
 504
 505
 506
 507
 508
 509
 510
 511
 512
 513
 514
 515
 516
 517
 518
 519
 520
 521
 522
 523
 524
 525

Form approved
CMB No. 444-C188

Day's work, see 224 6000 A 22294 4002

92 12 09 060

012200
92-31234

1. The first group of people who are interested in the results of the study are the researchers themselves. They want to know if the study was successful in achieving its goals and if the data collected is reliable and valid. They also want to know if the study has contributed to the field of research and if it has provided any new insights or findings.

235P8

FURTHER ONE-DIMENSIONAL ANALYSIS OF **LONG-ROD PENETRATION OF** **SEMI-INFINITE TARGETS**

Accession For	
NTIS CRA&I	<input checked="" type="checkbox"/>
DTIC TAB	<input type="checkbox"/>
Unannounced	<input type="checkbox"/>
Justification:	
By	
Distribution /	
Availability	
Dist	Avail
A-1	



APPROVED: Wallace T. Fowler
Wallace T. Fowler

George W. Botbyl
George W. Botbyl

Copyright

by

John Daniel Cinnamon

1992

All Rights Reserved

This work is dedicated to my wife, Tamara. Her love and support were invaluable.

**FURTHER ONE-DIMENSIONAL ANALYSIS OF
LONG-ROD PENETRATION OF
SEMI-INFINITE TARGETS**

by

JOHN DANIEL CINNAMON, B.S.

REPORT

Presented to the Faculty of the Graduate School of
The University of Texas at Austin
in Partial Fulfillment
of the Requirements
for the Degree of
Master of Science in Engineering

THE UNIVERSITY OF TEXAS AT AUSTIN

August 1992

Acknowledgements:

I would like to acknowledge the contributions of Dr. Stanley E. Jones from the University of Alabama. His guidance as a mentor and a friend was truly unparalleled. His role as a Distinguished Visiting Professor at The United States Air Force Academy placed him in a position to begin my intellectual development in this field.

Dr. Joseph C. Foster, Jr., Leo Wilson, and Joel House at the Armament Directorate (WL/MNMW) of the U.S. Air Force's Wright Laboratories were instrumental in aiding me in my research.

Special acknowledgement is given to Dr. Wallace T. Fowler at the University of Texas at Austin for his exceptional support and trust of my abilities to allow me the latitude to attempt this project.

Finally, the role of both the U.S. Air Force Academy and the Air Force Institute of Technology in providing me this opportunity to pursue graduate education must not be overlooked.

July 29, 1992

ABSTRACT

FURTHER ONE-DIMENSIONAL ANALYSIS OF LONG-ROD PENETRATION OF SEMI-INFINITE TARGETS

by

JOHN DANIEL CINNAMON, B.S.

SUPERVISING PROFESSOR: Wallace T. Fowler

A new one-dimensional analysis of long-rod penetration of semi-infinite targets is presented. Models in this field attempt to accurately describe the penetration process of a long rod of material into a semi-infinite construct of target material. This one-dimensional analysis predicts profile hole diameters and penetration depths over a wide range of material combinations and extends the previous analysis in this area to include hypervelocity impacts. This approach utilizes values of material dynamic yield strengths, known impact conditions, and the well established crater volume/kinetic energy relationship to predict crater hole characteristics over an impact velocity range of 1 to 6 km/s. The analysis

presented here includes an initial transient phase and modifies previous estimates for pressure on the penetrator tip at steady-state. The average pressure at steady state was found to be a constant value over the range of impact velocities for a particular shot combination. The specific value for the average pressure was found to be a direct function of target strength. The resulting equations retain computational simplicity by remaining completely algebraic in nature. Correlation with a majority of the readily available experimental data is given. The results are quite good for a one-dimensional model.

Table of Contents

Signature Page.....	i
Copyright Page.....	ii
Dedication.....	iii
Title Page.....	iv
Acknowledgements.....	v
Abstract.....	vi
Table of Contents.....	viii
List of Tables and Figures.....	ix
List of Symbols and Abbreviations.....	x
1.0 INTRODUCTION.....	1
2.0 THEORY.....	4
2.1 Primary Governing Equations.....	5
2.2 Previous Pressure Analysis.....	6
2.3 Transient Penetration Analysis.....	9
2.4 Impact Conditions.....	13
2.5 Cratering Analysis.....	13
2.6 Penetration Analysis.....	15
3.0 CURRENT PRESSURE PROFILE ANALYSIS.....	17
3.1 Previous Pressure Distributions.....	18
3.2 New Pressure Distribution.....	18
3.3 Revised Average Pressure Approach.....	20
4.0 RESULTS.....	20
5.0 CONCLUSION.....	30
APPENDIX A.....	32
6.0 REFERENCES.....	222
VITA.....	228

List of Tables and Figures

<u>Title</u>	<u>Page</u>
Table 1. Experimental Data Summary.....	22
Table 2. Correlation of Q to Target Strength.....	27
Figure A. Schematic of rod and penetration process.....	5
Figure B. Idealized Crater Geometry.....	14
Figure C. Actual Crater Geometry.....	15
Figure D. Average Pressure vs. Target Strength.....	28
Figure E. Comparative Case: Strain vs. Impact Velocity.....	29
Figure F. Comparative Case: Penetration Depth vs. Impact Velocity...	29
Figures 1 - 94.....	App A

List of Symbols and Abbreviations

a	slope of the crater volume/kinetic energy relationship
A	cross-sectional area of the mushroom of the rigid-plastic penetrator
A_i	initial cross-sectional area of the undeformed penetrator
A_0	cross-sectional area of the penetrator at impact
A_1	cross-sectional area of the penetrator at steady state
b	intercept of the crater volume/kinetic energy relationship
D	original diameter of the undeformed penetrator
e	engineering strain in the mushroom of the penetrator
e_0	engineering strain in the mushroom at impact
e_1	engineering strain in the mushroom at steady state
E_0	kinetic energy of the penetrator at impact
ℓ	current undeformed section length
L	original length of the undeformed penetrator
p_a	pressure on the axis of the penetrator tip
p_0	pressure on the axis of the penetrator tip at impact
p_1	pressure on the axis of the penetrator tip at steady state
P	average pressure on the penetrator tip
P_0	average pressure on the penetrator tip at impact
P_1	average pressure on the penetrator tip at steady state
Q	average pressure on the penetrator tip at steady state, independent of v_0

r	radial distance from the axis of the penetrator
R	original undeformed penetrator rod radius
R_t	dynamic yield strength of target
u	current penetration velocity
u_0	penetration velocity at impact
v	current velocity of the undeformed section
v_0	impact velocity
V_c	crater volume of the recovered target
Y_p	dynamic yield strength of penetrator
z	penetration depth
ρ	penetrator density
μ^2	ratio of target density to penetrator density

1.0 INTRODUCTION

In 1967, Tate [1] and simultaneously Alekseevskii [2], published a one-dimensional theory for the penetration of semi-infinite targets by long rods. Tate [3] published a second paper in 1969. These papers form the basis upon which the accepted theory of one-dimensional rod penetration rests. This theory attempts to accurately describe the penetration process of a long rod of material into a semi-infinite construct of target material. A prediction of the resulting penetration hole characteristics is available from this analysis. By comparing the theoretical predictions to experimental data, we can evaluate the accuracy of these one-dimensional models.

In 1987, Jones, *et al.* [4] modified the equations of motion for the undeformed rod section by employing a balance of linear impulse and momentum. In subsequent papers [5,6] an improvement in the correlation between theoretical and experimental data was observed. However, this approach relied upon post-test measurements for estimates of the engineering strain in the mushroom of the penetrator tip. The strain was assumed to be constant throughout the process and equal to that measured from the profile hole diameter. By using the modified Bernoulli Equation proposed by Tate, the pressure, penetration velocity, and undeformed section velocity were coupled with the modified equation of motion and an equation for the conservation of mass passing from the undeformed section of the penetrator. This system was solved by integration and the resulting prediction of penetration

depths were compared to experimentally observed values from the recovered targets. The penetrator and target dynamic yield strengths were taken to be constant during the event and estimated from laboratory values for yield strengths at the highest available strain-rates.

These results were satisfying and showed promise, but based analysis of key parameters on post-experiment measurement. Kerber, *et al.* [7], in 1990, utilized a well established crater volume - kinetic energy relationship, e.g. [8], to remove some of the dependence on post-test measurements. The aim was to produce engineering strain as a by-product of the solution of the model. However, because the penetration process was treated as being dominated by the steady-state, the results did not correlate well over a large range of impact velocities and rod lengths. The correlations with experiment were satisfactory for longer rods and higher impact velocities where steady state penetration can be presumed to dominate the event. The initial and terminal transients were neglected in this and previous analysis. The initial transient would appear to become more important in shorter rods and lower impact velocities.

In 1992, Cinnamon, *et al.* [9,10] reported a significant increase in accuracy by incorporating an initial transient phase to the penetration process. This analysis was based on observations by Ravid, *et al.* [11], Gillis, *et al.* [12], and Jones, *et al.* [13]. This latest approach yielded good accuracy for a one-dimensional model in the 1 to 3 km/s velocity range. The results depended only on physical parameters determined before testing and the well

established crater volume/kinetic energy relationship. The terminal transient was neglected in this model. The resulting equations were completely algebraic in nature. Of some concern in this approach was that the trends in the predicted penetration depth curves were tending toward significantly high values for impact velocities above 3 km/s. When experimental data for 3 - 6 km/s were evaluated, the model's accuracy indeed deteriorated. In examining the model, it became obvious that the predictions of pressure available from the modified Bernoulli Equation were simply too high. In fact, the correlation discovered by Cinnamon, *et al.* [9,10] indicated that the pressure profile could be successfully modified in such a way that the average pressure at steady-state predicted by the Bernoulli Equation was *reduced* by a specific factor (which depended exclusively on target strength) to match experimental penetration depths. The parabolic nature in which the modified Bernoulli Equation predicts the interface pressure at steady state as impact velocity increases was somewhat minimized by this technique.

In 1992, Jones, *et al.* [14], the pressure distribution on the penetrator tip was modified to attempt to correct for the deteriorating results above 2.5 km/s. With a judicious choice of two dimensionless parameters, slight improvement was observed. However, a physical relationship between these parameters and the model was not discovered. The pressures predicted by the modified Bernoulli Equation were once again reduced to achieve acceptable results. However, this new pressure

distribution contained the same parabolic component as the previous approach.

In this paper, several approaches to the choice of pressure at steady state are evaluated. It became clear that past successful solution forms for the pressure distribution were those that cancelled out the parabolic nature of the modified Bernoulli Equation. As a consequence, when the average pressure at steady state is taken to be a particular value for a specific material combination over all impact velocities and directly related to target strength, a significant increase in model accuracy resulted. The model was successfully extended up to 6 km/s. This paper includes a large body of results reflecting analysis of all readily available experimental data in this field of research, a great majority of which has been compiled by Anderson, *et al.* [15].

2.0 THEORY

The general concepts of the rod penetration process are detailed in Figure A. The undeformed penetrator is a cylinder of known length and diameter which impacts the target at a nominal normal incidence at a known velocity. The penetrator enters the target and experiences mushrooming in the tip. When the event has concluded, a crater with a measurable diameter and depth remains.

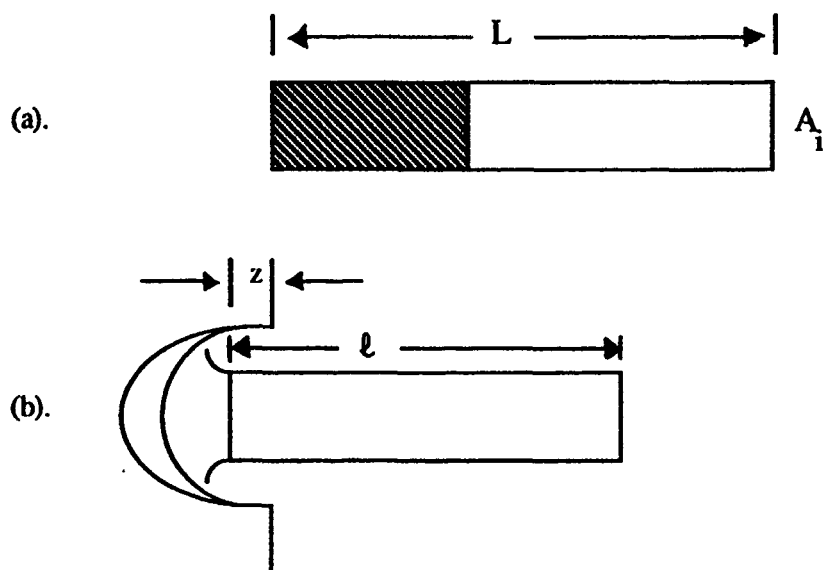


Figure A. Schematic of Rod and Penetration Process.
 (a) shows the undeformed rod of length L and initial cross-sectional area A_i . The shaded portion will be lost to erosion.
 (b) shows the penetration event. l is the undeformed section length and z is the penetration depth.

2.1 Primary Governing Equations

In [4], Jones, *et al.* proposed a modification to the equation of motion of the undeformed section of a rod penetrator. This equation is

$$l \ddot{v} + \dot{l} (v-u) = \frac{-P}{\rho(1+e)} \quad (1)$$

where l is the undeformed section length, v is the current undeformed section velocity, u is the penetration velocity, P is the average pressure on the penetrator tip, ρ is the penetrator density, and e is the engineering strain in the

penetrator mushroom. The details behind the development of this equation are contained in [4].

Wilson, *et al.* in [5] added another key equation to the analysis. The conservation of mass across the plastic interface between the mushroom and the undeformed section of the penetrator was given in the form

$$e \dot{\ell} = v - u \quad (2)$$

The penetrator is assumed to be rigid-plastic during the event. In both (1) and (2), dots over the symbols represent differentiation with respect to time. The engineering strain in the mushroom is compressive and therefore negative. The current value of the engineering strain in the mushroom is defined to be

$$e = \frac{A_i}{A} - 1 \quad (3)$$

where A_i is the initial cross-sectional area of the undeformed penetrator and A is the current cross-sectional area of the mushroom.

2.2 Previous Pressure Analysis

The average pressure on the penetrator tip, P , can be varied by considering various pressure profiles. In [4] and [5], the pressure was assumed to be uniform across the mushroom face. The intensity of the pressure was assumed to be the solution of the modified Bernoulli equation. This

equation, from [1 - 3], is applied at steady state and relates pressure on the axis of the specimen at the penetrator tip, p_a , to the undeformed section speed v , the penetration velocity u , and material properties of the target and penetrator. The modified Bernoulli equation is

$$p_a = \frac{1}{2} \mu^2 \rho u^2 + R_t = \frac{1}{2} \rho (v - u)^2 + Y_p \quad (4)$$

where R_t and Y_p are dynamic yield strengths of the target and penetrator at suitably high strain rates respectively, and μ^2 is the ratio of the penetrator to target density. The pressure was taken in [4] and [5] not to vary across the mushroom face.

Gillis, *et al.*, in [12] suggested that the uniform pressure profile was not realistic and proposed a parabolic form which was symmetric about the axis of the specimen and zero on the edge of the mushroom. In this case, the pressure p had the form

$$p = p_a \left(1 - \frac{r^2}{R^2} \right) \quad (5)$$

where p_a is the current pressure on the rod axis, R is the original rod radius, and r is the radial distance from the axis. The factor $(1+e)$ in the denominator of the pressure term in (1) forces the pressure to act over the deformed mushroom face with area A , even though (5) refers to the original rod configuration.

The average pressure P can be computed, in general, by

$$P = \frac{1}{A_i} \int_{A_i} p \, dA_i \quad (6)$$

When P was calculated for (5), the result was $\frac{p_a}{2}$. The predictions for penetration depths were somewhat improved over the previously assumed uniform pressure distribution. The results still suffered from ignoring the initial and final transients in the penetration event. This parabolic pressure distribution effectively reduced the parabolic nature of (4) by a factor of two. Although this improved the model by reducing the effect of (4), the addition of at least an initial transient seemed warranted.

In Cinnamon, *et al.* [9,10], the pressure distribution was generalized to the form

$$p = p_a \left(1 - \frac{r^2}{R^2}\right)^n \quad (7)$$

which made the average pressure term become

$$P = \frac{p_a}{(n+1)} \quad (8)$$

This new pressure distribution was successfully employed with an initial transient phase to correlate to a large number of experimental cases. The pressure exponent n was found to be a direct function of target strength. Although this approach provided improved results over

previous approaches, the analysis could not be successfully extended beyond 3 km/s.

Jones, *et al.* [14] attempted to correct the problem by adding a uniform component to the pressure profile. The distribution had the form

$$p = q + (p_a - q) \left(1 - \frac{r^2}{R^2}\right)^n \quad (9)$$

and the average pressure became

$$P = \frac{nq}{(n+1)} + \frac{p_a}{(n+1)} \quad (10)$$

This new pressure profile improved results slightly and extended them into the hypervelocity range (3 - 6 km/s). However, q and n were not successfully correlated to any physical parameters.

In this paper, another approach to the determination of the average pressure will be explored and a successful correlation to target strength will be presented. In addition, the widest possible body of available data will be used in the correlation.

2.3 Transient Penetration Analysis

In Cinnamon, *et al.* [9,10], an initial transient phase of penetration was added to the model. The transient phase is characterized by impact shock effects and complete mushroom growth which occurs between impact and the beginning of steady state penetration. We assume that the

penetrator impacts the target at a known velocity, v_0 , of sufficient magnitude (i.e. $v_0 > 1$ km/s) such that the undeformed section cannot sustain any appreciable deceleration (i.e. $\dot{v} \approx 0$) during the initial transient. This means that $v = v_0$ throughout the transient or mushrooming phase of penetration. During the initial transient, the mushroom develops from a cross-sectional area A_0 at impact to A_1 , when steady state begins. The mushroom retains an area of A_1 throughout the steady state portion of the penetration process until the end of the event.

Ravid, *et al.* [11] reported that there was little change in penetration velocity u during the shock/impact stage of the initial transient phase. Motivated by this observation, we assumed that the penetration velocity was approximately constant (i.e. $u = u_0$) throughout the initial transient. Hence, (1) becomes

$$\dot{\ell} (v_0 - u_0) = \frac{-P}{\rho(1+e)} \quad (11)$$

and (2) is modified to

$$e \dot{\ell} = v_0 - u_0 \quad (12)$$

These two equations, (11) and (12), govern the mushrooming of the rod during the initial transient phase of the penetration event which precedes the steady state. At impact, the engineering strain in the mushroom is e_0 . When steady state is reached, the strain becomes e_1 .

By eliminating \dot{e} between (11) and (12) and solving for e , we arrive at an expression for the engineering strain.

$$e = \frac{-(v_0 - u_0)^2}{(v_0 - u_0)^2 + \frac{P}{\rho}} \quad (13)$$

This relationship provides us with an explicit formula for the strain in the mushroom as it develops during the transient phase. This equation governs the behavior until the beginning of the steady state penetration phase. The pressure on the axis, p_a , is changing rapidly during mushroom formation. It has a large value, p_0 , at impact and a reduced value, p_1 , at steady state.

When steady state is reached, we assume that the modified Bernoulli Equation, (4), is valid. At the transition point between the transient and steady state portions of the event, (4) can be expressed as

$$p_1 = \frac{1}{2} \mu^2 \rho u_0^2 + R_1 = \frac{1}{2} \rho (v_0 - u_0)^2 + Y_p \quad (14)$$

and (13) can be written as

$$e_1 = \frac{-(v_0 - u_0)^2}{(v_0 - u_0)^2 + \frac{P_1}{\rho}} \quad (15)$$

where P_1 is the average pressure on the penetrator tip at the beginning of steady state.

Equation (14) can then be used to solve for u_0 in terms of the known quantities v_0 , ρ , μ^2 , R_t , and Y_p . The remaining variable in the system of equations is P_1 . The determination of P_1 is the primary focus of this paper.

The penetration velocity u_0 can be found algebraically from (14). The three primary cases are outlined below.

For equal penetrator and target dynamic yield strength (i.e. $R_t = Y_p$) and equal densities (i.e. $\mu^2 = 1$), u_0 reduces to

$$u_0 = \frac{1}{2} v_0 \quad (16)$$

For unequal penetrator and target dynamic yield strength (i.e. $R_t \neq Y_p$) and equal densities (i.e. $\mu^2 = 1$), u_0 becomes

$$u_0 = \frac{\rho v_0^2 + 2(Y_p - R_t)}{2\rho v_0} \quad (17)$$

In the general case, u_0 is given by

$$u_0 = \frac{-v_0}{\mu^2 - 1} + \frac{1}{\rho(\mu^2 - 1)} \left[\rho^2 v_0^2 - 2\rho(\mu^2 - 1)(R_t - Y_p - \frac{1}{2}\rho v_0^2) \right]^{1/2} \quad (18)$$

In each of these cases, then, u_0 can be determined algebraically from known material properties and impact conditions. This leaves e_1 in (15) as a function of known parameters and the average pressure on the penetrator tip at steady state.

2.4 Impact Conditions

The model outlined above also provides some information about conditions at impact. The strain on impact e_0 can be calculated from (13) if we know the average pressure on the penetrator tip at impact, P_0 .

$$e_0 = \frac{-(v_0 - u_0)^2}{(v_0 - u_0)^2 + \frac{P_0}{\rho}} \quad (19)$$

The impact pressure can be estimated from elementary shock physics, using

$$P_0 = \rho u_s u_0 \quad (20)$$

where u_s is the shock speed in the target. Values for u_s as a function of u_0 can be found in shock Hugoniot tables, e.g. [16]. Calculation of P_0 from a known value of p_0 can typically be accomplished using the same approach as the calculation of P_1 from p_a .

2.5 Cratering Analysis

The mathematical model for the behavior of the penetrator is a rigid-plastic, instantaneously eroding rod model. As a result, the penetrator enters the target with some impact engineering strain e_0 which expands to e_1 during the transient. The impact pressure p_0 is usually very high relative to the steady state pressure p_1 . Although this pressure decreases rapidly during mushroom

formation in the transient phase, the values for p_0 can be significant. The mushroom diameter grows from the time of impact through the transient phase, and ceases at the beginning of the steady state portion of the event. The shock/impact stage takes place in a period of a few microseconds, see [11].

The instantaneous erosion assumption prevents the model from accounting for any additional erosion of the target - which occurs in actual practice. There is typically appreciable change in target geometry due to penetrator and target material ejection from the crater. As a consequence, the recovered targets will appear to have more cylindrical-type craters than the model would predict. Figure B illustrates the crater predicted by the mathematical model, and Figure C indicates how the actual geometry frequently appears.

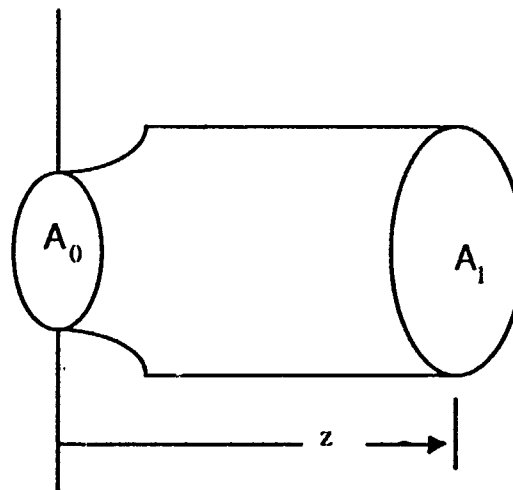


Figure B. Idealized Crater Geometry

A_0 and A_1 are the cross-sectional areas at impact and at steady state respectively. z is the penetration depth.

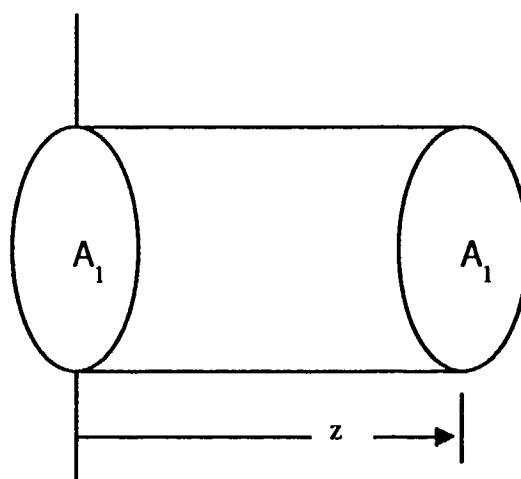


Figure C. Actual Crater Geometry

A_1 is the observed crater cross-sectional area. The crater is assumed cylindrical with altitude z .

2.6 Penetration Analysis

Predicting penetration depths from the above model is made possible through the use of a somewhat empirical approach. For a number of years, researchers have observed a significant correlation between crater volume in the recovered targets and impact kinetic energy, e.g. [8]. This relationship appears to be linear for impact cases of sufficiently, but not excessively, high energy and can be expressed in the form

$$V_c = a E_0 + b \quad (21)$$

where V_c is the crater volume, E_0 is the impact kinetic energy and is equal to $\frac{1}{2} \rho A_1 L v_0^2$, and the variables a and b

are regression constants determined from the available experimental data. The linear fit is performed for each shot combination.

These crater volume/kinetic energy relationships are computed from data points for a particular shot combination. The reliability of the linear fit is, of course, a function of the number of data points available. Since most experimental tests are quite expensive, frequently the data is sparse and/or somewhat scattered. When the linear fit predicts cratering at zero impact kinetic energy, or in some other way reflects erroneous trends, the usefulness of the particular case is significantly reduced. This phenomenon is typically avoided by a sufficient number of experimental points. The accuracy of the penetration prediction is extremely dependent on the crater volume/kinetic energy relationship arrived at using this technique.

By adopting the cylindrical approximation for the crater geometry discussed above, we can generate predictions for the penetration depths. Because of the ejection of material from the crater, the cross-sectional area of the recovered target hole, A_1 , will be

$$A_1 = \frac{A_i}{(1 + e_1)} \quad (22)$$

The crater volume can be expressed as

$$V_c = A_1 z \quad (23)$$

where z is the penetration depth. The penetration depth can be predicted by applying the crater volume/kinetic energy relationship to V_c . From (21) and (23), z is given by

$$z = \frac{1}{A_i} (1+e_1) V_c = \frac{1}{A_i} (1 + e_1) (aE_0 + b) \quad (24)$$

Thus, the penetration depth can be expressed as an algebraic function of known material properties and impact conditions, and as a function of the average pressure on the penetrator tip at steady state.

3.0 CURRENT PRESSURE PROFILE ANALYSIS

In the previous work outlined above, it was noted that one of the primary difficulties in achieving good predictions for the crater characteristics was the manner in which the modified Bernoulli Equation (4) predicted pressure as a function of u and v . The parabolic nature of (4) tended to over-predict penetration depths for the higher velocity cases (3 - 6 km/s). Earlier successes, particularly in the intermediate velocity range (1 - 3 km/s), were the result of pressure distributions that tended to reduce the effect of (4). In this paper, additional pressure distribution analysis is performed to address this problem.

3.1 Previous Pressure Distributions

An obvious departure point for the attempt to improve the one-dimensional analysis and extend it into the hypervelocity range was to begin with the previous pressure distributions. A great body of additional experimental data became available in [15] that expanded the range of materials, greatly increased the number of shot combinations accessible for analysis, and provided data in the hypervelocity range. The pressure profiles detailed in (7) and (9) were examined for possible application in these new cases.

The distribution in (7) was unable to compensate for the parabolic nature of (4) while maintaining accuracy in the intermediate velocity ranges if n was considered a constant as it was in [9,10]. Attempts to model n as a function of material properties or impact conditions were not successful. In general, it was observed that n needed to increase with impact velocity to essentially cancel the effects of the modified Bernoulli Equation. The distribution in (9) followed the same trend. Although the results improved, the net effect was to choose n and q to counter the dramatic pressure increase dictated by equation (4).

3.2 New Pressure Distribution

To attempt to find a solution to this dilemma, a new, more general, pressure distribution was proposed by Jones [17]. This pressure profile takes the form

$$p = q + (p_a - q) \left(1 - \left(\frac{r}{R}\right)^m\right)^n \quad (25)$$

This profile is a more complex and versatile one. A great deal of additional control over the shape of the pressure distribution was provided by (25). The average pressure then is given by

$$P = q + 2(p_a - q) \frac{\Gamma\left(\frac{2}{m}\right) \Gamma(1+n)}{m \Gamma\left(1 + \frac{2}{m} + n\right)} \quad (26)$$

where Γ is the well known mathematical gamma function.

As a significant number of cases were examined, it became increasingly clear that in order to achieve the desired trends in the theoretical penetration curves, n and m were chosen in such a way as to essentially eliminate the effect of the second term in (26). That is, an average pressure comprised of a single value, q , which was unvarying over the range of impact velocities, achieved the best results. This discovery matched our previous experience with (7) and (9). Apparently, the magnitude and trends in the pressures predicted by the modified Bernoulli Equation were not leading to acceptable results. All previous successes were based on choices that reduced or eliminated the contribution of the velocity dependent axial pressure in (4) to the value of P_1 .

3.3 Revised Average Pressure Approach

With the results described above, another approach was required. It became clear that the previous calculation of the average pressure at steady state, P_1 , was not acceptable. To simplify the analysis, the connection of P_1 to a particular pressure distribution is ignored.

The problem is further simplified by the fact that the desired trends in the penetration depths result from a constant value for P_1 over the entire velocity range.

This approach does not imply that the pressure distributions have the same shape for differing velocities, or that p_a is equivalent for all velocities, simply that the value of P_1 is constant for a particular shot combination over all impact velocities.

4.0 RESULTS

When P_1 was assumed to be some constant average pressure on the penetrator tip independent of v_0 , defined here to be Q , for all impact velocities in a particular shot combination, the results of this model improved tremendously. The penetration depth theoretical curves adopted the trends present in the experimental data (i.e. penetration depths leveling off as velocity increases toward 6 km/s). In addition, the values for Q which yielded the best results correlated strongly to target strength.

In order to establish the most credible and most complete correlation possible, all available data were employed. As a consequence, this report includes a large number of figures. In order for this theory to be applied

effectively, experimental data sets must have included crater diameters. A number of the cases in [15] did not provide this information. In addition, a minimum of two data points were required to construct the crater-volume/kinetic energy relationship. Hence, some other cases could not be evaluated. With those limitations in mind, the author applied all readily available cases to this model and reports the results.

Table 1 summarizes all the cases and provides essential data about each shot combination. The figure numbers referred to can be found in Appendix A. One figure number is assigned to each shot combination. For each case, several figures denoted by the figure number and lower case letters are to be found. The first three figures of each case (corresponding to a, b, and c) are the strain vs. impact velocity, crater volume vs. impact kinetic energy, and penetration depth vs. impact velocity graphs. Any additional graphs will occur in pairs. These additional figures (i.e. d and e, etc.) refer to cases in which the crater volume/kinetic energy relationship was modified by removing certain data points that appear erroneous or that may skew the general trend. When these points are removed, the relationship changes - which modifies the resulting penetration curve. Of course this does not alter the strain curve in any way - avoiding the necessity of including an additional one. The first three figures for each case include all reported data.

The figures report theoretical curves superimposed on discrete experimental points. The upper curve in the

Table 1. Experimental Data Summary

Fig. #	Pene- trator	Y_p (MPa)	ρ ($\frac{\text{kg}}{\text{m}^3}$)	L (mm)	$\frac{L}{D}$	Target	R_t (MPa)	$\mu^2 \rho$ ($\frac{\text{kg}}{\text{m}^3}$)	Ref.
1	Alum Alloy	200	2700	63.5	10	Lead	200	11200	[18]
2	1100-O Al	250	2720	9.525	3	1100-O Al	250	2720	[19]
3	2024-T3 Al	675	2770	9.525	3	1100-O Al	250	2720	[19]
4	7075-T6 Al	600	2804	9.525	3	1100-O Al	250	2720	[19]
5	C1015 St.	600	7600	9.525	3	1100-O Al	250	2720	[19]
6	Soft 4340	1263	7850	31.75	5	2024-T4 Al	400	2770	[20]
7	7075-T6 Al	600	2804	31.75	5	2024-T4 Al	400	2770	[20]
8	Hard 4340	1826	7850	31.75	5	7075-T6 Al	600	2804	[20]
9	Soft 4340	1263	7850	31.75	5	7075-T6 Al	600	2804	[20]
10	7075-T6 Al	600	2804	31.75	5	7075-T6 Al	600	2804	[20]
11	1100-O Al	250	2720	9.525	3	C1015 St.	600	7600	[19]
12	2024-T3 Al	675	2770	9.525	3	C1015 St.	600	7600	[19]
13	7075-T6 Al	600	2804	9.525	3	C1015 St.	600	7600	[19]
14	C1015 St.	600	7600	9.525	3	C1015 St.	600	7600	[19]
15	4340 Steel	1600	7810	68.58	18	6061-T651 Al	600	2710	[21]
16	1100-O Al	250	2720	9.525	3	2024-T3 Al	675	2770	[19]

Fig. #	Pene- trator	Y_p (MPa)	ρ ($\frac{kg}{m^3}$)	L (mm)	$\frac{L}{D}$	Target:	R_t (MPa)	$\mu^2 \rho$ ($\frac{kg}{m^3}$)	Ref.
17	1100-O Al	250	2720	9.525	3	304 St.St.	675	7900	[19]
18	2024-T3 Al	675	2770	9.525	3	2024-T3 Al	675	2770	[19]
19	2024-T3 Al	675	2770	9.525	3	304 St.St.	675	7900	[19]
20	C1015 St.	600	7600	9.525	3	2024-T3 Al	675	2770	[19]
21	C1015 St.	600	7600	9.525	3	304 St.St.	675	7900	[19]
22	304 St.St.	675	7900	9.525	3	2024-T3 Al	675	2770	[19]
23	304 St.St.	675	7900	9.525	3	304 St.St.	675	7900	[19]
24	C110 W1	1200	7850	25	10	St37	750	7850	[22]
25	C110 W1	1200	7850	43	10	St37	750	7850	[22]
26	C110 W1	1200	7850	54	10	St37	750	7850	[22]
27	C110 W1	1200	7850	25	10	St52	850	7850	[22]
28	C110 W1	1200	7850	43	10	St52	850	7850	[22]
29	C110 W1	1200	7850	54	10	St52	850	7850	[22]
30	D17	2500	17000	28	10	St52	850	7850	[22]
31	D17	2500	17000	60	10	St52	850	7850	[22]
32	C110 W2	1100	7850	58	10	H2B,A	850	7850	[22]
33	Marag St	1000	7850	58	10	H2B,A	850	7850	[22]
34	Marag St	1000	7850	116	20	H2B,A	850	7850	[22]
35	35CrNiMo	2200	7850	54	10	H2B,A	850	7850	[22]
36	elmet	2000	15500	58	10	H2B,A	850	7850	[22]

Fig. #	Pene- trator	Y_p (MPa)	ρ ($\frac{kg}{m^3}$)	L (mm)	$\frac{L}{D}$	Target	R_t (MPa)	$\mu^2 \rho$ ($\frac{kg}{m^3}$)	Ref.
37	D17K	2500	17300	58	10	H ₂ B,A	850	7850	[22]
38	D17	2500	17000	58	10	H ₂ B,A	850	7850	[22]
39	W	2500	19300	60	10	H ₂ B,A	850	7850	[22]
40	W75	2500	15500	58	10	H ₂ B,A	850	7850	[22]
41	W90	2500	17000	58	10	H ₂ B,A	850	7850	[22]
42	D18	2500	18000	58	10	H ₂ B,A	850	7850	[22]
43	H01T	2000	14500	58	10	H ₂ B,A	850	7850	[22]
44	D17.6	2000	17600	41.7	10	H ₂ B,A	850	7850	[22]
45	D17.6	2000	17600	58	10	H ₂ B,A	850	7850	[22]
46	Steel	1600	7850	58	10	H ₂ B,A	850	7850	[22]
47	D17	2500	17000	116	20	H ₂ B,A	850	7850	[22]
48	D18.5	2500	18500	58	10	H ₂ B,A	850	7850	[22]
49	H01T	2000	14500	58	10	H ₂ B,A	850	7850	[22]
50	H60T	1600	13500	60	10	H ₂ B,A	850	7850	[22]
51	H60T	1600	13500	58	10	H ₂ B,A	850	7850	[22]
52	H70T	1400	13500	60	10	H ₂ B,A	850	7850	[22]
53	H70T	1400	13500	58	10	H ₂ B,A	850	7850	[22]
54	D17.6	2000	17600	101.5	17.5	H ₂ B,A	850	7850	[22]
55	D17.6	2000	17600	107.8	22	H ₂ B,A	850	7850	[22]
56	D17.6	2000	17600	110.2 5	22.5	H ₂ B,A	850	7850	[22]
57	D17.6	2000	17600	156.8	32	H ₂ B,A	850	7850	[22]
58	D17.6	2000	17600	163.2	32	H ₂ B,A	850	7850	[22]
59	Hard 4340	1826	7850	60	6	RHA	1000	7850	[23]
60	OFHC Cu	300	8900	60	6	RHA	1000	7850	[24]
61	Tantal um	500	16600	60	6	RHA	1000	7850	[24]
62	Hard 4340	1826	7850	95.25	7.5	RHA	1000	7850	[24]
63	Kenn W10	2500	17300	155.8	23	RHA	1000	7850	[25]
64	Kenn W10	2500	17300	121.7 5	23	RHA	1000	7850	[25]
65	D17	2500	17000	28	10	W8	1000	7850	[22]

Fig. #	Pene- trator	Y_p (MPa)	ρ ($\frac{\text{kg}}{\text{m}^3}$)	L (mm)	$\frac{L}{C}$	Target	R_t (MPa)	$\mu^2 \rho$ ($\frac{\text{kg}}{\text{m}^3}$)	Ref.
66	U- 3/4Ti	7000	18600	266.7	20	RHA	1000	7850	[26]
67	W92.5	2500	17590	75	10	Ger RHA	1000	7850	[27]
68	Kenn W10	2500	17200	50	10	Ger RHA	1000	7850	[27]
69	Teledy X27	2500	17330	78.74	10	RHA	1000	7850	[28]
70	C110 W1	1200	7850	25	10	Ger Arm St	1100	7850	[22]
71	C110 W1	1200	7850	43	10	Ger Arm St	1100	7850	[22]
72	C110 W1	1200	7850	54	10	Ger Arm St	1100	7850	[22]
73	D17	2500	17000	28	10	Ger Arm St	1100	7850	[22]
74	D17	2500	17000	60	10	Ger Arm St	1100	7850	[22]
75	D17.6	2000	17600	17.4	3	Ger St	1200	7850	[22]
76	D17.6	2000	17600	29	5	Ger St	1200	7850	[22]
77	D17.6	2000	17600	42	10	Ger St	1200	7850	[22]
78	Soft 4340	1263	7850	31.75	5	Soft 4340	1263	7850	[20]
79	7075- T6 Al	600	2804	31.75	5	Soft 4340	1263	7850	[20]
80	Hard 4340	1826	7850	31.75	5	Soft 4340	1263	7850	[20]
81	X21C	3500	17650	45.7	10	4340 Steel	1600	7810	[21]
82	Teledy X27C	2500	17400	81.6	10	4340 Steel	1600	7810	[29]

Fig. #	Pene- trator	Y_p (MPa)	ρ ($\frac{kg}{m^3}$)	L (mm)	$\frac{L}{D}$	Target	R_t (MPa)	$\mu^2 \rho$ ($\frac{kg}{m^3}$)	Ref.
83	Teledy X27C	2500	17400	81.6	15	4340 Steel	1600	7810	[29]
84	Hard 4340	1826	7850	63.5	10	Hard 4340	1826	7850	[20]
85	Hard 4340	1826	7850	47.63	7.5	Hard 4340	1826	7850	[20]
86	Hard 4340	1826	7850	47.63	5	Hard 4340	1826	7850	[20]
87	Hard 4340	1826	7850	31.75	5	Hard 4340	1826	7850	[20]
88	Hard 4340	1826	7850	63.5	5	Hard 4340	1826	7850	[20]
89	Hard 4340	1826	7850	31.75	3.33	Hard 4340	1826	7850	[20]
90	Hard 4340	1826	7850	31.75	2.5	Hard 4340	1826	7850	[20]
91	Soft 4340	1263	7850	31.75	5	Hard 4340	1826	7850	[20]
92	OFHC Cu	300	8900	60	6	Hard 4340	1826	7850	[24]
93	Tantal um	500	16600	60	6	Hard 4340	1826	7850	[24]
94	D17	2500	17000	28	10	D17	2500	17000	[22]

strain vs. impact velocity figures represents the estimate for θ_0 .

When these cases were evaluated, a certain value for Q could be chosen to match the experimental data. This Q was found to strongly correlate to target strength. Table 2 reports each of the different targets present in the data and their corresponding Q value.

Table 2. Correlation of Q to Target Strength

Target Material	R_t (MPa)	Q (GPa)
Lead	200	0.128
1100-O Al	250	0.28
2024-T4 Al	400	0.6
7075-T6 Al	600	1.05
C1015 St.	600	1.05
6061-T651 Al	600	1.05
2024-T3 Al	675	1.3
304 St. St.	675	1.3
St37	750	1.4
St52	850	1.7
HzB,A	850	1.7
RHA	1000	2.2
W8	1000	2.2
Ger RHA	1000	2.2
Ger Arm St	1100	2.275
Ger St	1200	2.35
Soft 4340	1263	2.4
4340 Steel	1600	2.5
Hard 4340	1826	2.6
D17	2500	2.9

With this information, it was immediately evident that some strong relationship existed between Q and target strength. Figure D depicts the values for Q chosen to allow the model to predict penetration depths and crater diameters accurately against R_t . A curve is fit through the data to both illustrate the correlation and provide a functional relationship between Q and R_t . The best fit is

$$Q = 3.8 (1 - e^{(-0.00135 R_t)}) - 0.8 \quad (27)$$

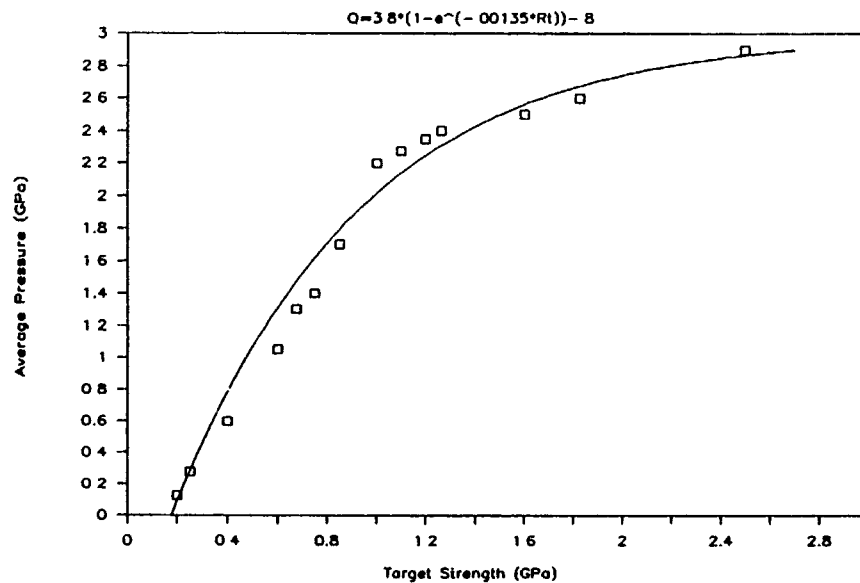


Figure D. Average Pressure vs. Target Strength
Q is the average pressure.

With Q as a direct function of target strength, this one-dimensional penetration model can be expressed in terms of known material properties and impact conditions. The crater volume/kinetic energy curve is still needed to allow for the calculation of penetration depths, however.

To place this revised model into context with regard to those used in [9,10] and [14], Figures E and F are presented. These figures illustrate the comparative results between these three different approaches to the calculation of the average pressure at steady state.

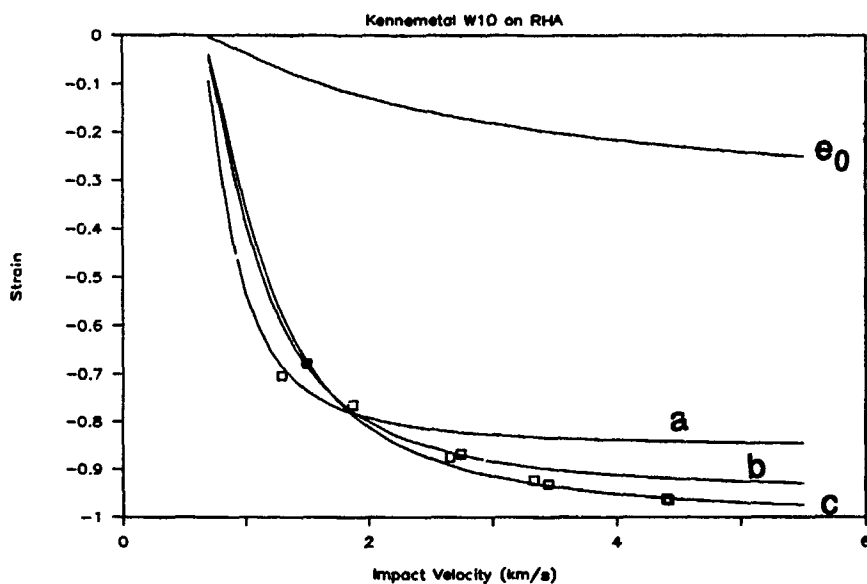


Figure E. Comparative Case: Strain vs. Impact Velocity
 (a) indicates theory from [9,10]
 (b) indicates theory from [14]
 (c) indicates current model

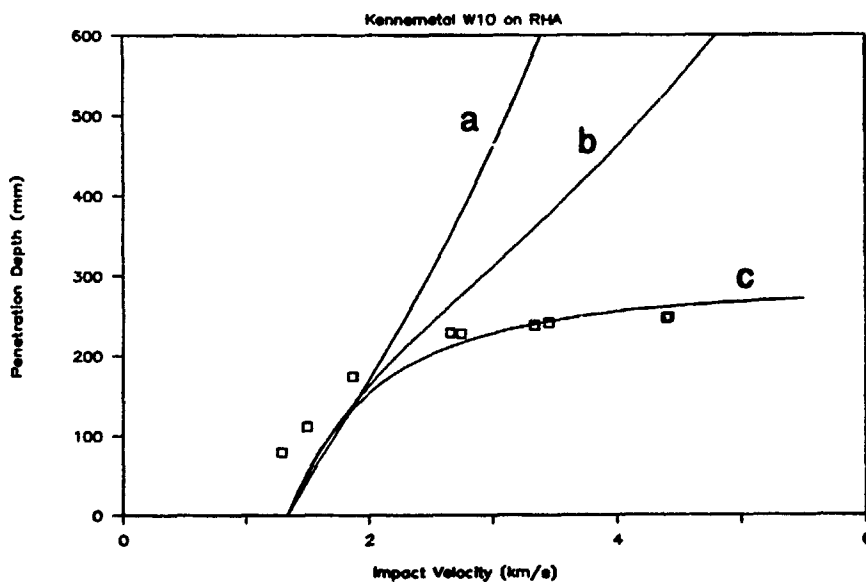


Figure F. Comparative Case: Penetration Depth vs. Impact Velocity
 (a) indicates theory from [9,10]
 (b) indicates theory from [14]
 (c) indicates current model

It is clear from the above comparative figures (i.e. E & F) that each subsequent theory lowered the average pressure in such a way as to lower the penetration and strain curves. This particular case that appears in Figures E and F was chosen for its higher velocity data and its presentation in [14].

5.0 CONCLUSION

In this paper, a new one-dimensional model for the penetration of semi-infinite targets by long rods was developed. Its basis was the revision of the previous techniques employed to calculate the average pressure at steady state. The modified Bernoulli Equation appears to result in values for P_1 that are simply too high for the impact cases in the hypervelocity range.

By correlating a new approach to a great body of data, it was discovered that a single value for the average pressure on the penetrator tip at steady state, Q , could successfully represent the pressure at steady state over the impact velocity range of 1 to 6 km/s. This formulation for Q allowed the model to improve its accuracy and its trends at higher velocities. In addition, this value Q was shown to have a strong correlation to target strength. This approach has resulted in a completely algebraic solution that relies only on known test parameters and the well established crater volume/kinetic energy relationship.

Future work will involve an effort to revise or replace the modified Bernoulli Equation's estimate for pressure at steady state. Additional analysis also needs to be conducted to ascertain the form of the pressure distribution that leads to a constant Q over all impact velocities.

The aim of this paper was to extend the one-dimensional penetration analysis into the hypervelocity range. The resulting model offers good accuracy for a one-dimensional description of the penetration event.

Appendix A:

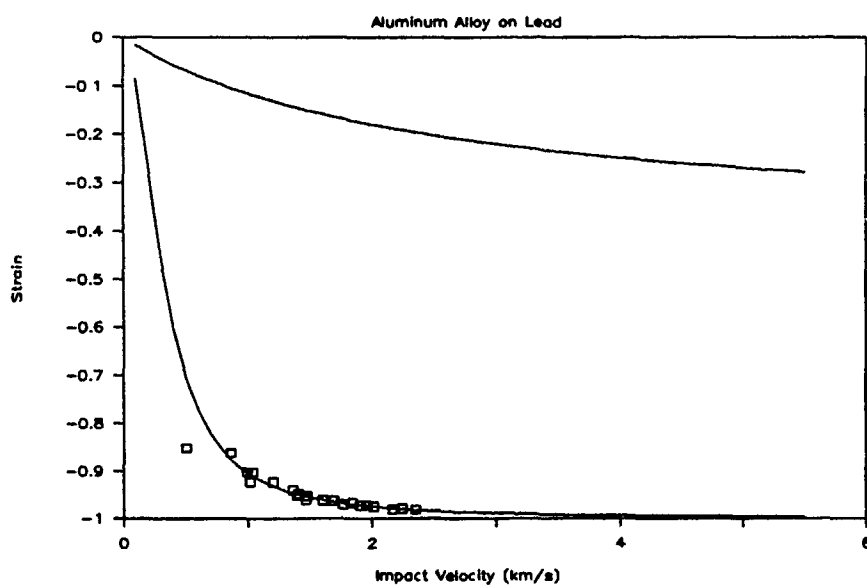


Figure 1a. Strain vs. Impact Velocity

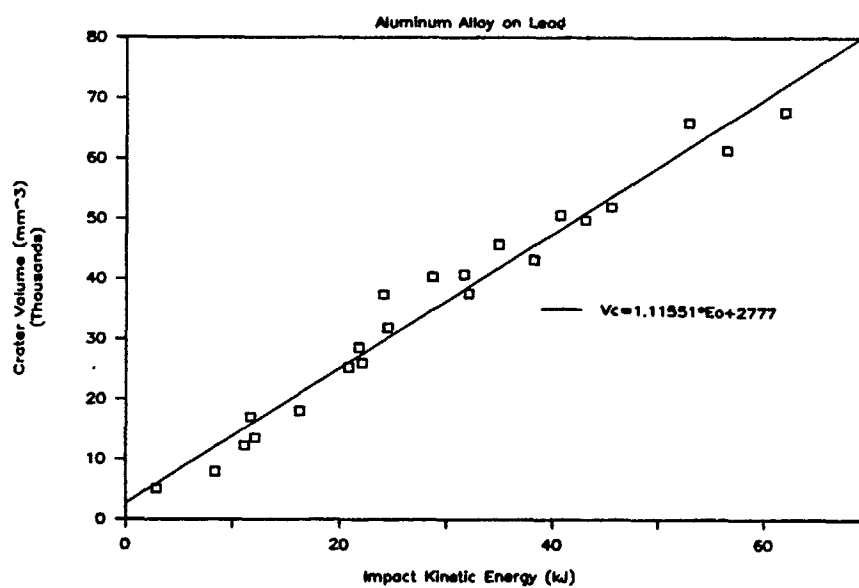


Figure 1b. Crater Volume vs. Impact Kinetic Energy

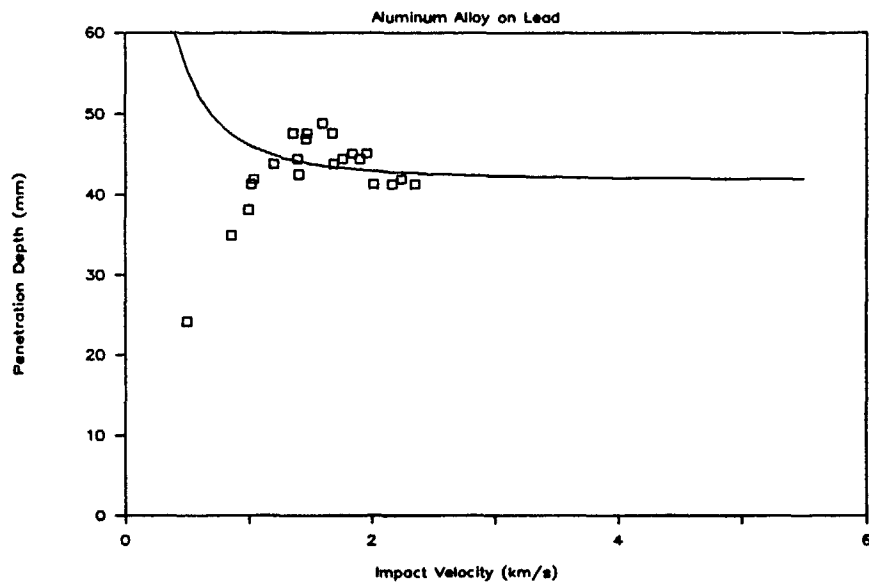


Figure 1c. Penetration Depth vs. Impact Velocity

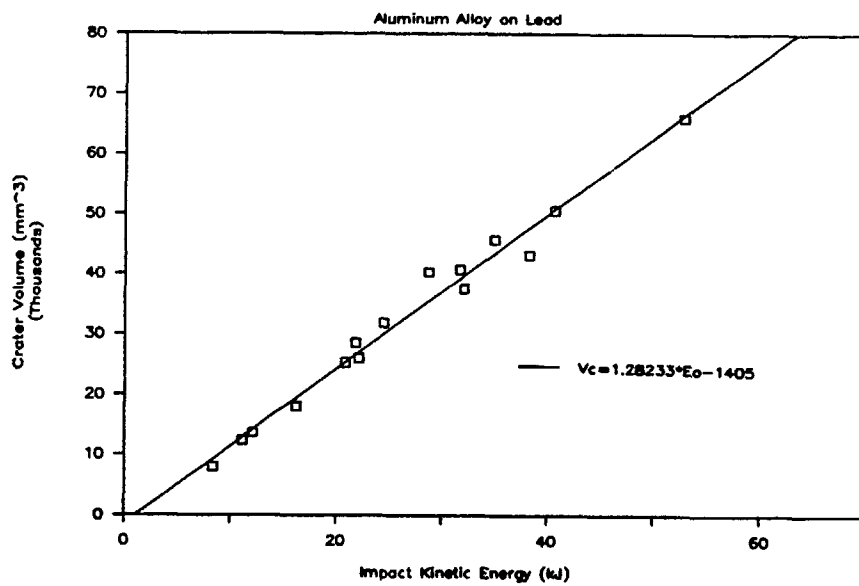


Figure 1d. Crater Volume vs. Impact Kinetic Energy

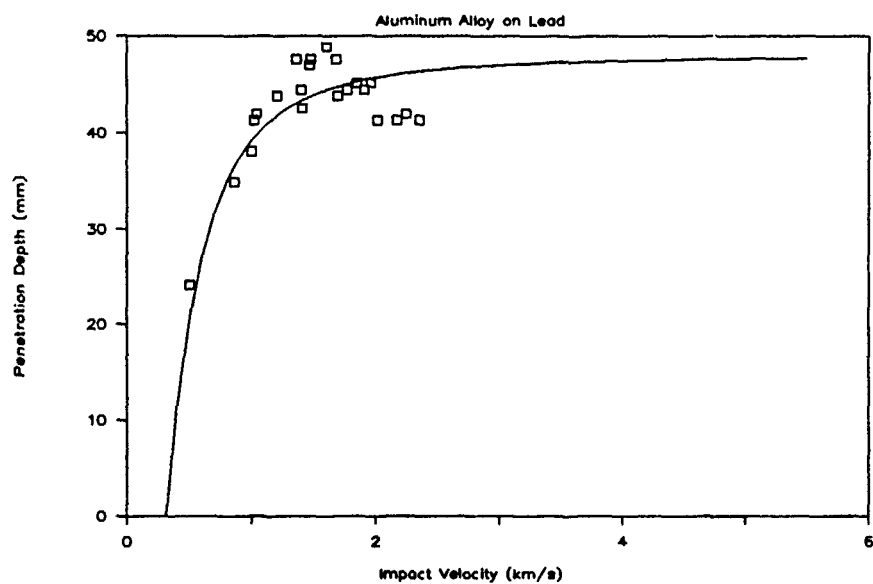


Figure 1e. Penetration Depth vs. Impact Velocity

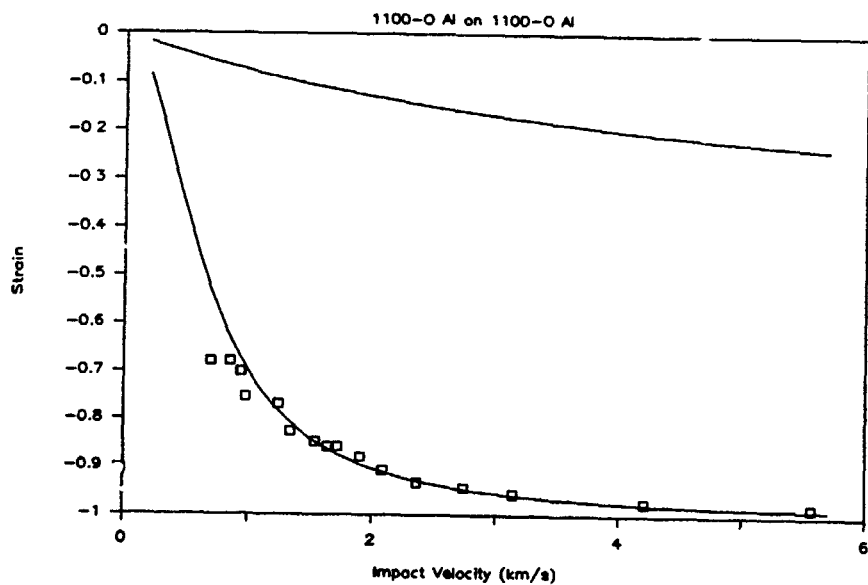


Figure 2a. Strain vs. Impact Velocity

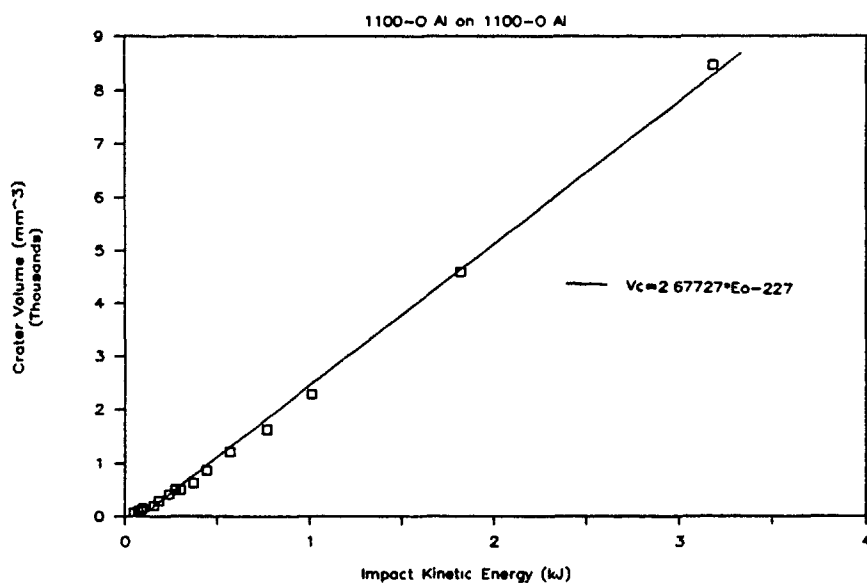


Figure 2b. Crater Volume vs. Impact Kinetic Energy

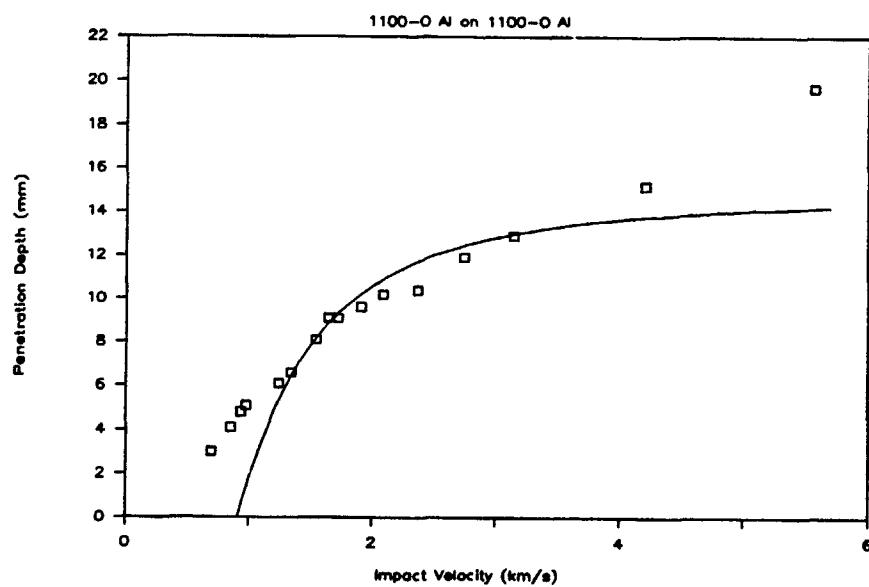


Figure 2c. Penetration Depth vs. Impact Velocity

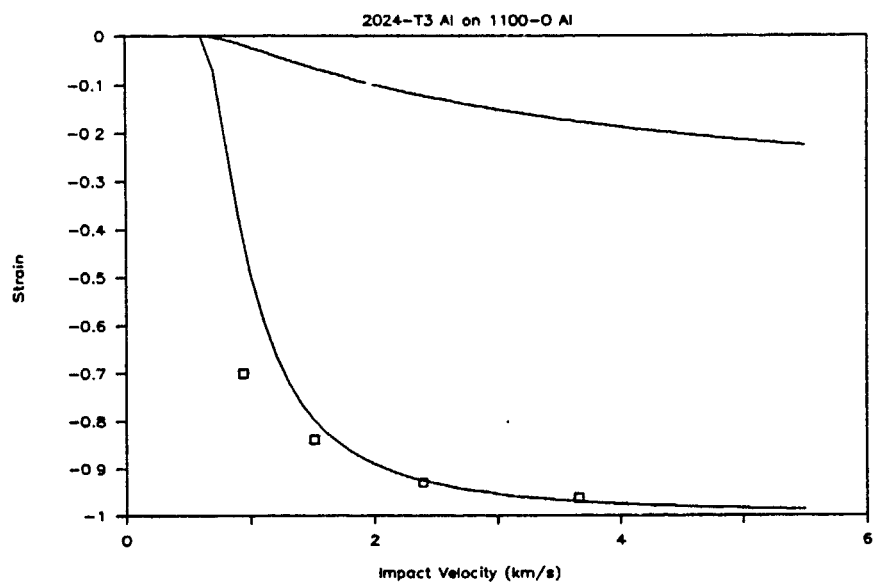


Figure 3a. Strain vs. Impact Velocity

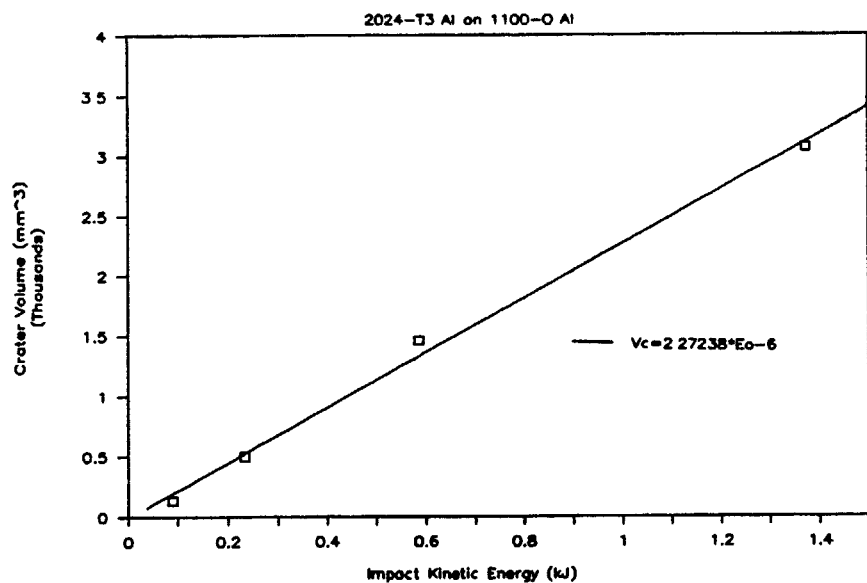


Figure 3b. Crater Volume vs. Impact Kinetic Energy

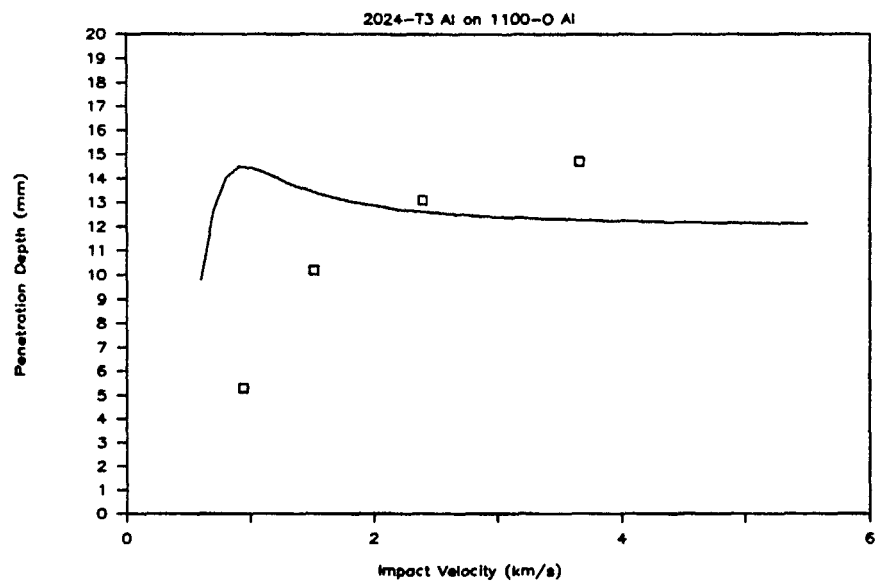


Figure 3c. Penetration Depth vs. Impact Velocity

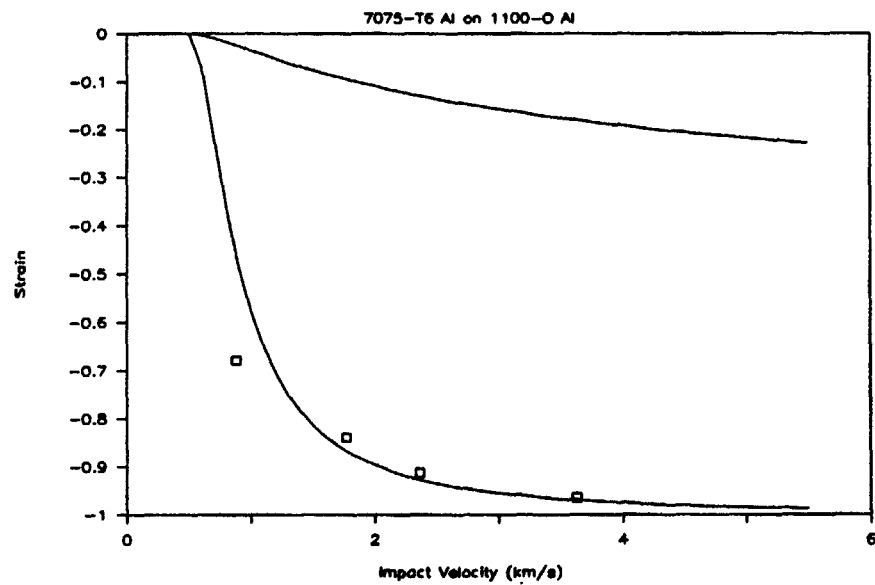


Figure 4a. Strain vs. Impact Velocity

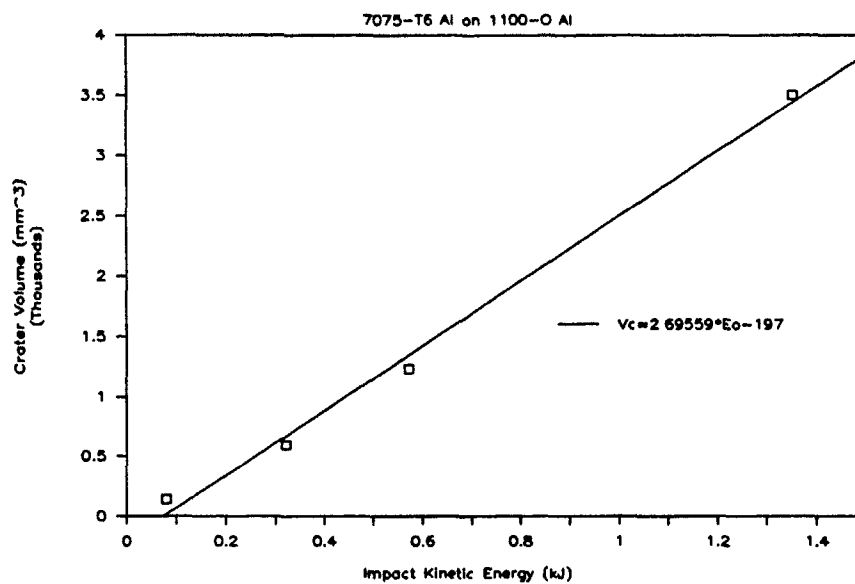


Figure 4b. Crater Volume vs. Impact Kinetic Energy

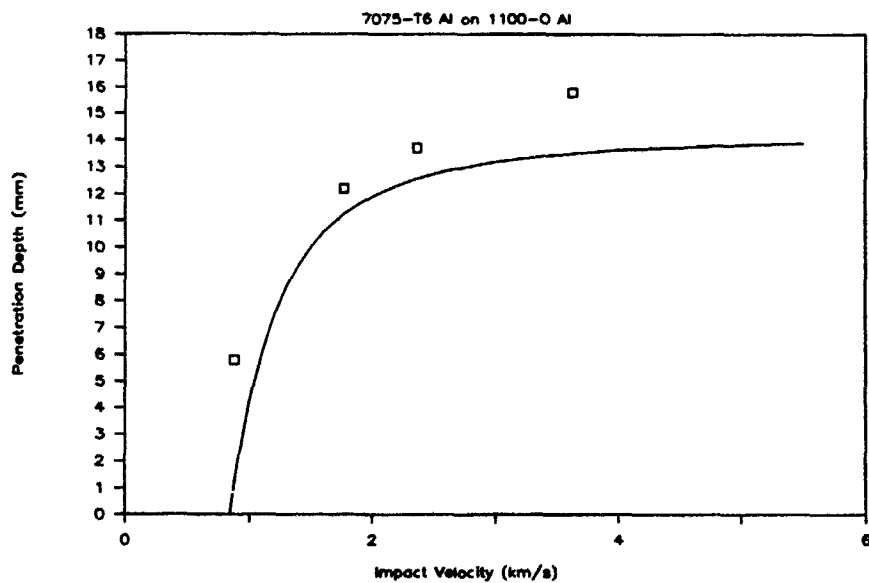


Figure 4c. Penetration Depth vs. Impact Velocity

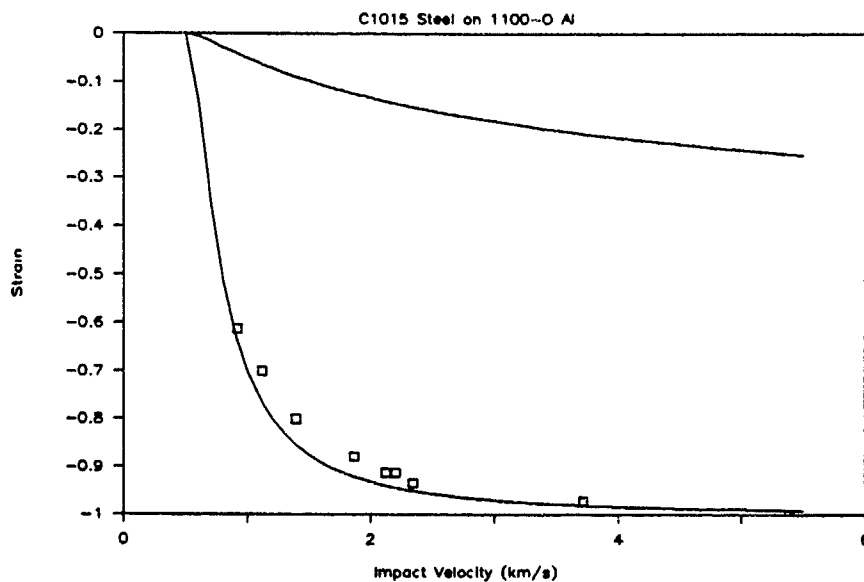


Figure 5a. Strain vs. Impact Velocity

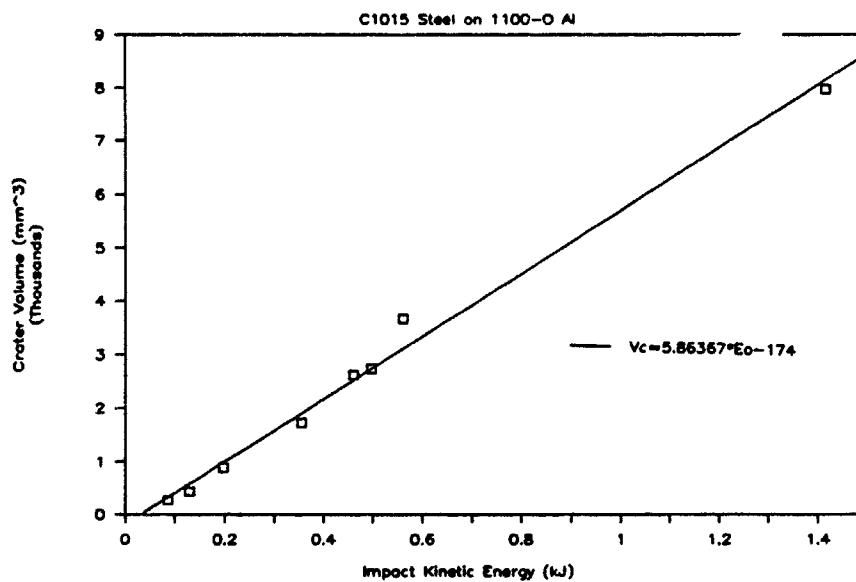


Figure 5b. Crater Volume vs. Impact Kinetic Energy

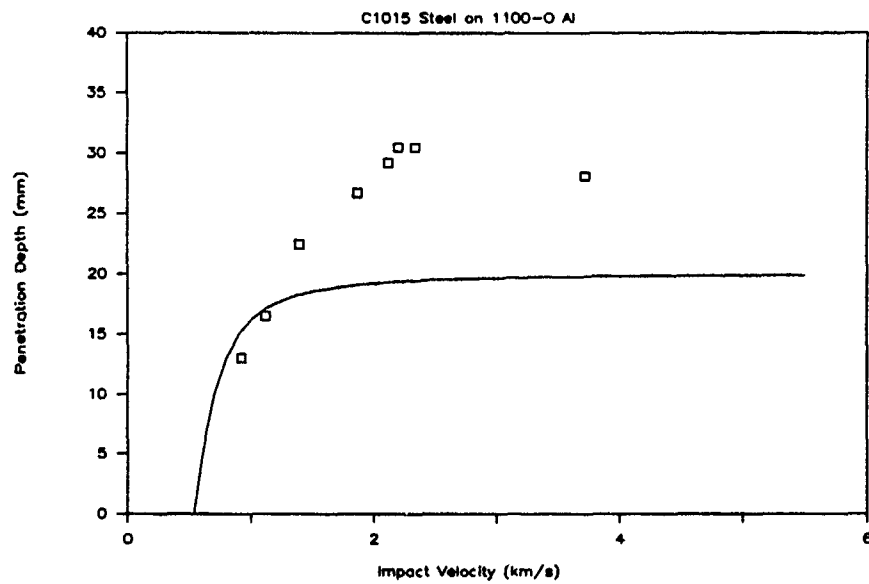


Figure 5c. Penetration Depth vs. Impact Velocity

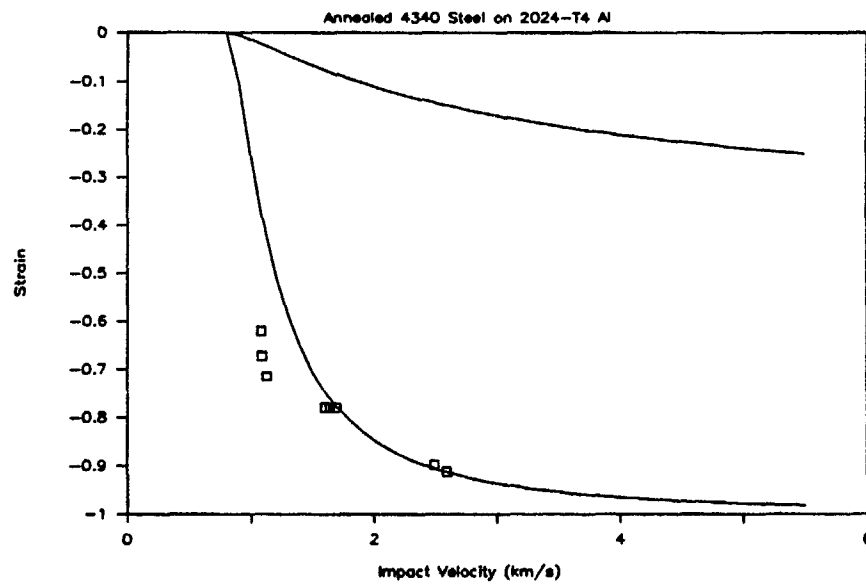


Figure 6a. Strain vs. Impact Velocity

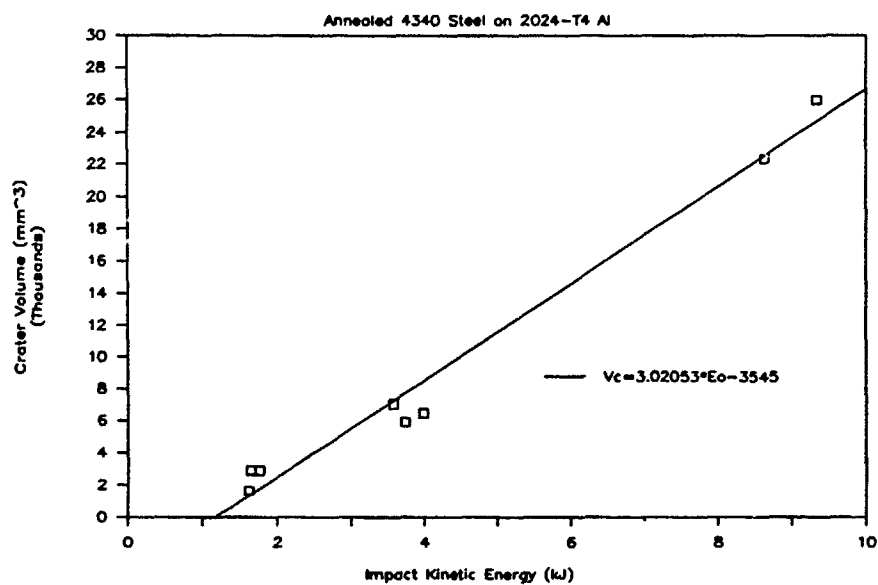


Figure 6b. Crater Volume vs. Impact Kinetic Energy

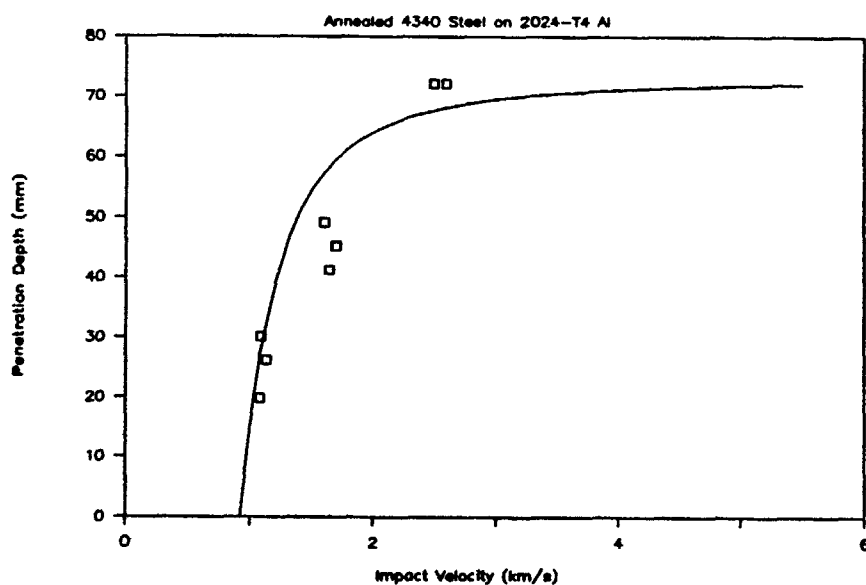


Figure 6c. Penetration Depth vs. Impact Velocity

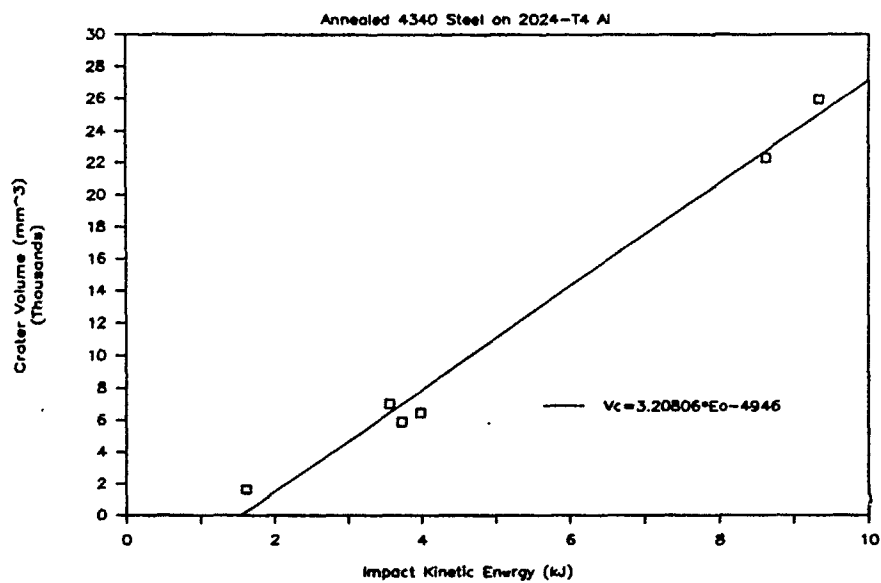


Figure 6d. Crater Volume vs. Impact Kinetic Energy

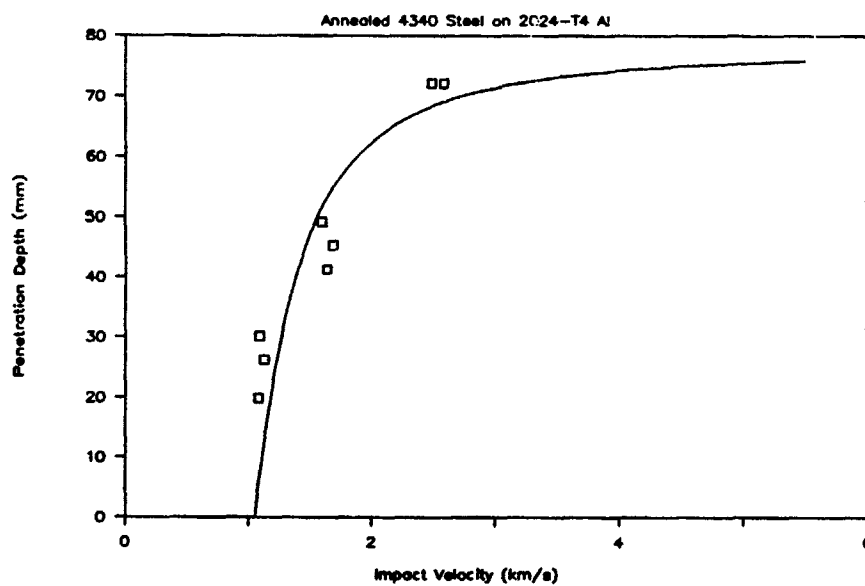


Figure 6e. Penetration Depth vs. Impact Velocity

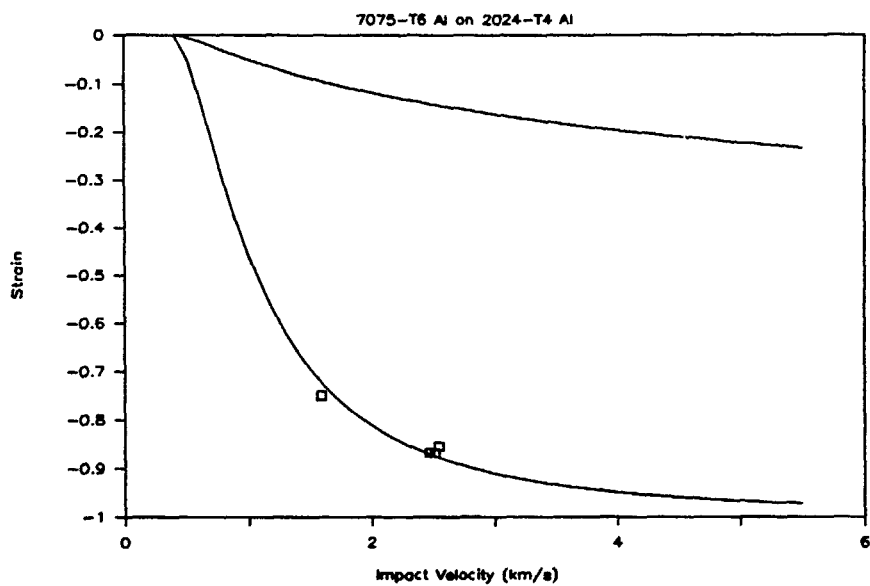


Figure 7a. Strain vs. Impact Velocity

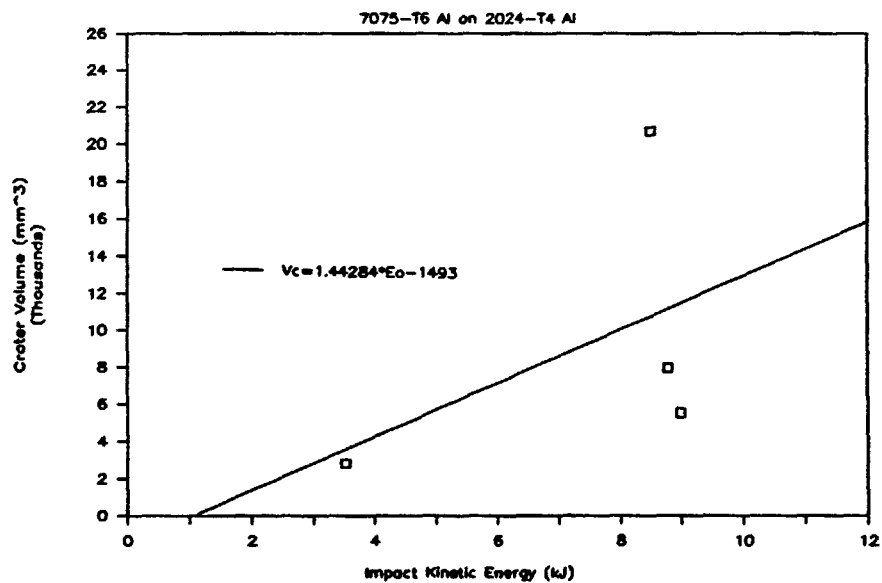


Figure 7b. Crater Volume vs. Impact Kinetic Energy

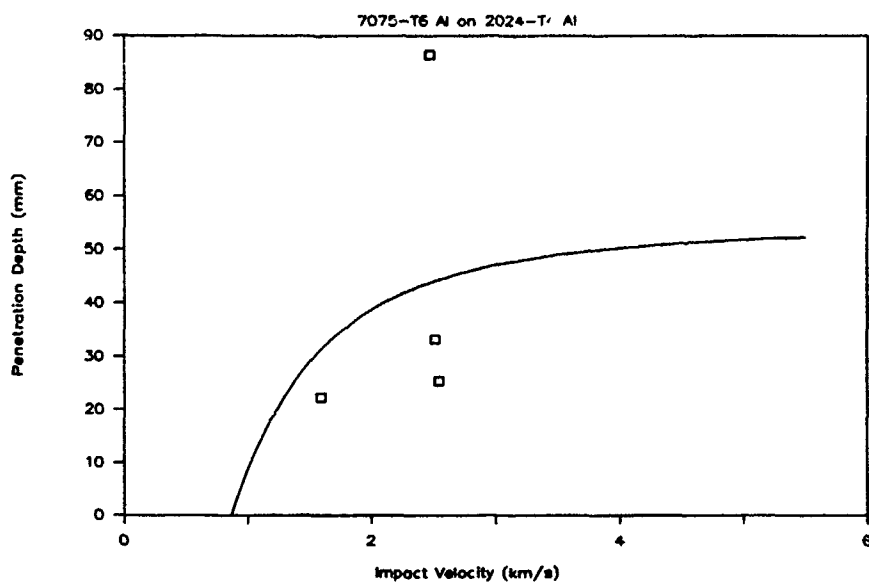


Figure 7c. Penetration Depth vs. Impact Velocity

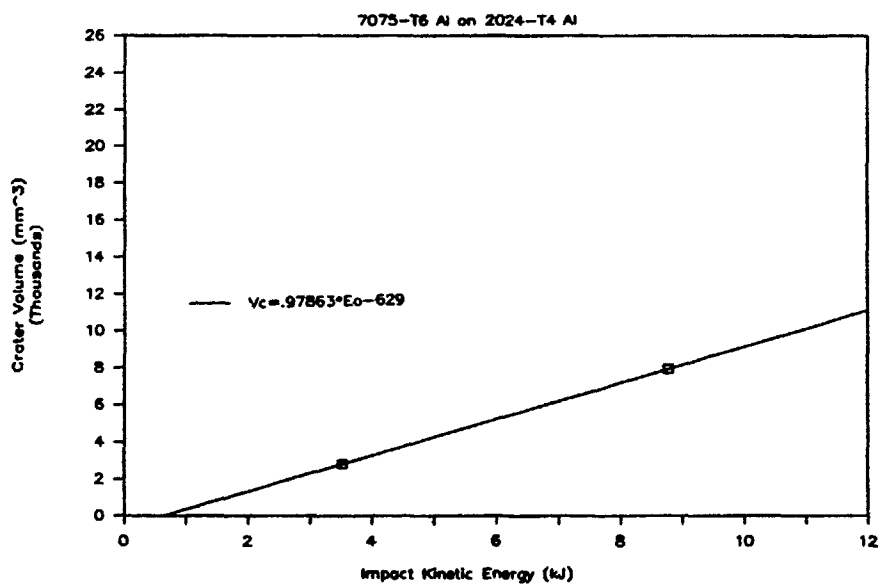


Figure 7d. Crater Volume vs. Impact Kinetic Energy

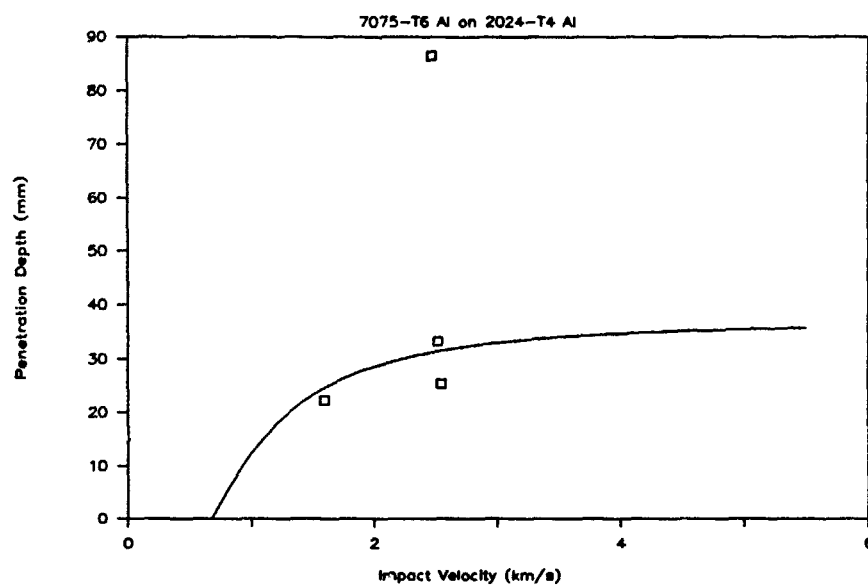


Figure 7e. Penetration Depth vs. Impact Velocity

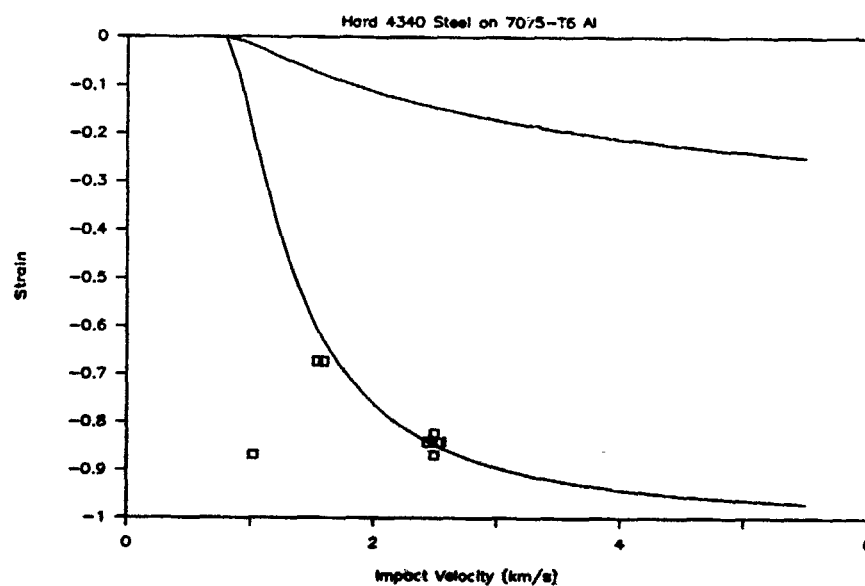


Figure 8a. Strain vs. Impact Velocity

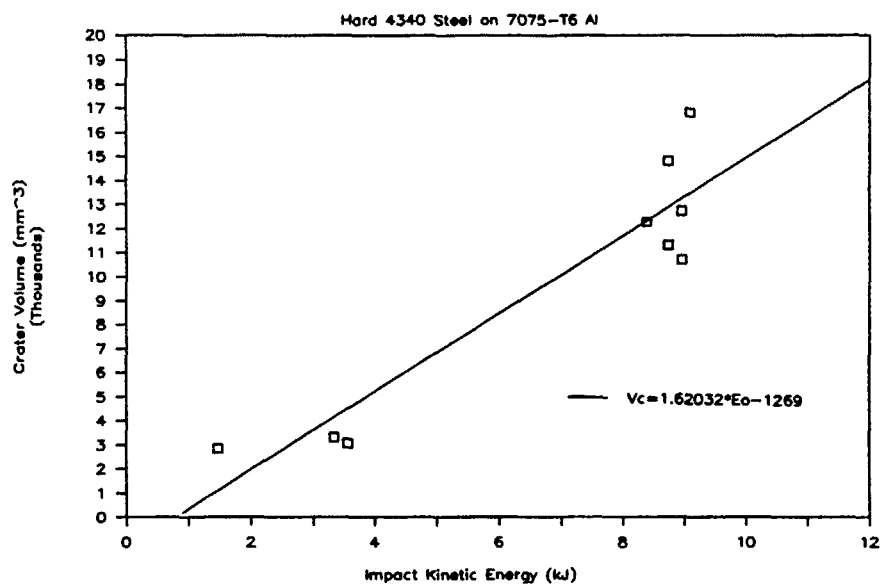


Figure 8b. Crater Volume vs. Impact Kinetic Energy

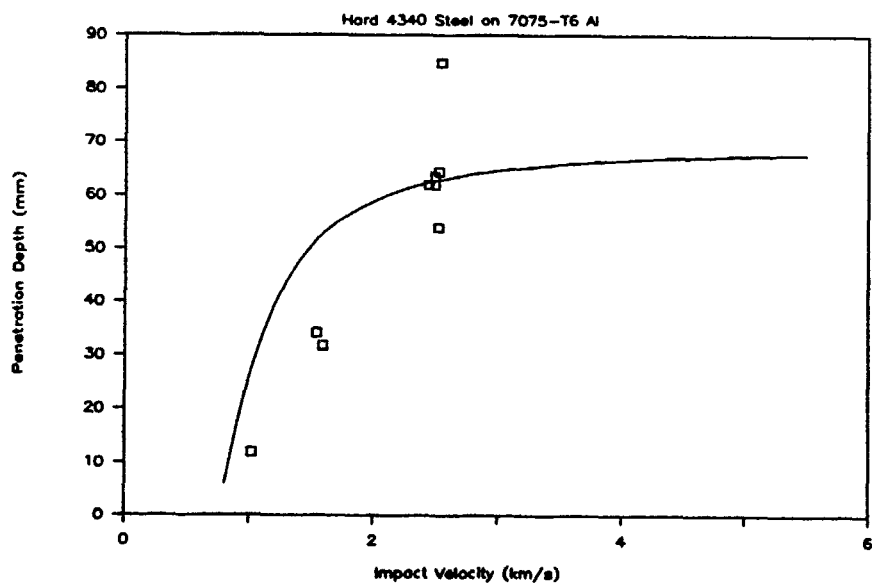


Figure 8c. Penetration Depth vs. Impact Velocity

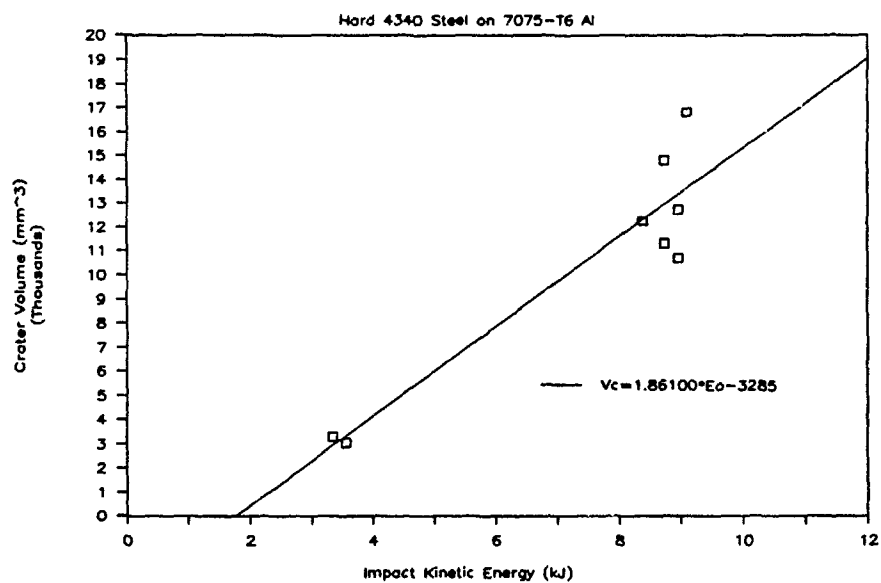


Figure 8d. Crater Volume vs. Impact Kinetic Energy

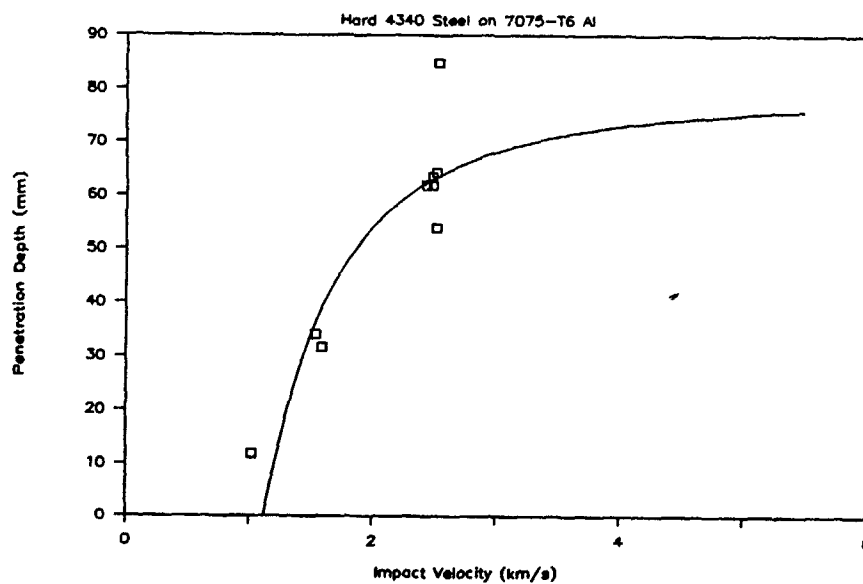


Figure 8e. Penetration Depth vs. Impact Velocity

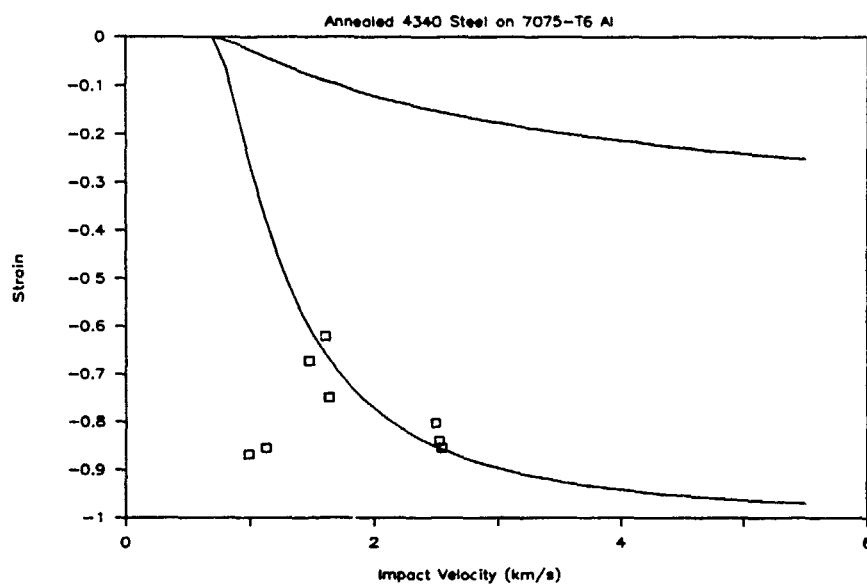


Figure 9a. Strain vs. Impact Velocity

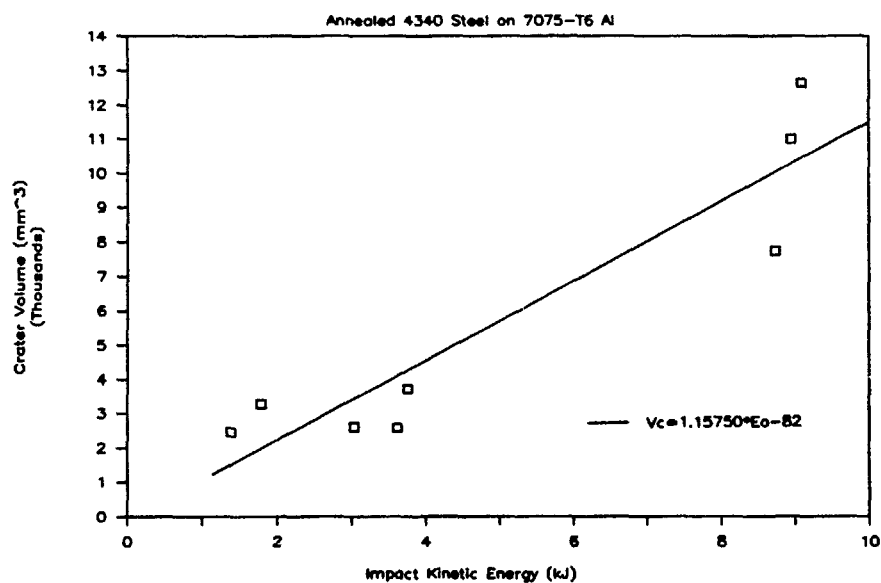


Figure 9b. Crater Volume vs. Impact Kinetic Energy

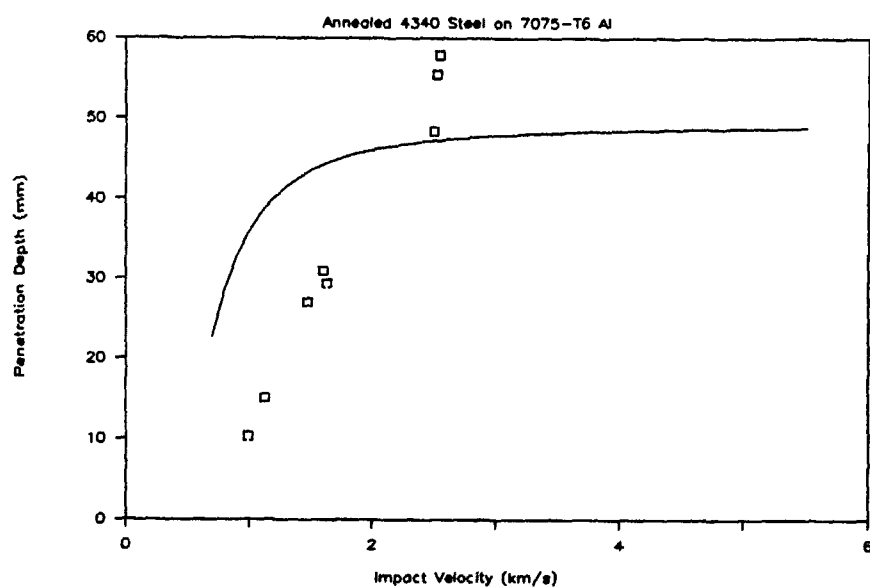


Figure 9c. Penetration Depth vs. Impact Velocity

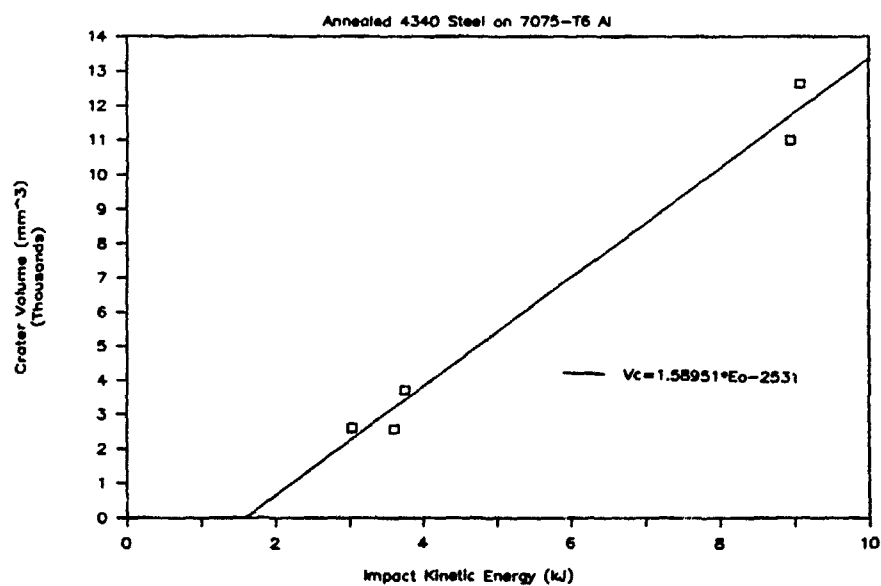


Figure 9d. Crater Volume vs. Impact Kinetic Energy

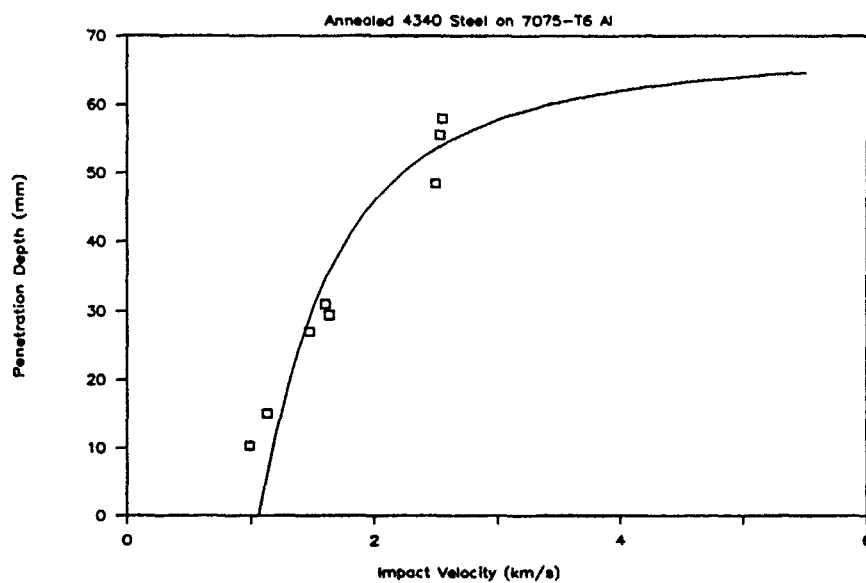


Figure 9e. Penetration Depth vs. Impact Velocity

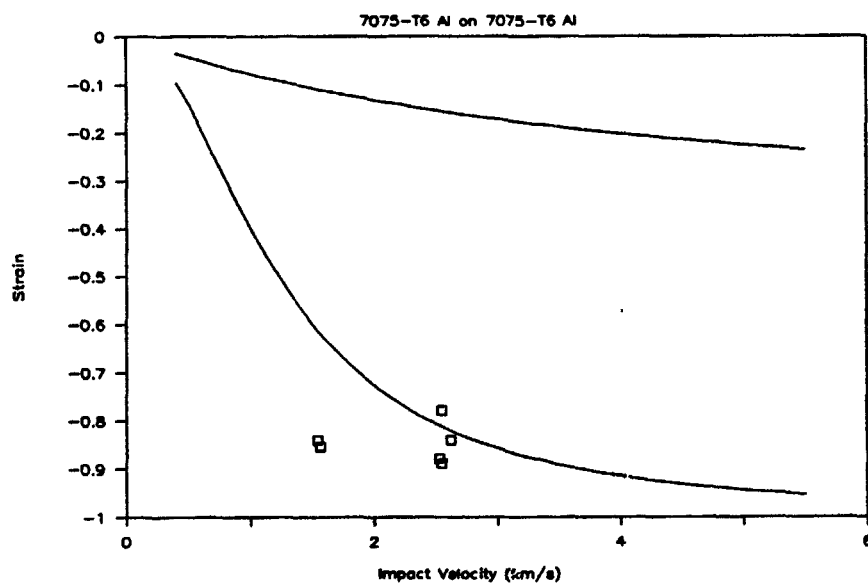


Figure 10a. Strain vs. Impact Velocity

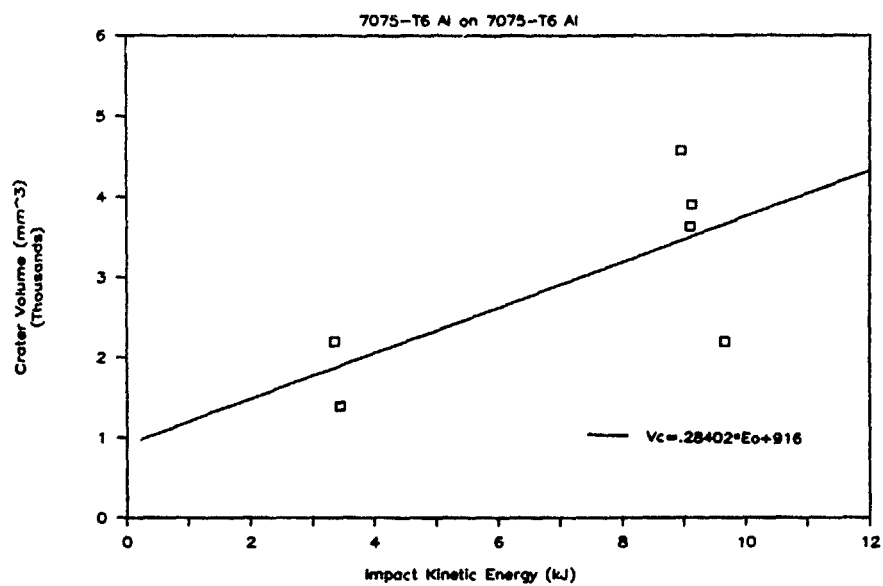


Figure 10b. Crater Volume vs. Impact Kinetic Energy

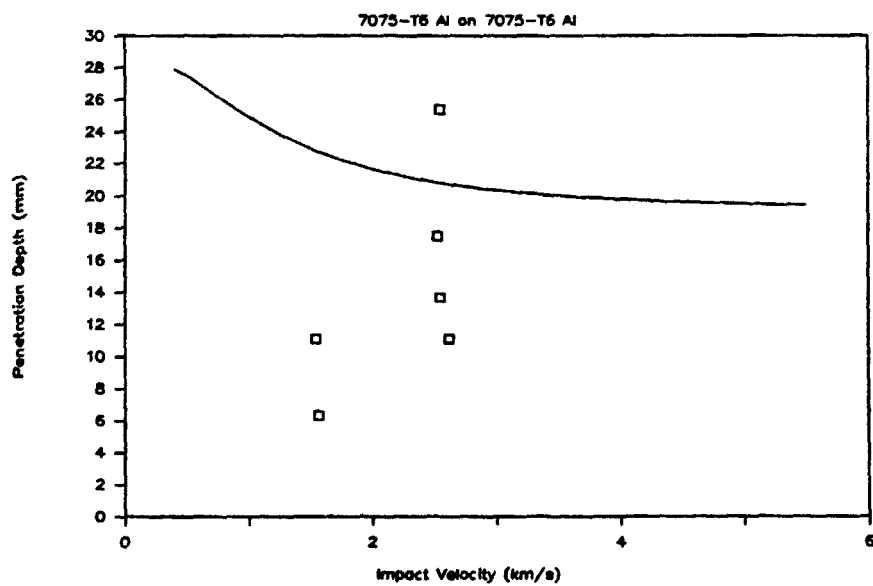


Figure 10c. Penetration Depth vs. Impact Velocity

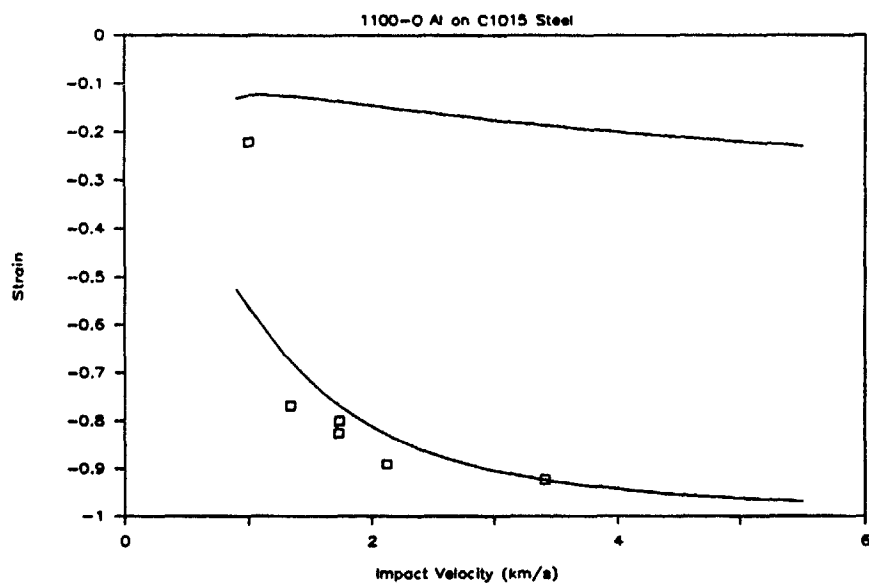


Figure 11a. Strain vs. Impact Velocity

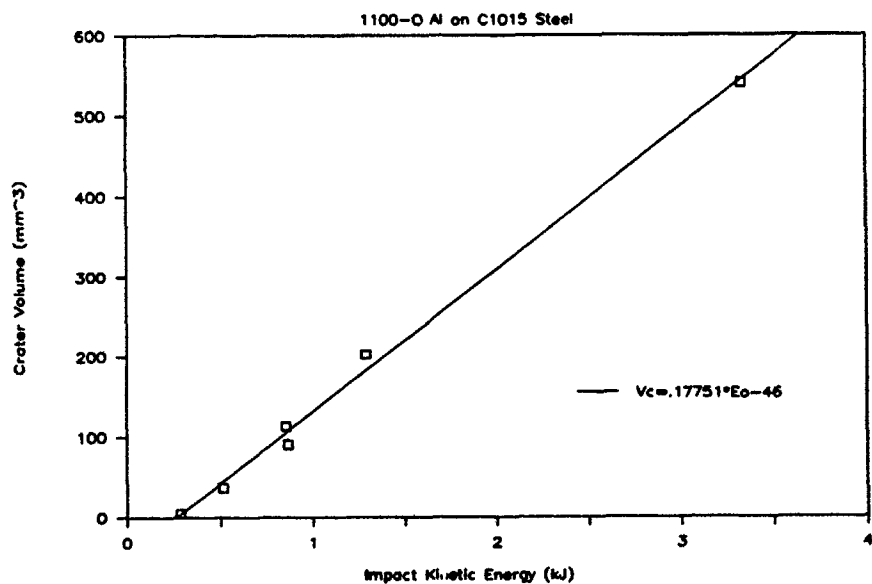


Figure 11b. Crater Volume vs. Impact Kinetic Energy

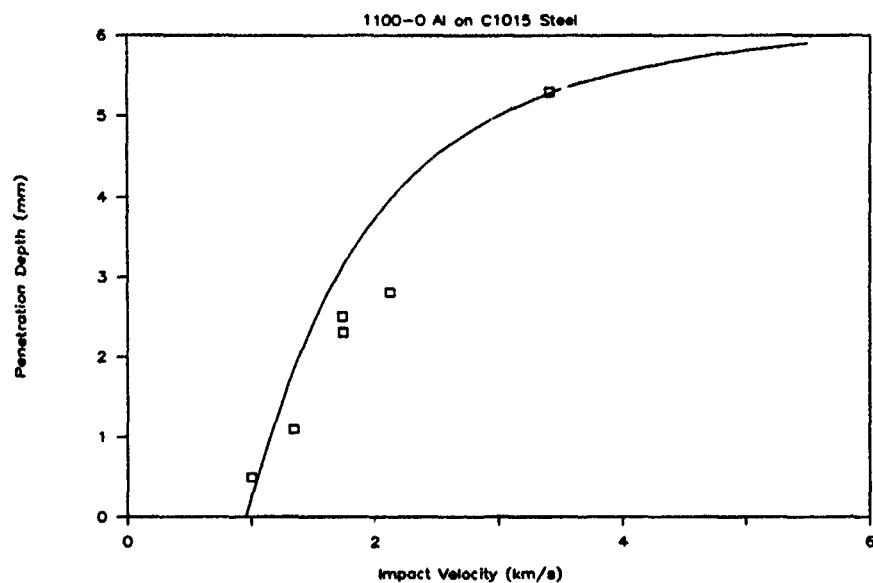


Figure 11c. Penetration Depth vs. Impact Velocity

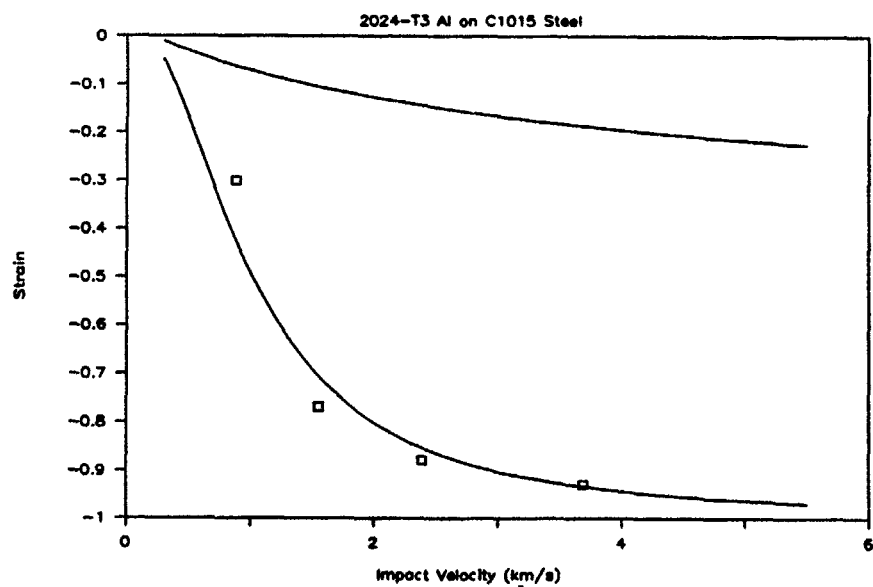


Figure 12a. Strain vs. Impact Velocity

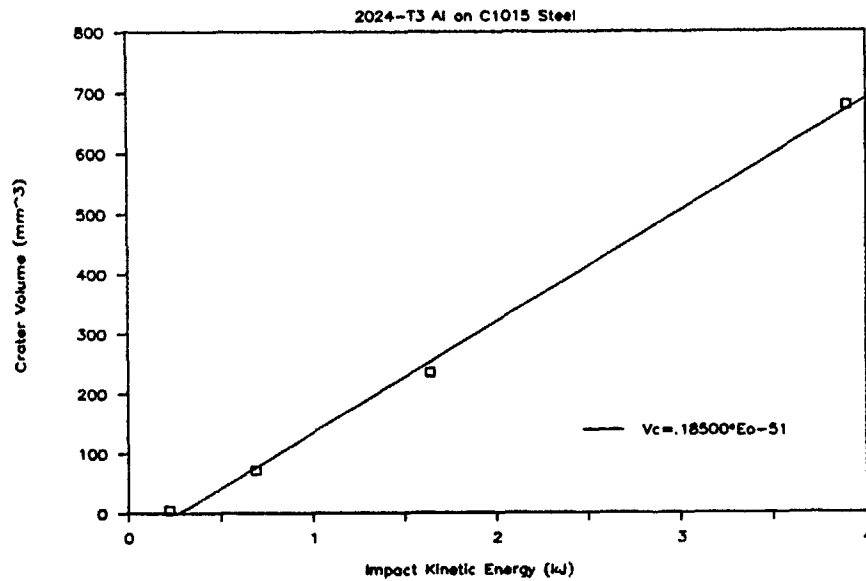


Figure 12b. Crater Volume vs. Impact Kinetic Energy

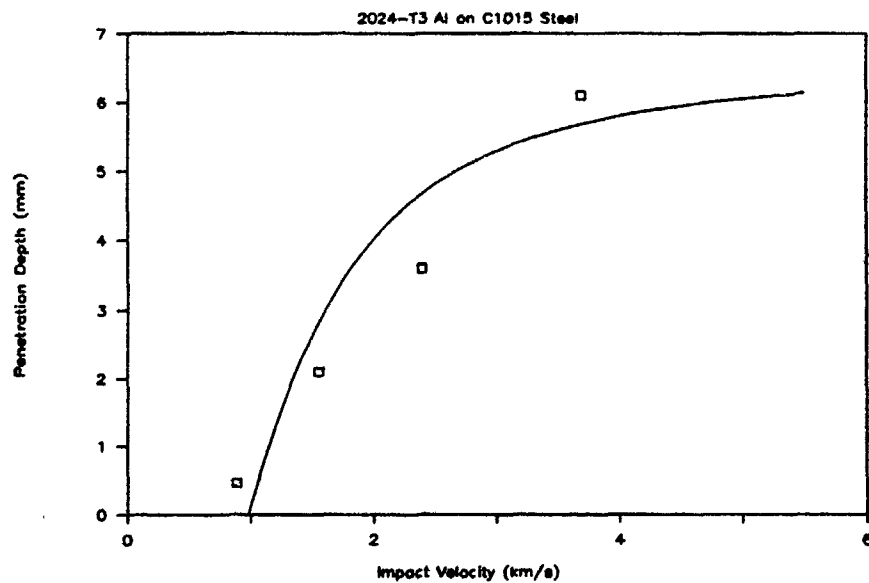


Figure 12c. Penetration Depth vs. Impact Velocity

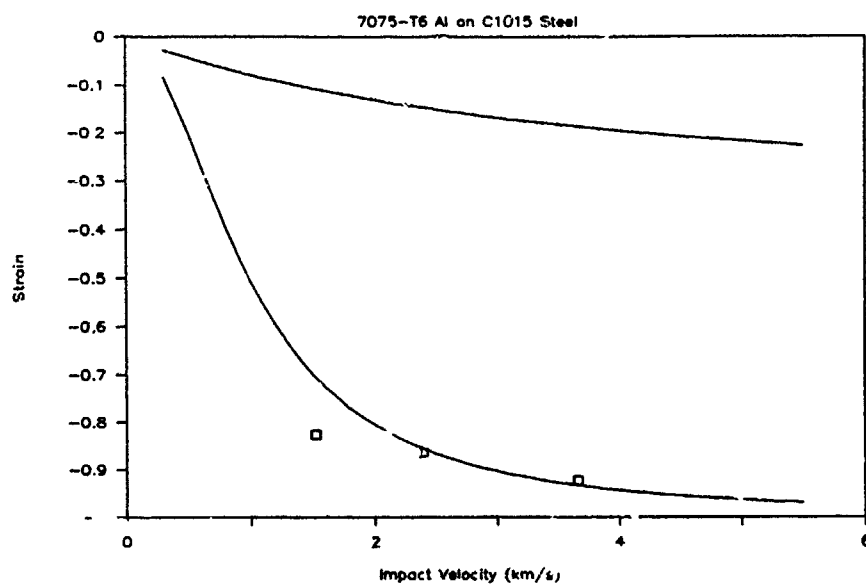


Figure 13a. Strain vs. Impact Velocity

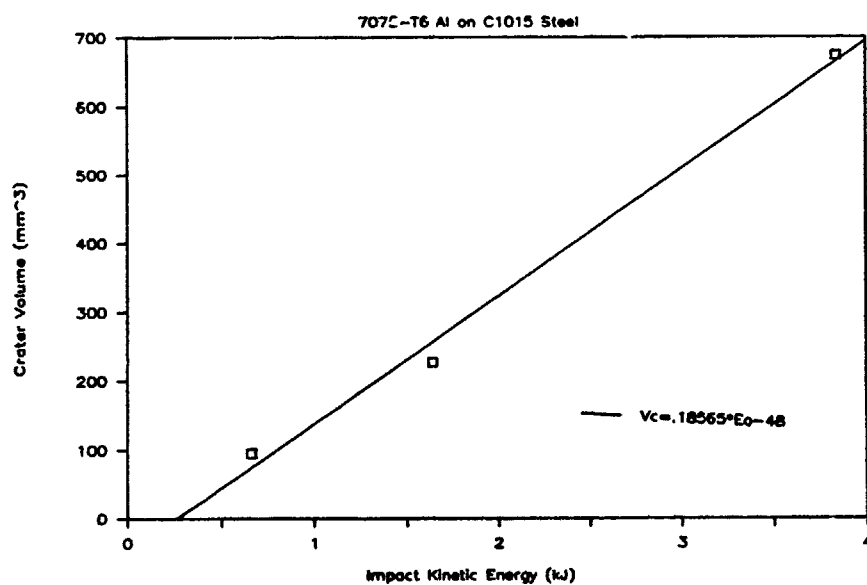


Figure 13b. Crater Volume vs. Impact Kinetic Energy

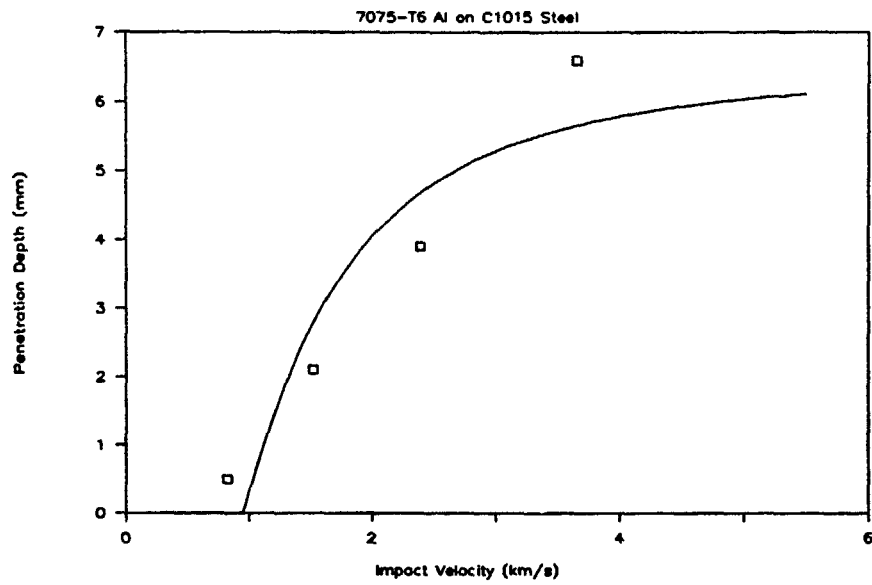


Figure 13c. Penetration Depth vs. Impact Velocity

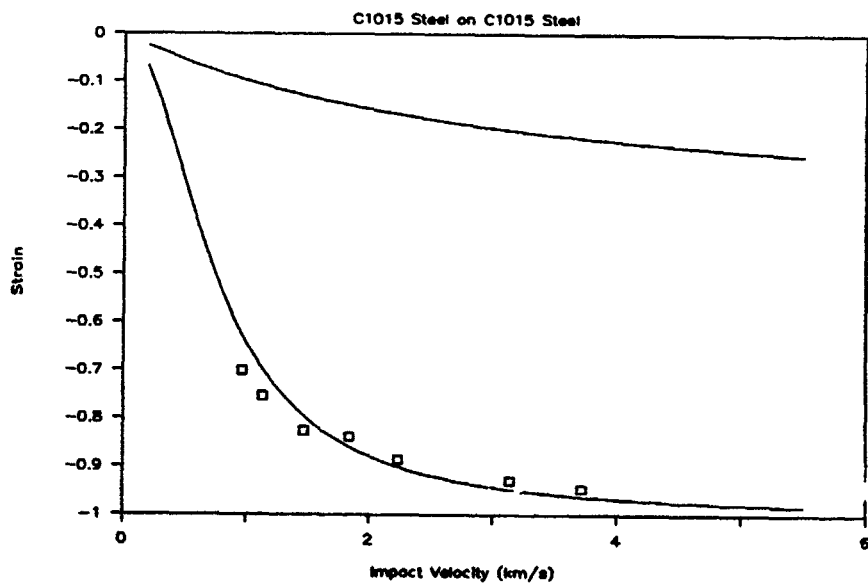


Figure 14a. Strain vs. Impact Velocity

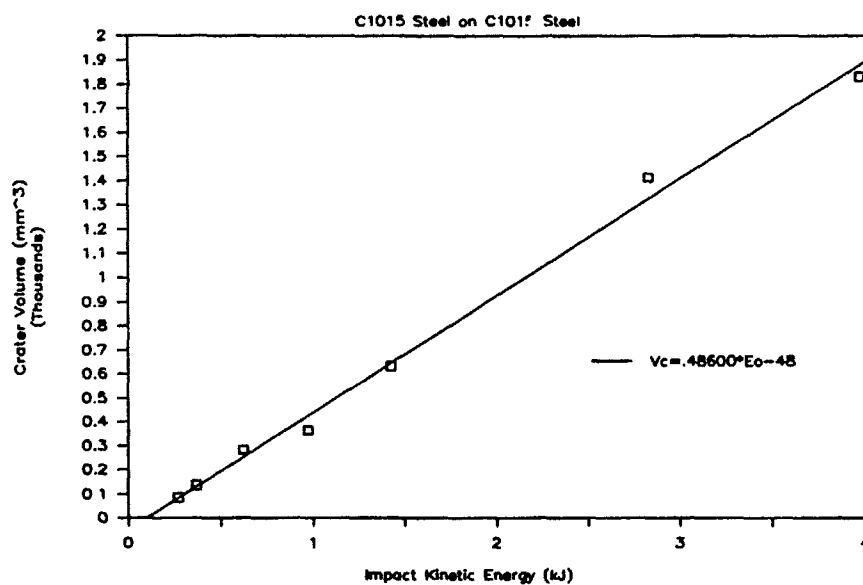


Figure 14b. Crater Volume vs. Impact Kinetic Energy

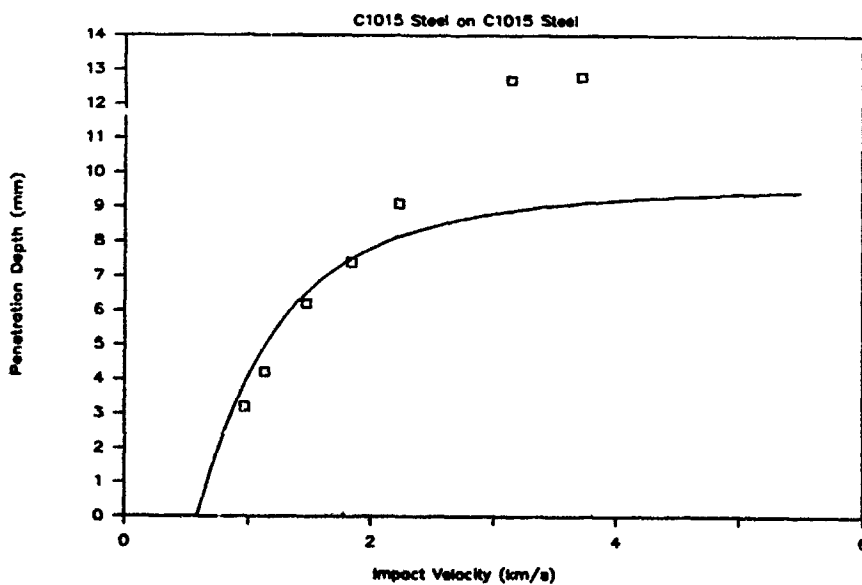


Figure 14c. Penetration Depth vs. Impact Velocity

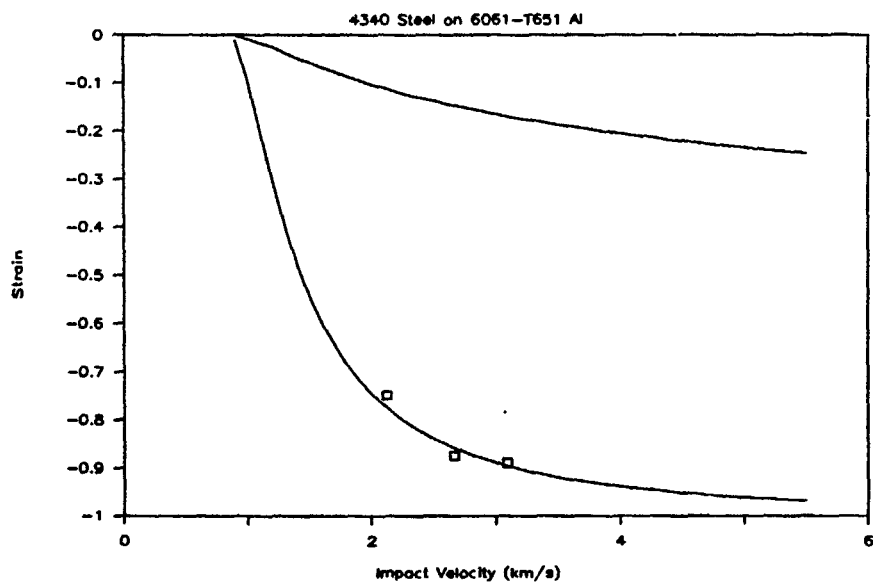


Figure 15a. Strain vs. Impact Velocity

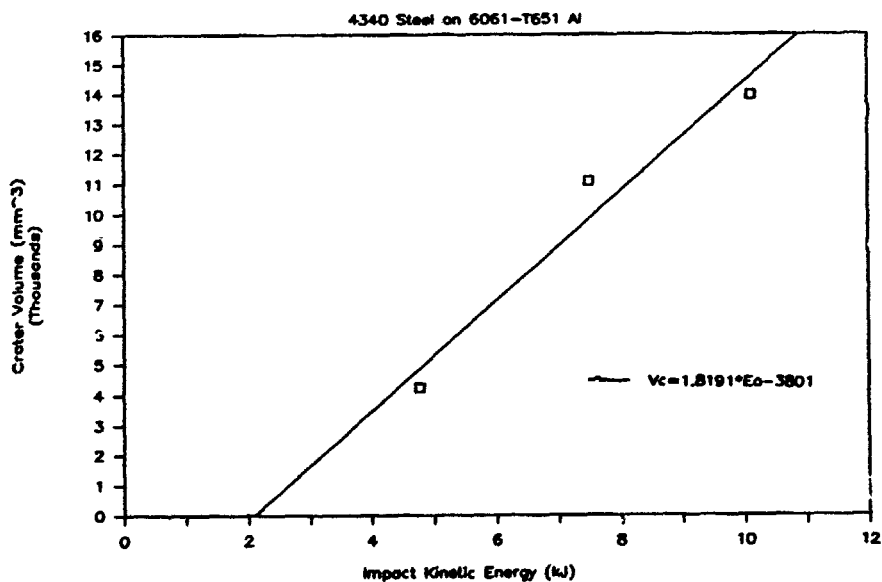


Figure 15b. Crater Volume vs. Impact Kinetic Energy

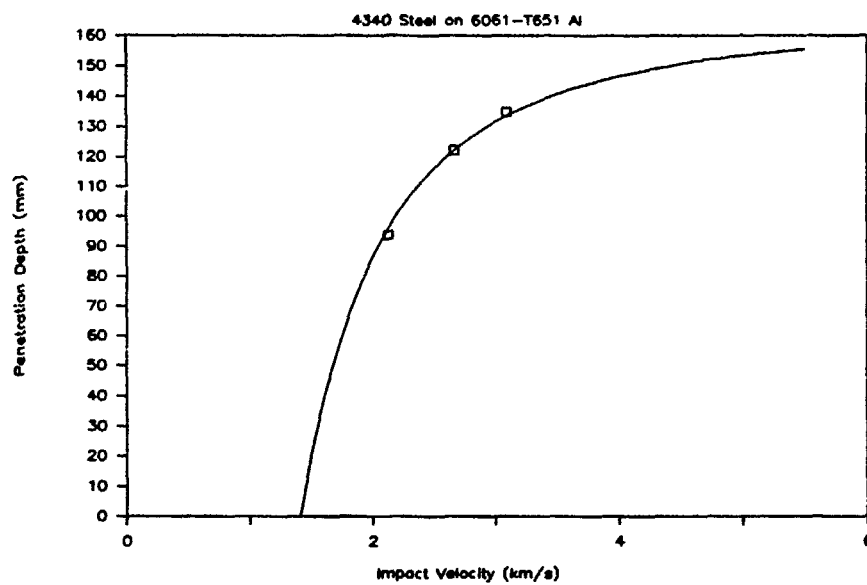


Figure 15c. Penetration Depth vs. Impact Velocity

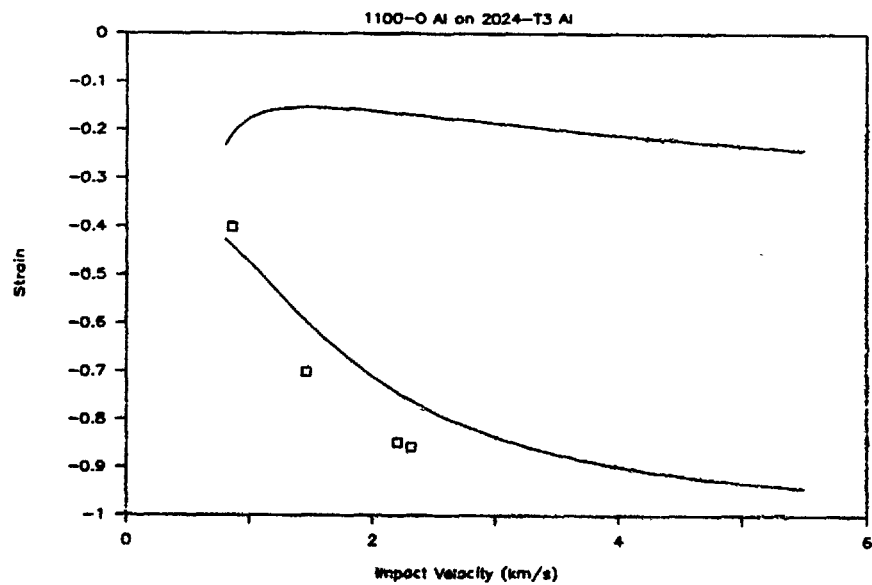


Figure 16a. Strain vs. Impact Velocity

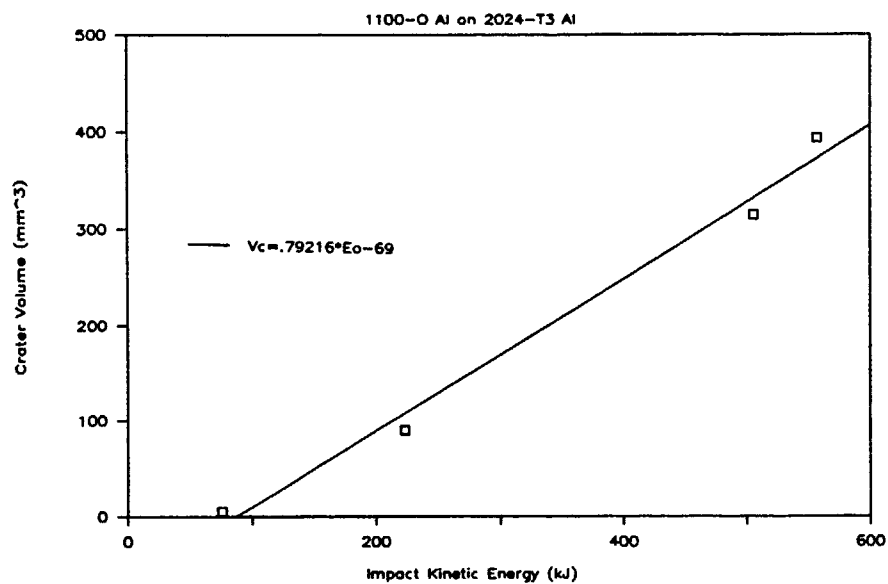


Figure 16b. Crater Volume vs. Impact Kinetic Energy

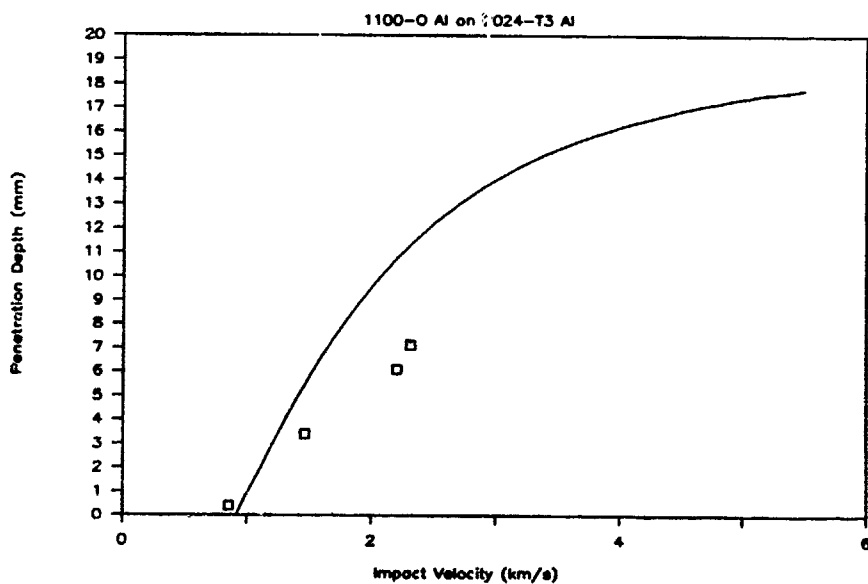


Figure 16c. Penetration Depth vs. Impact Velocity

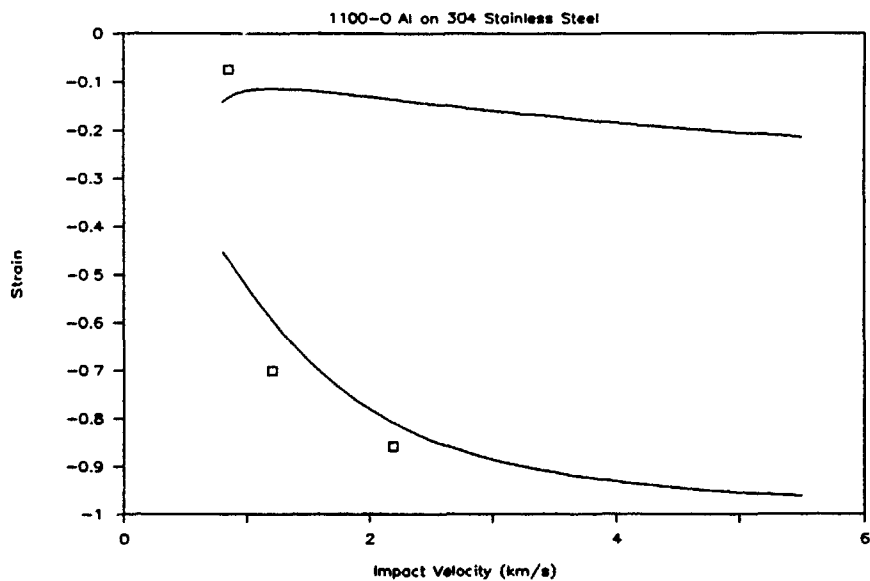


Figure 17a. Strain vs. Impact Velocity

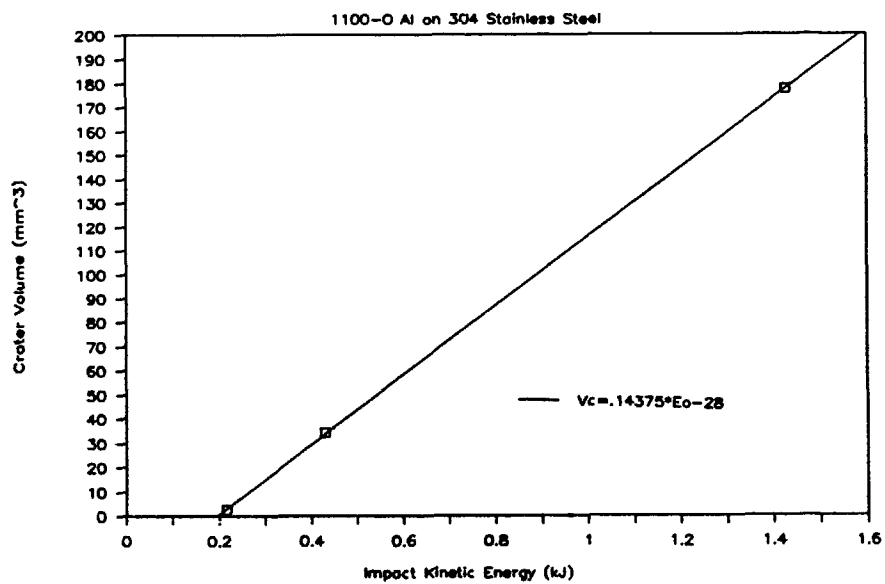


Figure 17b. Crater Volume vs. Impact Kinetic Energy

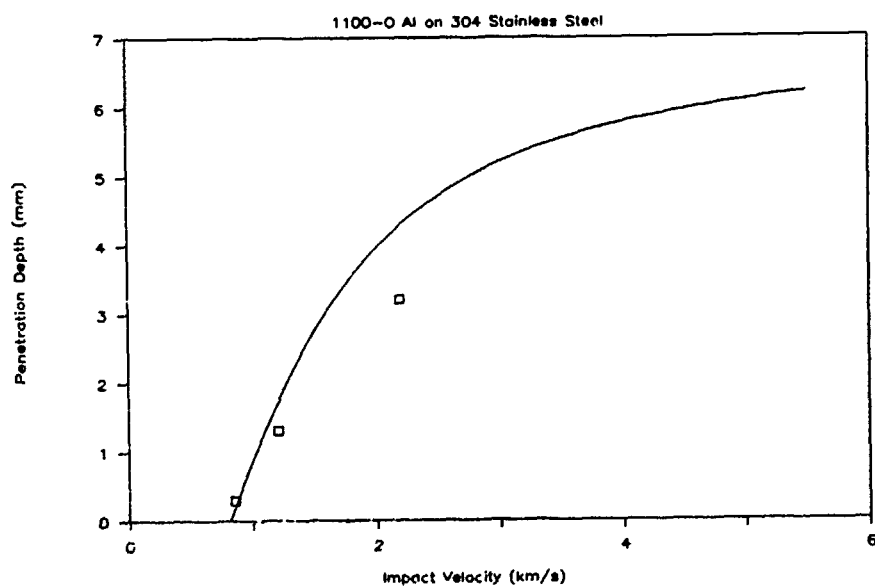


Figure 17c. Penetration Depth vs. Impact Velocity

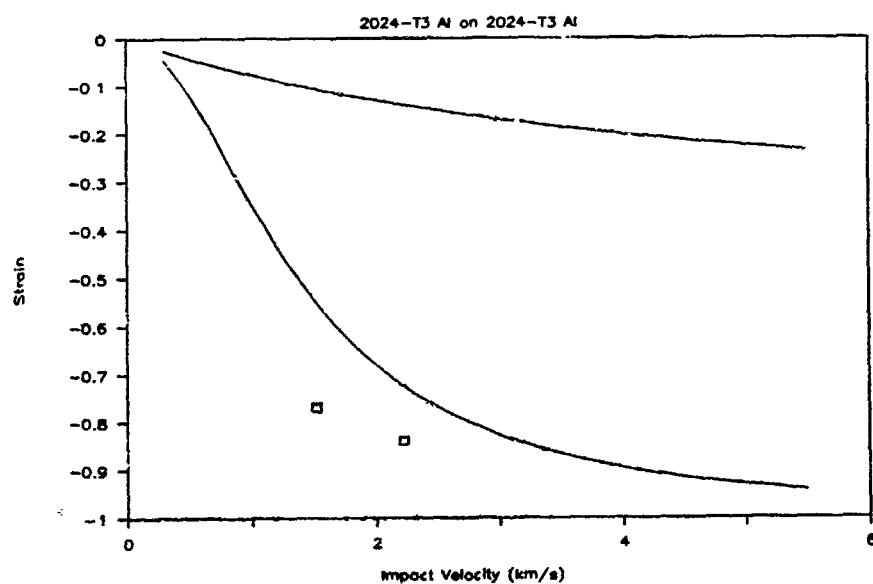


Figure 18a. Strain vs. Impact Velocity

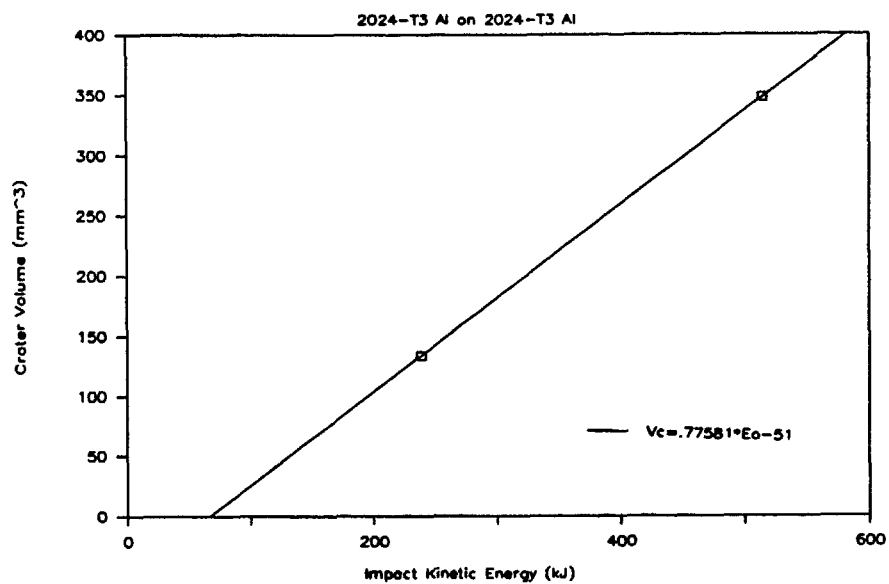


Figure 18b. Crater Volume vs. Impact Kinetic Energy

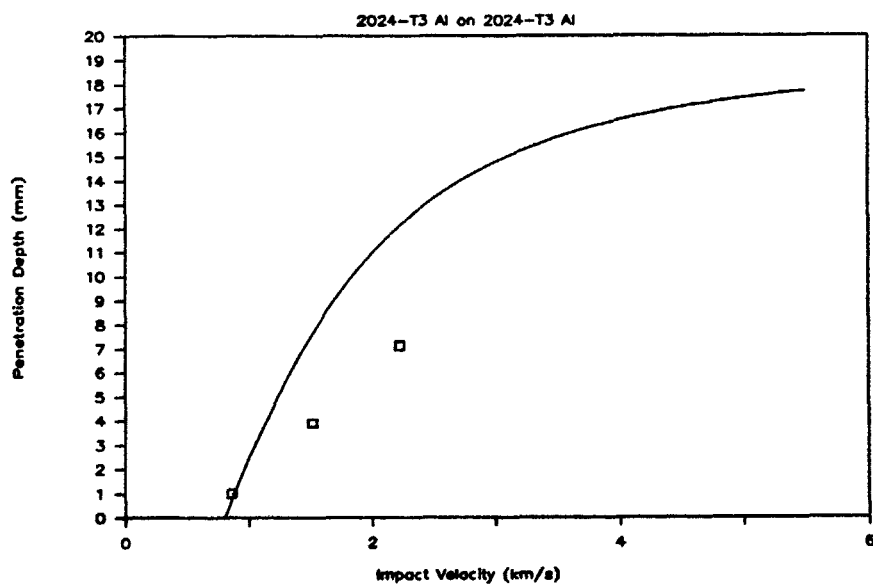


Figure 18c. Penetration Depth vs. Impact Velocity

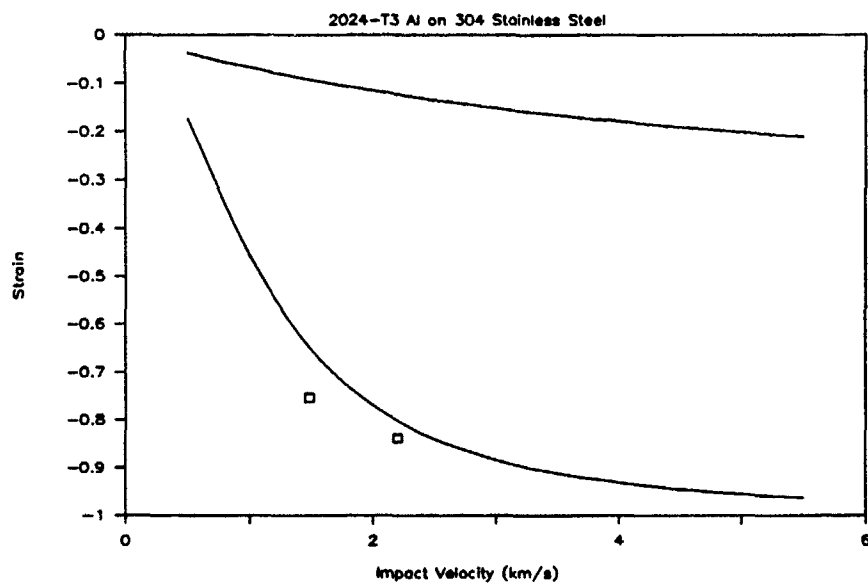


Figure 19a. Strain vs. Impact Velocity

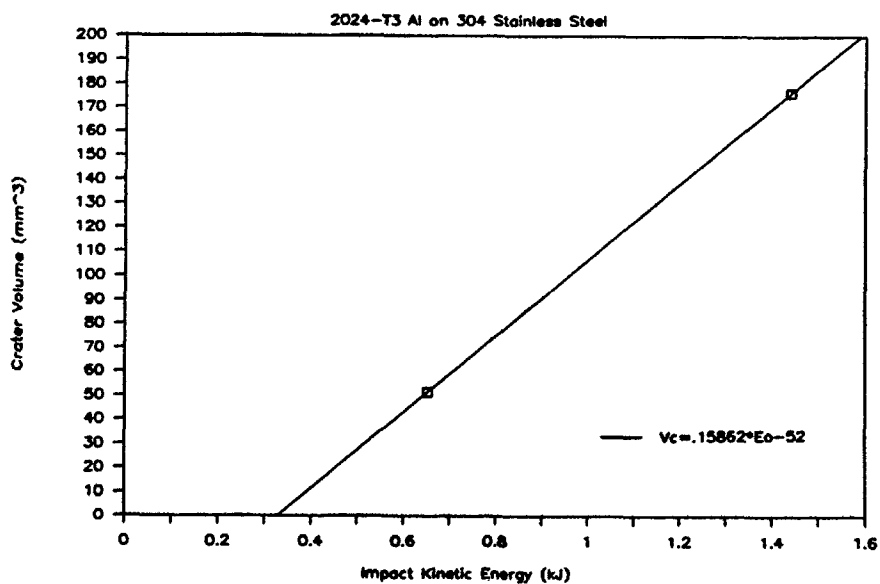


Figure 19b. Crater Volume vs. Impact Kinetic Energy

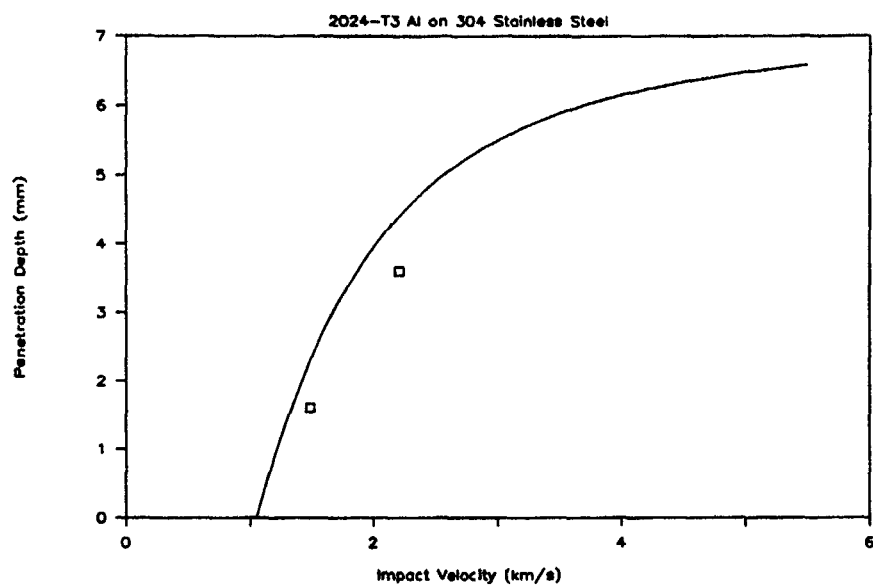


Figure 19c. Penetration Depth vs. Impact Velocity

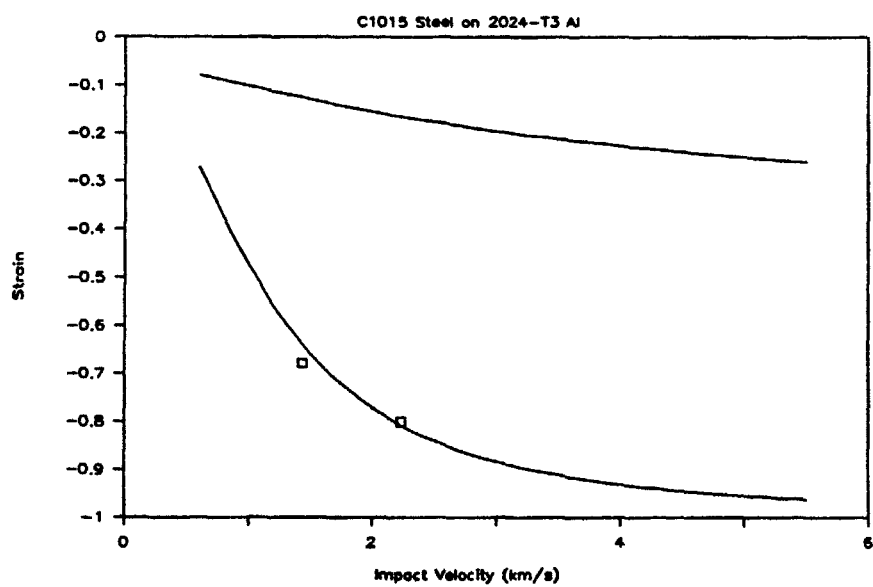


Figure 20a. Strain vs. Impact Velocity

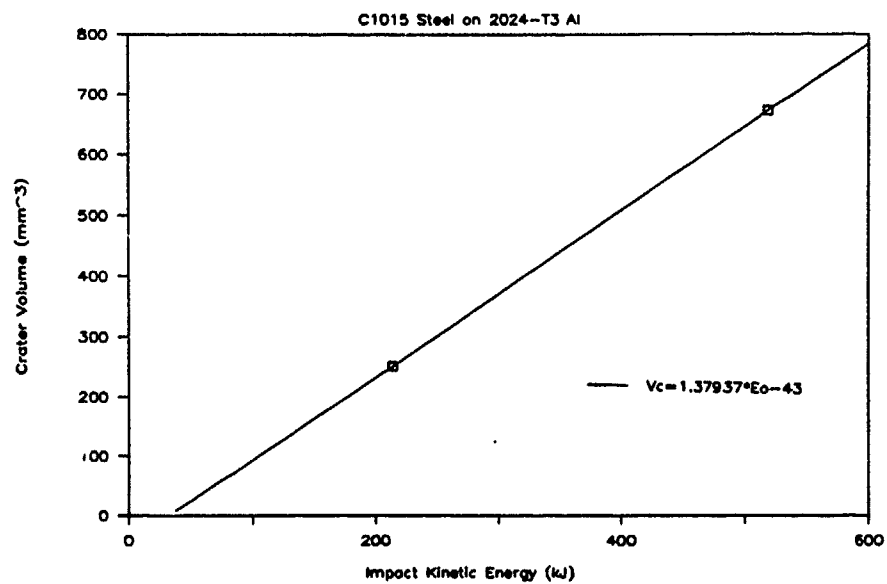


Figure 20b. Crater Volume vs. Impact Kinetic Energy

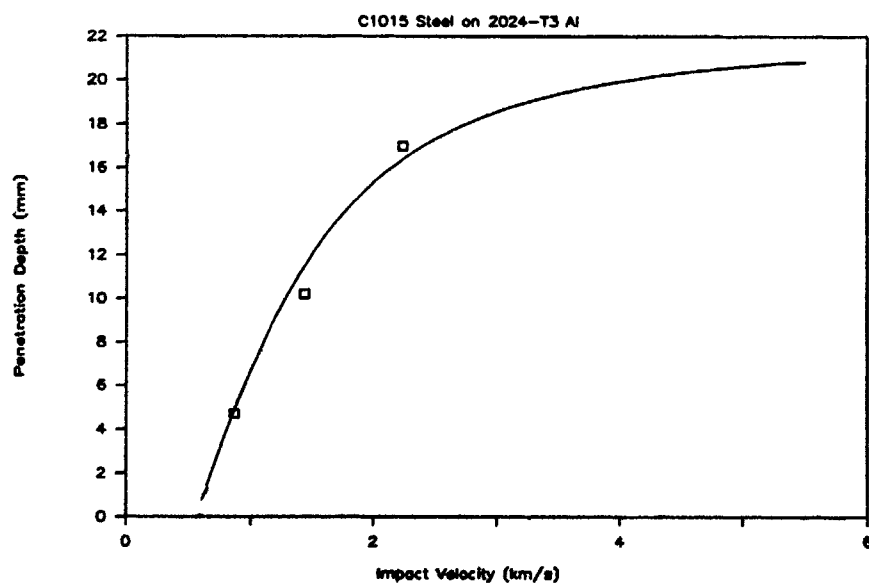


Figure 20c. Penetration Depth vs. Impact Velocity

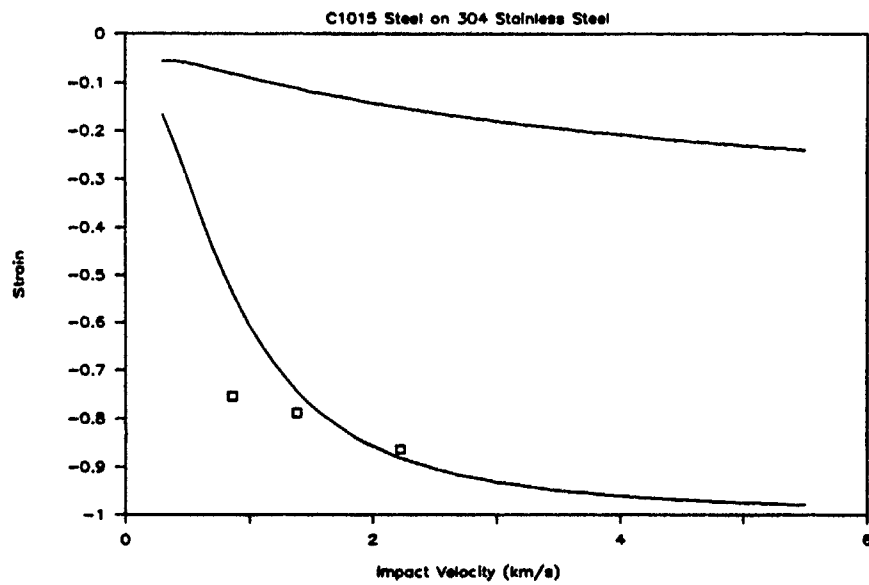


Figure 21a. Strain vs. Impact Velocity

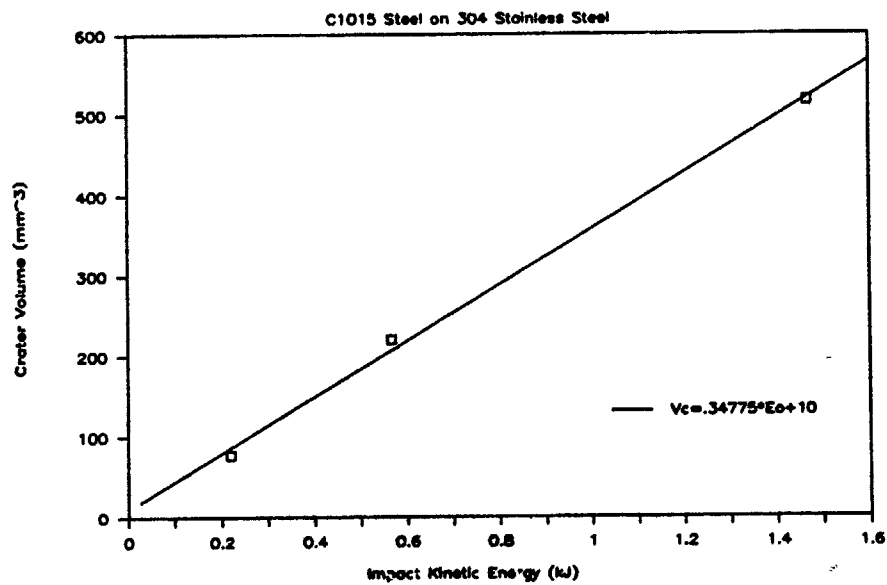


Figure 21b. Crater Volume vs. Impact Kinetic Energy

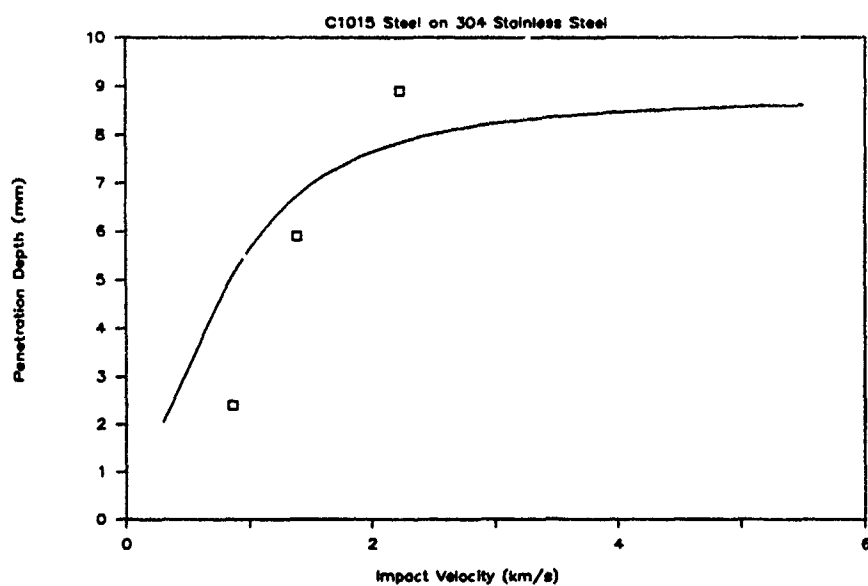


Figure 21c. Penetration Depth vs. Impact Velocity

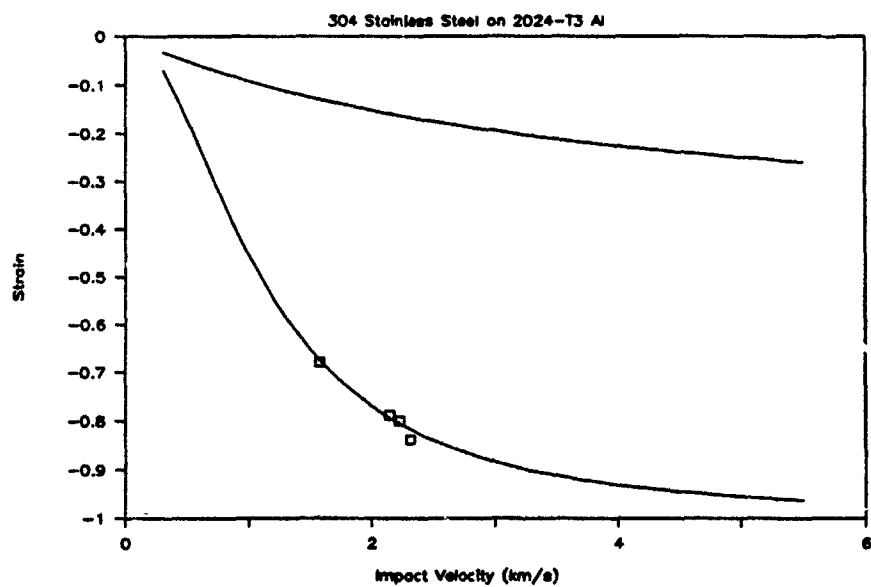


Figure 22a. Strain vs. Impact Velocity

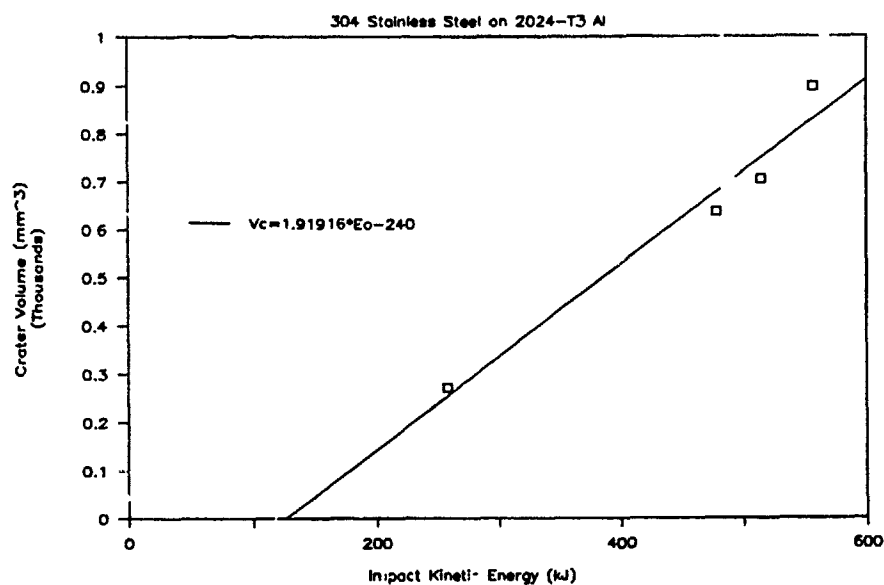


Figure 22b. Crater Volume vs. Impact Kinetic Energy

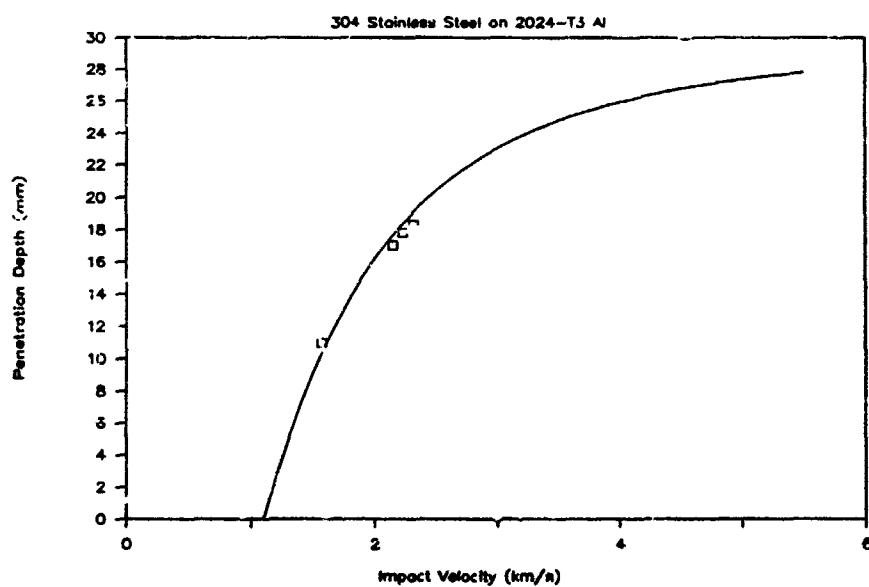


Figure 22c. Penetration Depth vs. Impact Velocity

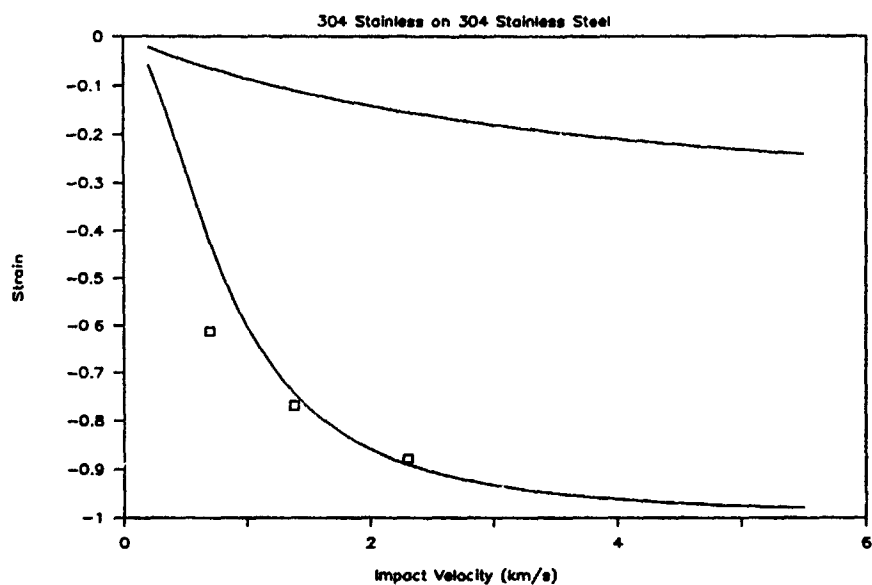


Figure 23a. Strain vs. Impact Velocity

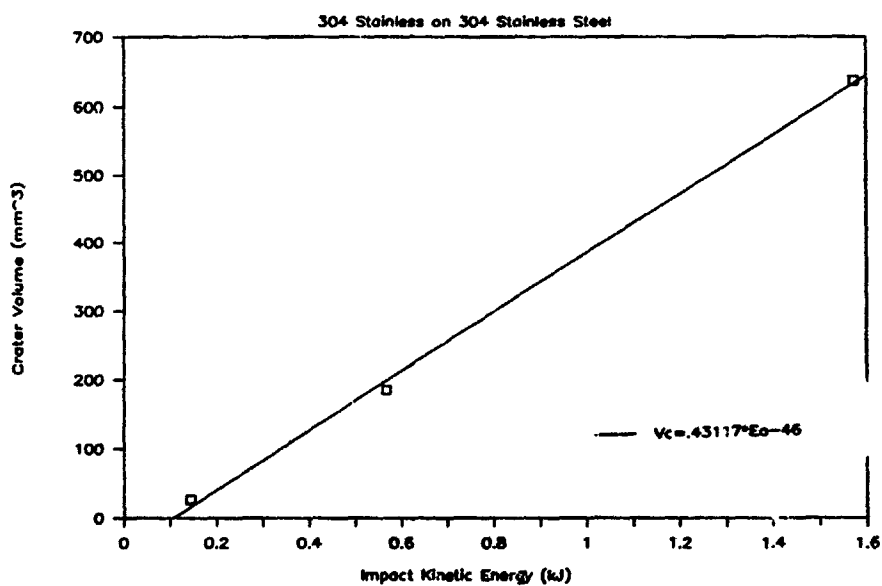


Figure 23b. Crater Volume vs. Impact Kinetic Energy

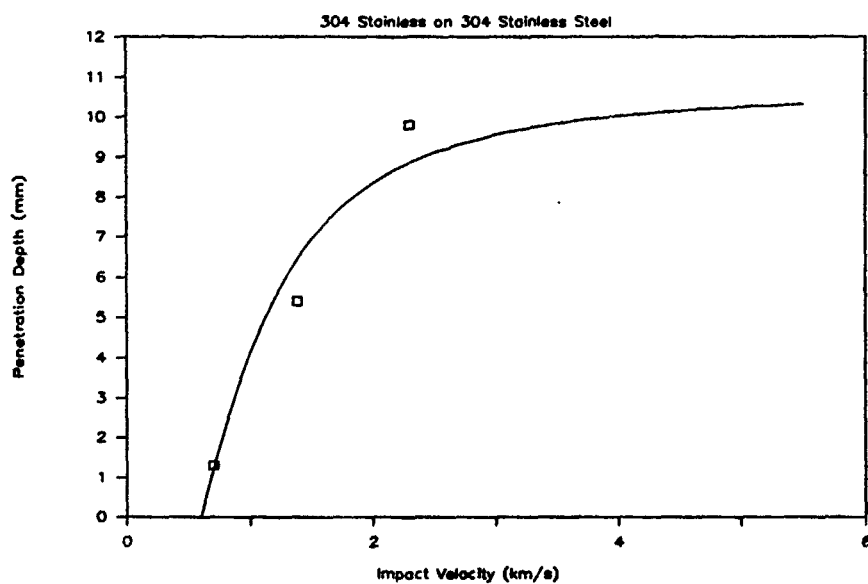


Figure 23c. Penetration Depth vs. Impact Velocity

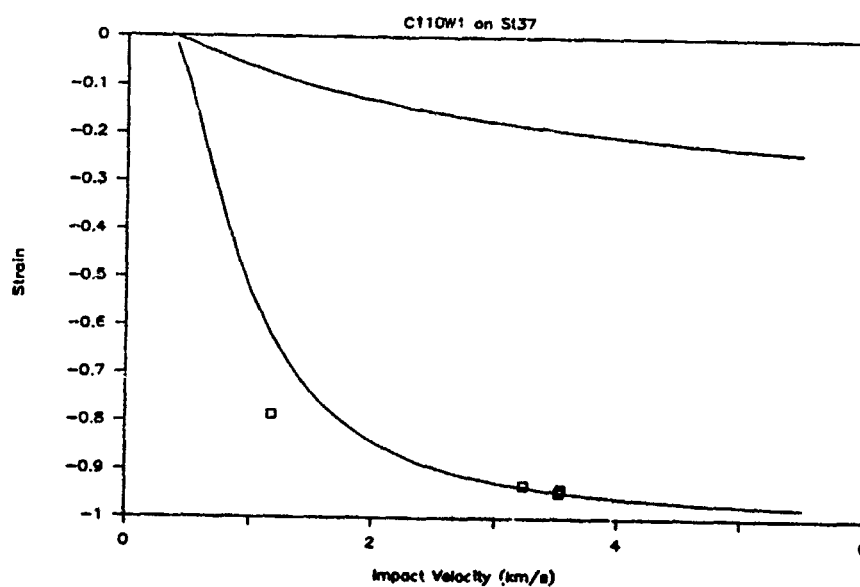


Figure 24a. Strain vs. Impact Velocity

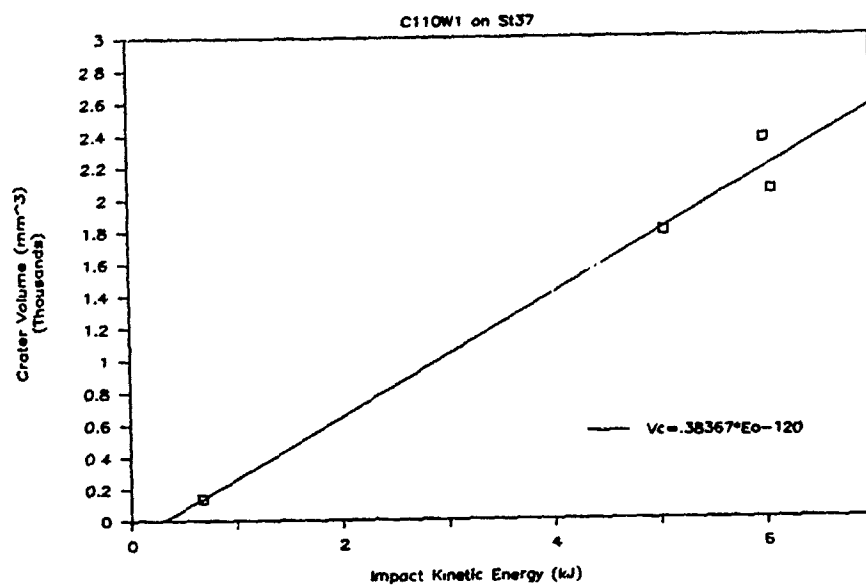


Figure 24b. Crater Volume vs. Impact Kinetic Energy

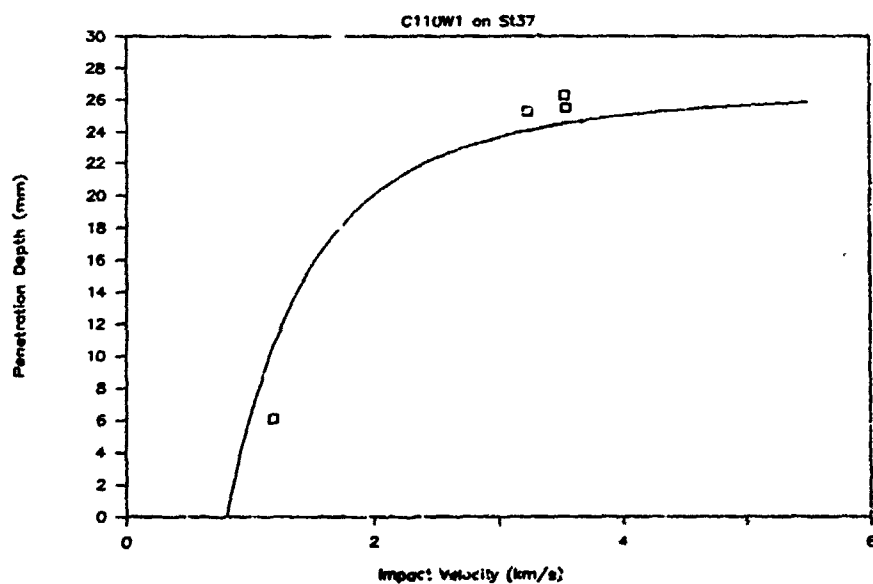


Figure 24c. Penetration Depth vs. Impact Velocity

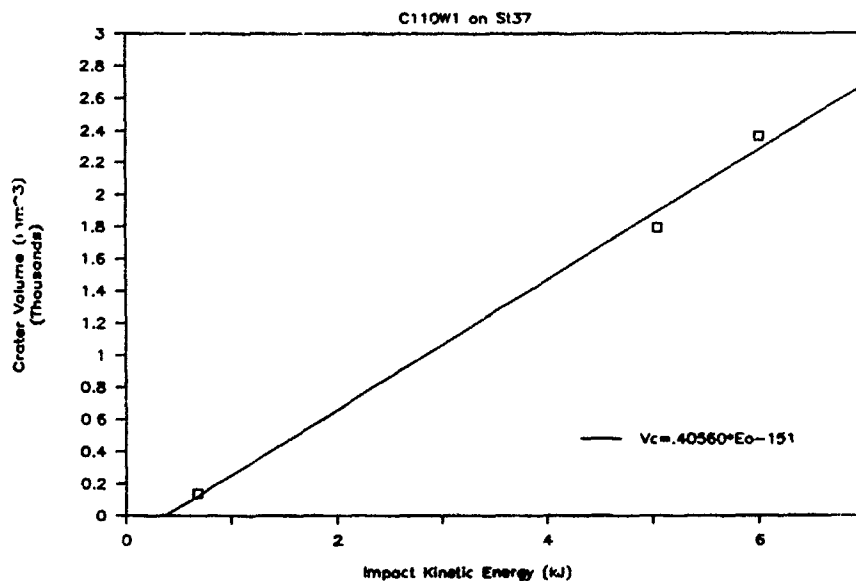


Figure 24d. Crater Volume vs. Impact Kinetic Energy

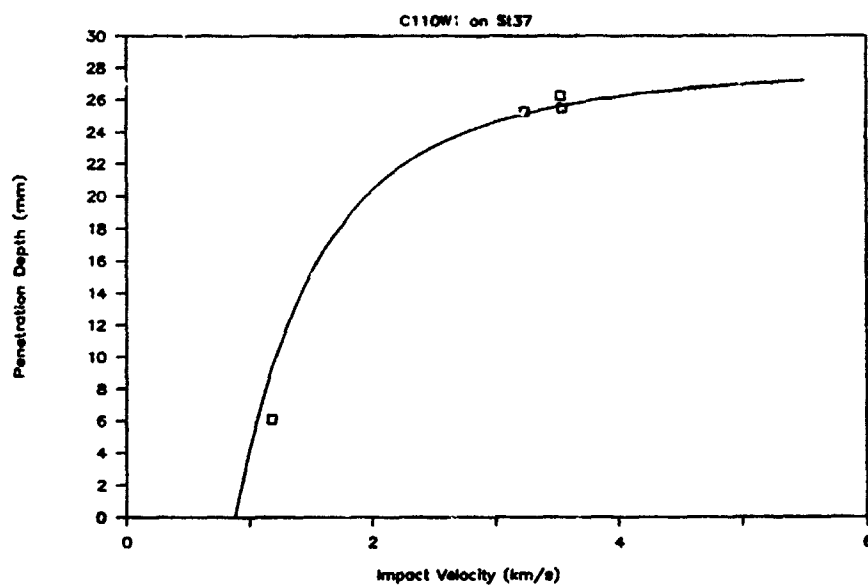


Figure 24e. Penetration Depth vs. Impact Velocity

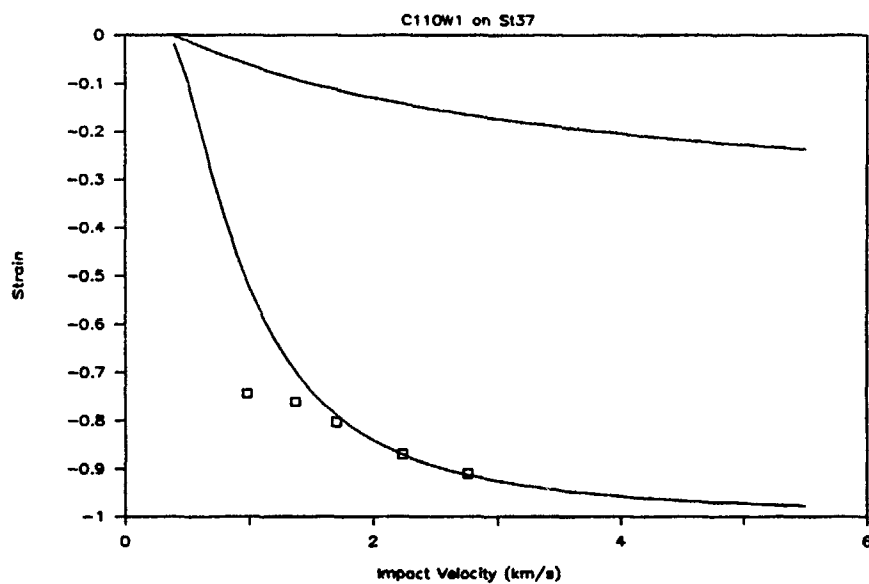


Figure 25a. Strain vs. Impact Velocity

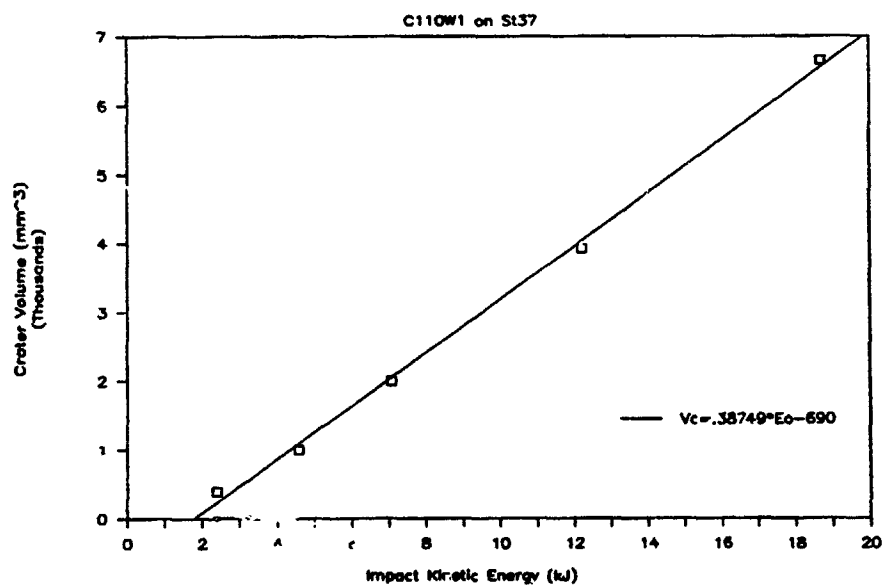


Figure 25b. Crater Volume vs. Impact Kinetic Energy

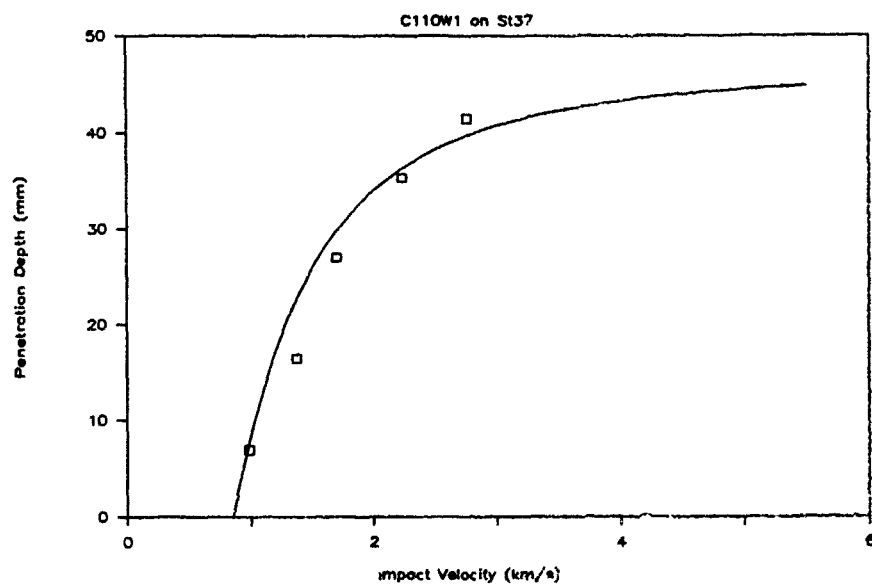


Figure 25c. Penetration Depth vs. Impact Velocity

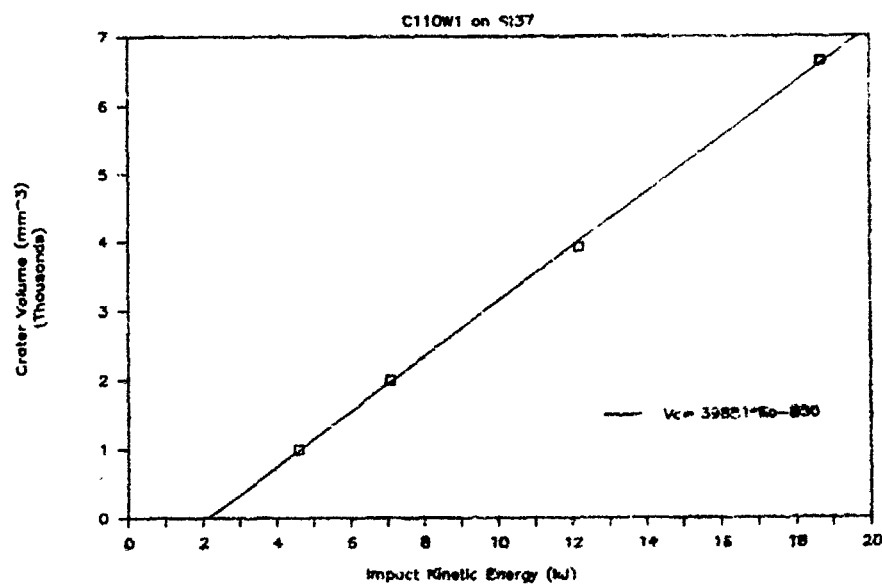


Figure 25d. Crater Volume vs. Impact Kinetic Energy

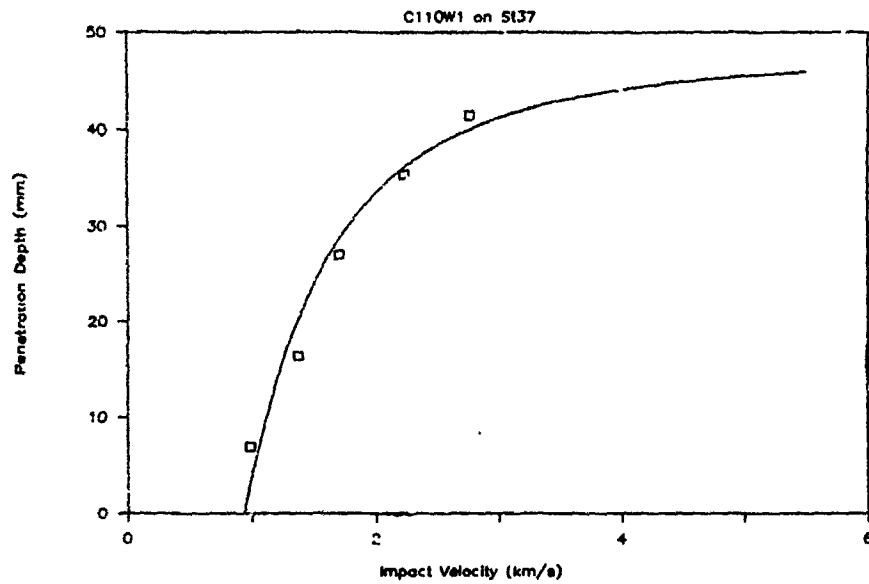


Figure 25e. Penetration Depth vs. Impact Velocity

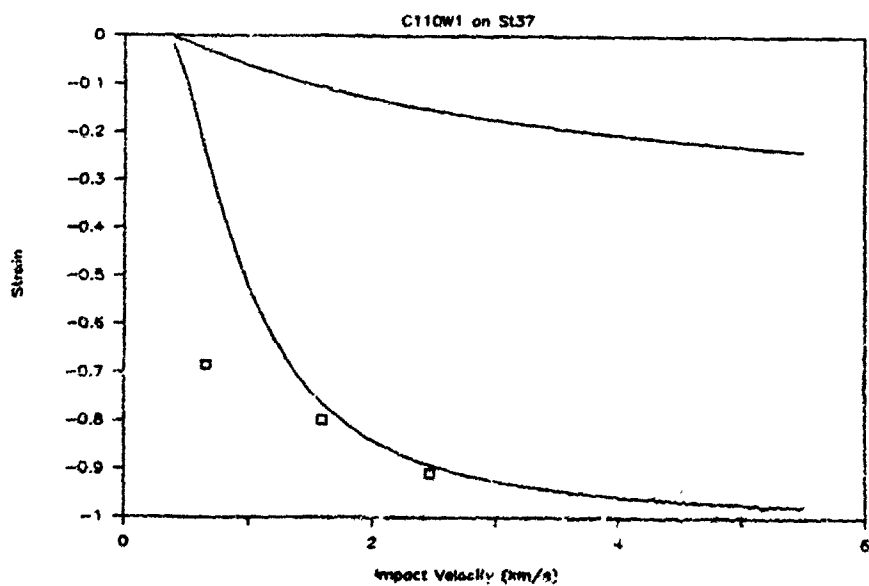


Figure 26a. Strain vs. Impact Velocity

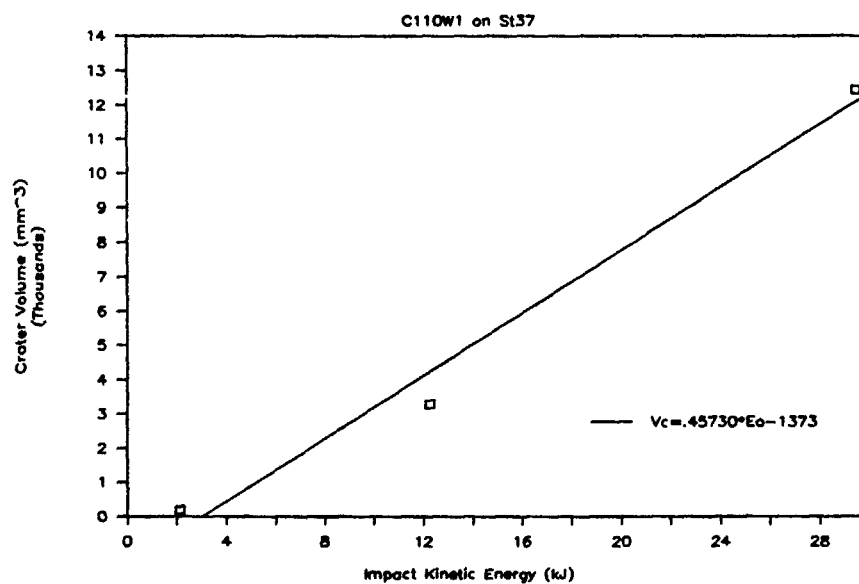


Figure 26b. Crater Volume vs. Impact Kinetic Energy

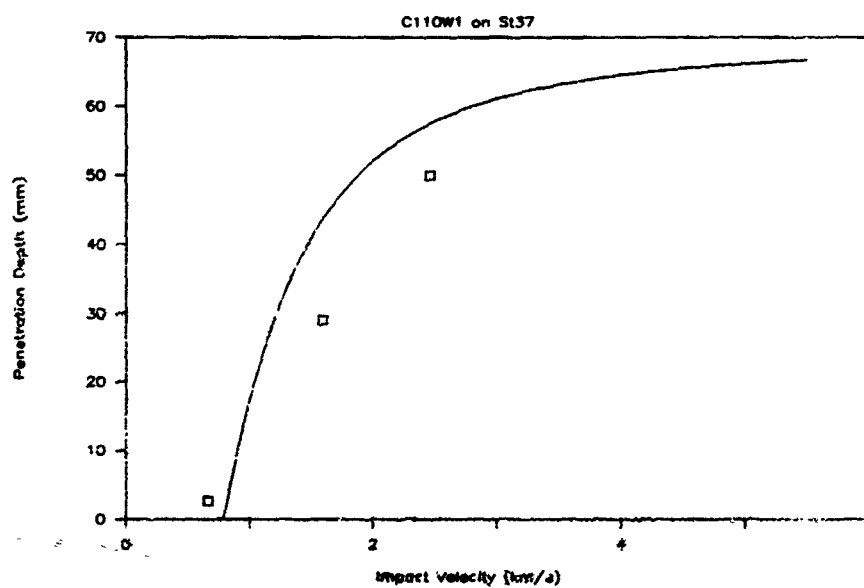


Figure 26c. Penetration Depth vs. Impact Velocity

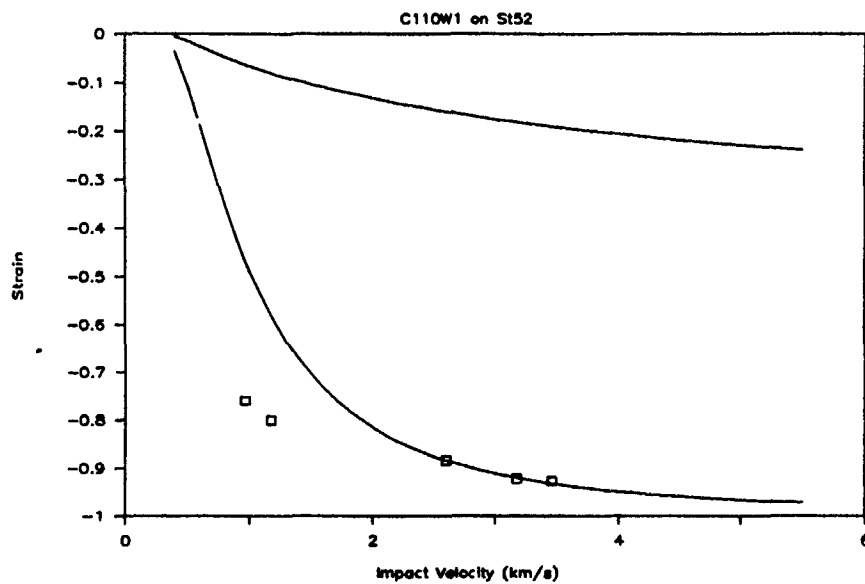


Figure 27a. Strain vs. Impact Velocity

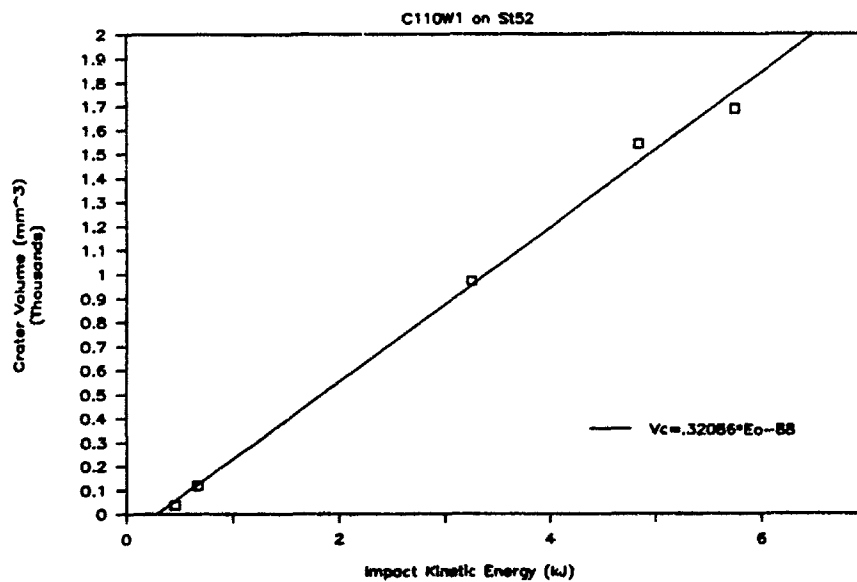


Figure 27b. Crater Volume vs. Impact Kinetic Energy

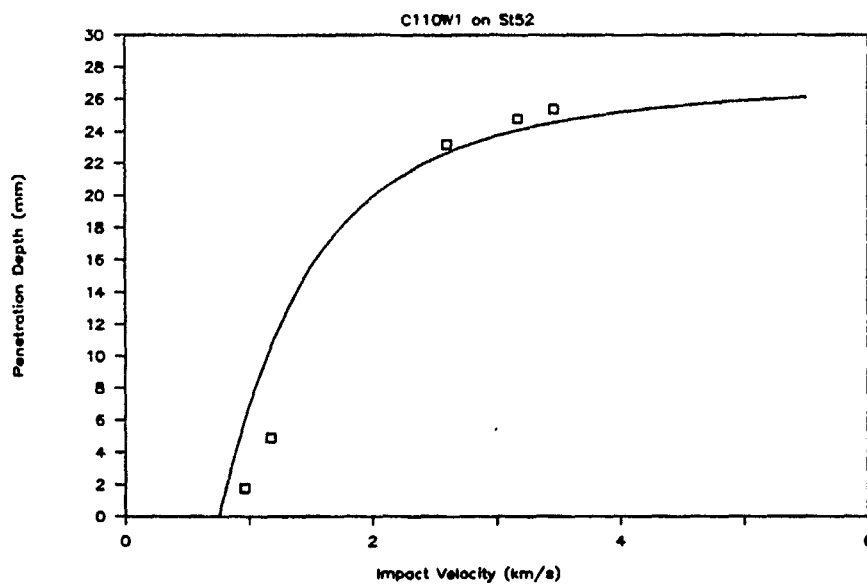


Figure 27c. Penetration Depth vs. Impact Velocity

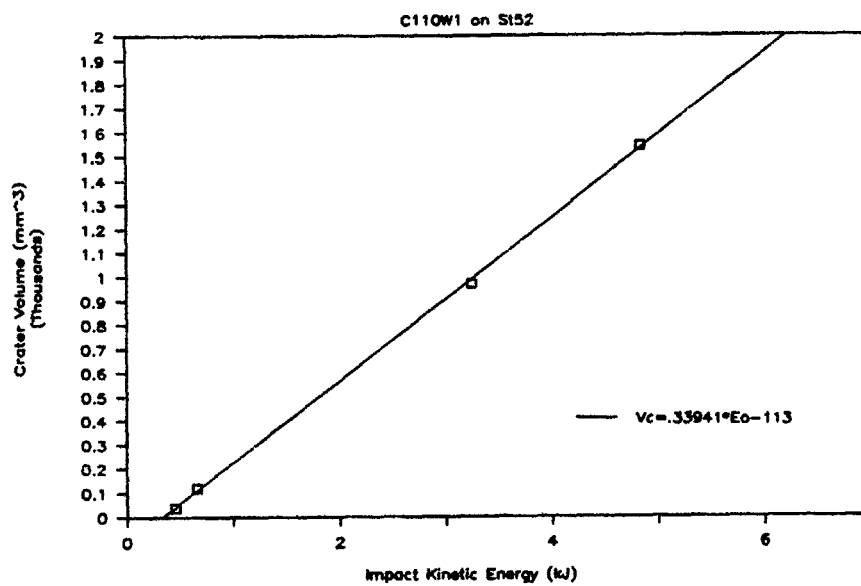


Figure 27d. Crater Volume vs. Impact Kinetic Energy

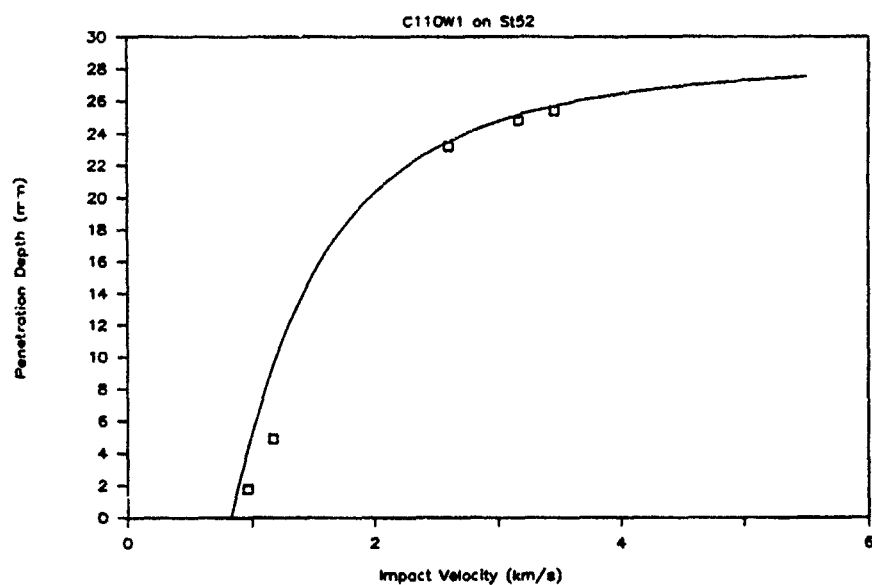


Figure 27e. Penetration Depth vs. Impact Velocity

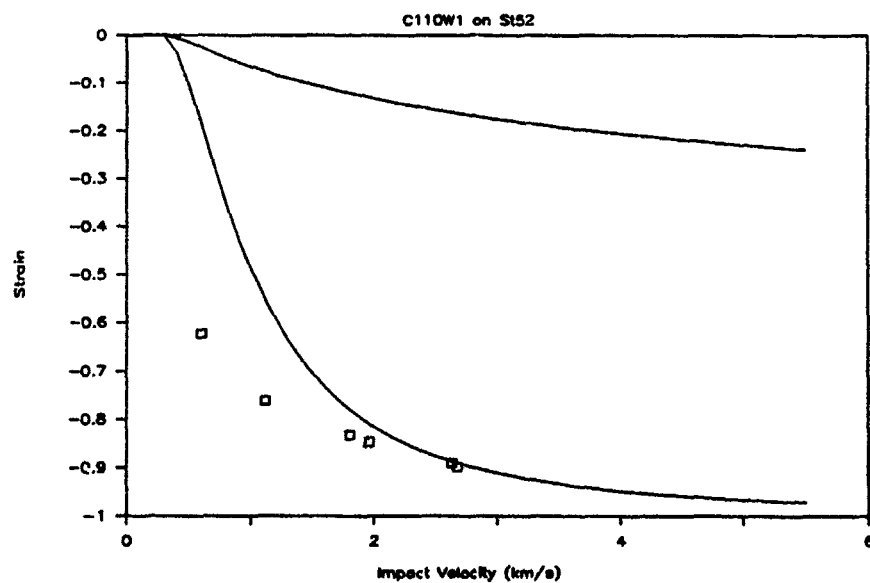


Figure 28a. Strain vs. Impact Velocity

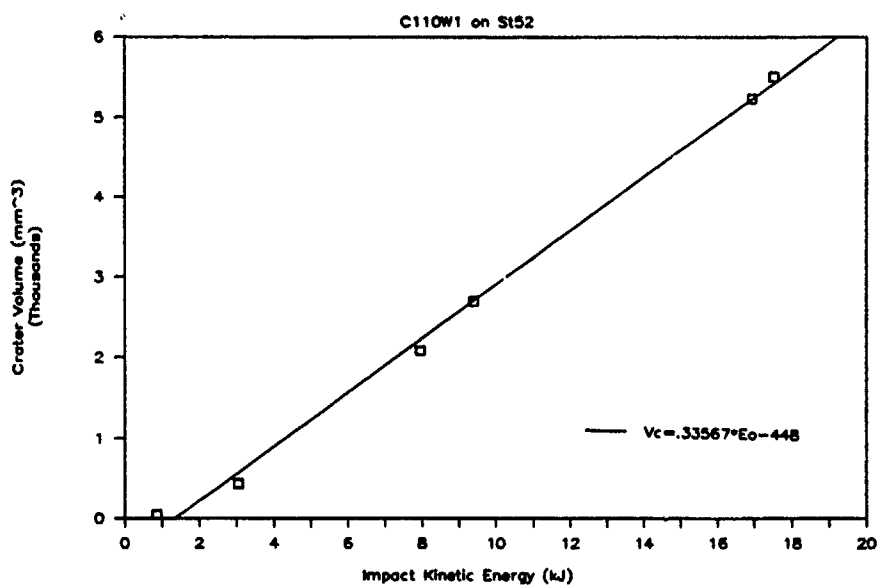


Figure 28b. Crater Volume vs. Impact Kinetic Energy

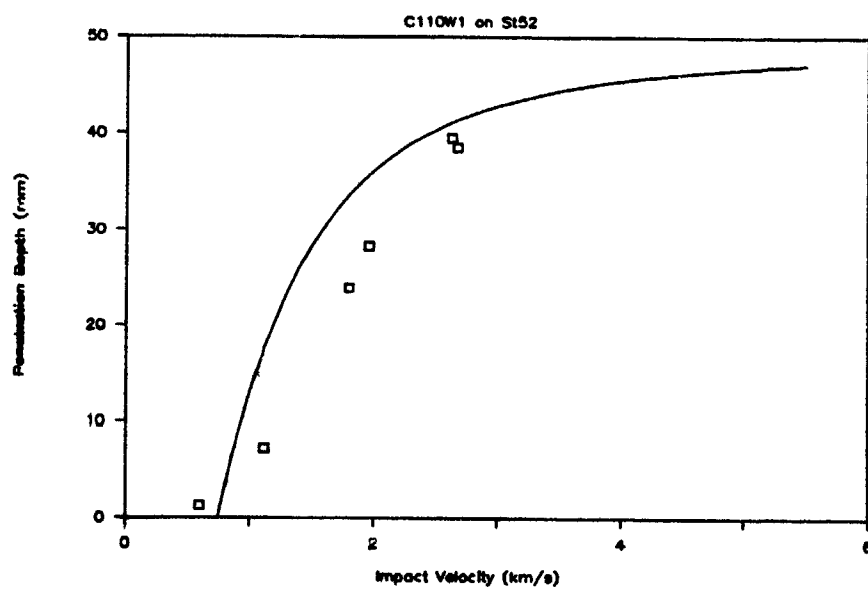


Figure 28c. Penetration Depth vs. Impact Velocity

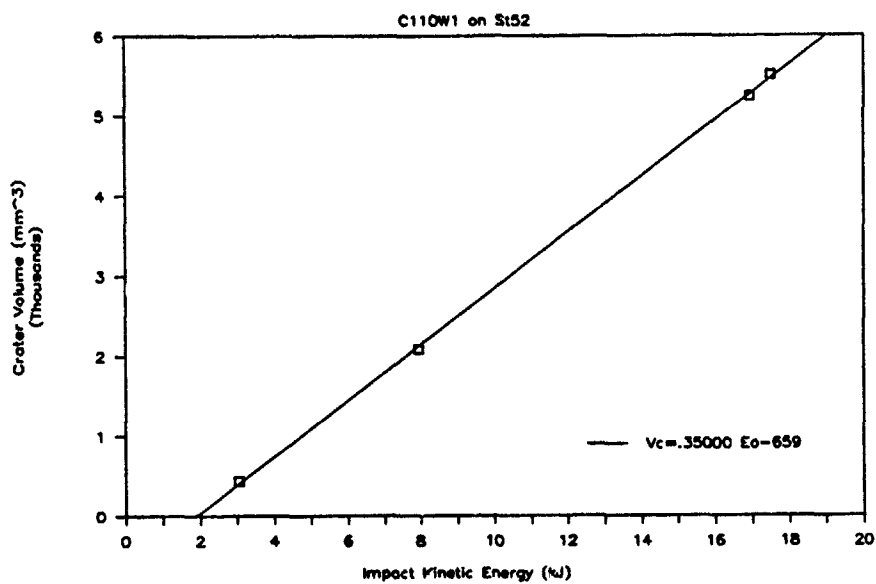


Figure 28d. Crater Volume vs. Impact Kinetic Energy

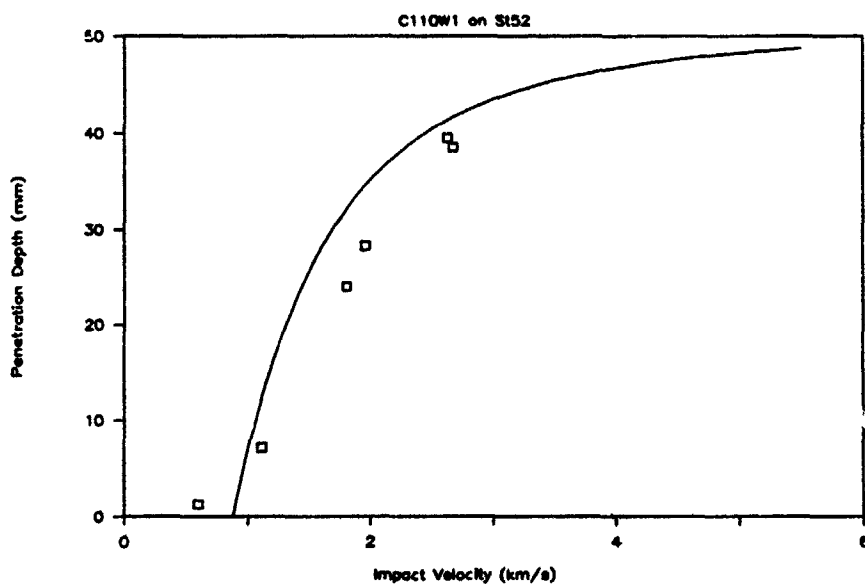


Figure 28e. Penetration Depth vs. Impact Velocity

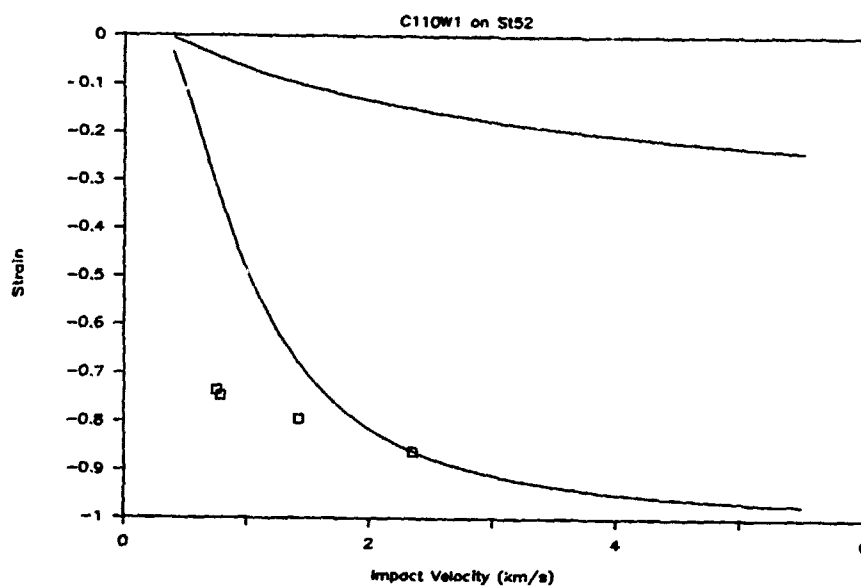


Figure 29a. Strain vs. Impact Velocity

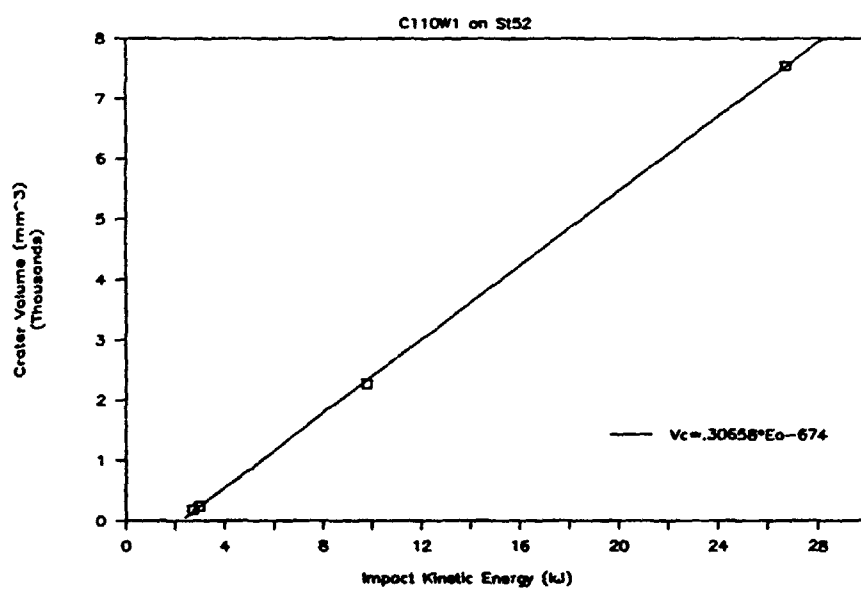


Figure 29b. Crater Volume vs. Impact Kinetic Energy

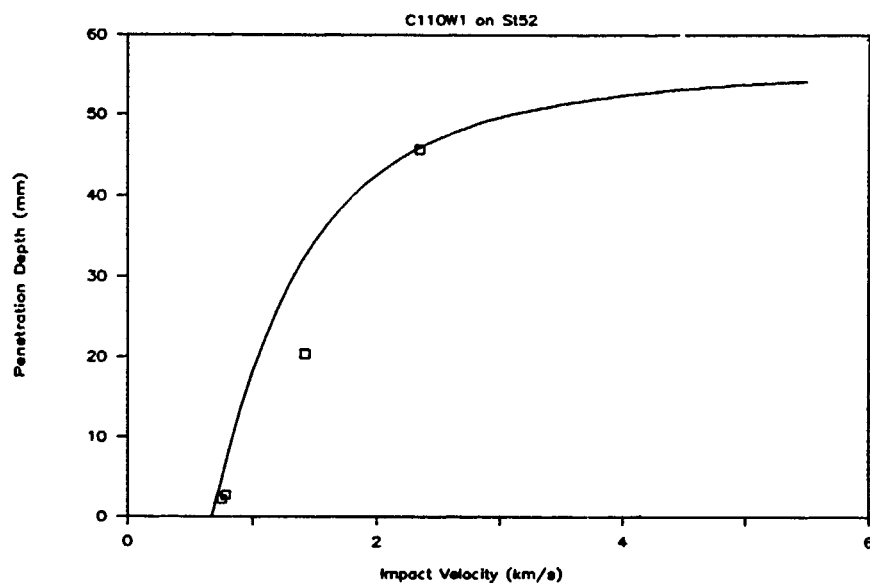


Figure 29c. Penetration Depth vs. Impact Velocity

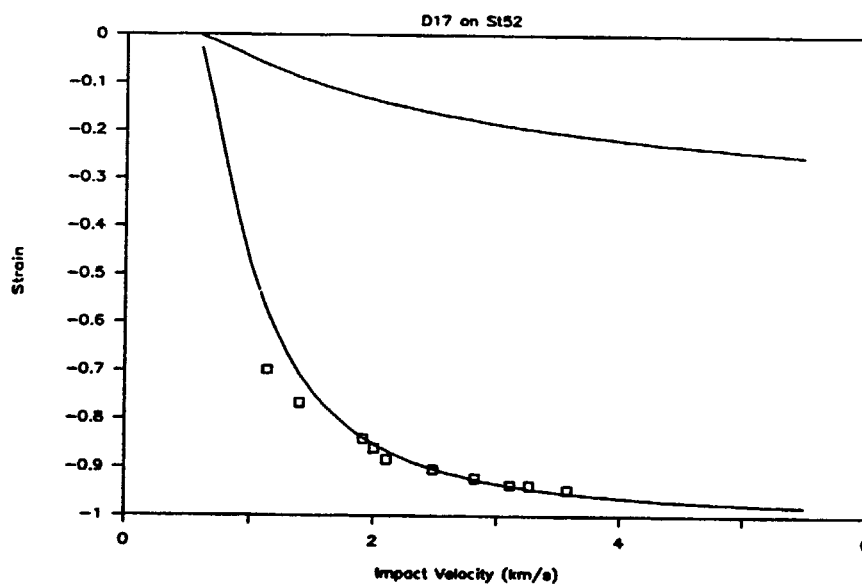


Figure 30a. Strain vs. Impact Velocity

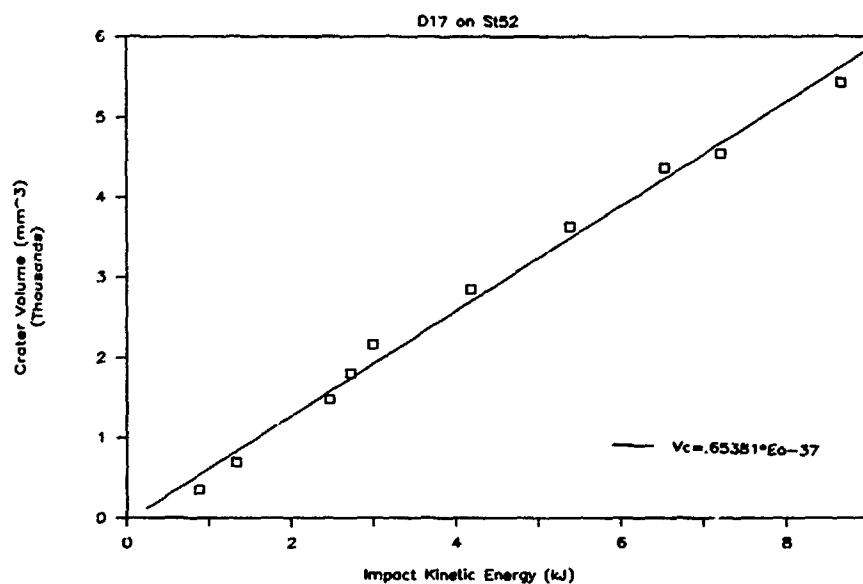


Figure 30b. Crater Volume vs. Impact Kinetic Energy

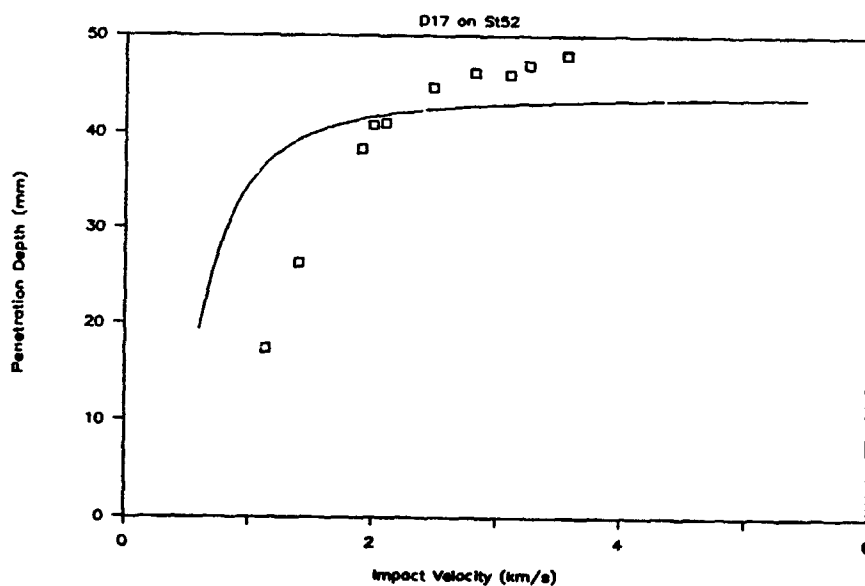


Figure 30c. Penetration Depth vs. Impact Velocity

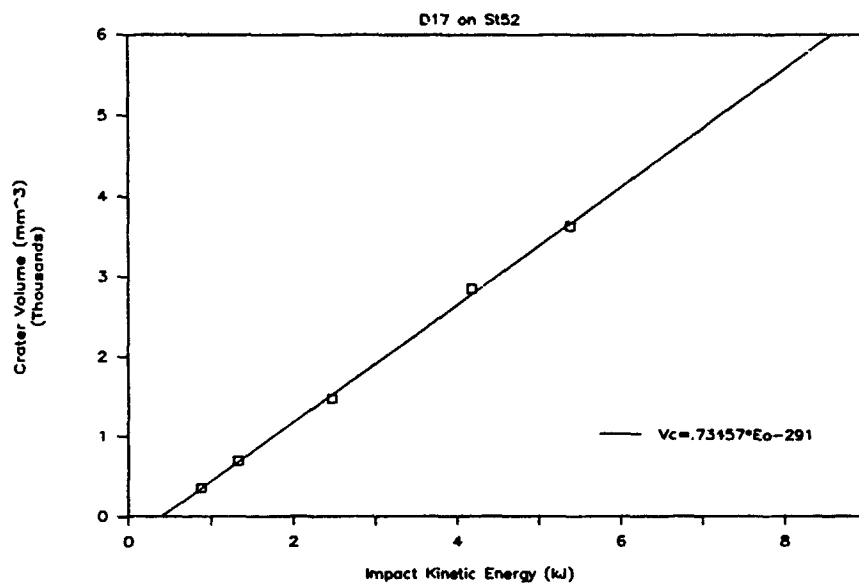


Figure 30d. Crater Volume vs. Impact Kinetic Energy

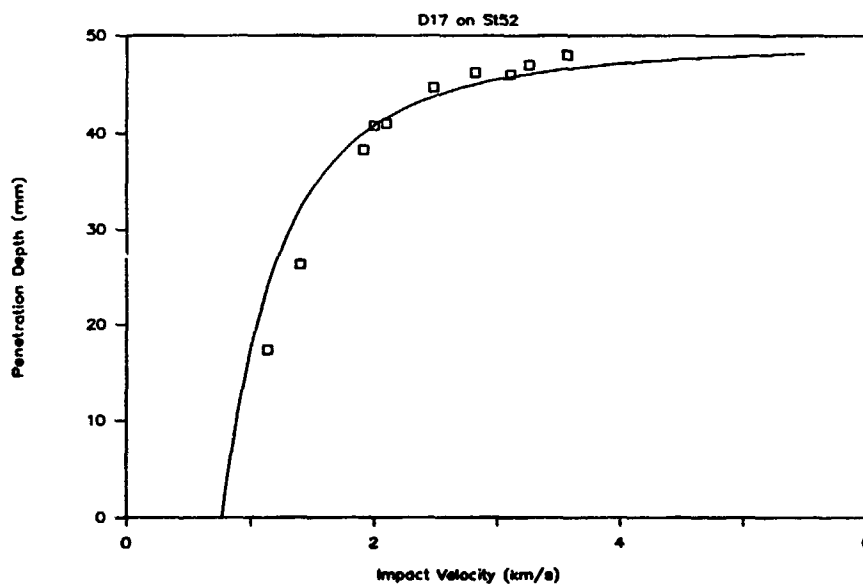


Figure 30e. Penetration Depth vs. Impact Velocity

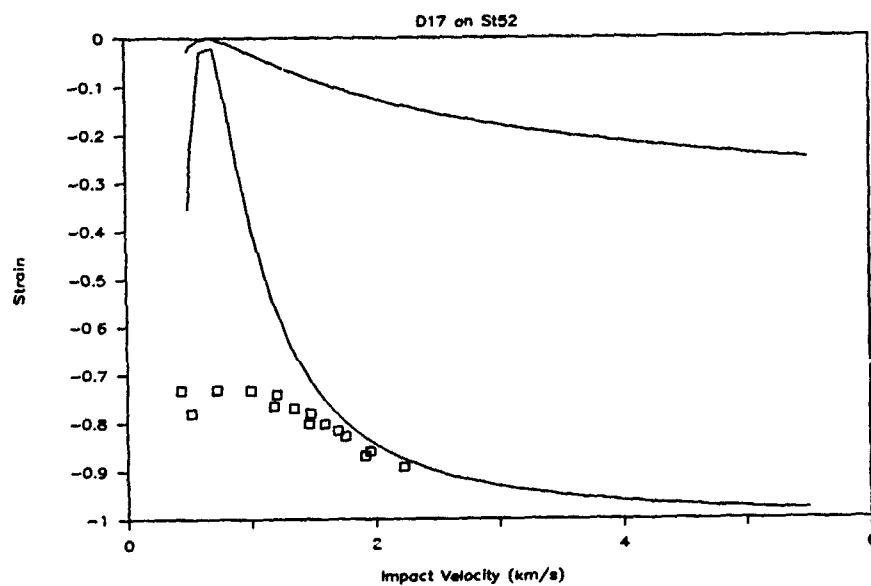


Figure 31a. Strain vs. Impact Velocity

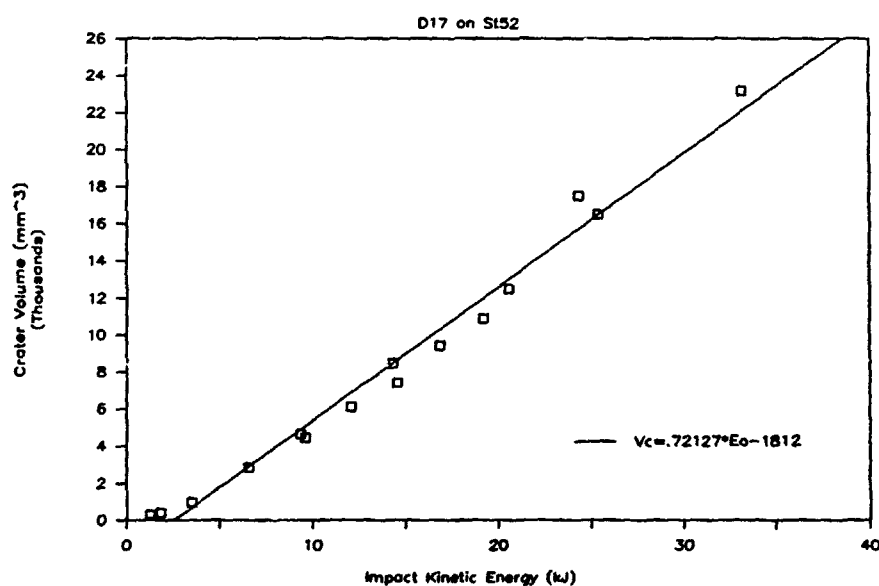


Figure 31b. Crater Volume vs. Impact Kinetic Energy

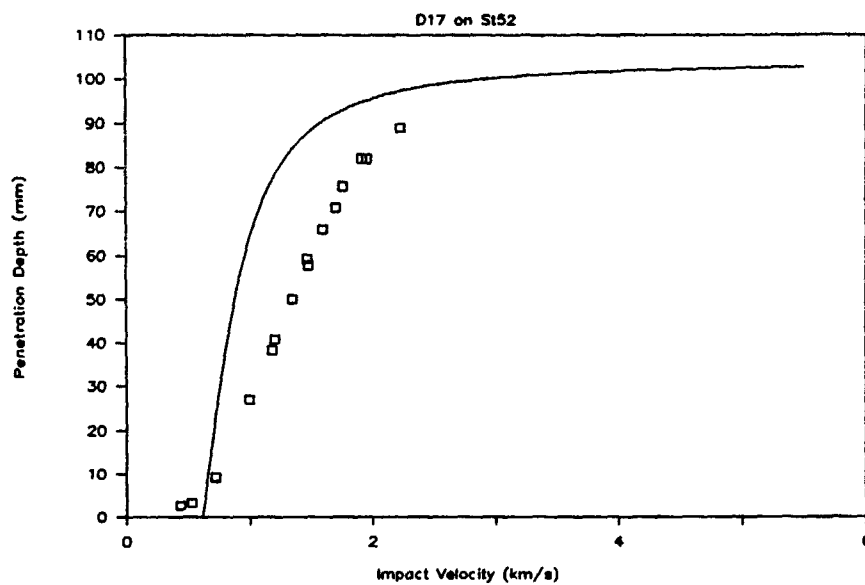


Figure 31c. Penetration Depth vs. Impact Velocity

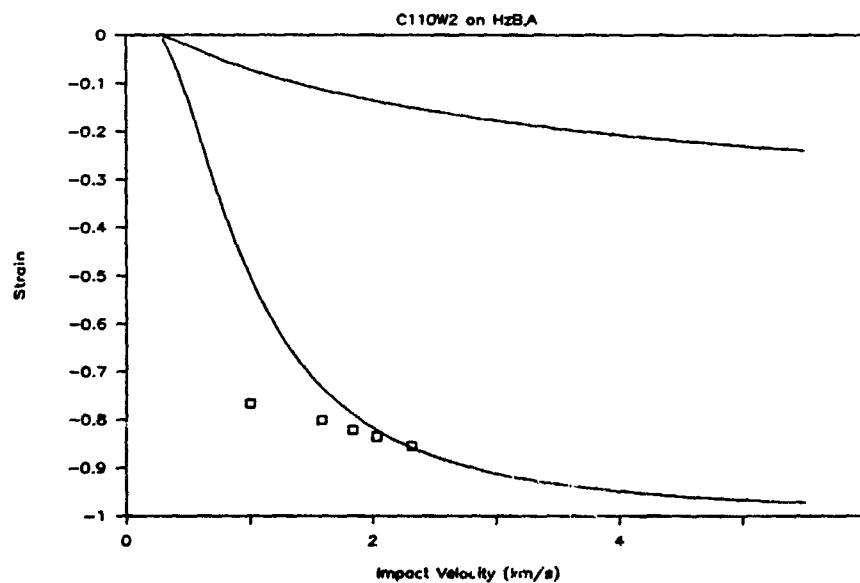


Figure 32a. Strain vs. Impact Velocity

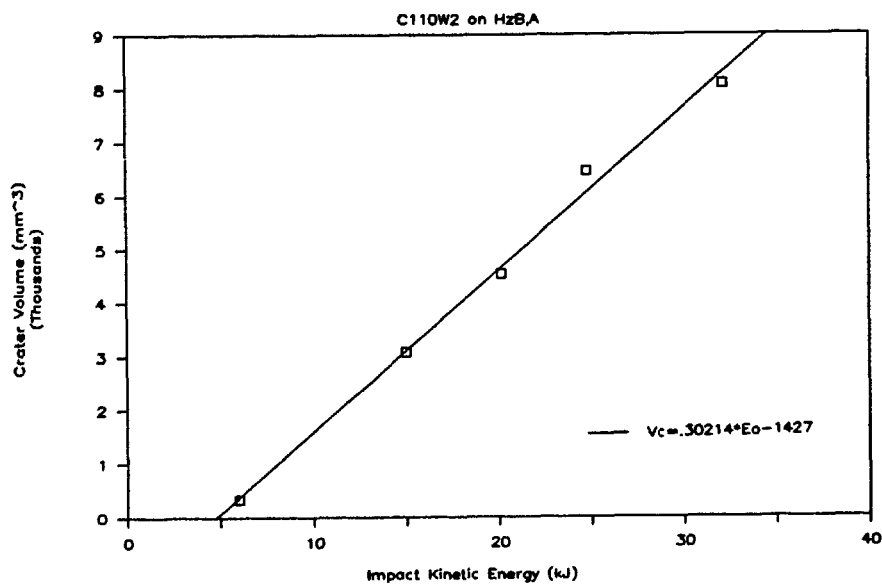


Figure 32b. Crater Volume vs. Impact Kinetic Energy

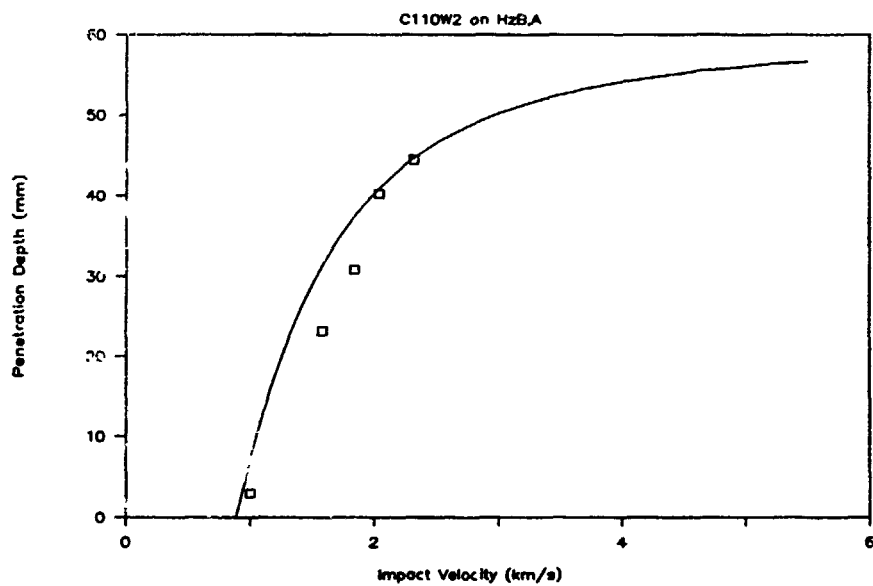


Figure 32c. Penetration Depth vs. Impact Velocity

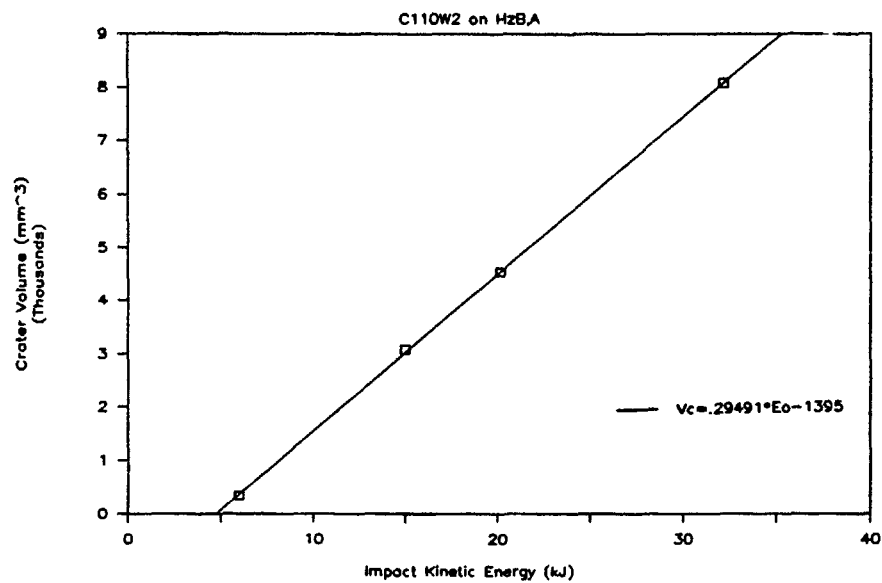


Figure 32d. Crater Volume vs. Impact Kinetic Energy

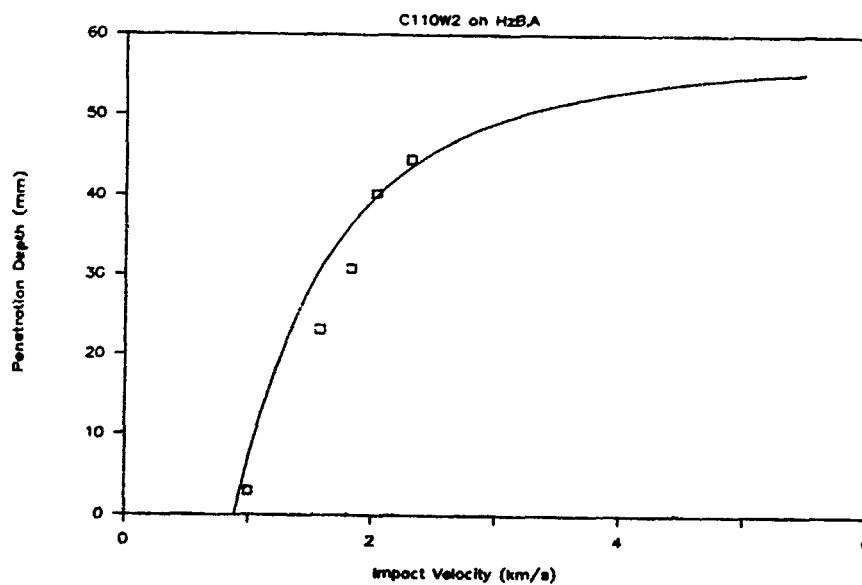


Figure 32e. Penetration Depth vs. Impact Velocity

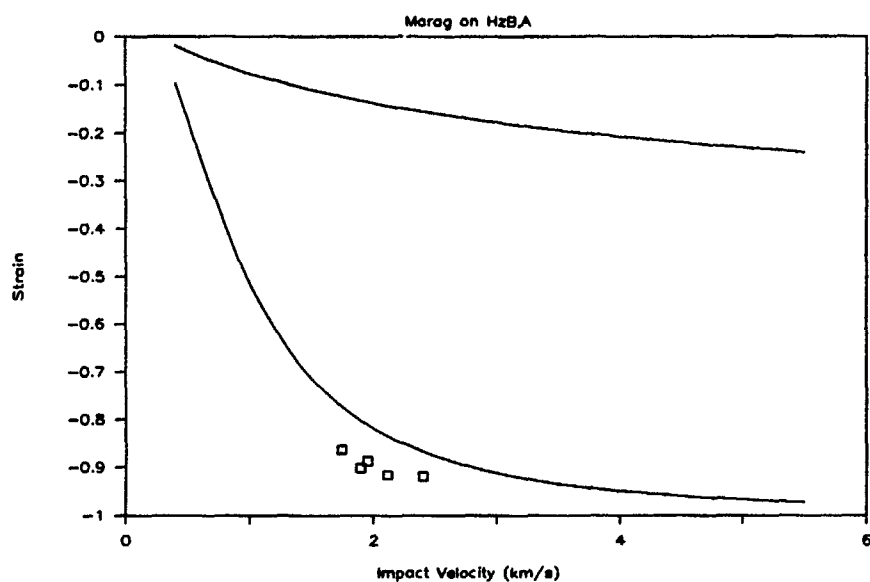


Figure 33a. Strain vs. Impact Velocity

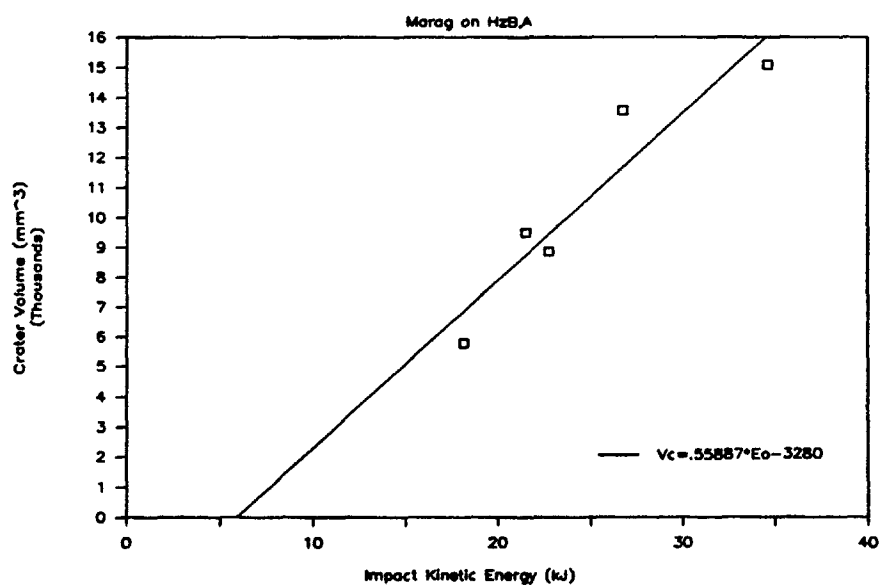


Figure 33b. Crater Volume vs. Impact Kinetic Energy

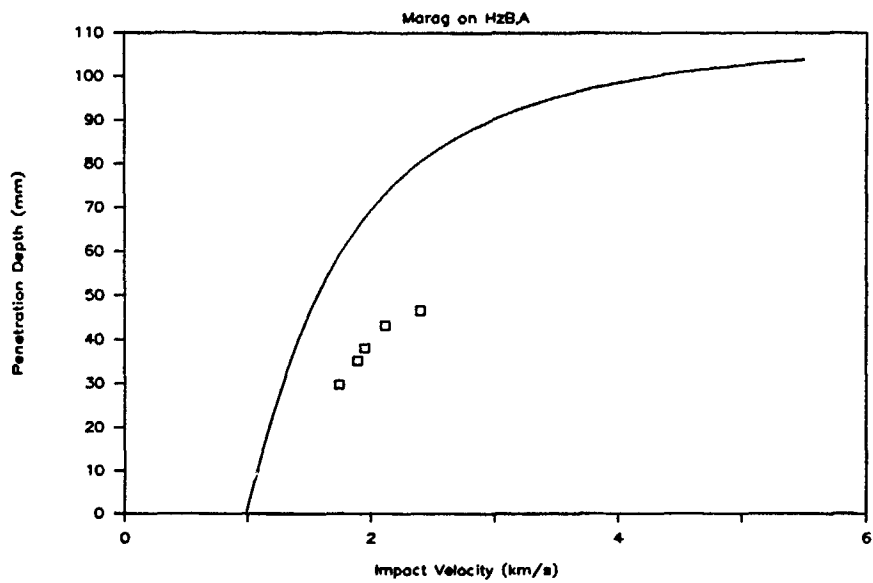


Figure 33c. Penetration Depth vs. Impact Velocity

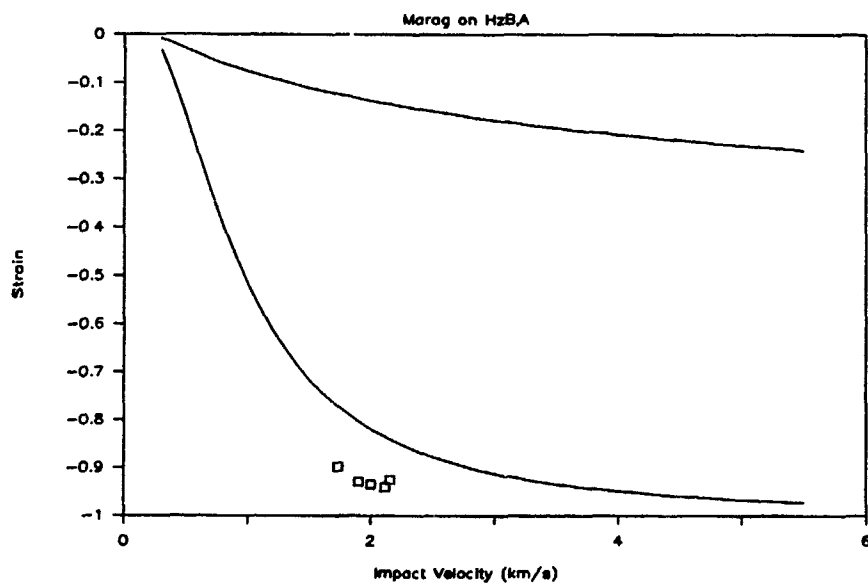


Figure 34a. Strain vs. Impact Velocity

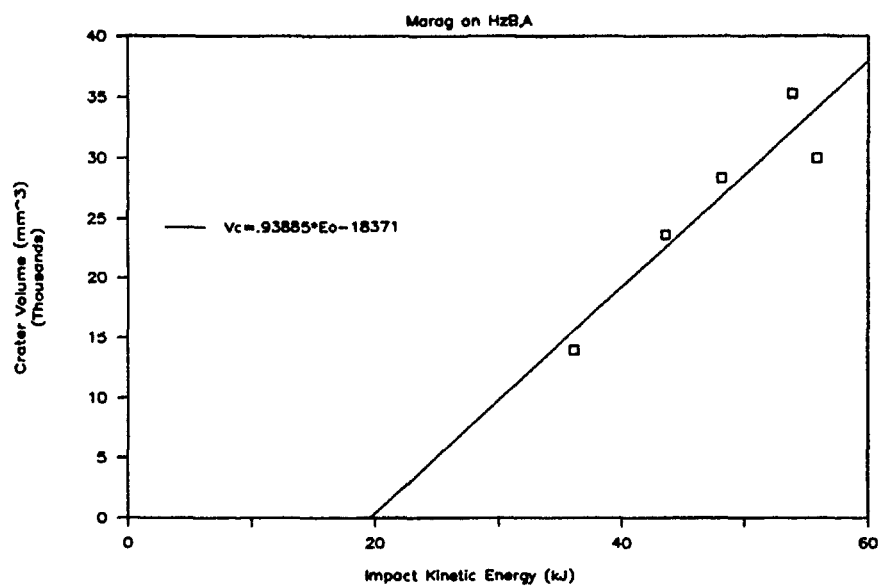


Figure 34b. Crater Volume vs. Impact Kinetic Energy

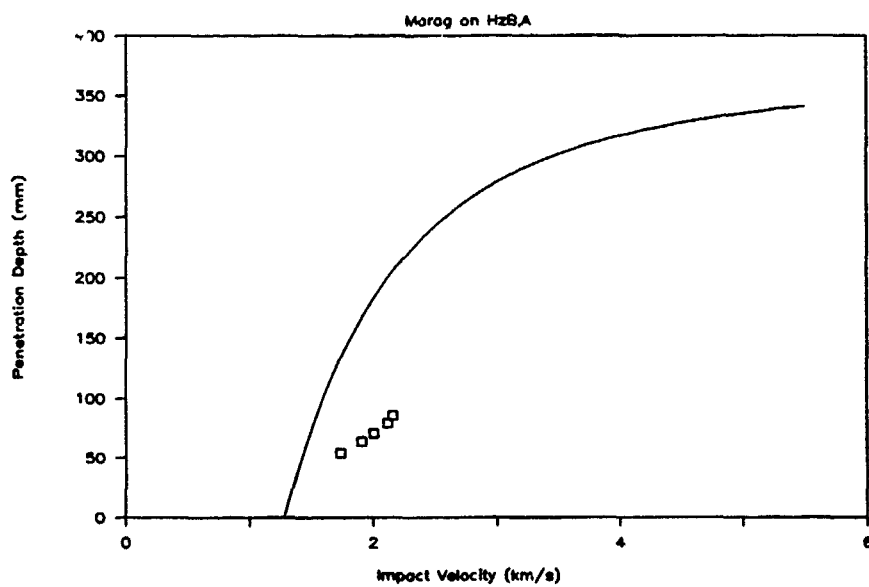


Figure 34c. Penetration Depth vs. Impact Velocity

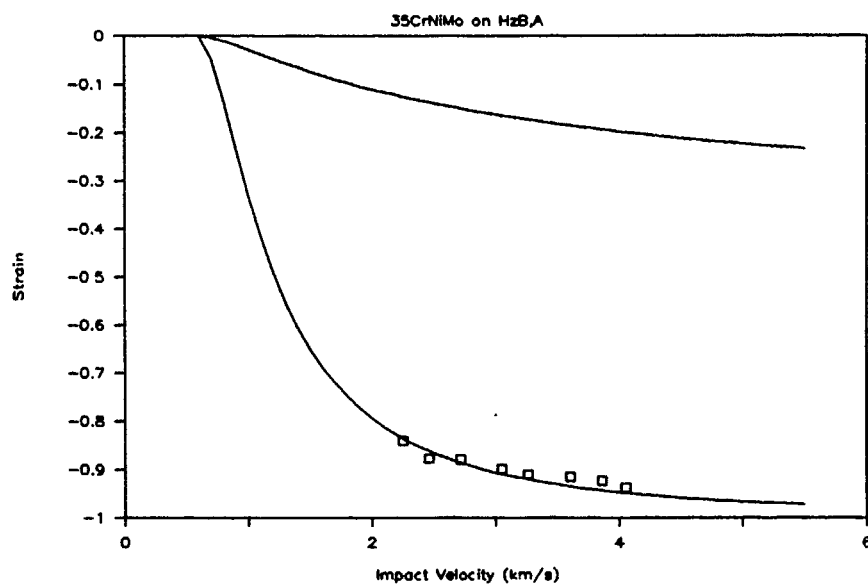


Figure 35a. Strain vs. Impact Velocity

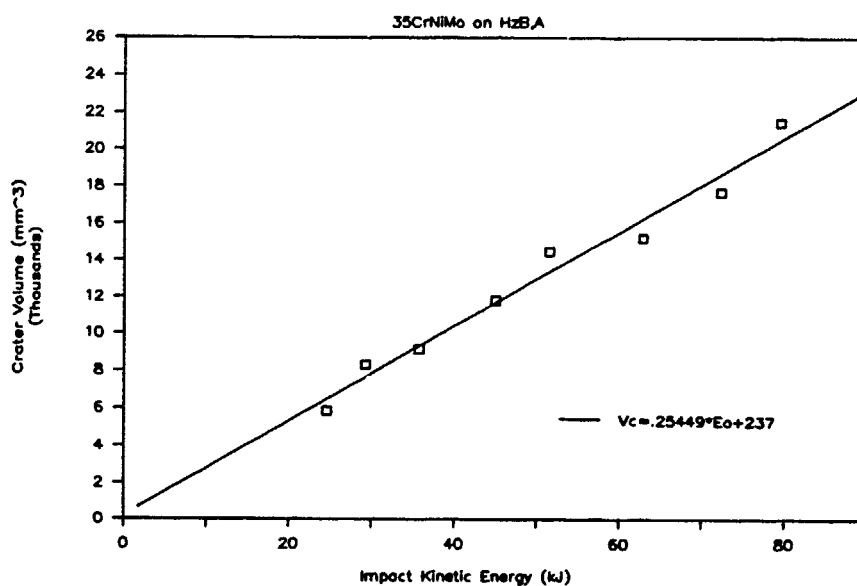


Figure 35b. Crater Volume vs. Impact Kinetic Energy

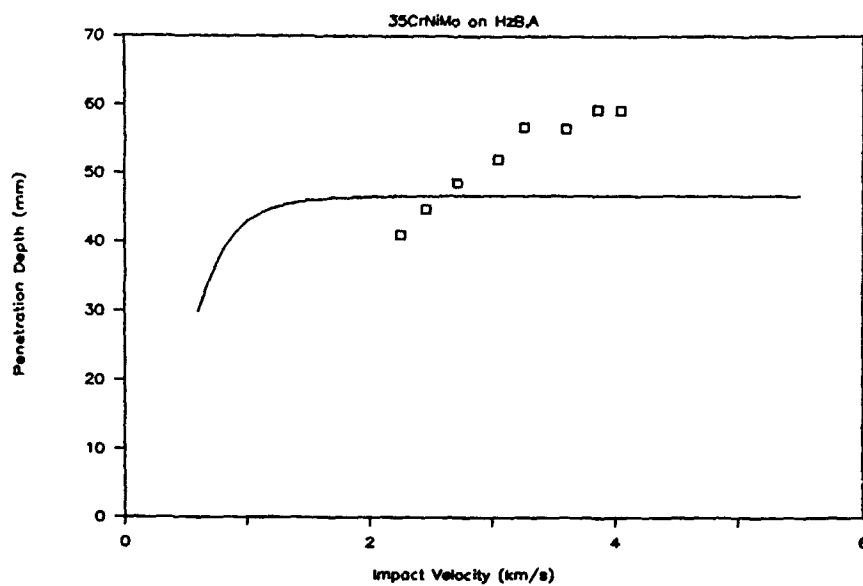


Figure 35c. Penetration Depth vs. Impact Velocity

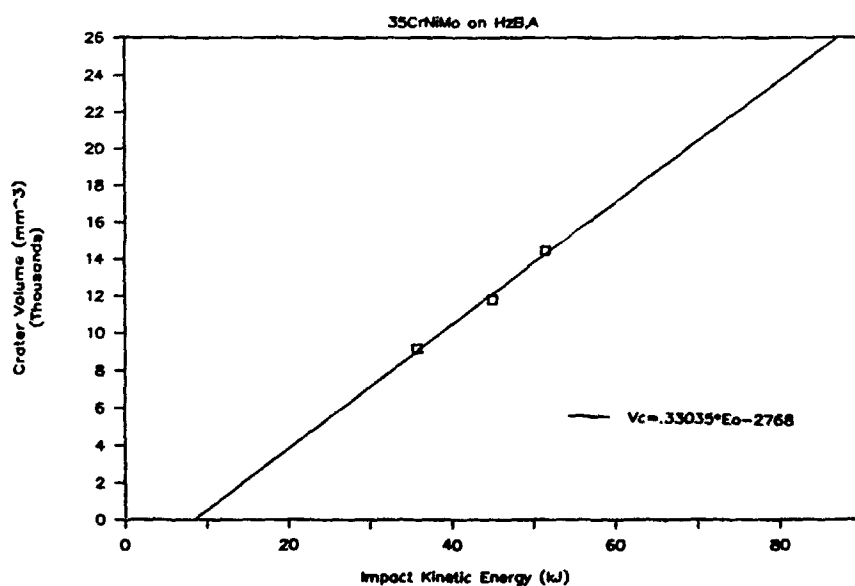


Figure 35d. Crater Volume vs. Impact Kinetic Energy

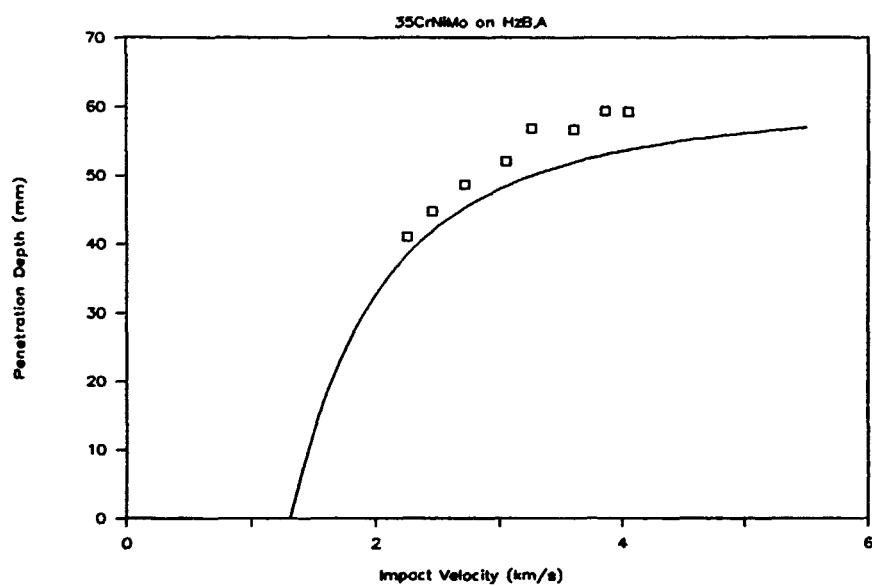


Figure 35e. Penetration Depth vs. Impact Velocity

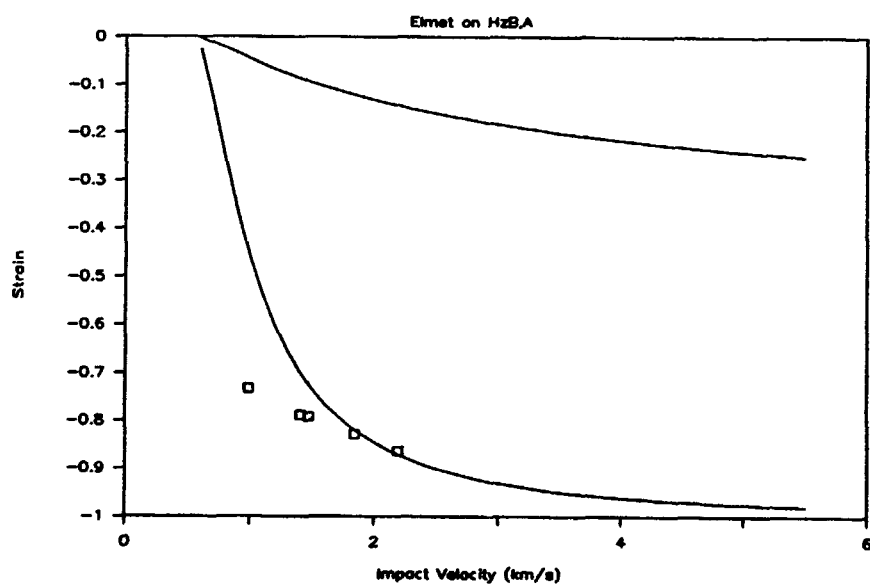


Figure 36a. Strain vs. Impact Velocity

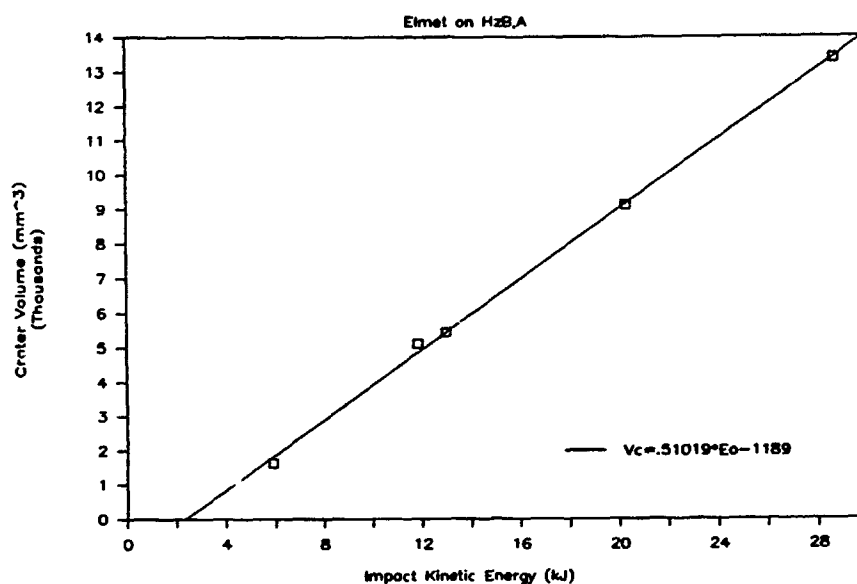


Figure 36b. Crater Volume vs. Impact Kinetic Energy

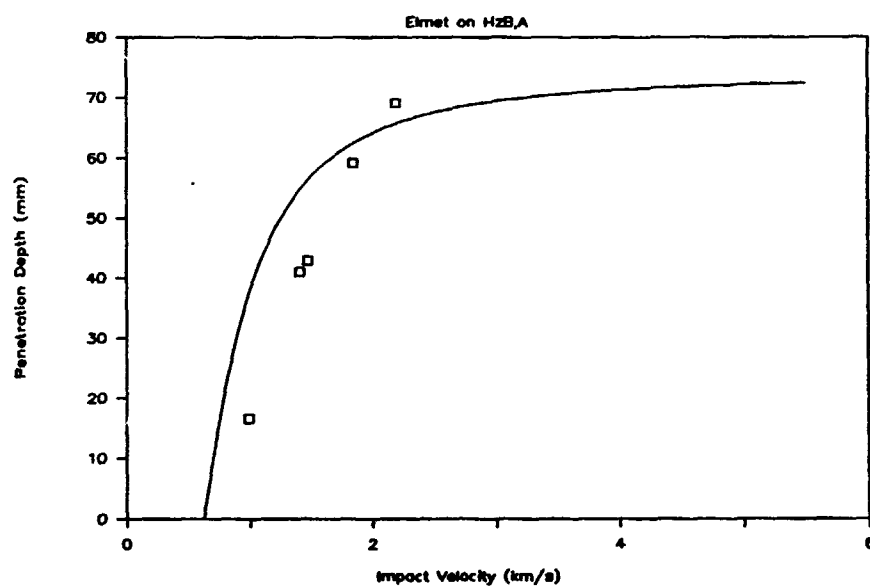


Figure 36c. Penetration Depth vs. Impact Velocity

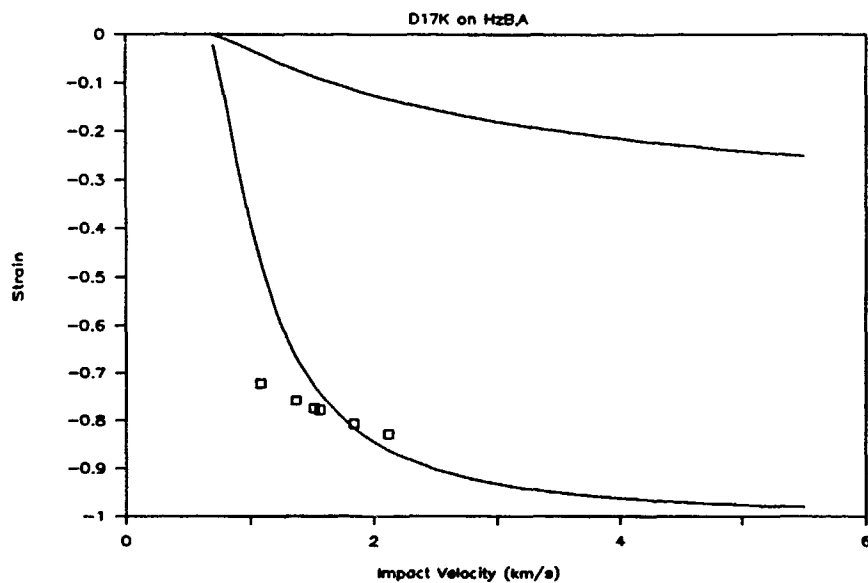


Figure 37a. Strain vs. Impact Velocity

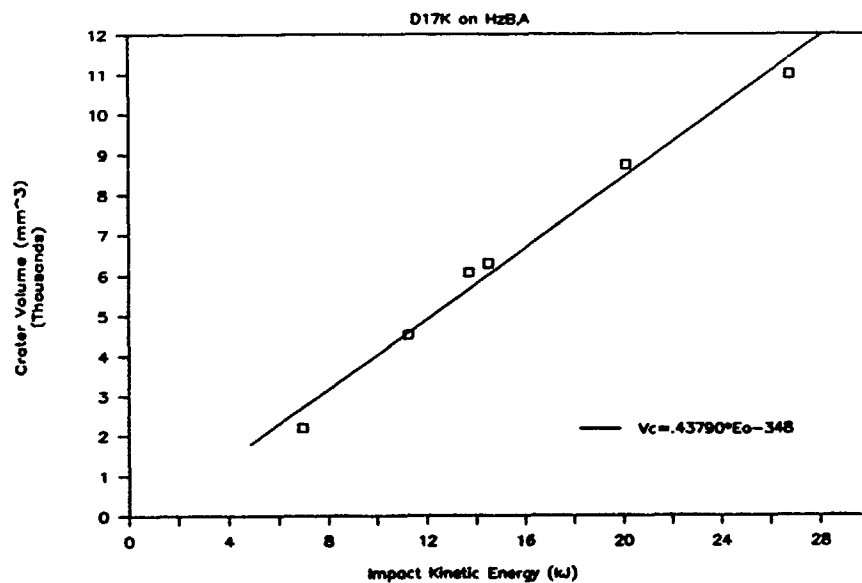


Figure 37b. Crater Volume vs. Impact Kinetic Energy

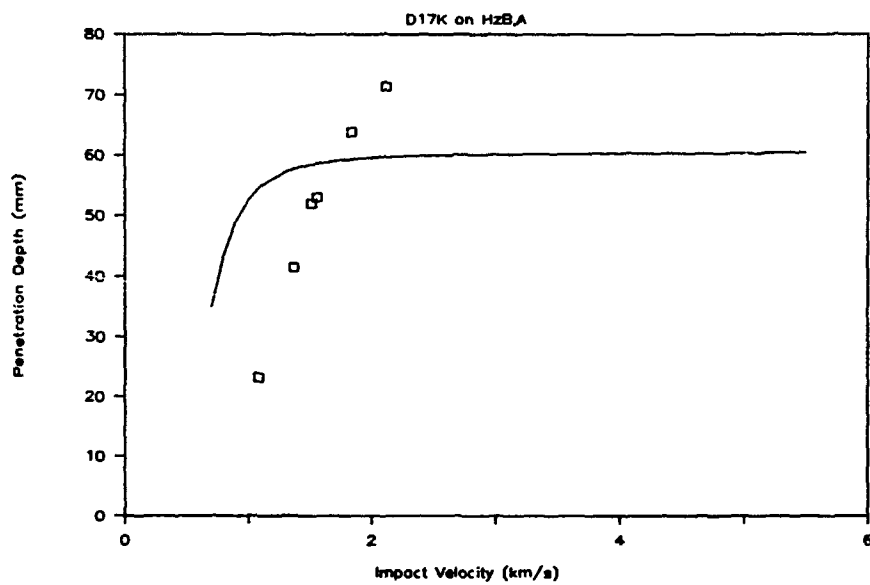


Figure 37c. Penetration Depth vs. Impact Velocity

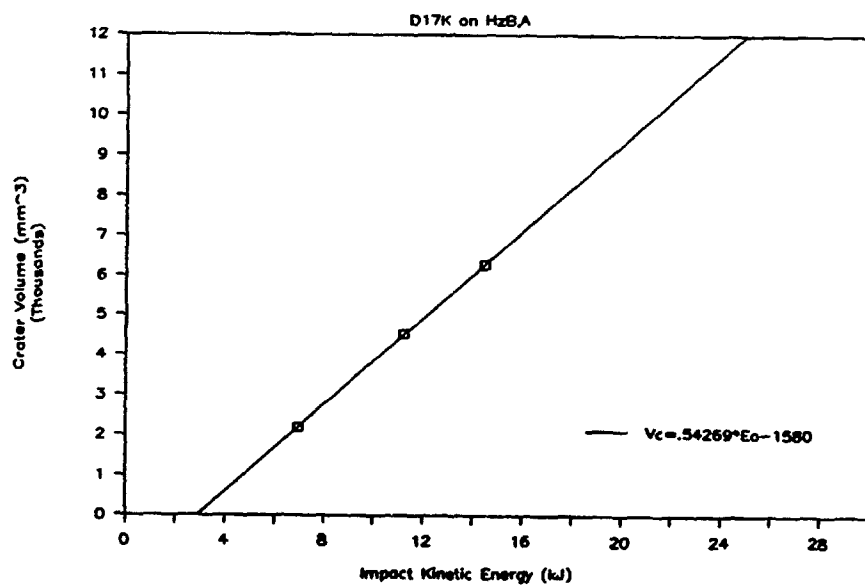


Figure 37d. Crater Volume vs. Impact Kinetic Energy

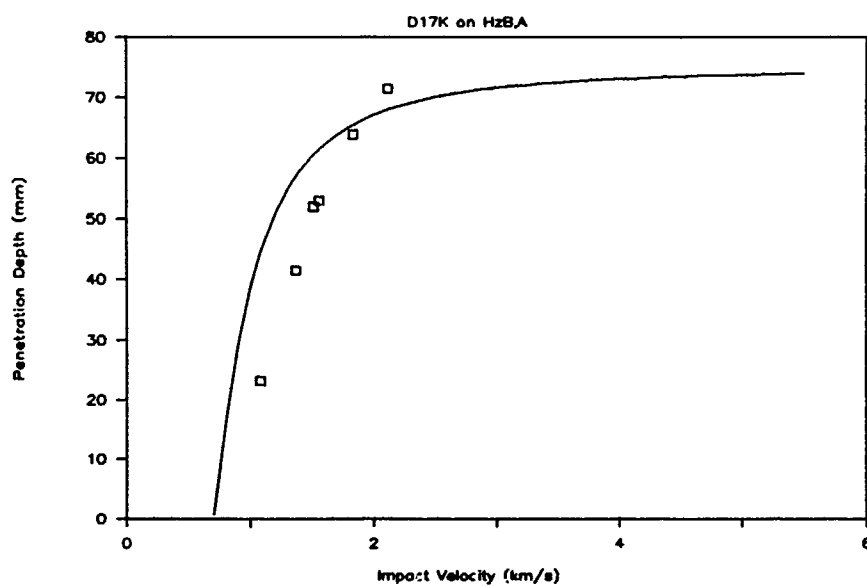


Figure 37e. Penetration Depth vs. Impact Velocity

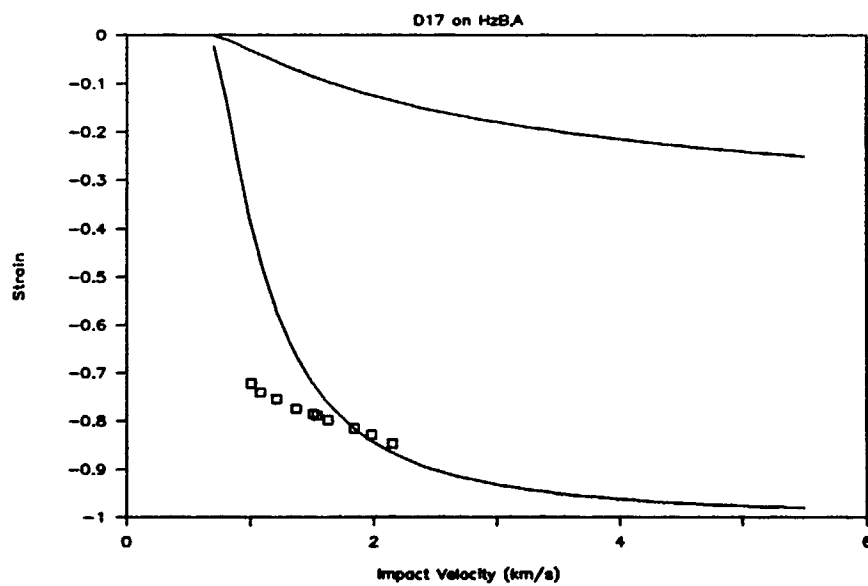


Figure 38a. Strain vs. Impact Velocity

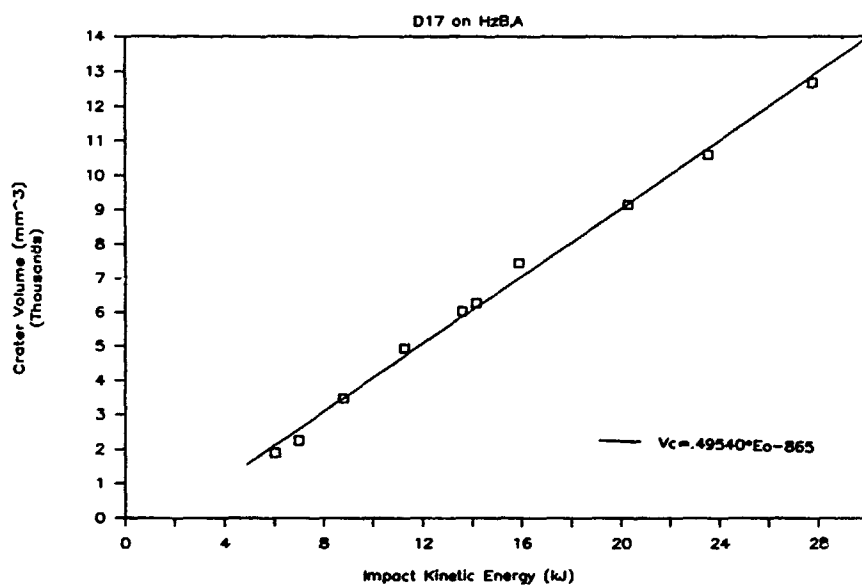


Figure 38b. Crater Volume vs. Impact Kinetic Energy

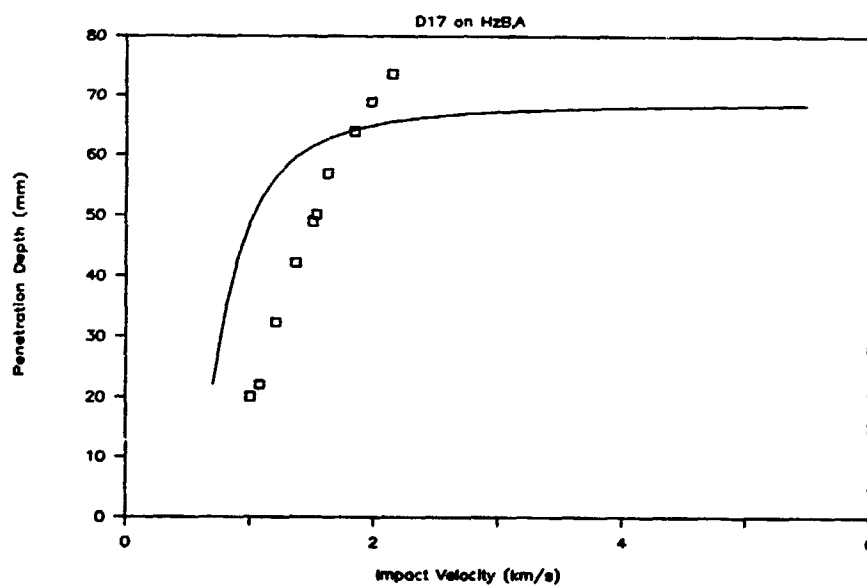


Figure 38c. Penetration Depth vs. Impact Velocity

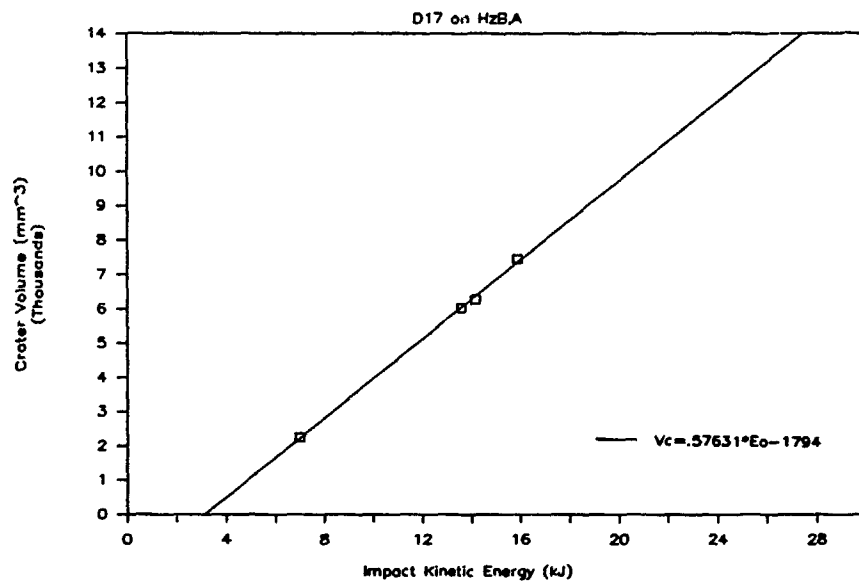


Figure 38d. Crater Volume vs. Impact Kinetic Energy

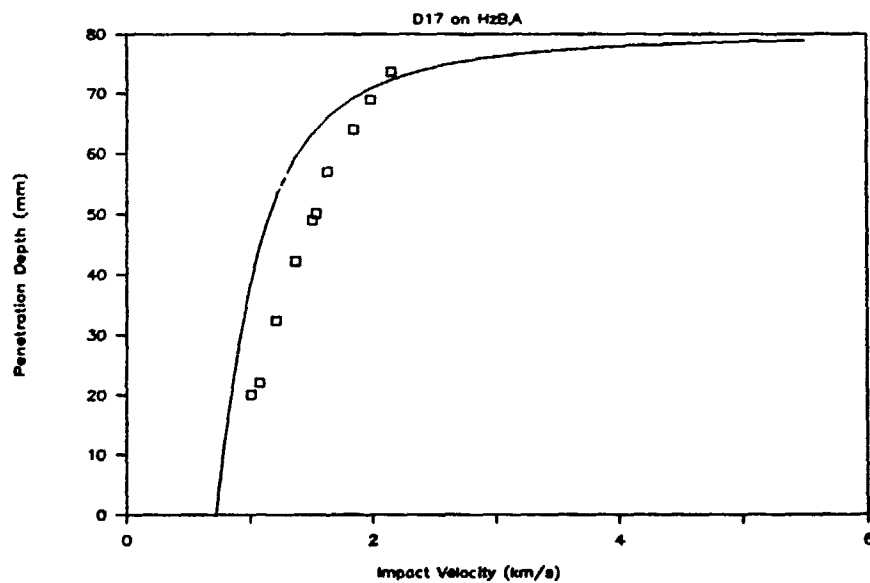


Figure 38e. Penetration Depth vs. Impact Velocity

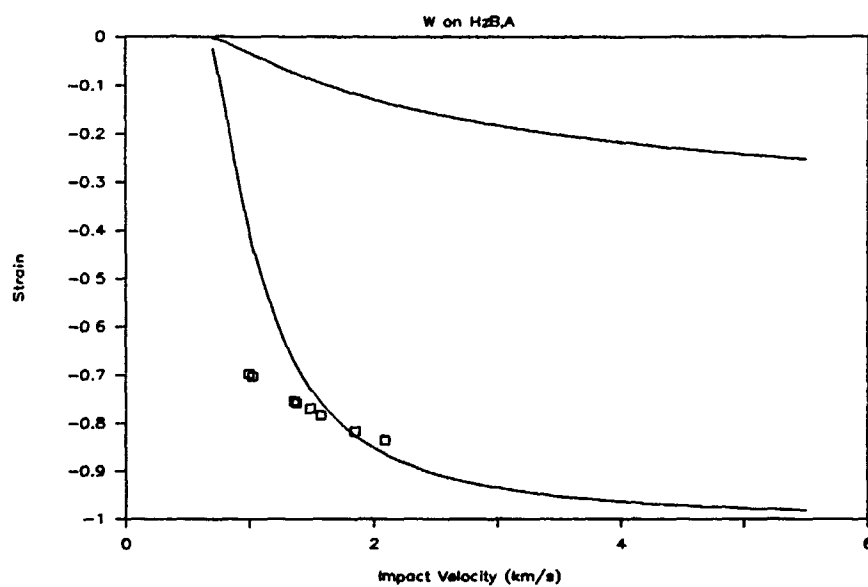


Figure 39a. Strain vs. Impact Velocity

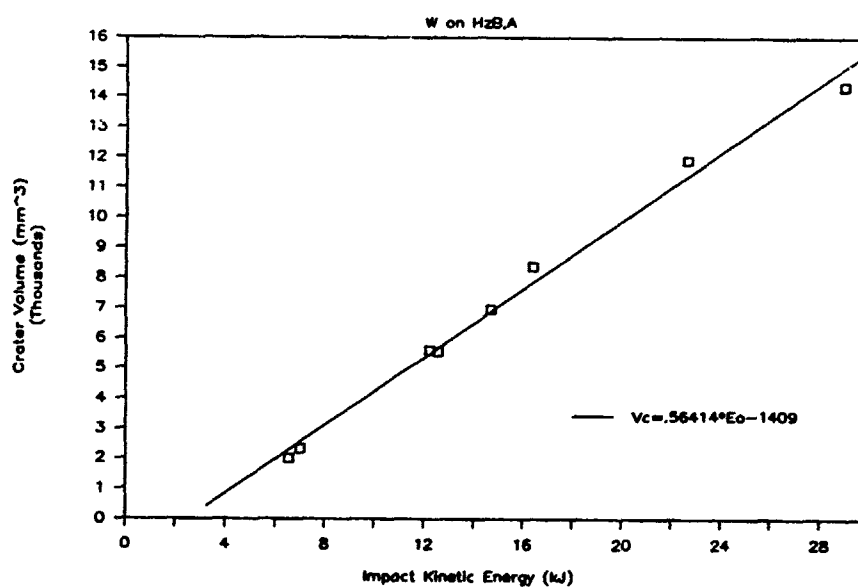


Figure 39b. Crater Volume vs. Impact Kinetic Energy

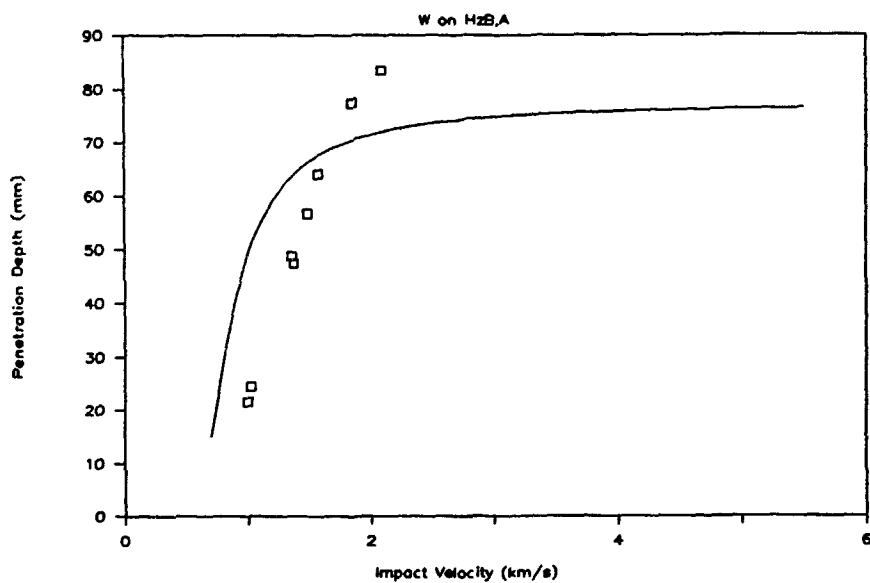


Figure 39c. Penetration Depth vs. Impact Velocity

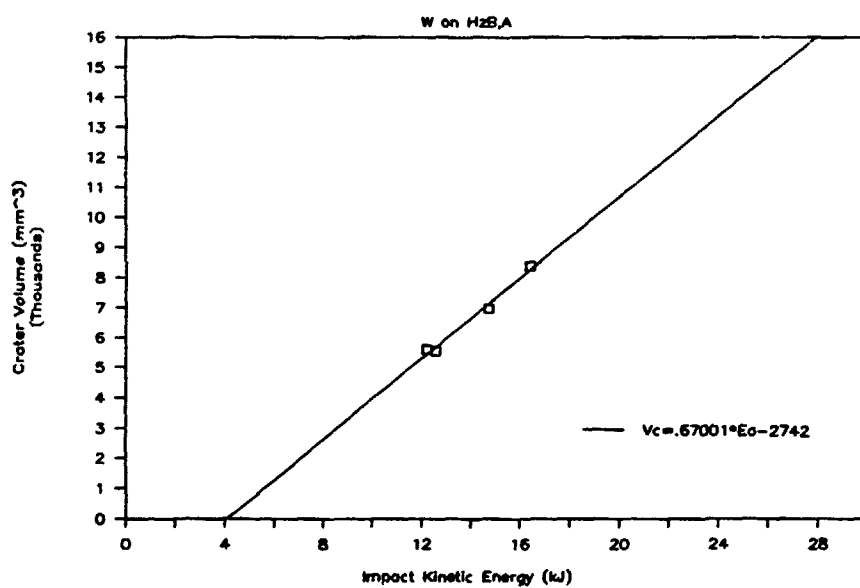


Figure 39d. Crater Volume vs. Impact Kinetic Energy

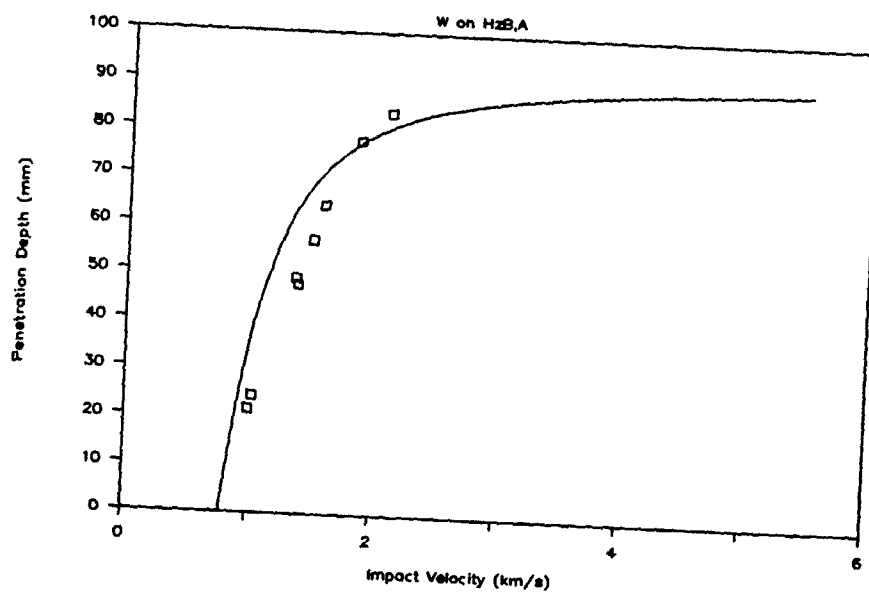


Figure 39e. Penetration Depth vs. Impact Velocity

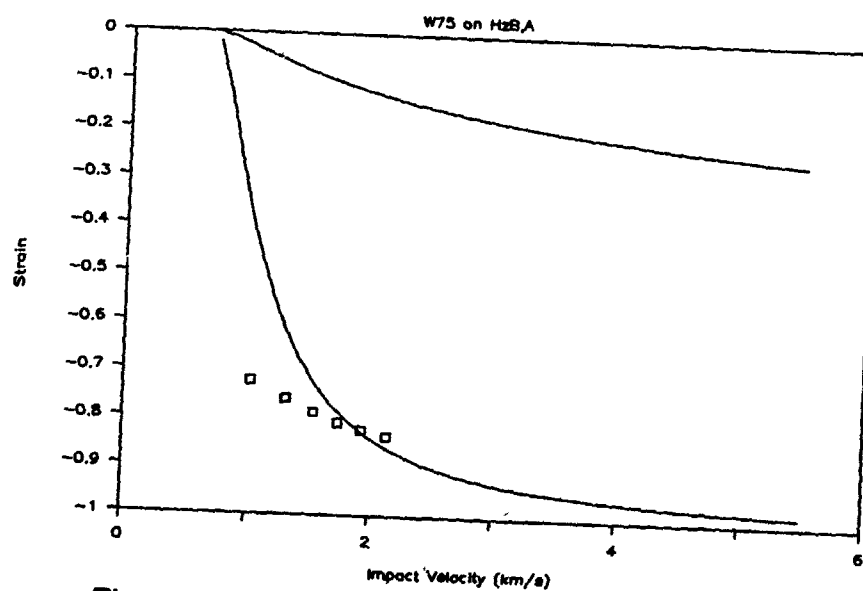


Figure 40a. Strain vs. Impact Velocity

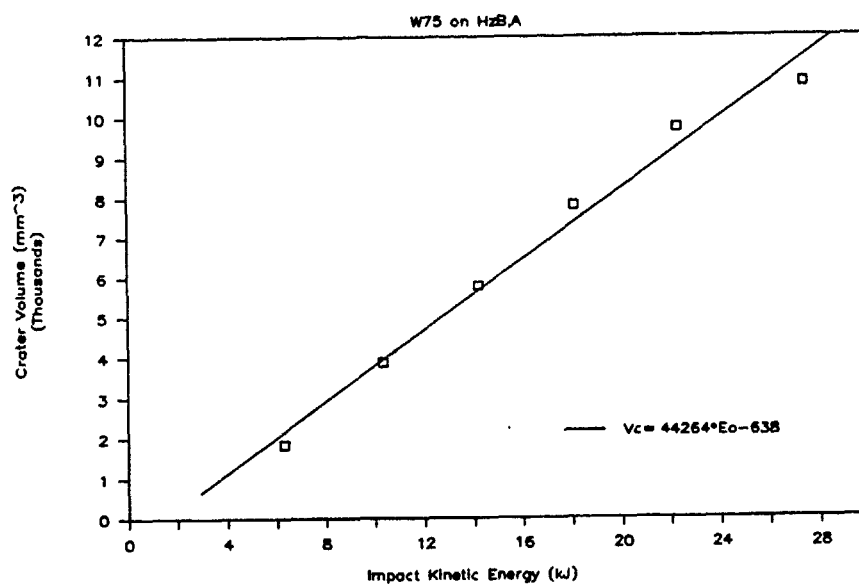


Figure 40b. Crater Volume vs. Impact Kinetic Energy

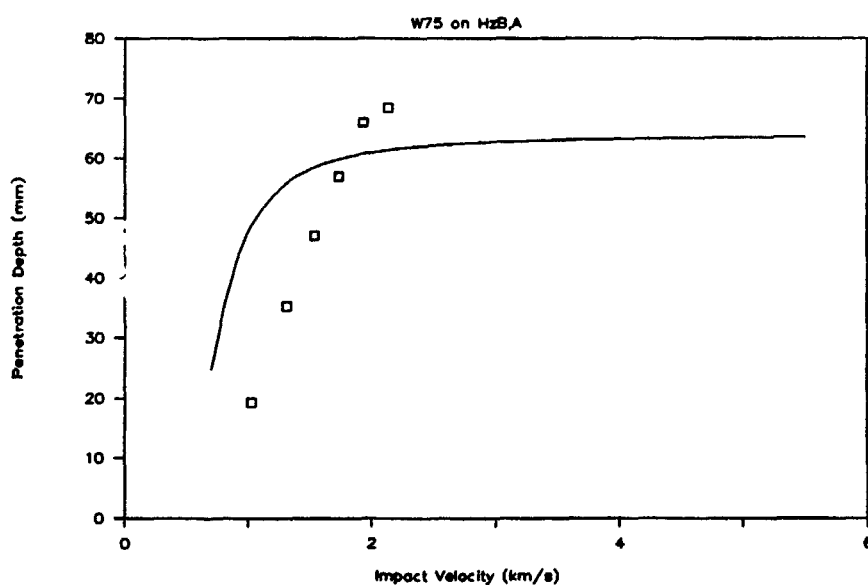


Figure 40c. Penetration Depth vs. Impact Velocity

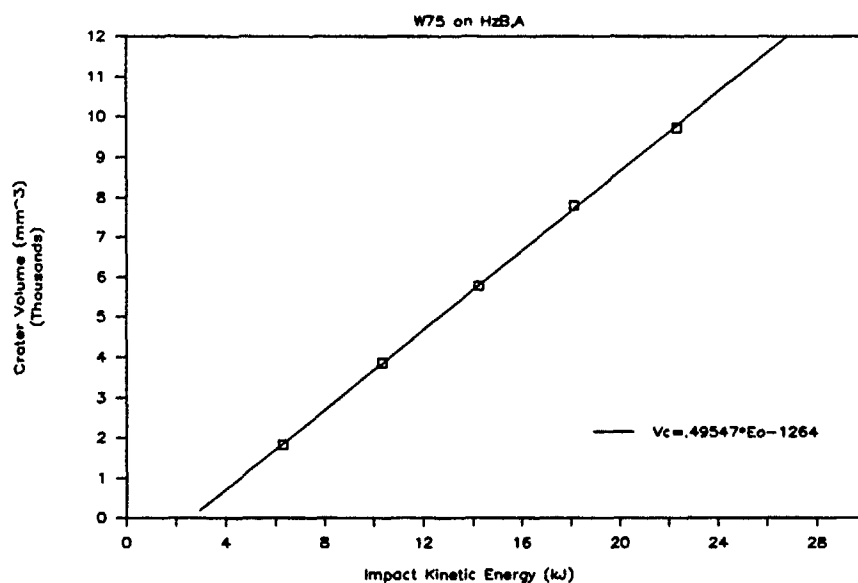


Figure 40d. Crater Volume vs. Impact Kinetic Energy

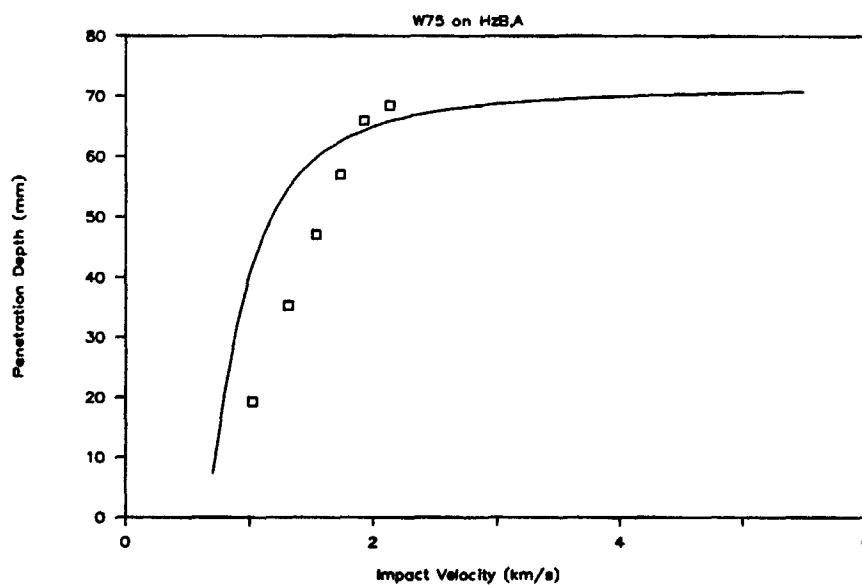


Figure 40e. Penetration Depth vs. Impact Velocity

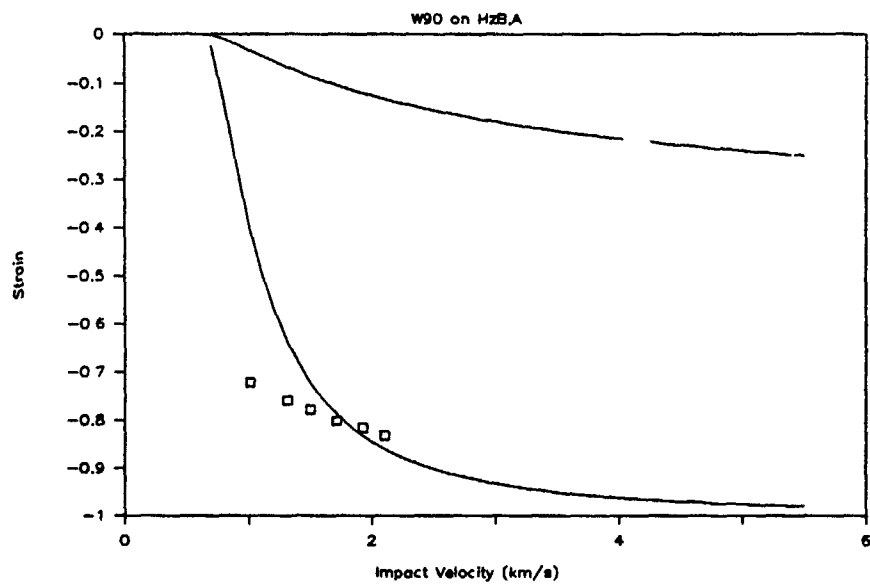


Figure 41a. Strain vs. Impact Velocity

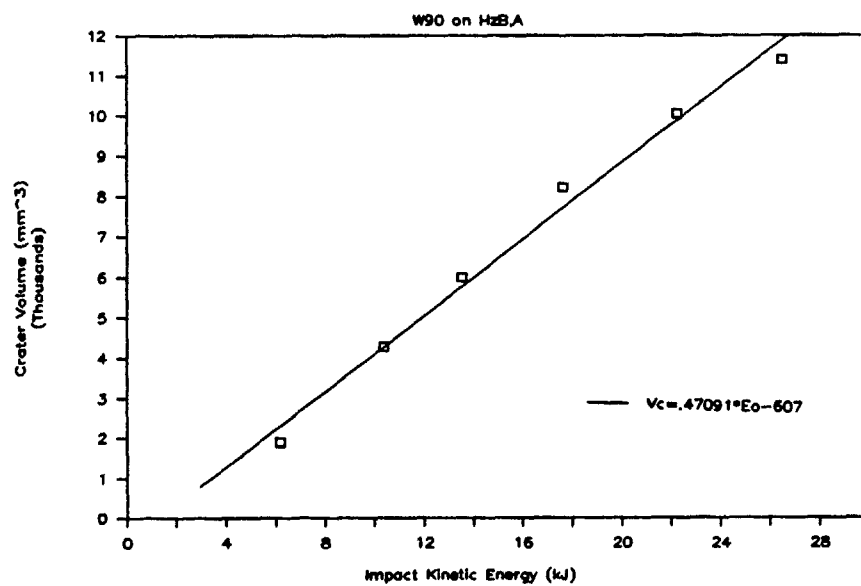


Figure 41b. Crater Volume vs. Impact Kinetic Energy

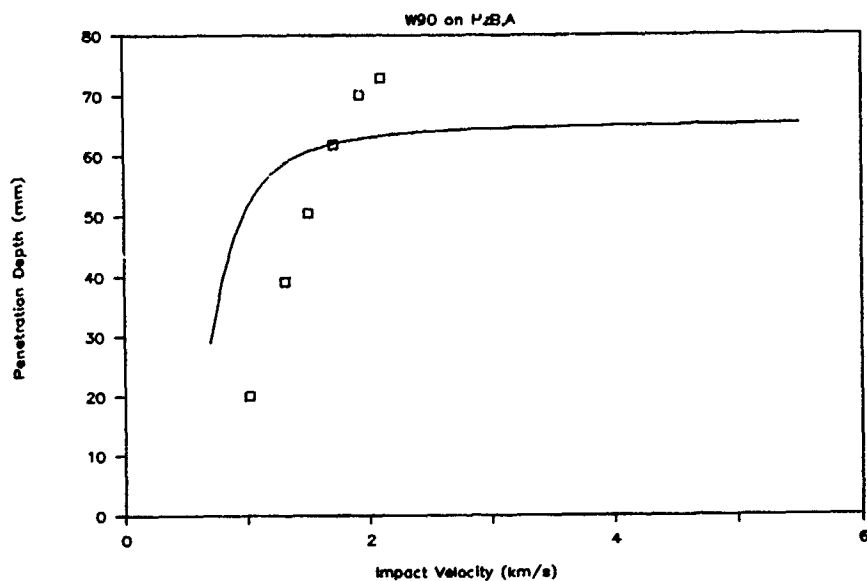


Figure 41c. Penetration Depth vs. Impact Velocity

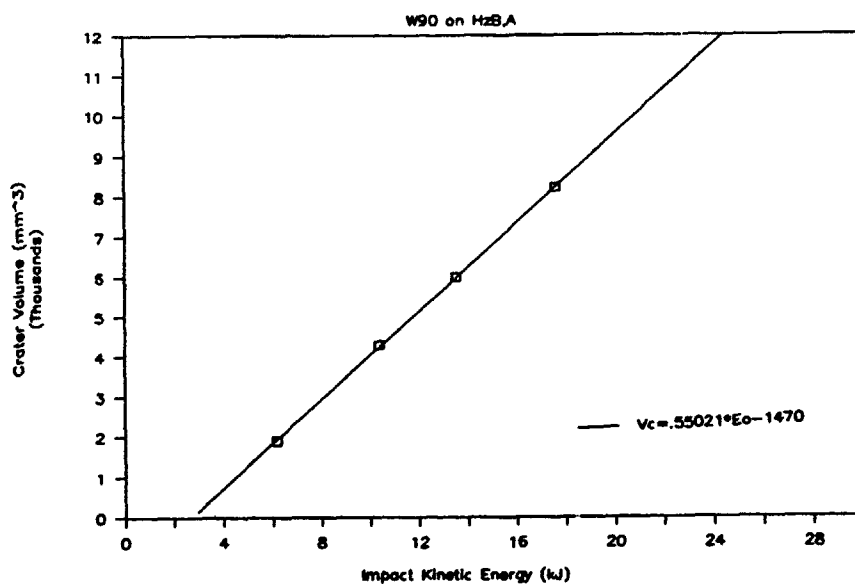


Figure 41d. Crater Volume vs. Impact Kinetic Energy

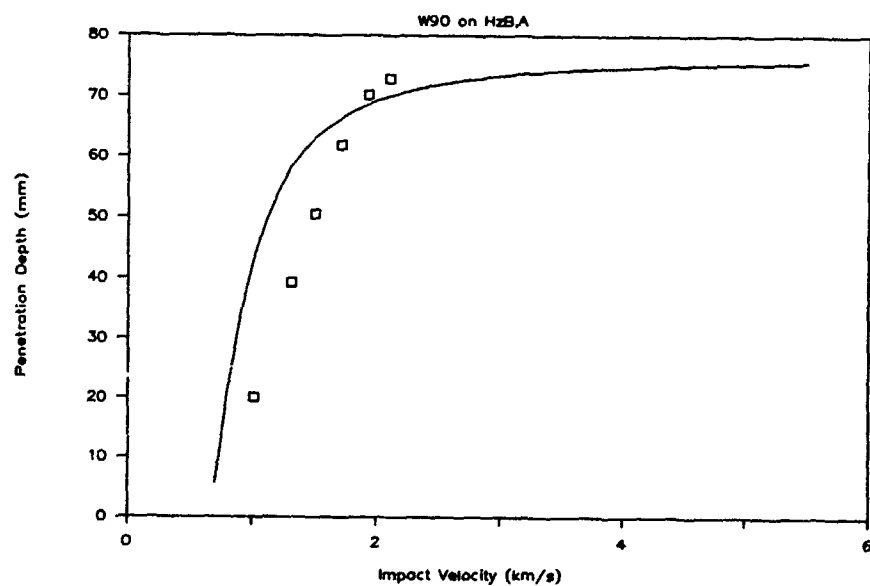


Figure 41e. Penetration Depth vs. Impact Velocity

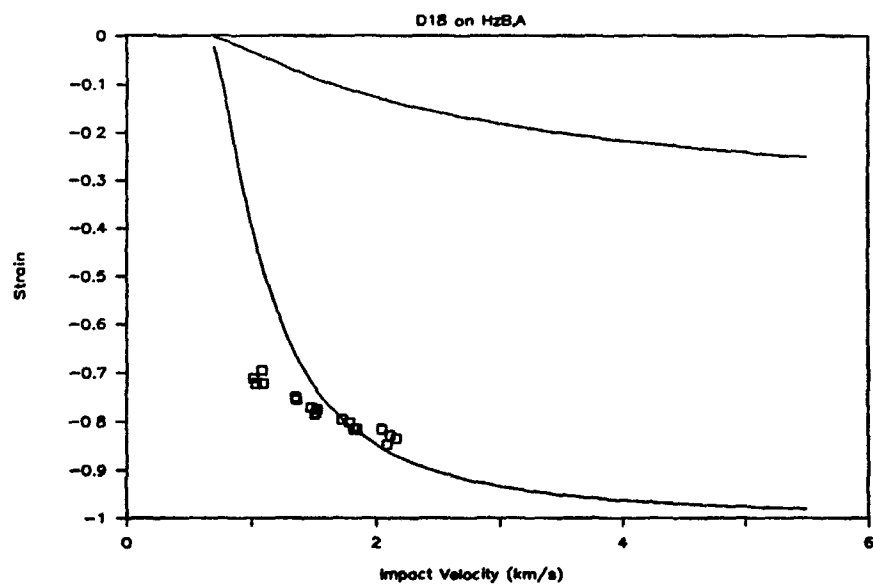


Figure 42a. Strain vs. Impact Velocity

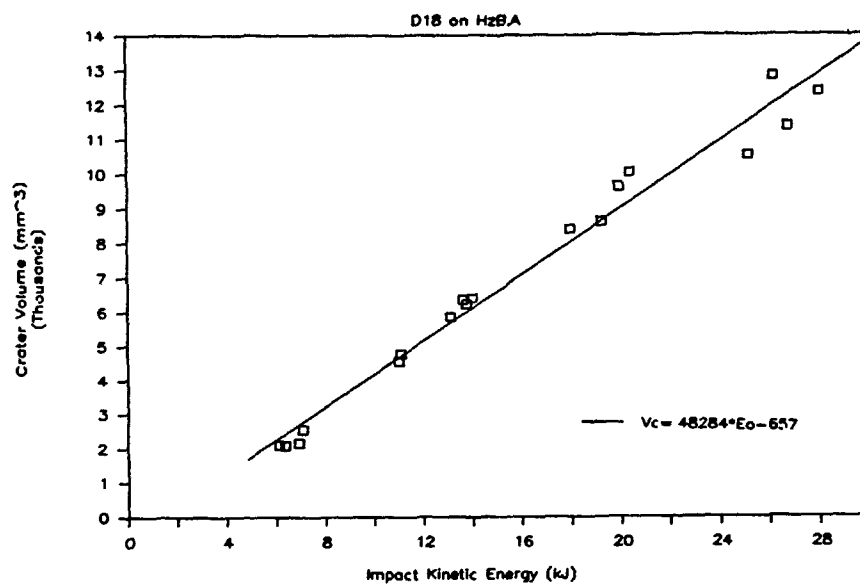


Figure 42b. Crater Volume vs. Impact Kinetic Energy

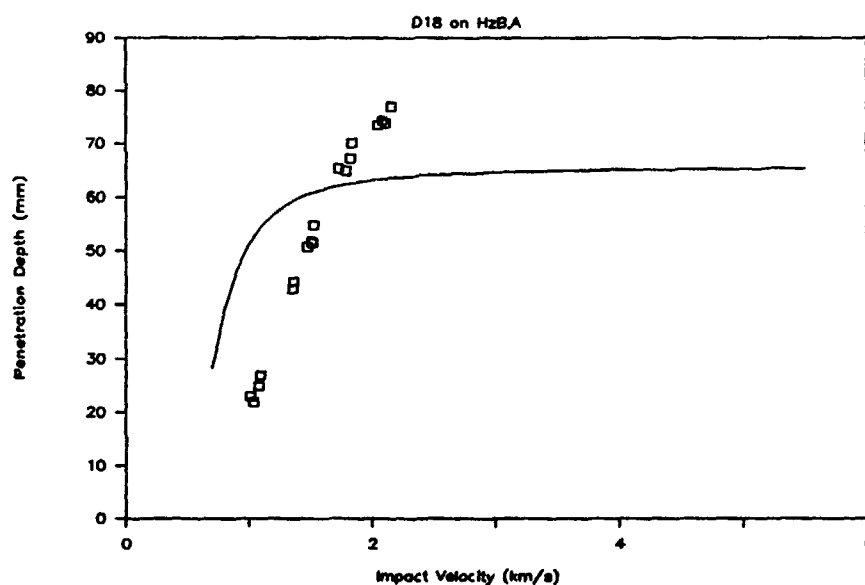


Figure 42c. Penetration Depth vs. Impact Velocity

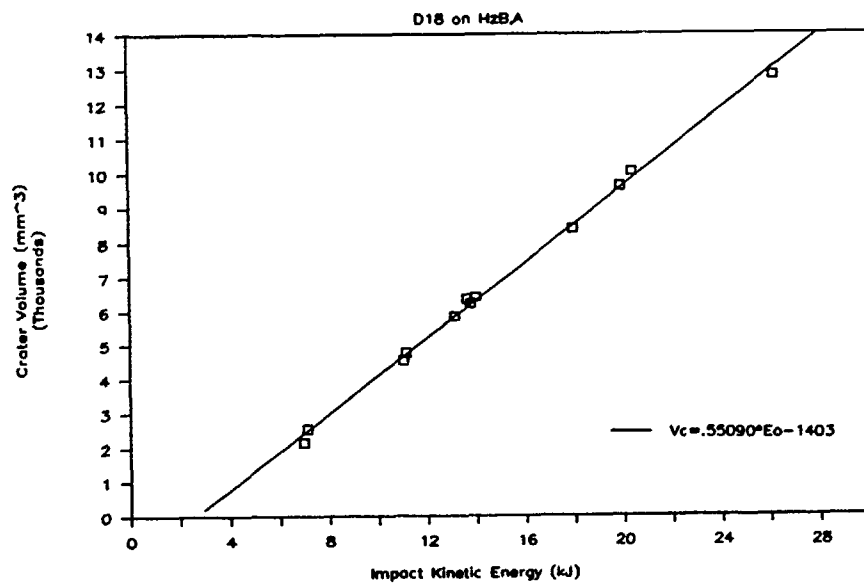


Figure 42d. Crater Volume vs. Impact Kinetic Energy

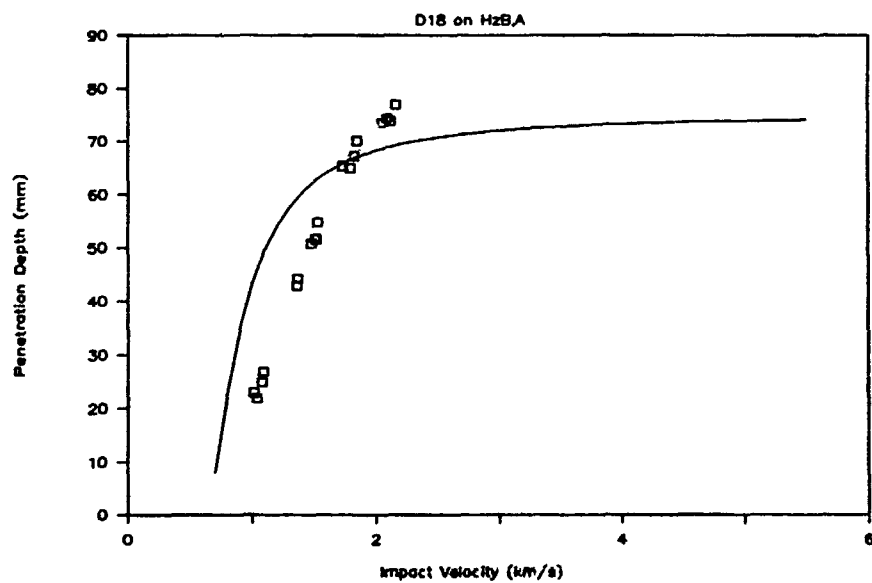


Figure 42e. Penetration Depth vs. Impact Velocity

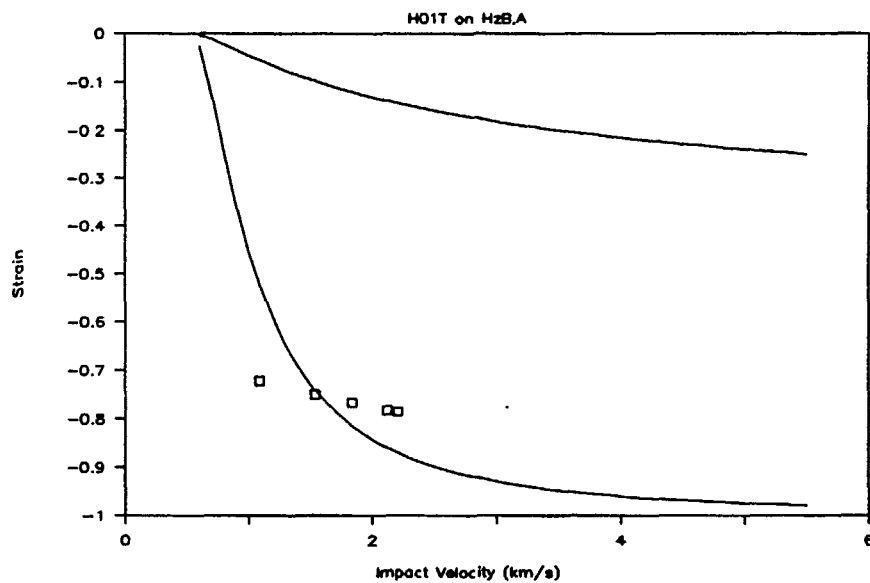


Figure 43a. Strain vs. Impact Velocity

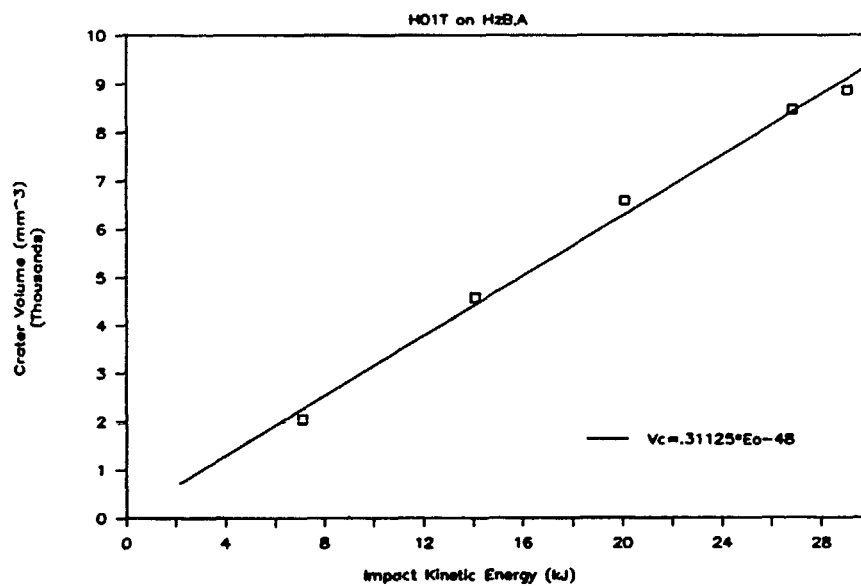


Figure 43b. Crater Volume vs. Impact Kinetic Energy

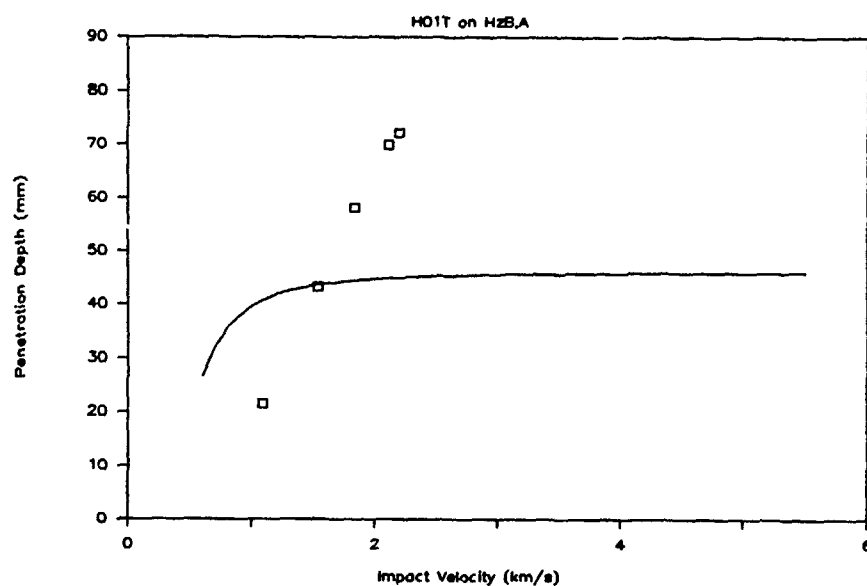


Figure 43c. Penetration Depth vs. Impact Velocity

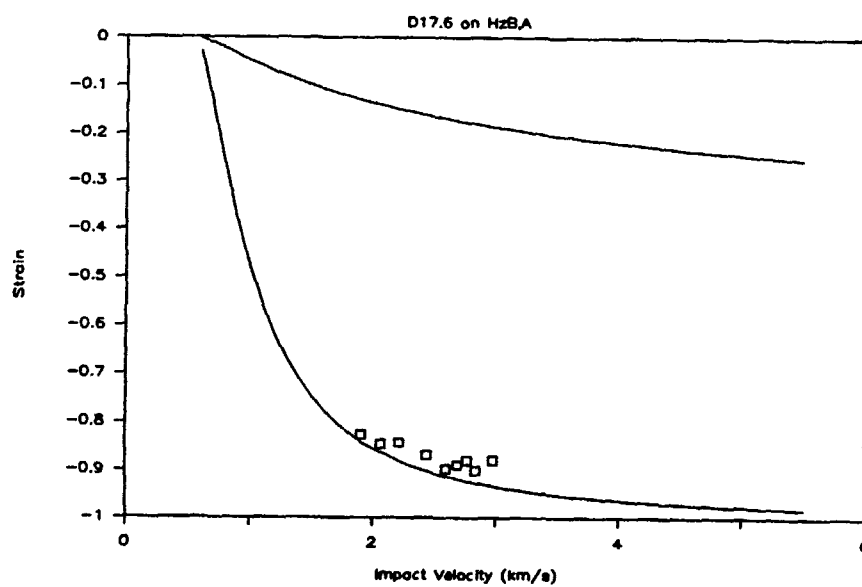


Figure 44a. Strain vs. Impact Velocity

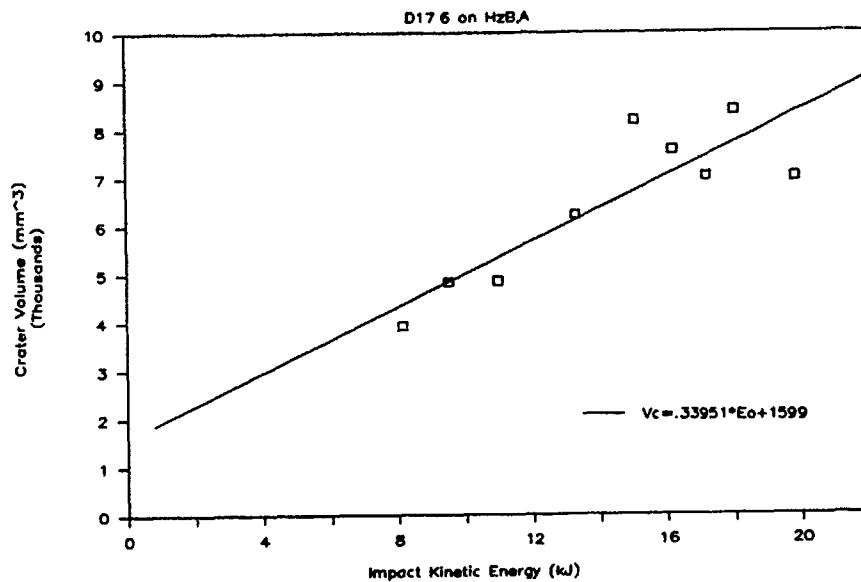


Figure 44b. Crater Volume vs. Impact Kinetic Energy

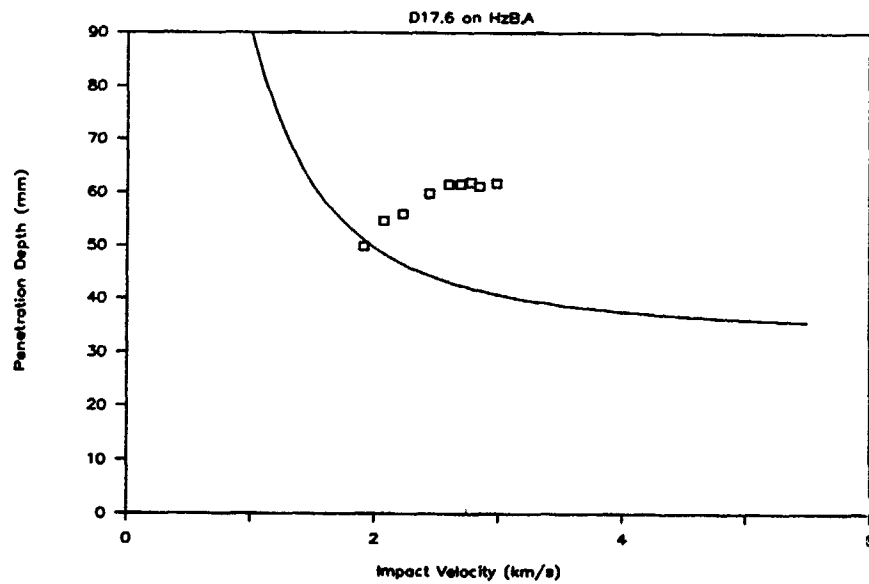


Figure 44c. Penetration Depth vs. Impact Velocity

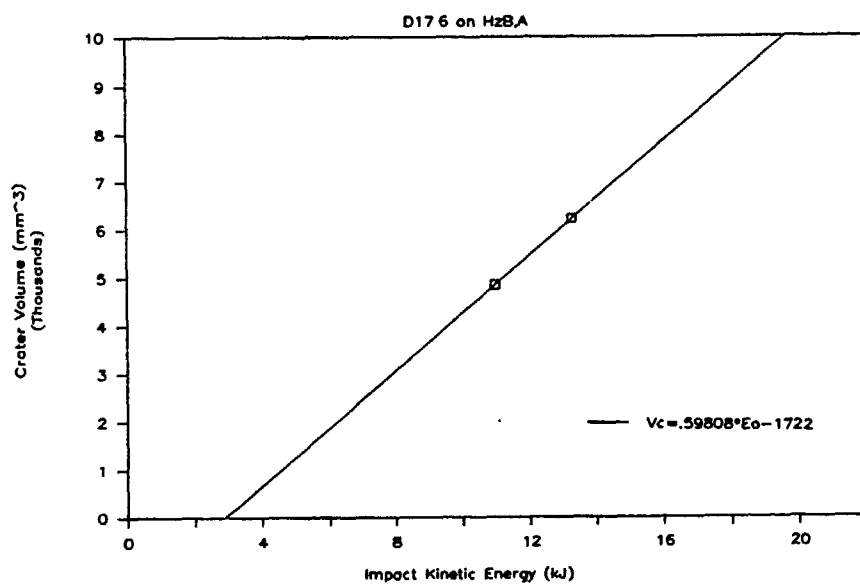


Figure 44d. Crater Volume vs. Impact Kinetic Energy

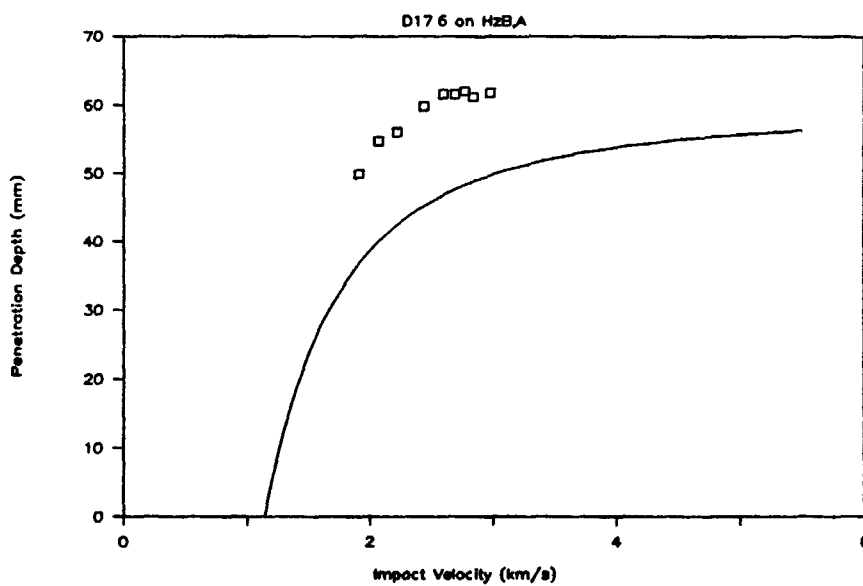


Figure 44e. Penetration Depth vs. Impact Velocity

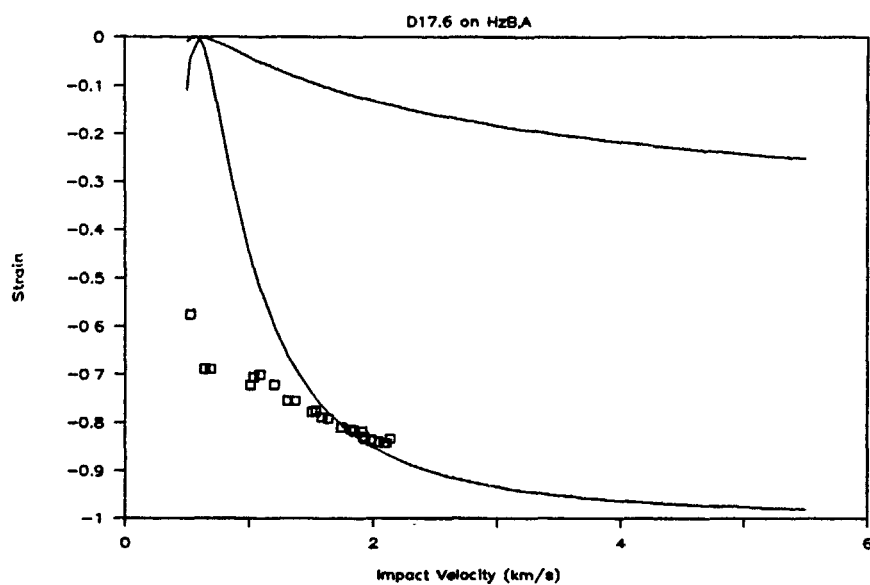


Figure 45a. Strain vs. Impact Velocity

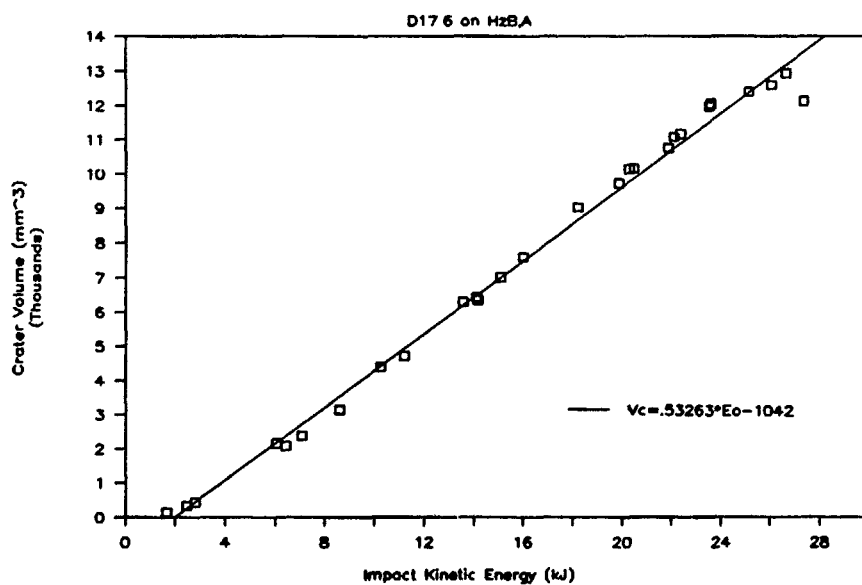


Figure 45b. Crater Volume vs. Impact Kinetic Energy

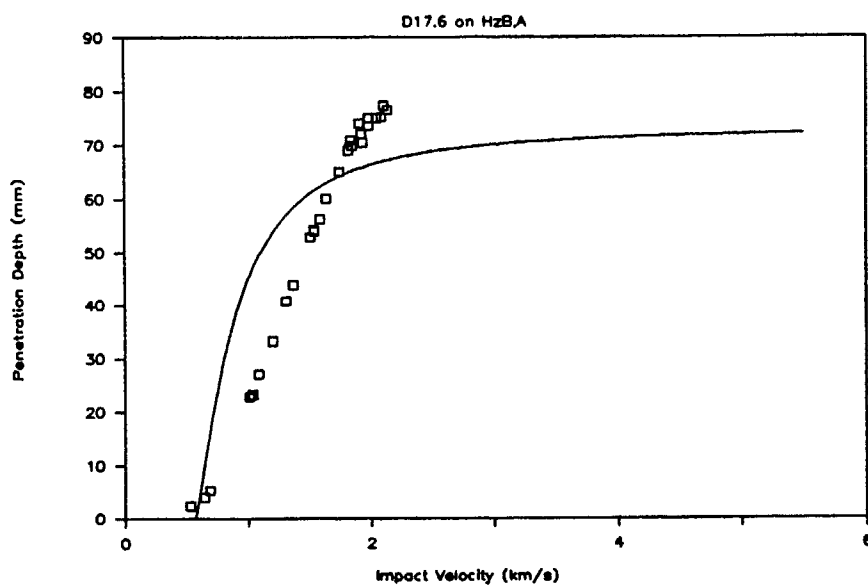


Figure 45c. Penetration Depth vs. Impact Velocity

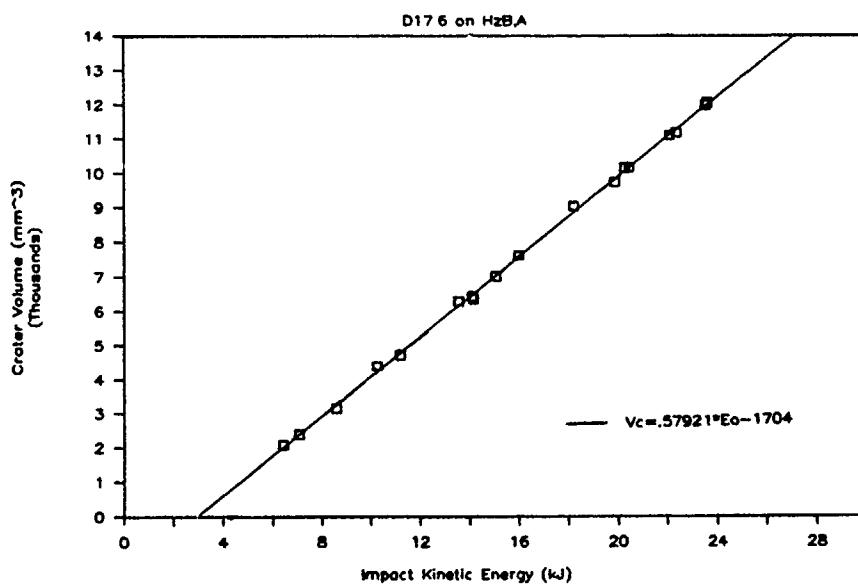


Figure 45d. Crater Volume vs. Impact Kinetic Energy

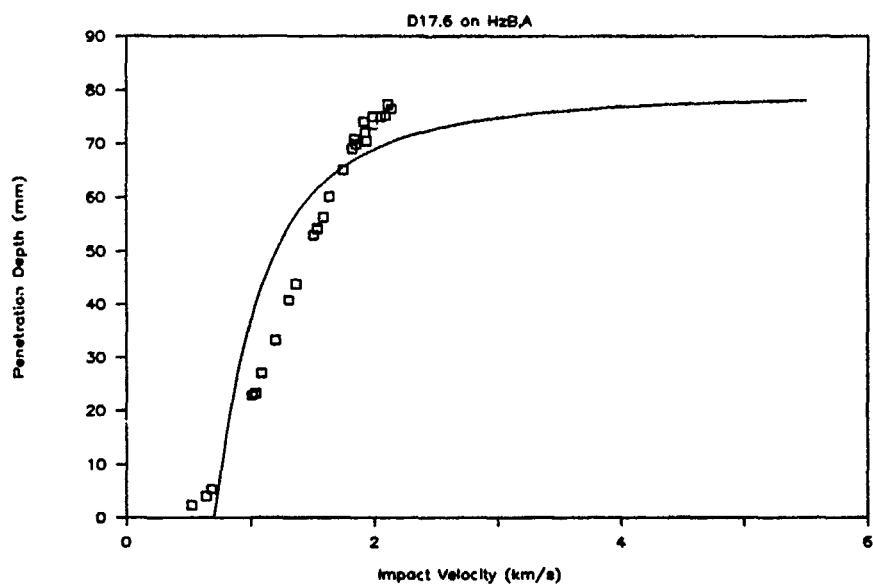


Figure 45e. Penetration Depth vs. Impact Velocity

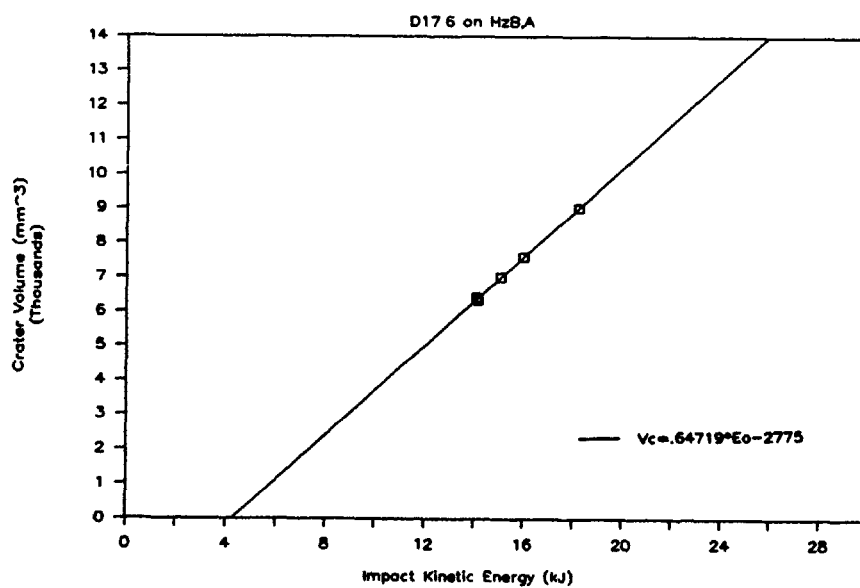


Figure 45f. Crater Volume vs. Impact Kinetic Energy

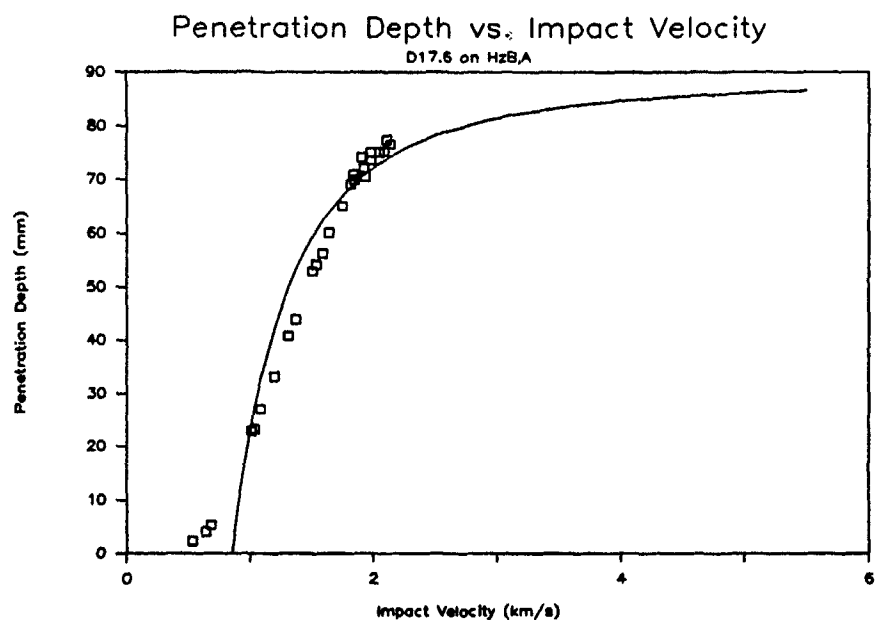


Figure 45g. Penetration Depth vs. Impact Velocity

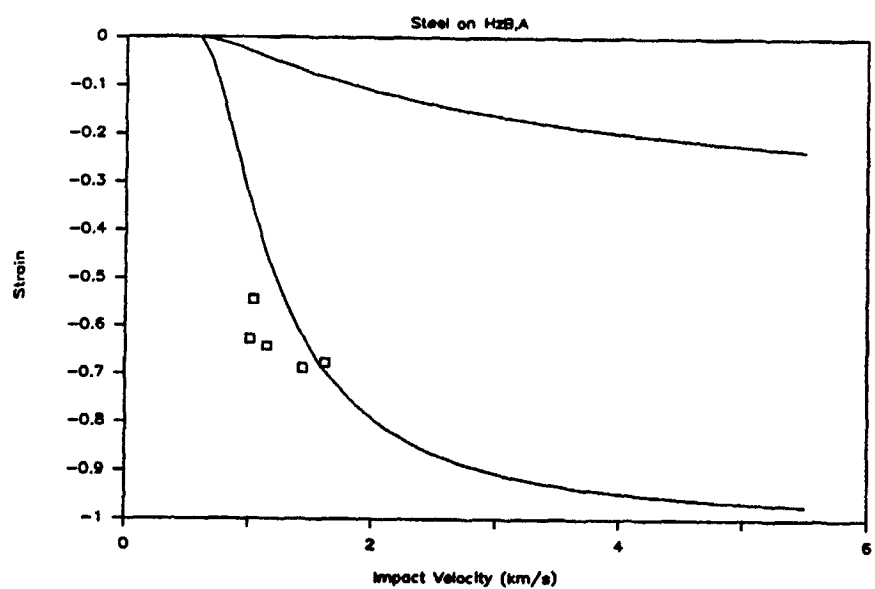


Figure 46a. Strain vs. Impact Velocity

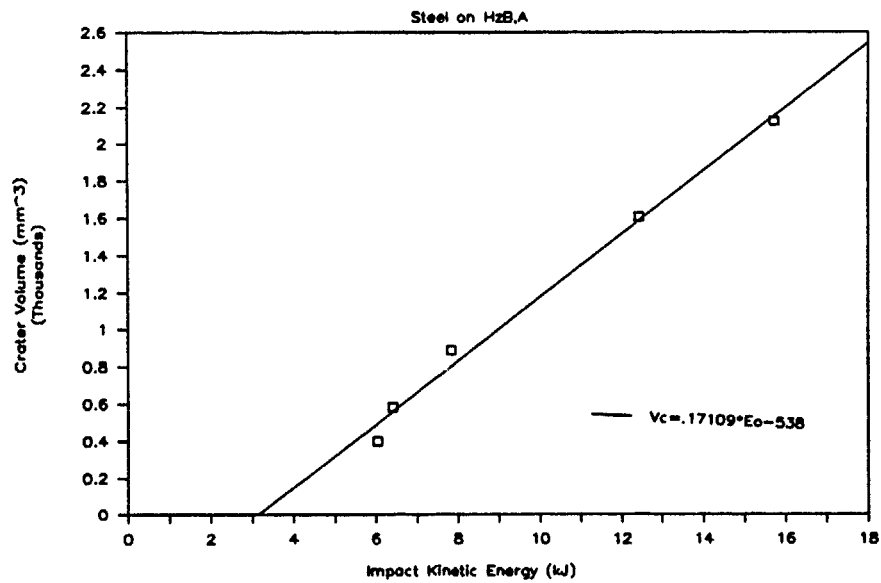


Figure 46b. Crater Volume vs. Impact Kinetic Energy

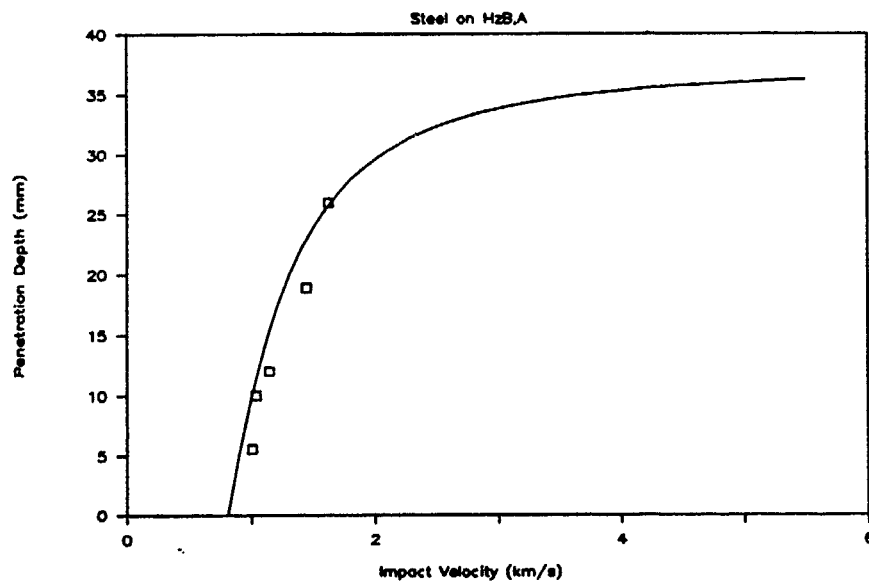


Figure 46c. Penetration Depth vs. Impact Velocity

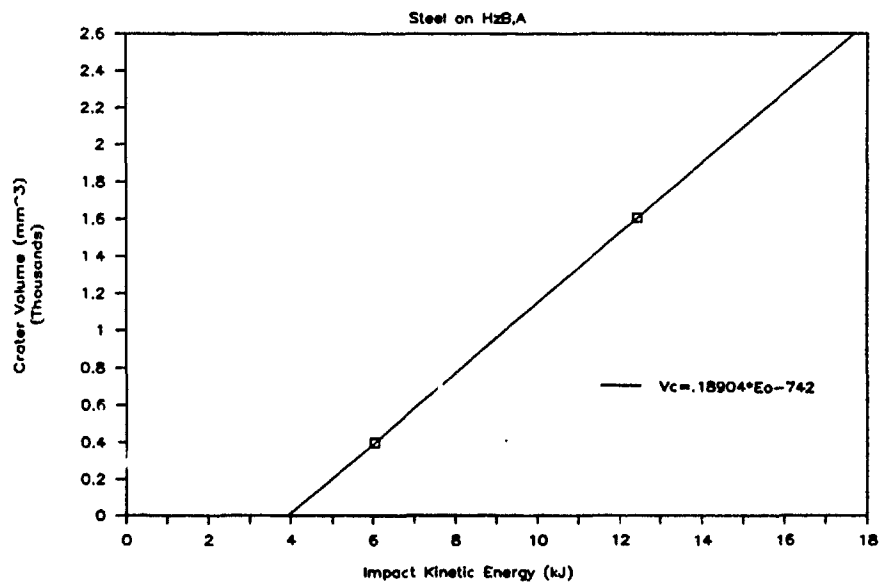


Figure 46d. Crater Volume vs. Impact Kinetic Energy

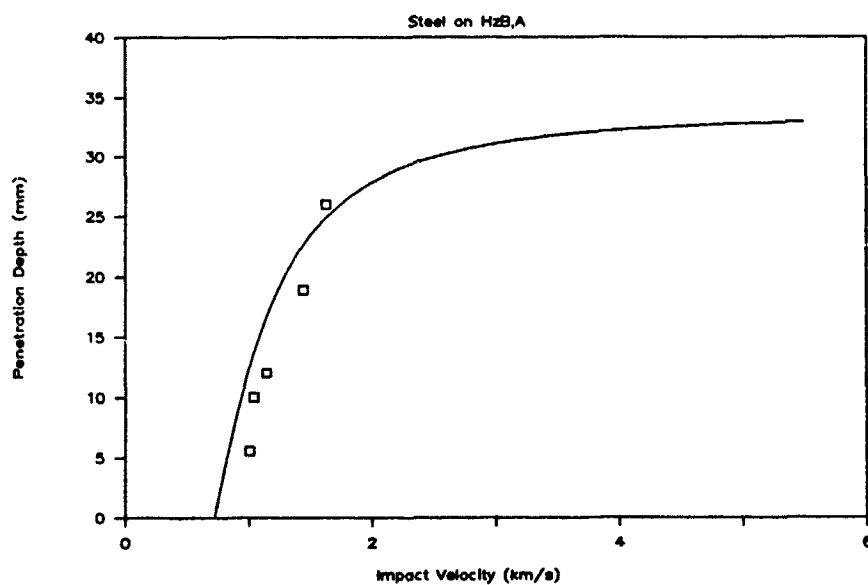


Figure 46e. Penetration Depth vs. Impact Velocity

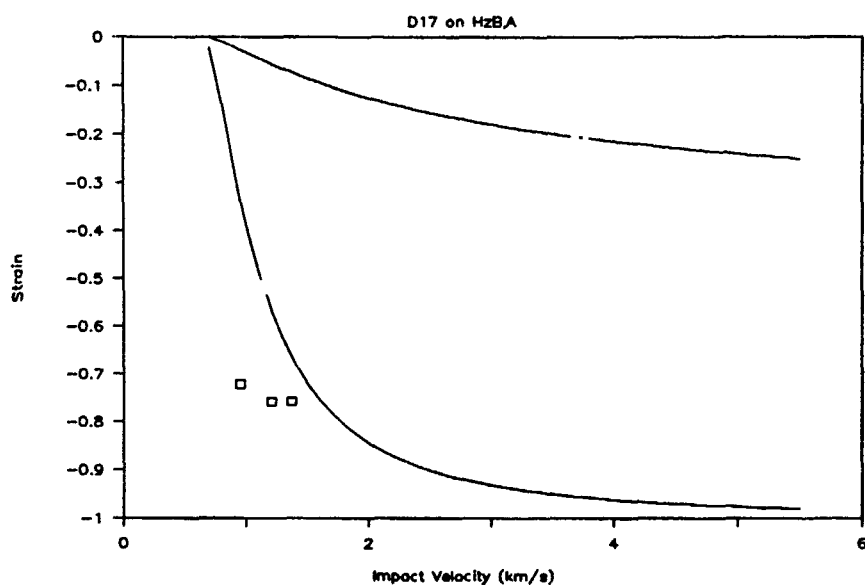


Figure 47a. Strain vs. Impact Velocity

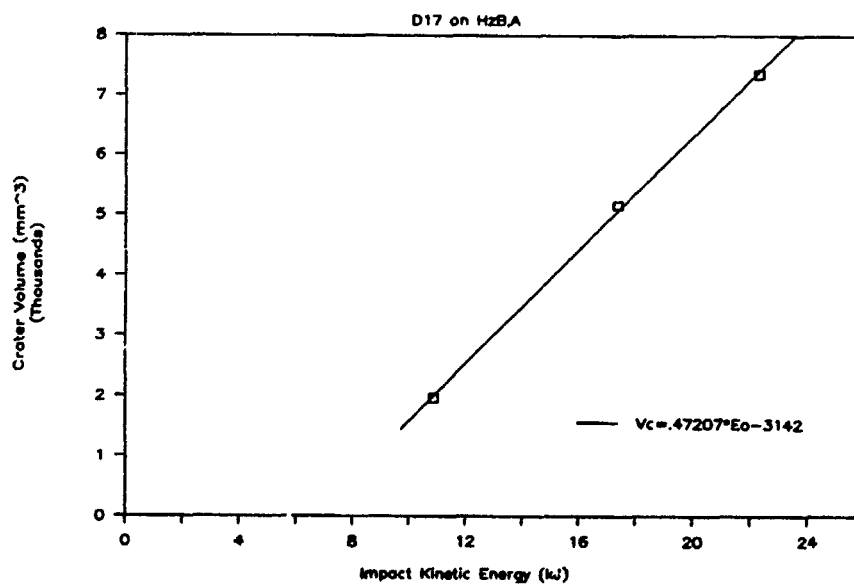


Figure 47b. Crater Volume vs. Impact Kinetic Energy

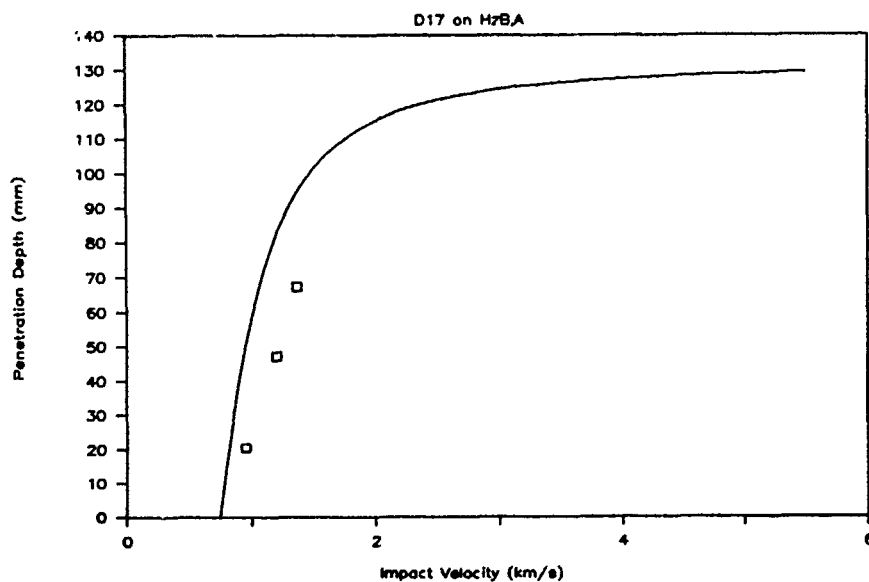


Figure 47c. Penetration Depth vs. Impact Velocity

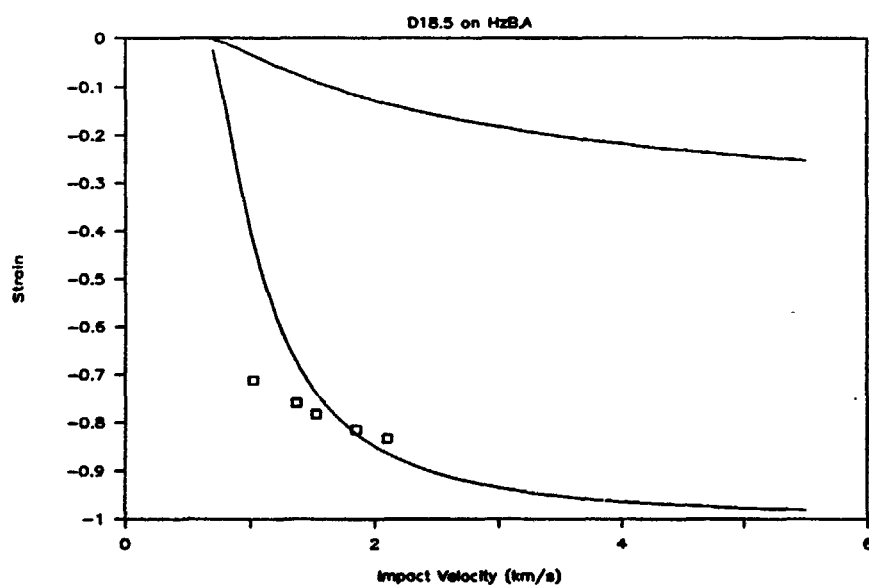


Figure 48a. Strain vs. Impact Velocity

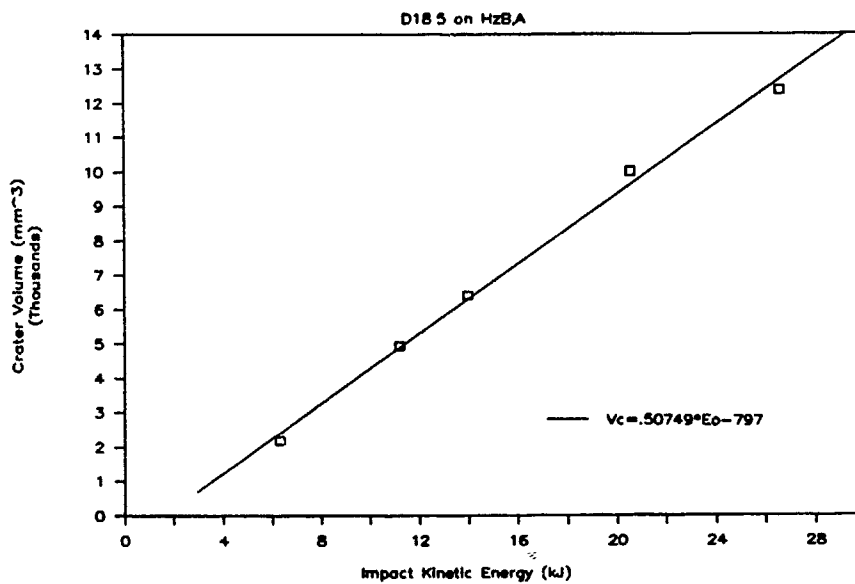


Figure 48b. Crater Volume vs. Impact Kinetic Energy

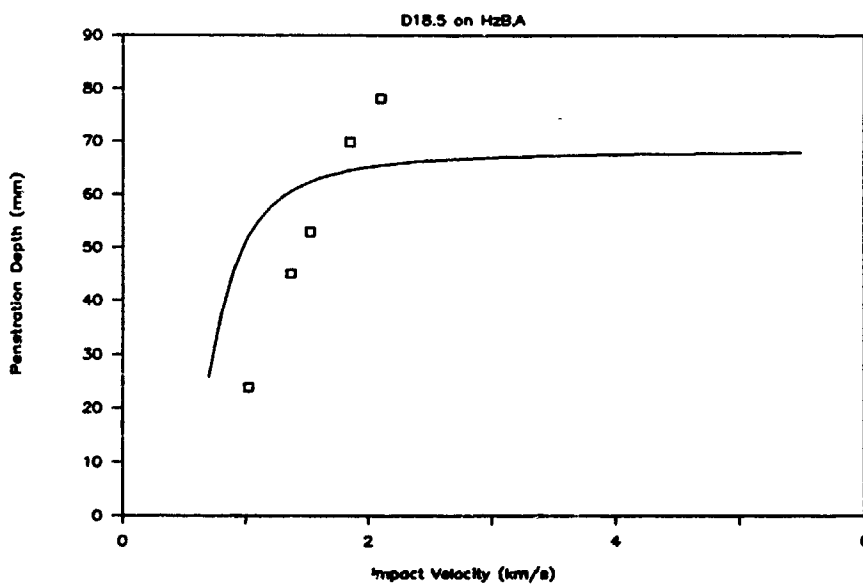


Figure 48c. Penetration Depth vs. Impact Velocity

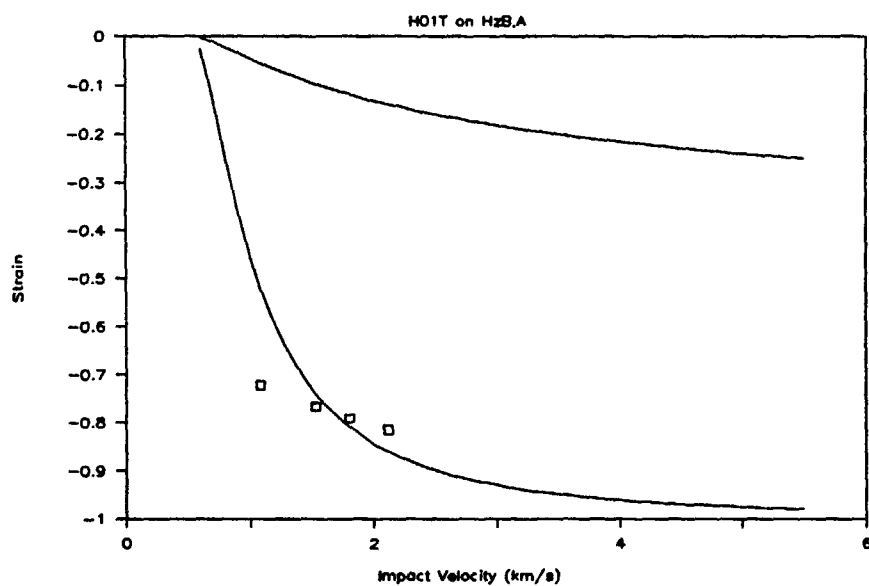


Figure 49a. Strain vs. Impact Velocity

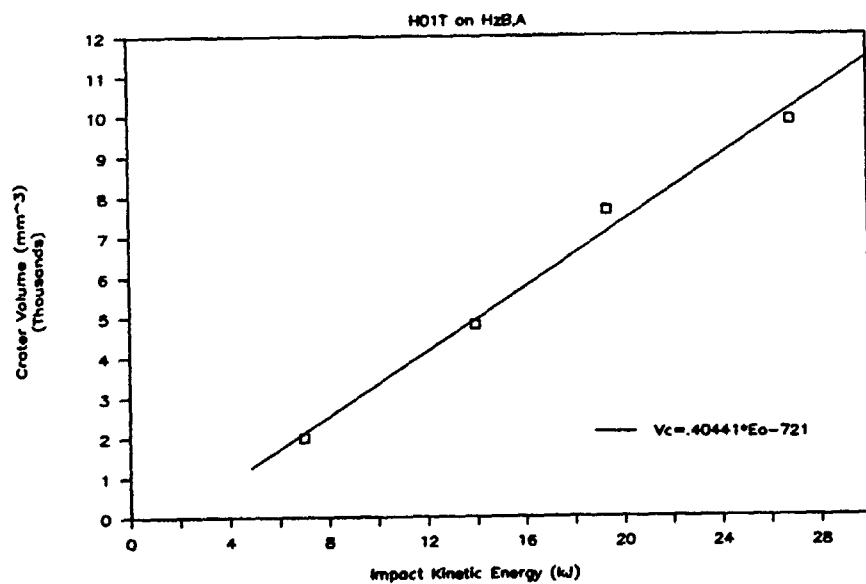


Figure 49b. Crater Volume vs. Impact Kinetic Energy

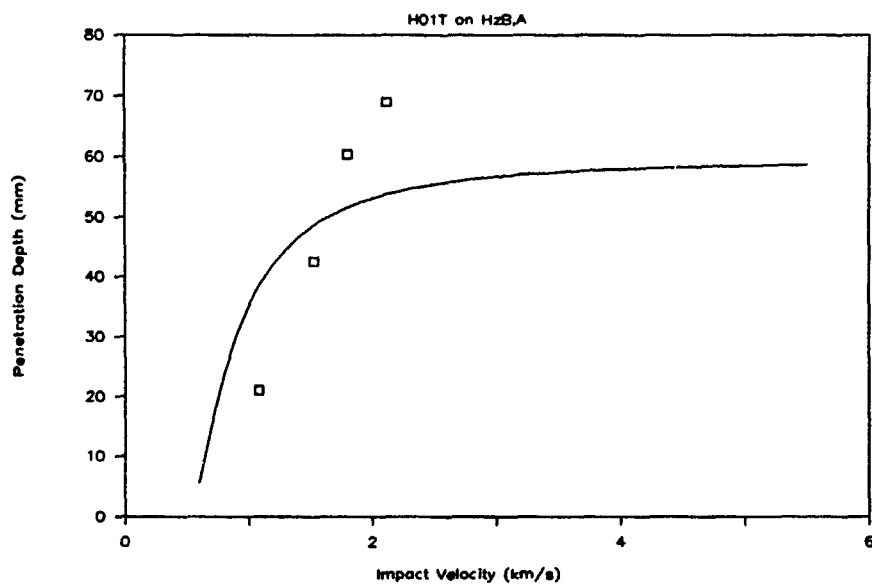


Figure 49c. Penetration Depth vs. Impact Velocity

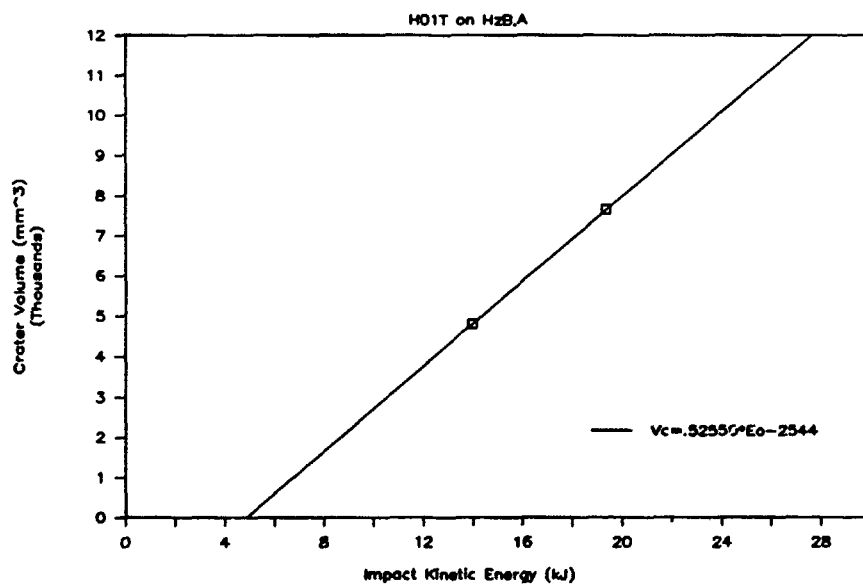


Figure 49d. Crater Volume vs. Impact Kinetic Energy

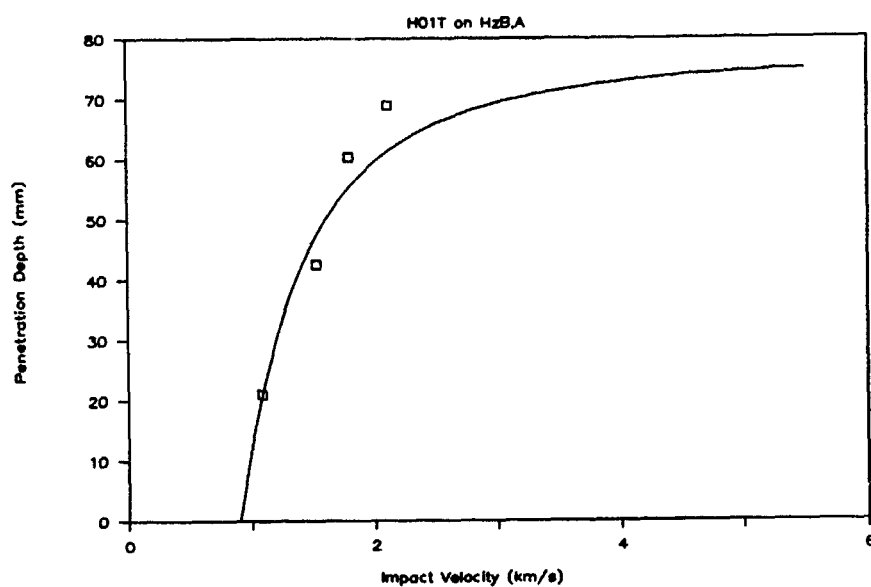


Figure 49e. Penetration Depth vs. Impact Velocity

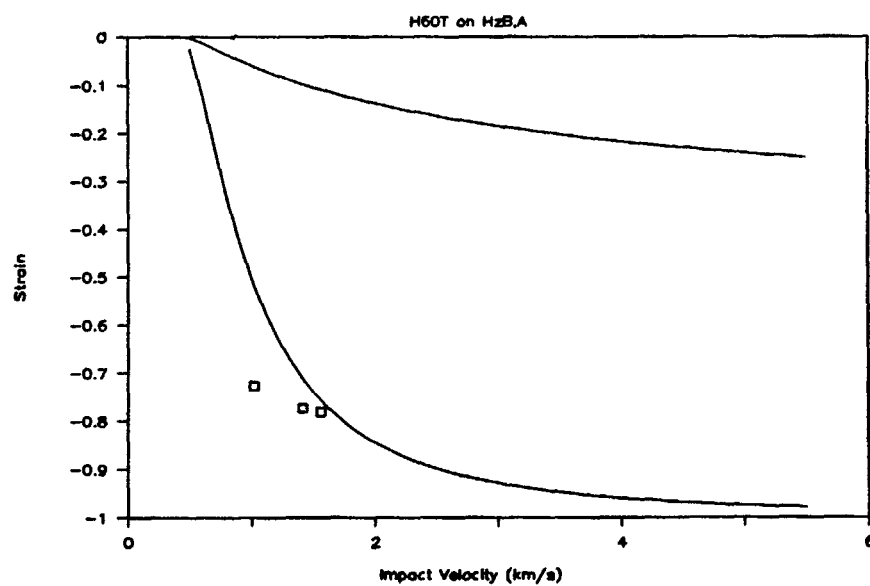


Figure 50a. Strain vs. Impact Velocity

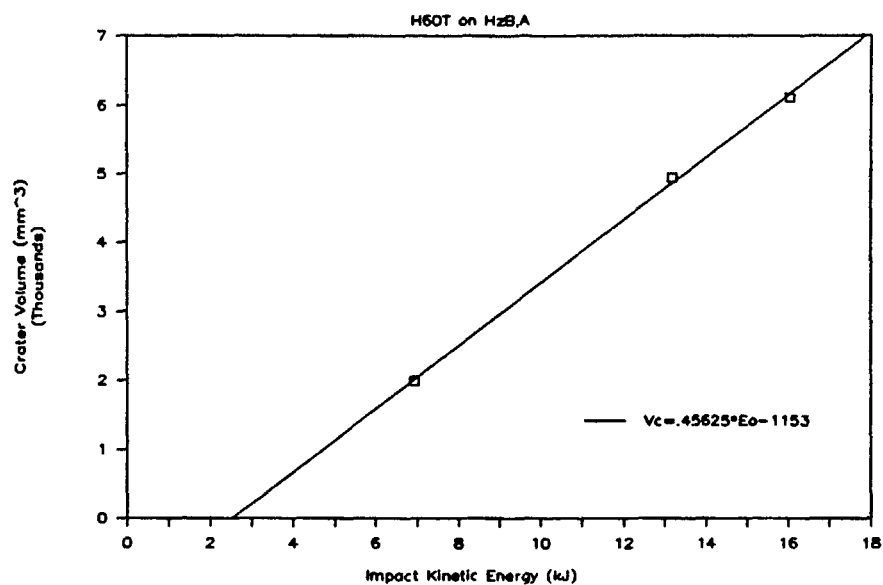


Figure 50b. Crater Volume vs. Impact Kinetic Energy

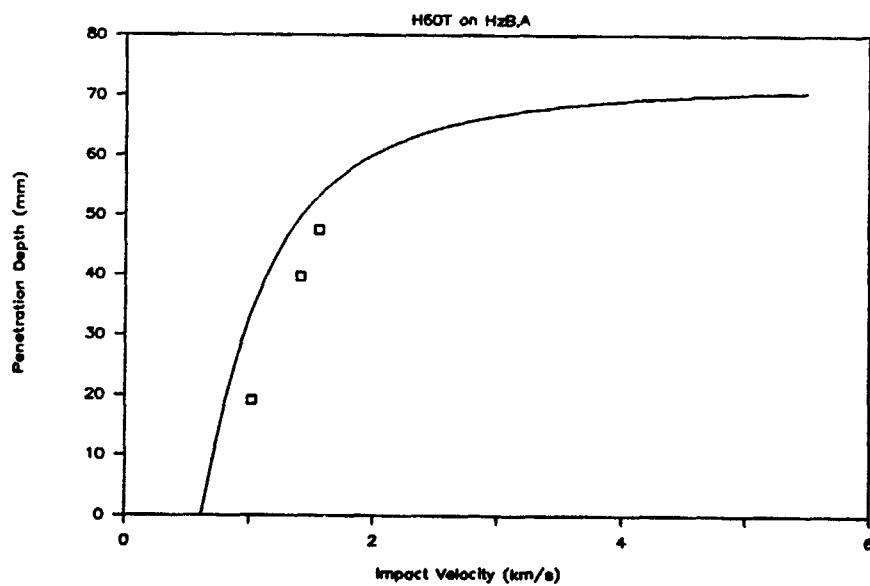


Figure 50c. Penetration Depth vs. Impact Velocity

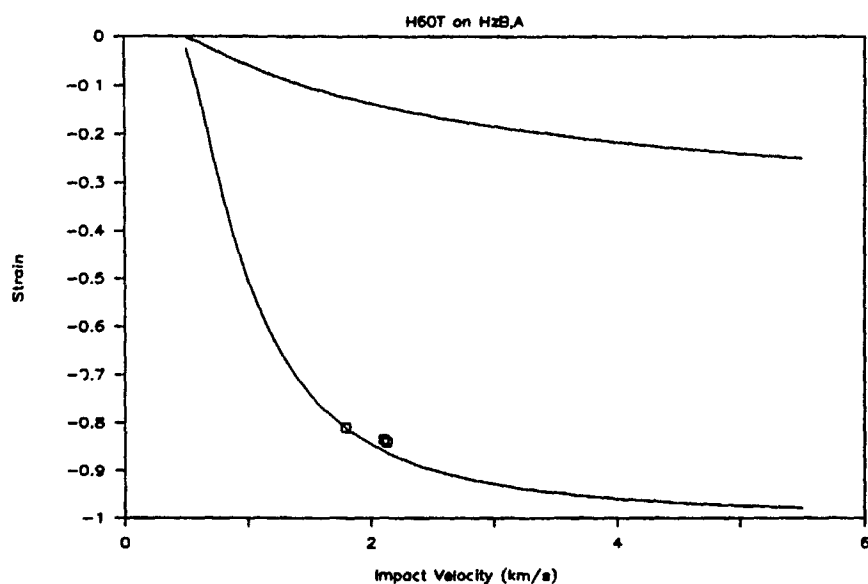


Figure 51a. Strain vs. Impact Velocity

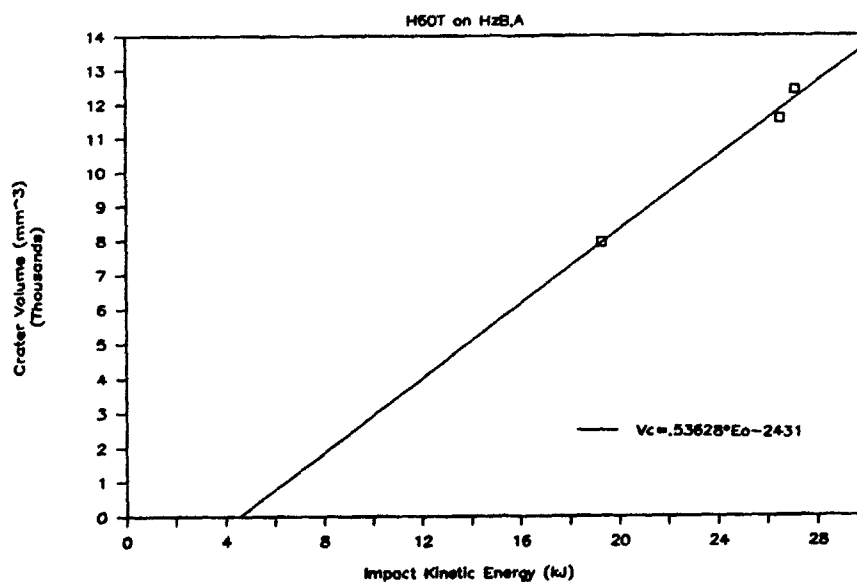


Figure 51b. Crater Volume vs. Impact Kinetic Energy

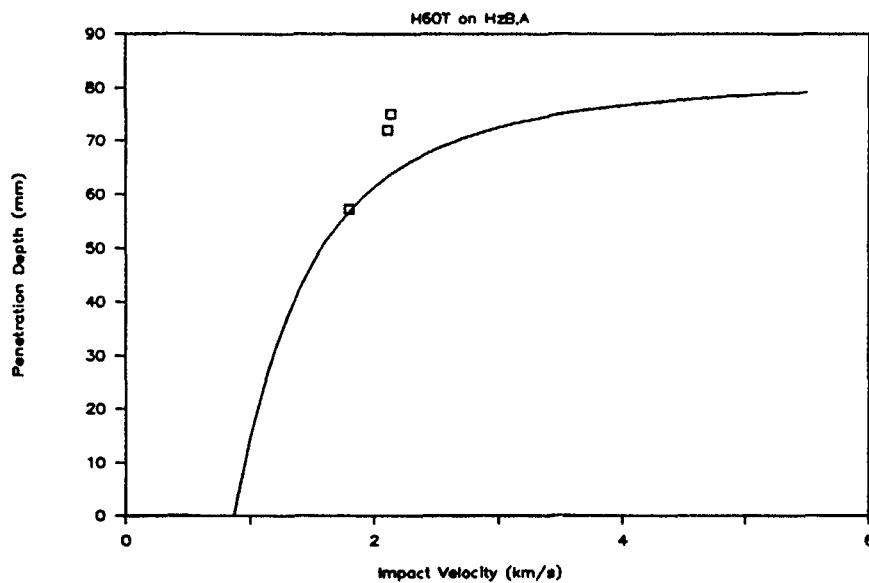


Figure 51c. Penetration Depth vs. Impact Velocity

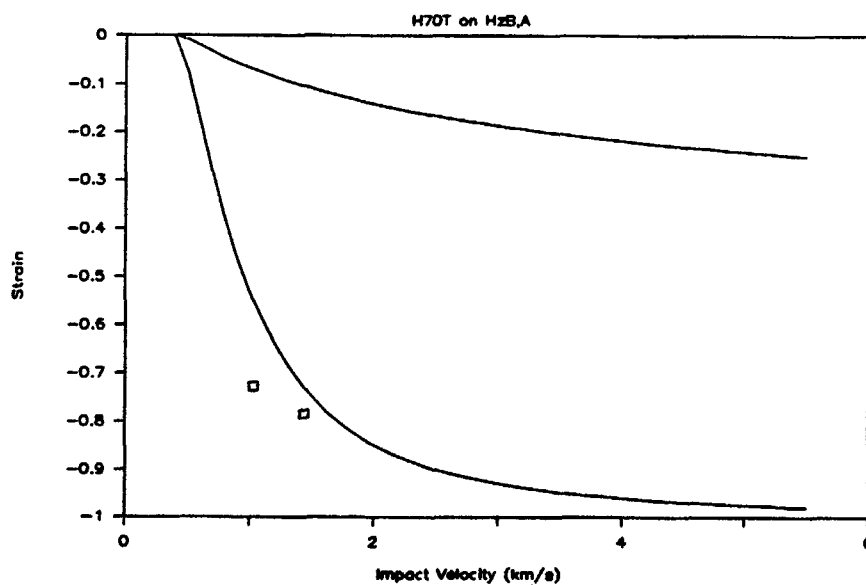


Figure 52a. Strain vs. Impact Velocity

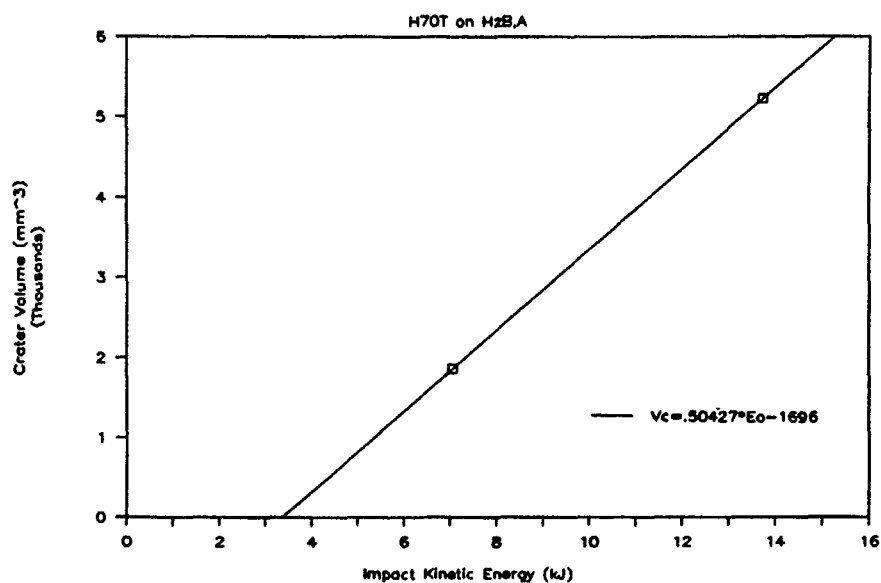


Figure 52b. Crater Volume vs. Impact Kinetic Energy

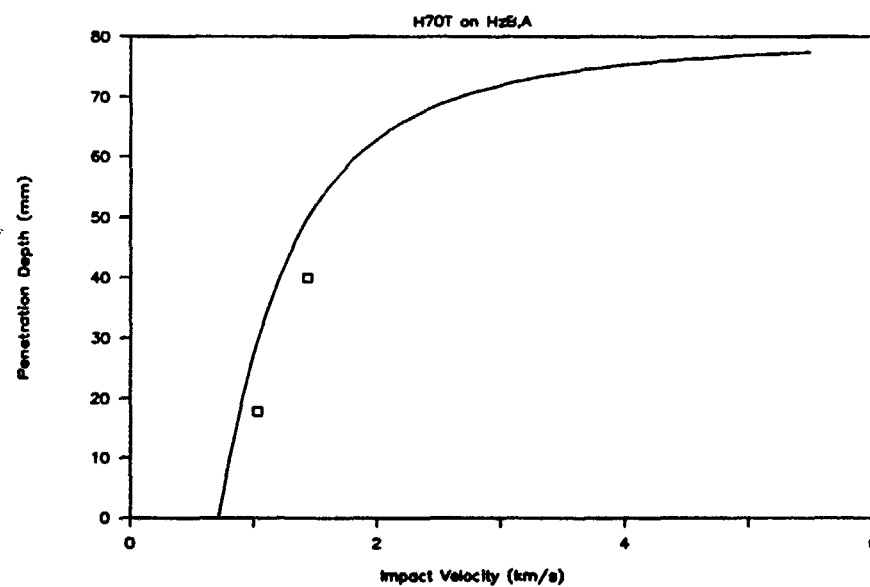


Figure 52c. Penetration Depth vs. Impact Velocity

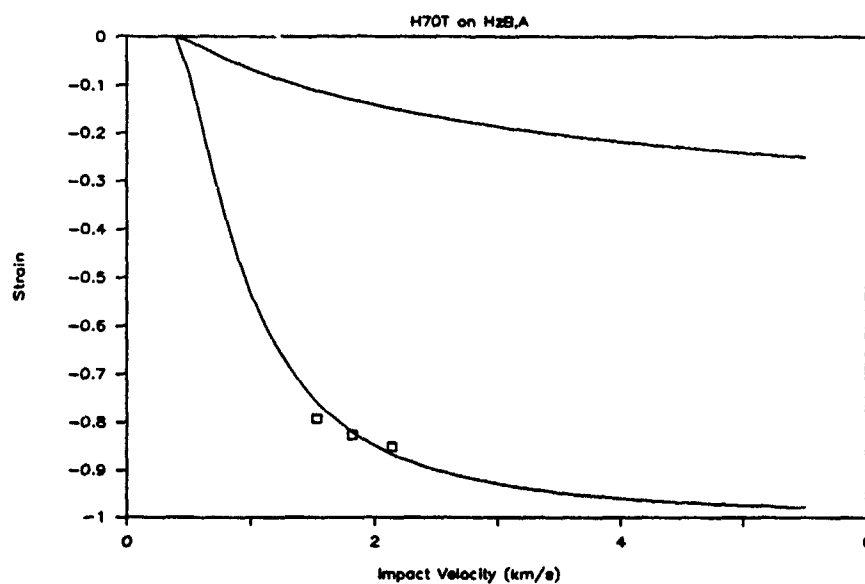


Figure 53a. Strain vs. Impact Velocity

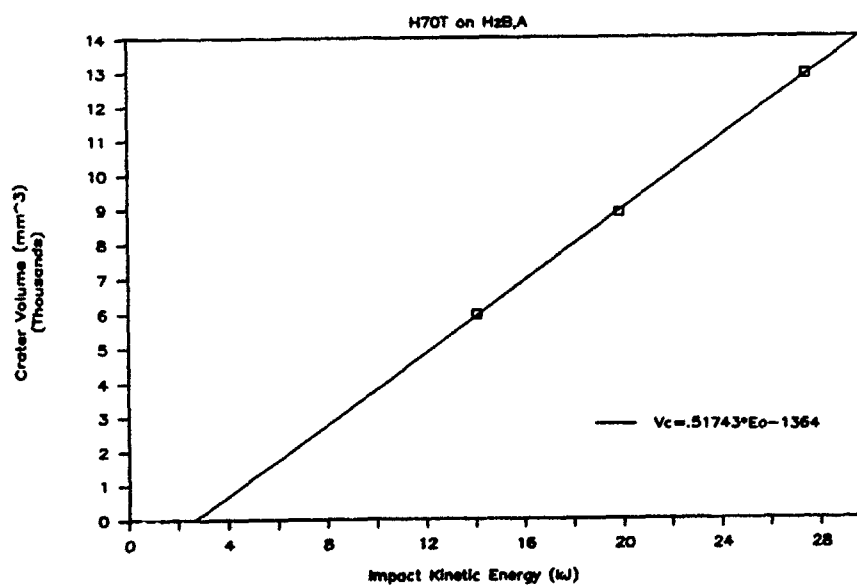


Figure 53b. Crater Volume vs. Impact Kinetic Energy

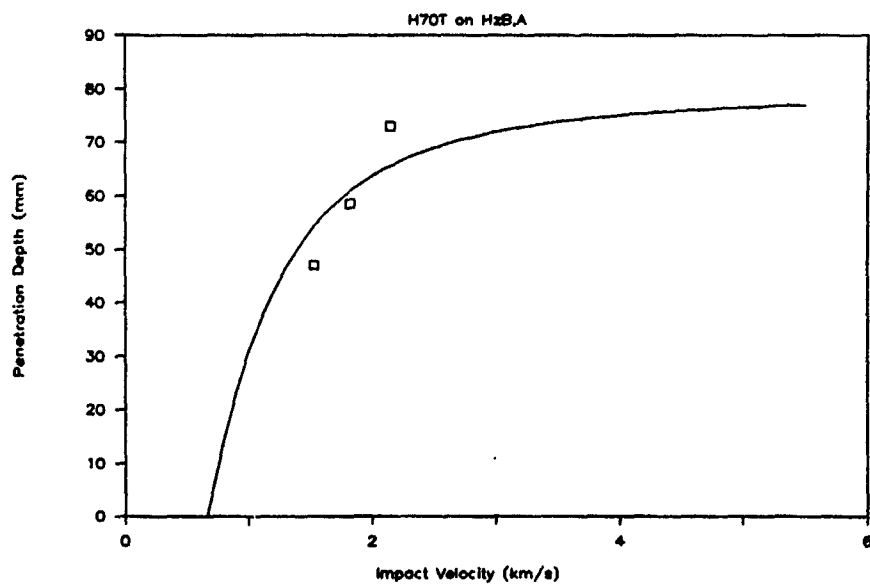


Figure 53c. Penetration Depth vs. Impact Velocity

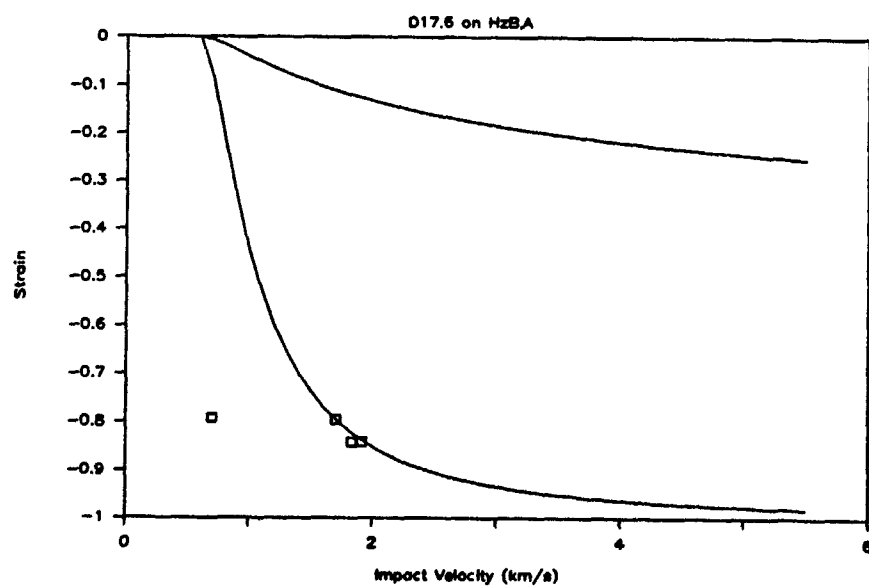


Figure 54a. Strain vs. Impact Velocity

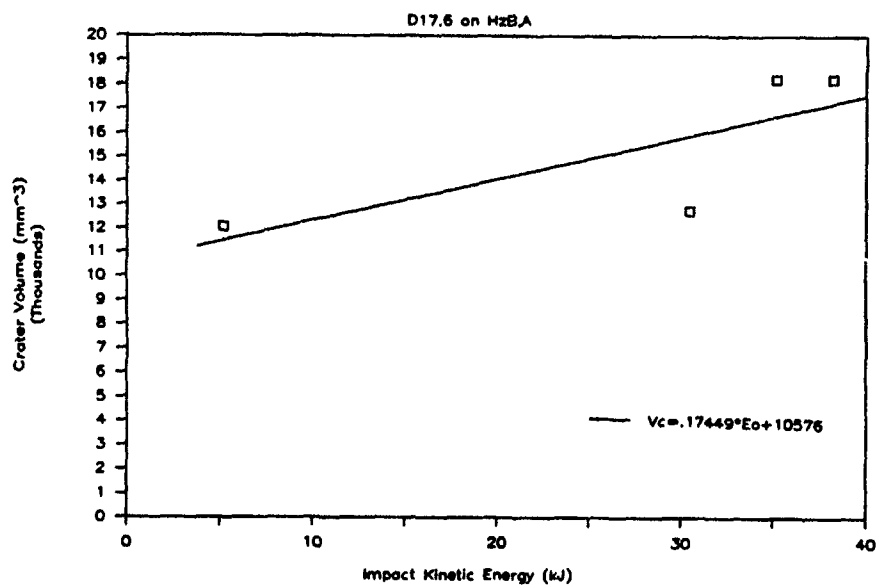


Figure 54b. Crater Volume vs. Impact Kinetic Energy

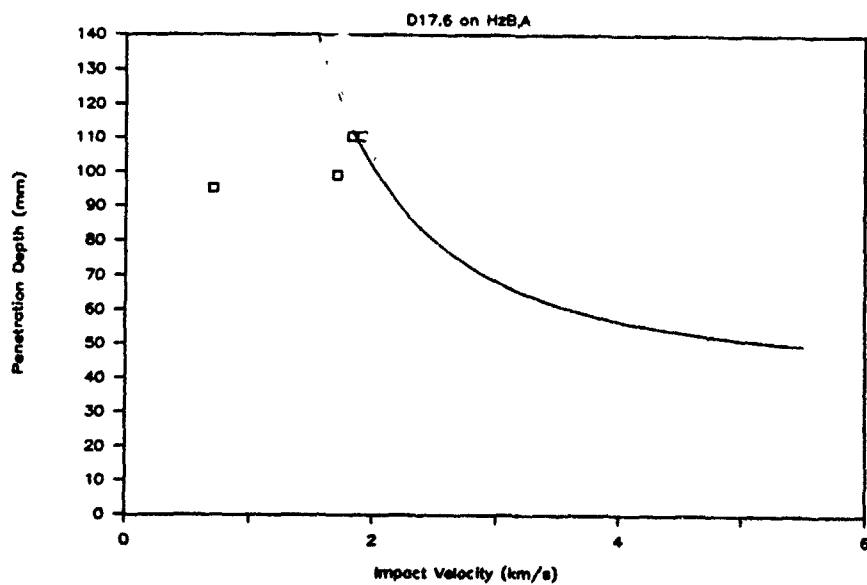


Figure 54c. Penetration Depth vs. Impact Velocity

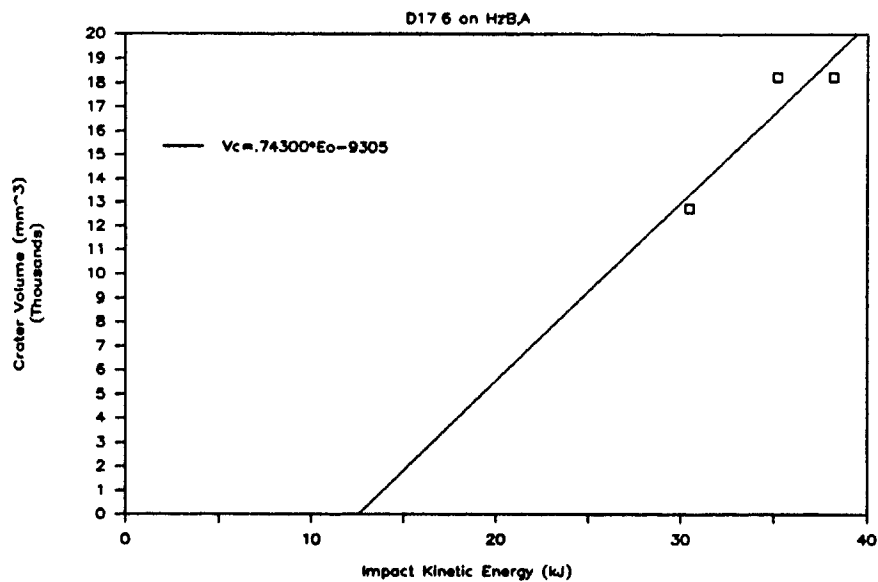


Figure 54d. Crater Volume vs. Impact Kinetic Energy

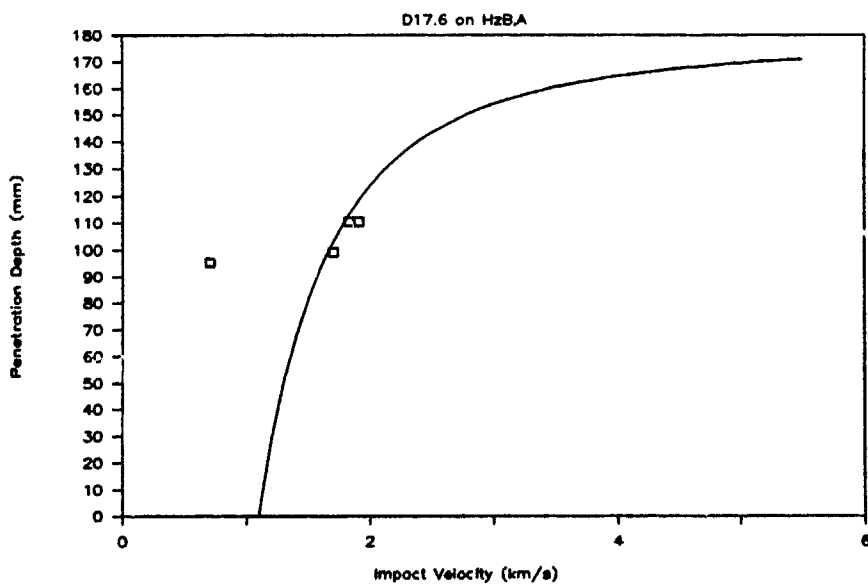


Figure 54e. Penetration Depth vs. Impact Velocity

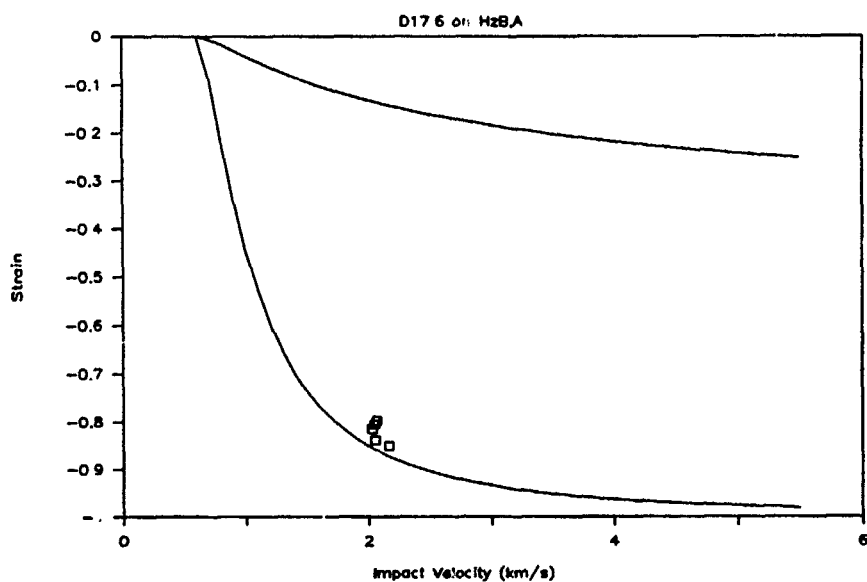


Figure 55a. Strain vs. Impact Velocity

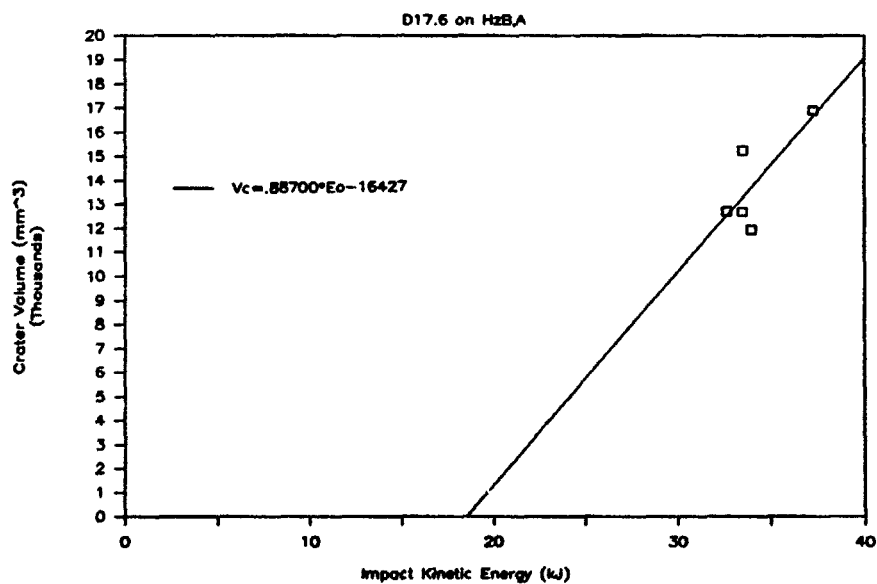


Figure 55b. Crater Volume vs. Impact Kinetic Energy

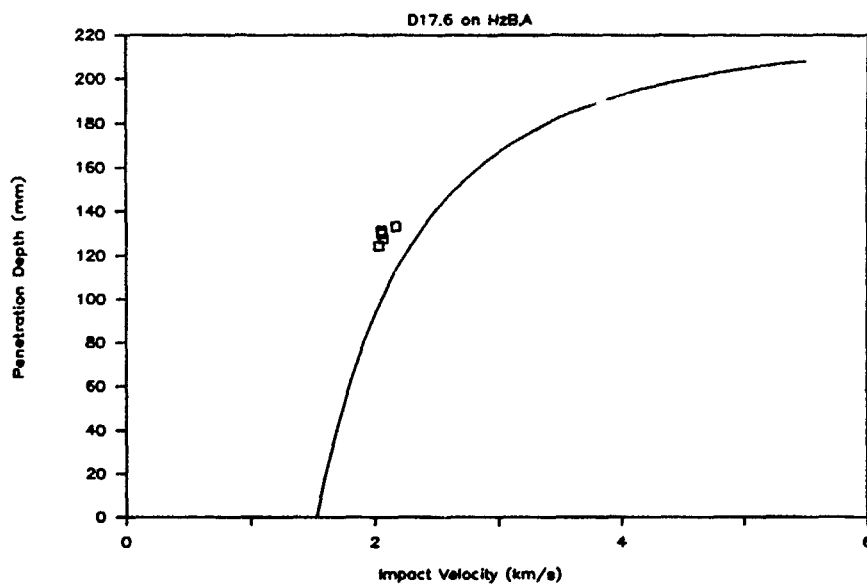


Figure 55c. Penetration Depth vs. Impact Velocity

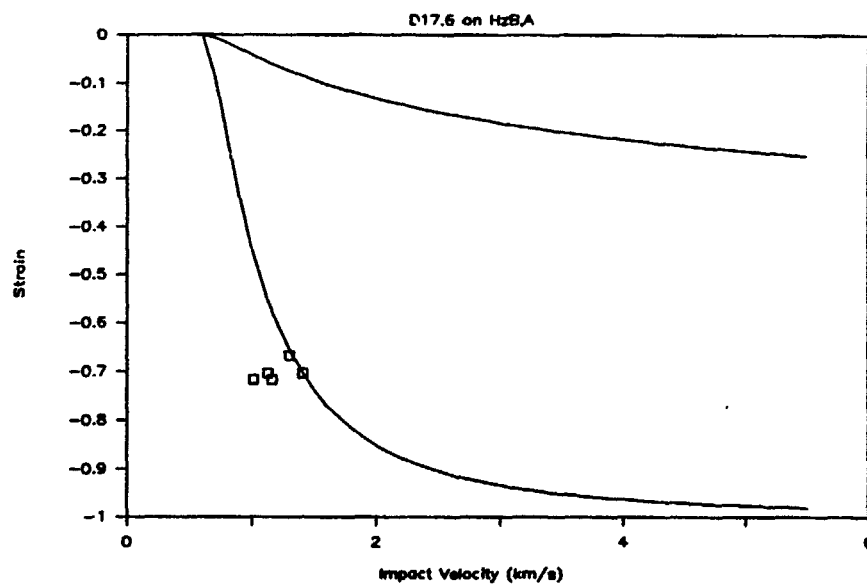


Figure 56a. Strain vs. Impact Velocity

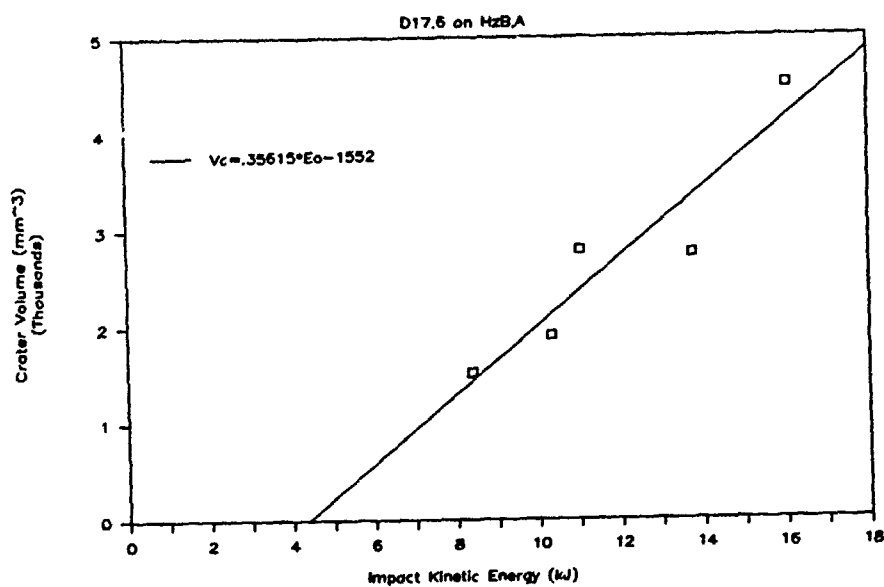


Figure 56b. Crater Volume vs. Impact Kinetic Energy

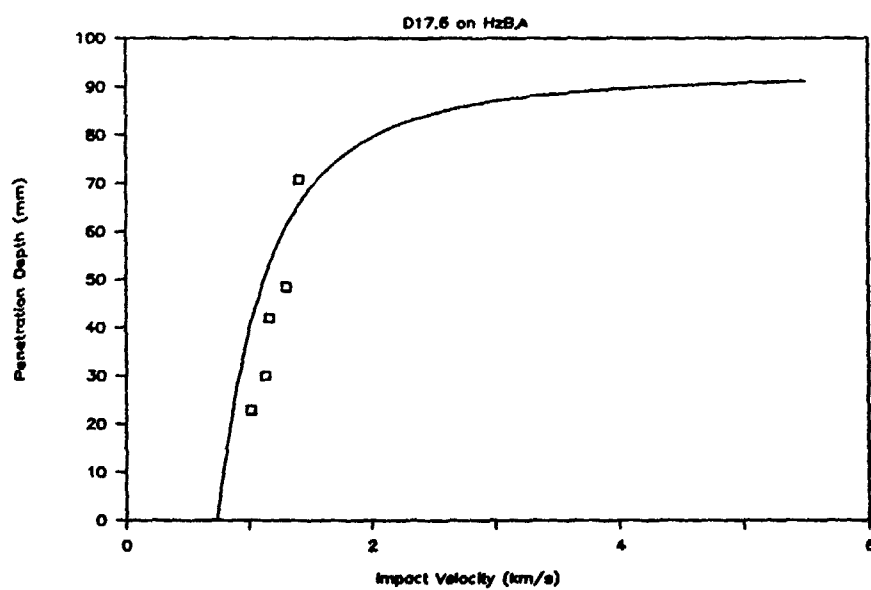


Figure 56c. Penetration Depth vs. Impact Velocity

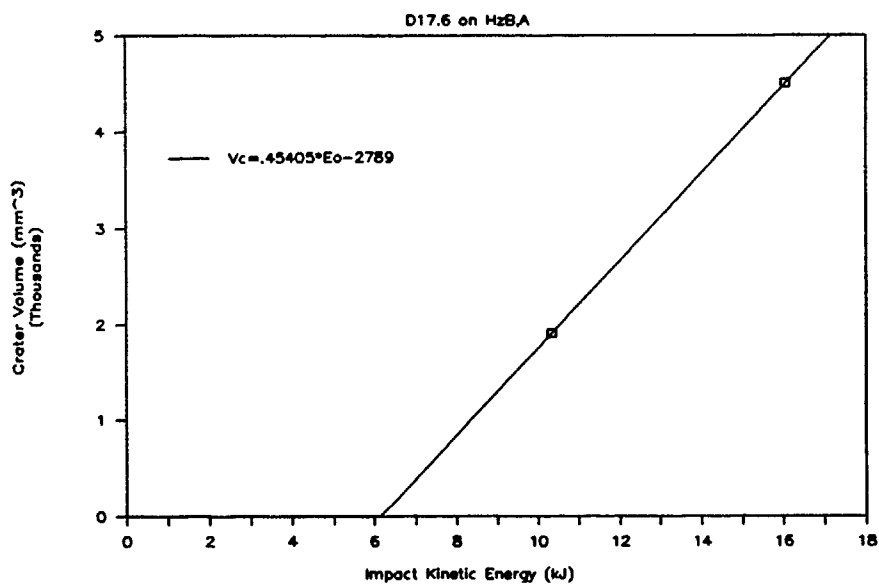


Figure 56d. Crater Volume vs. Impact Kinetic Energy

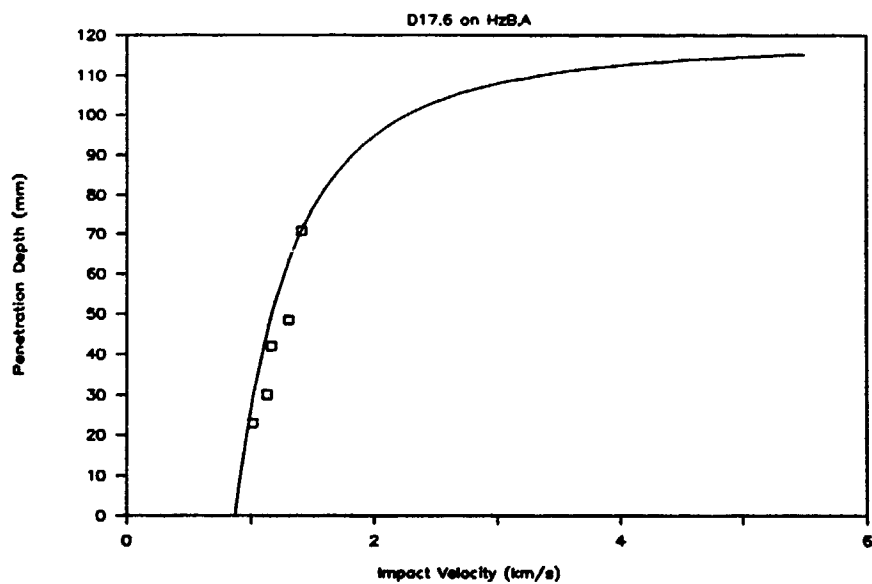


Figure 56e. Penetration Depth vs. Impact Velocity

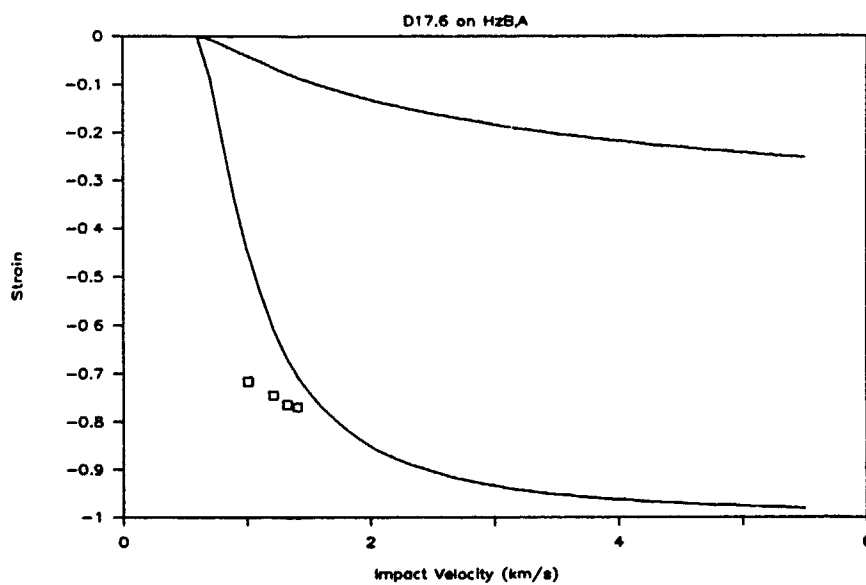


Figure 57a. Strain vs. Impact Velocity

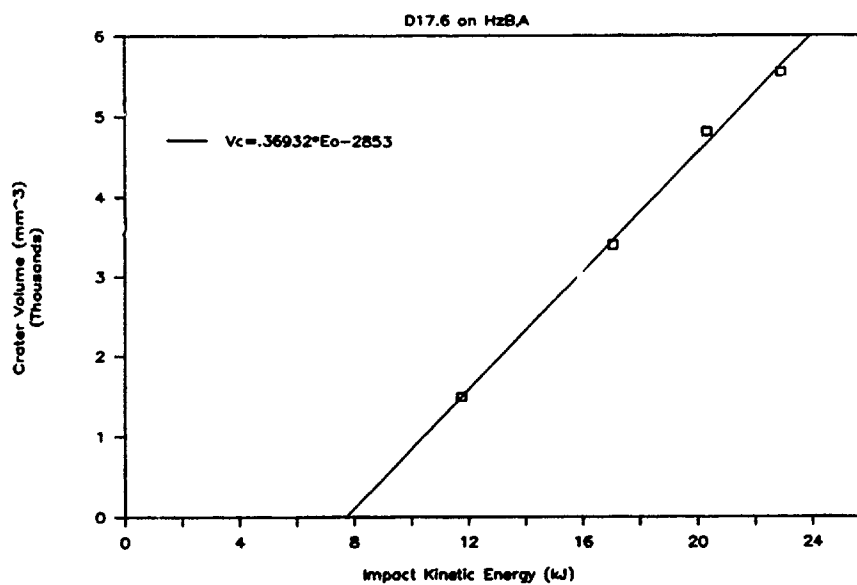


Figure 57b. Crater Volume vs. Impact Kinetic Energy

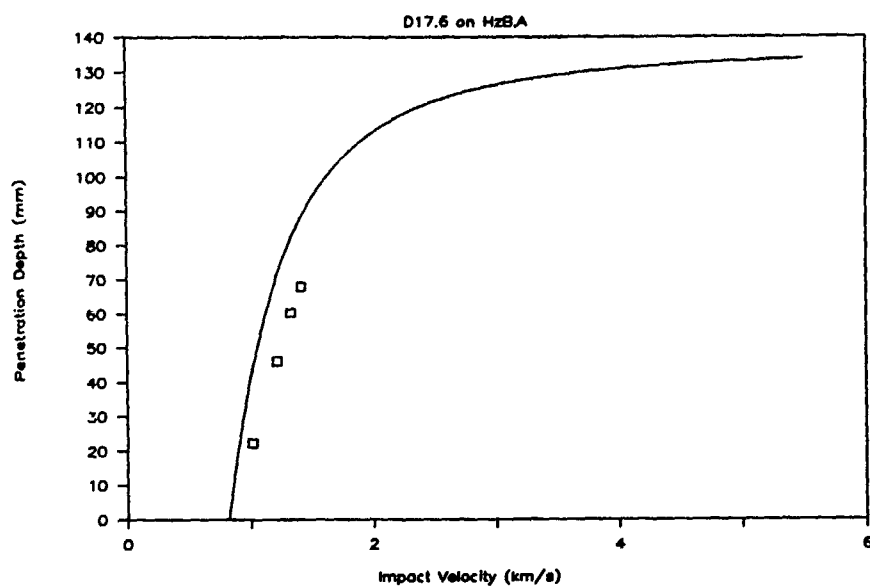


Figure 57c. Penetration Depth vs. Impact Velocity

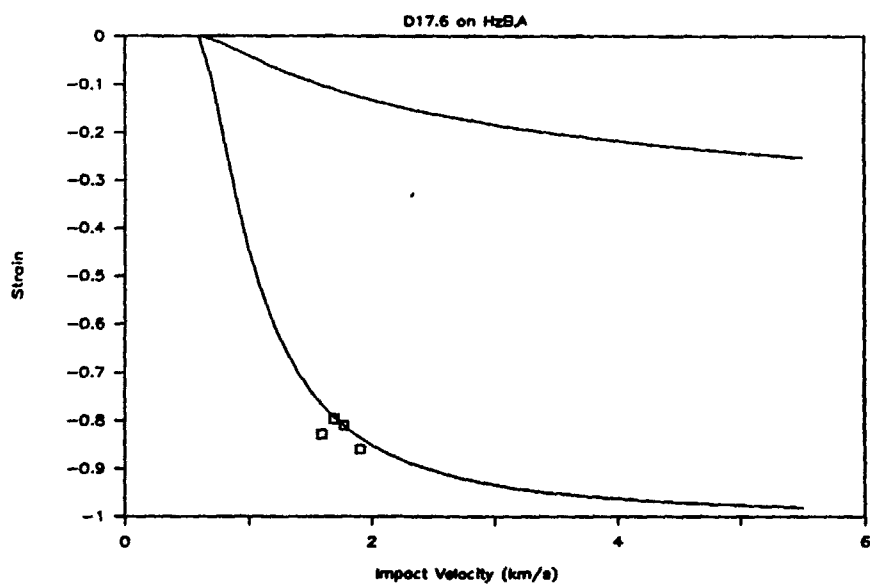


Figure 58a. Strain vs. Impact Velocity

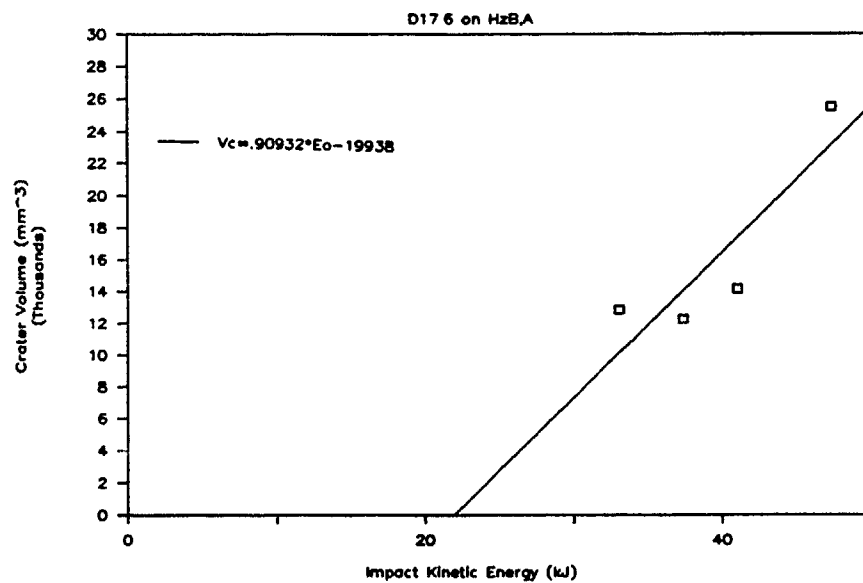


Figure 58b. Crater Volume vs. Impact Kinetic Energy

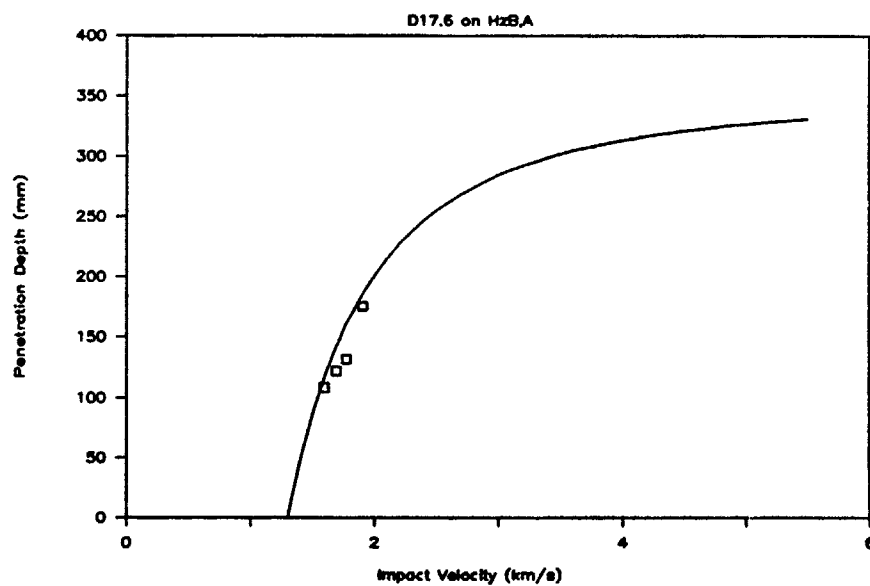


Figure 58c. Penetration Depth vs. Impact Velocity

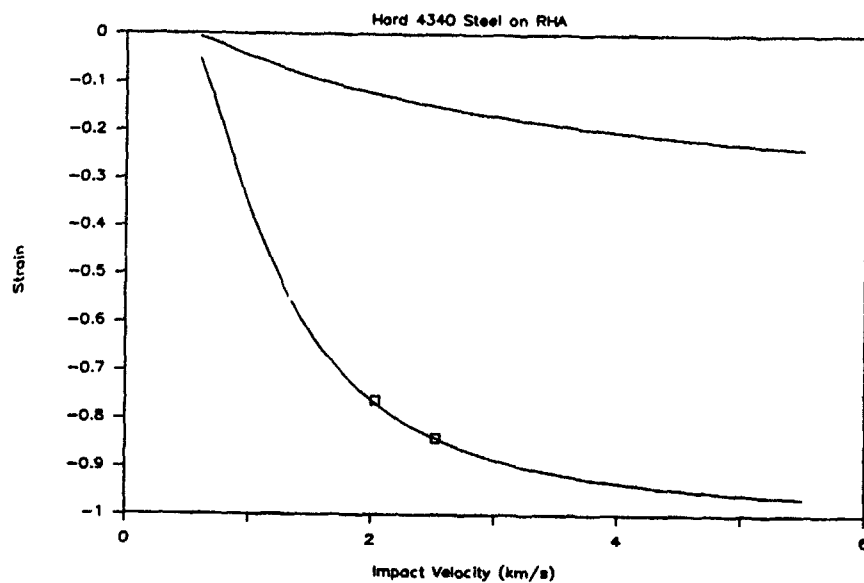


Figure 59a. Strain vs. Impact Velocity

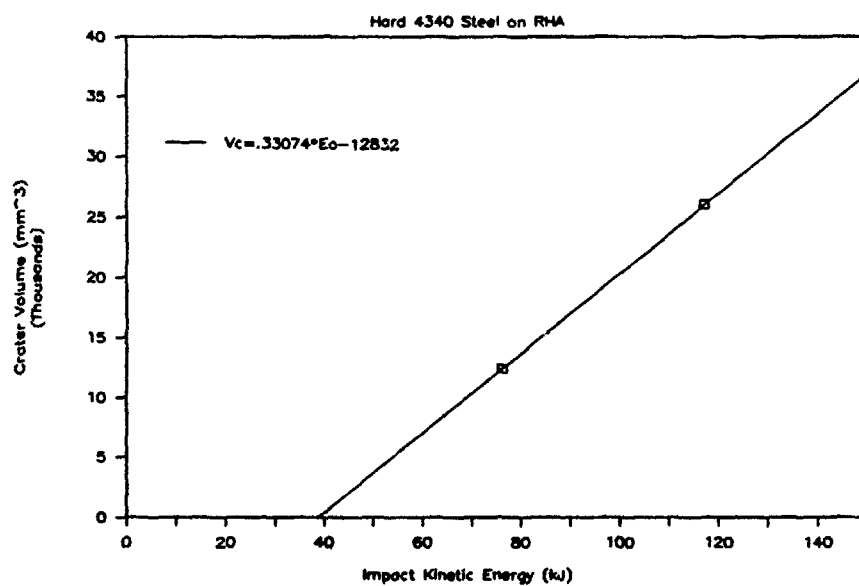


Figure 59b. Crater Volume vs. Impact Kinetic Energy

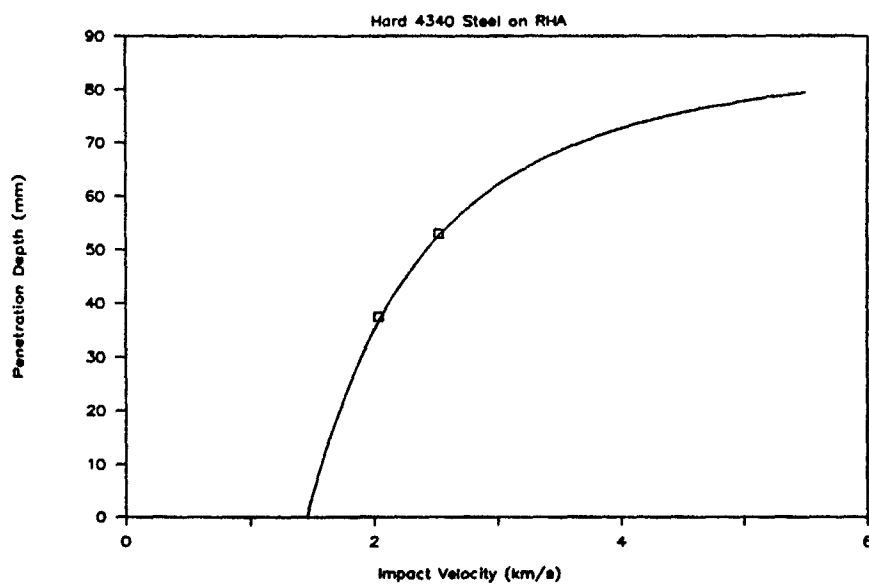


Figure 59c. Penetration Depth vs. Impact Velocity

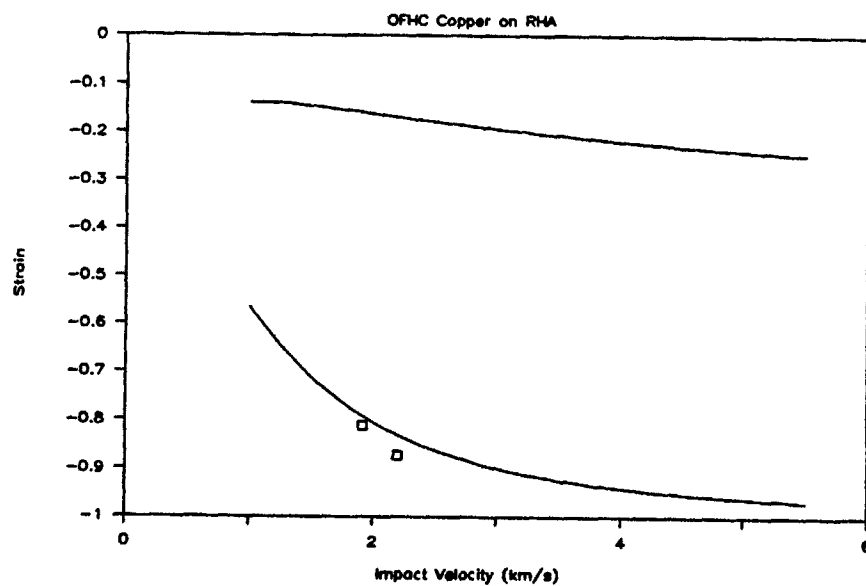


Figure 60a. Strain vs. Impact Velocity

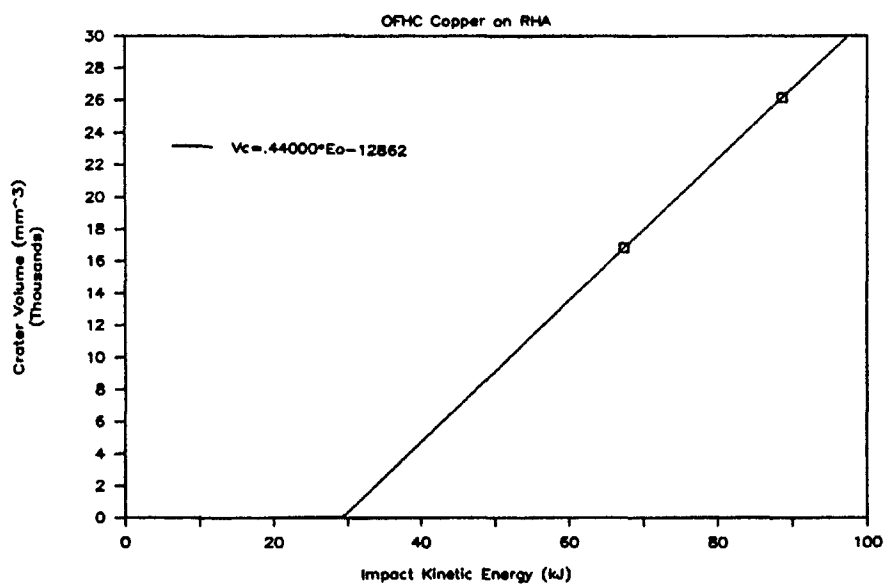


Figure 60b. Crater Volume vs. Impact Kinetic Energy

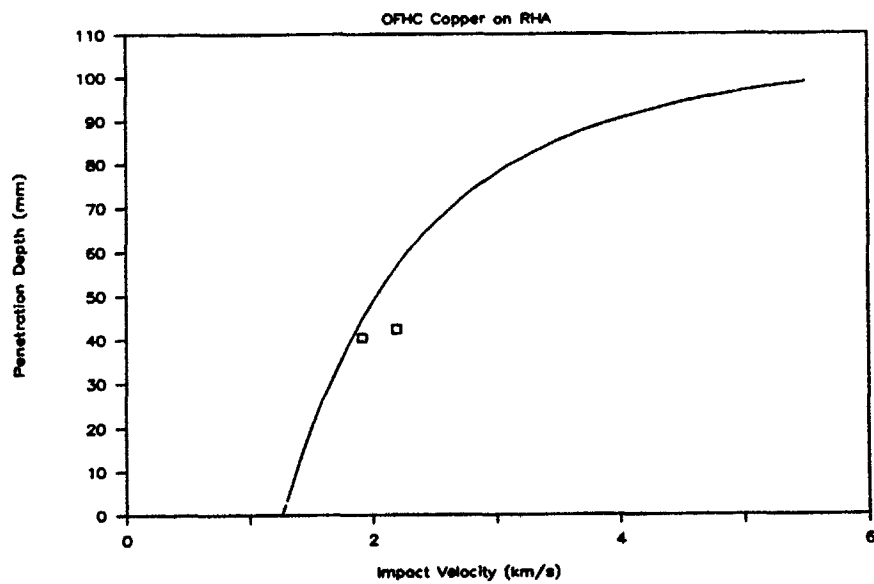


Figure 60c. Penetration Depth vs. Impact Velocity

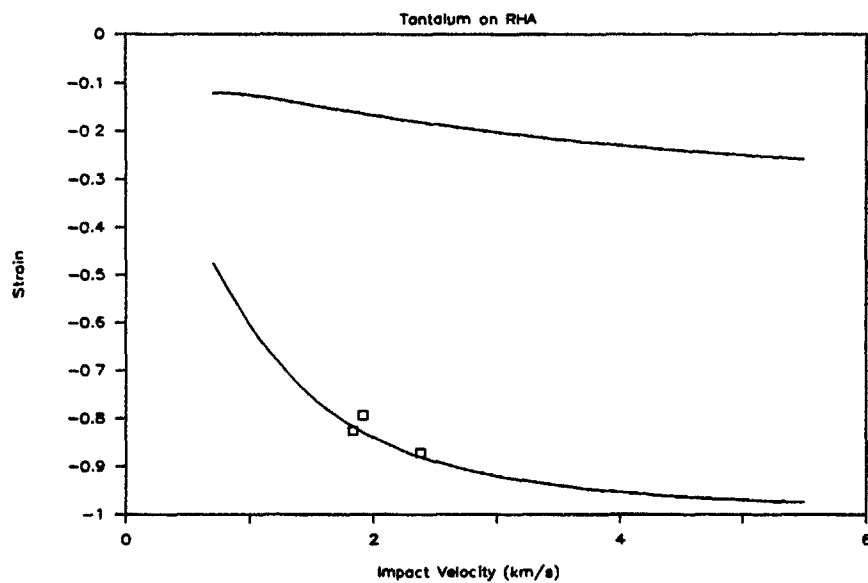


Figure 61a. Strain vs. Impact Velocity

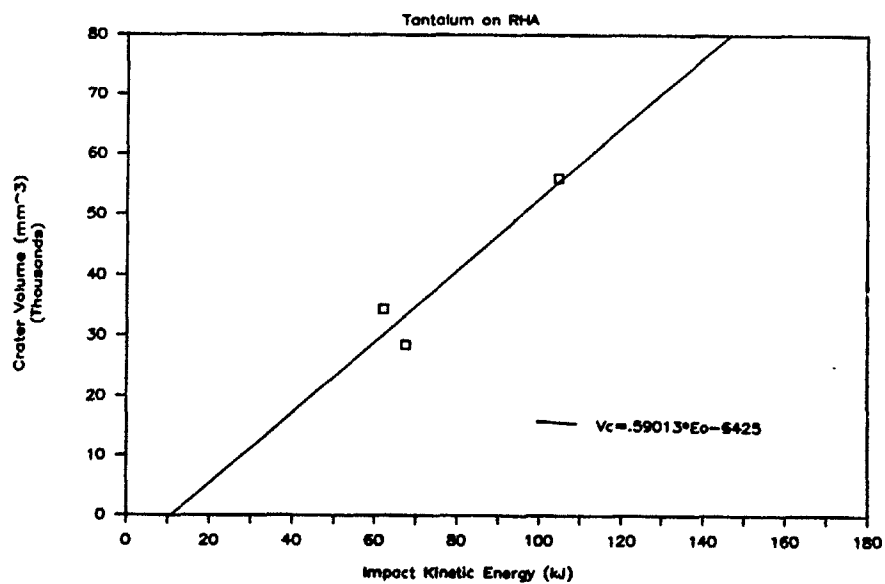


Figure 61b. Crater Volume vs. Impact Kinetic Energy

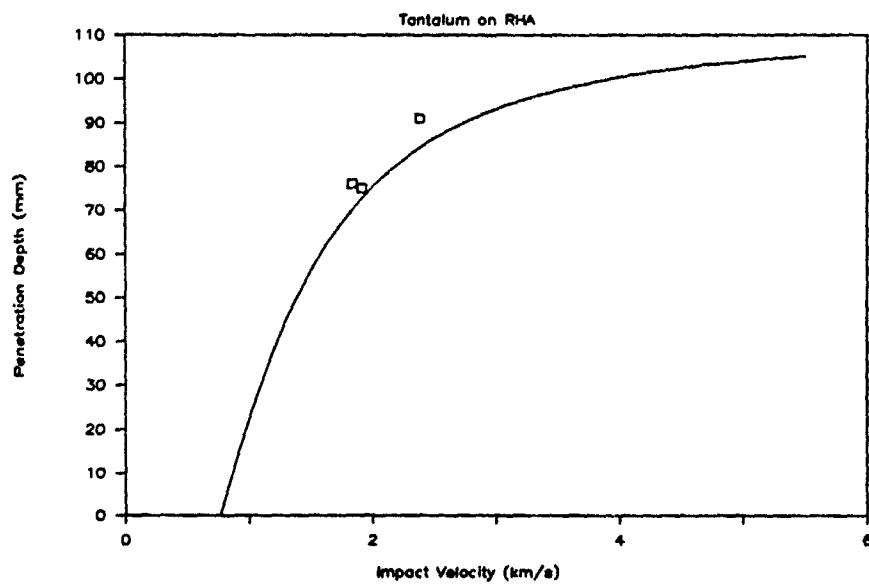


Figure 61c. Penetration Depth vs. Impact Velocity

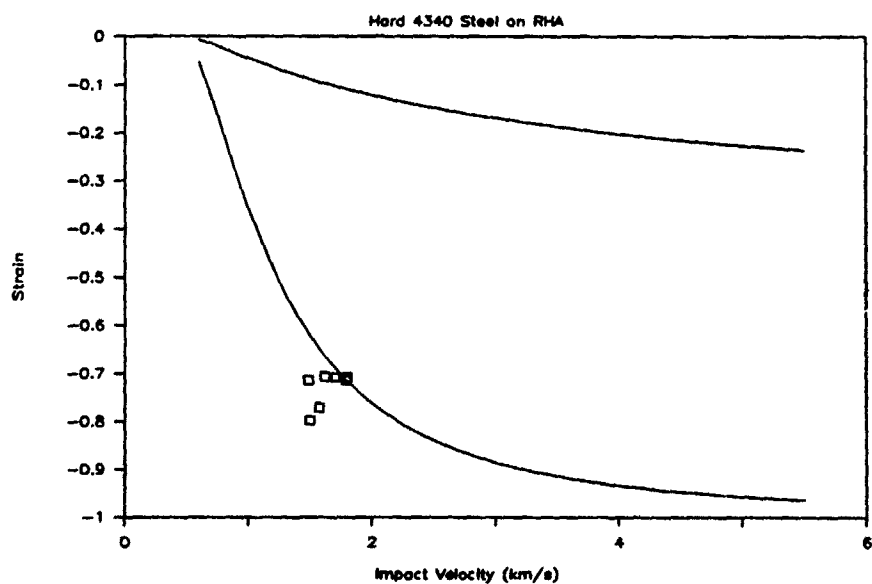


Figure 62a. Strain vs. Impact Velocity

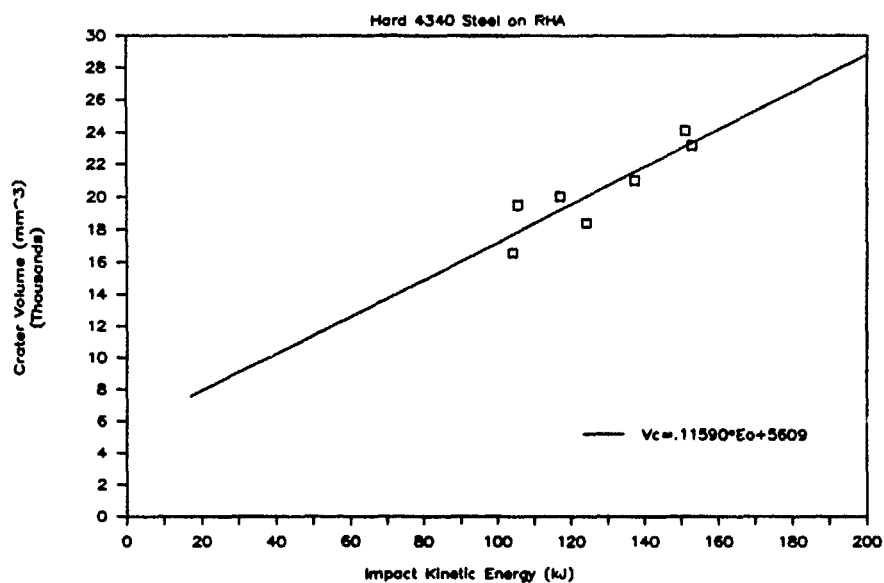


Figure 62b. Crater Volume vs. Impact Kinetic Energy

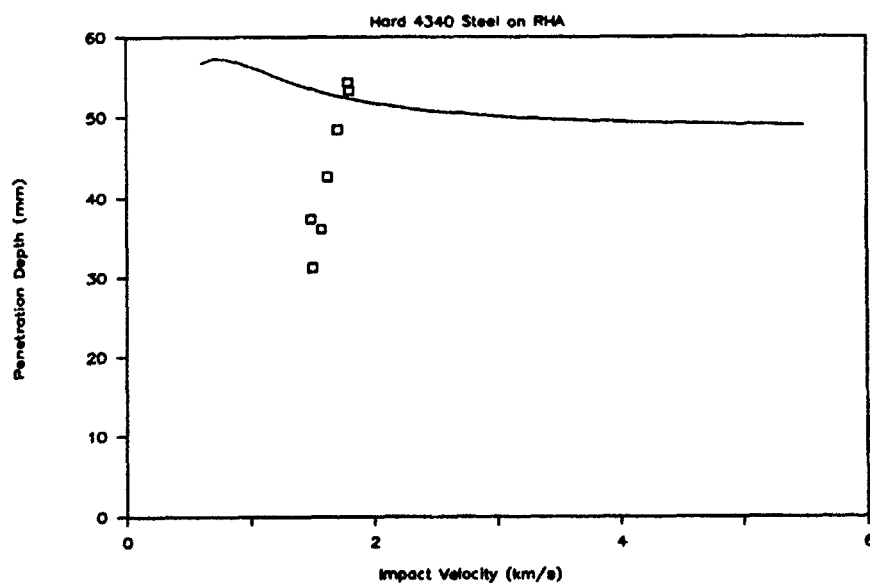


Figure 62c. Penetration Depth vs. Impact Velocity

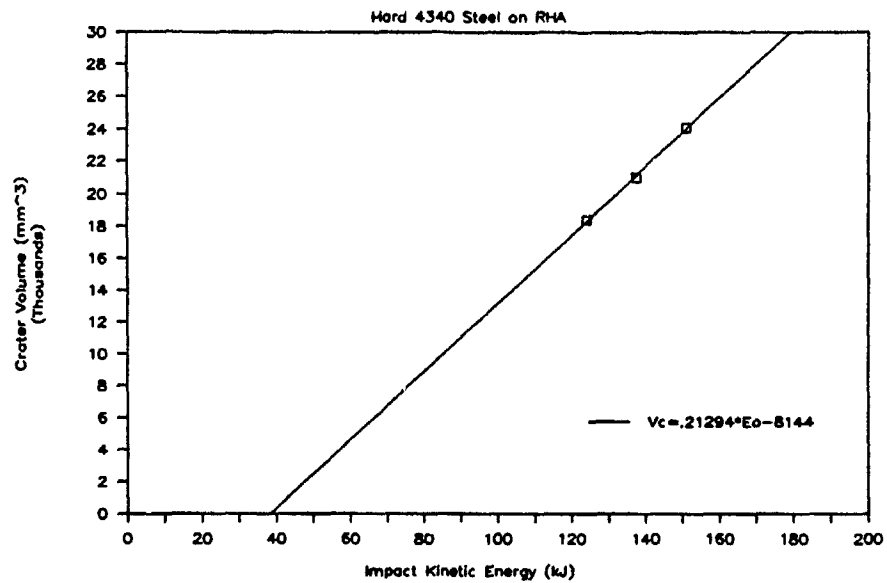


Figure 62d. Crater Volume vs. Impact Kinetic Energy

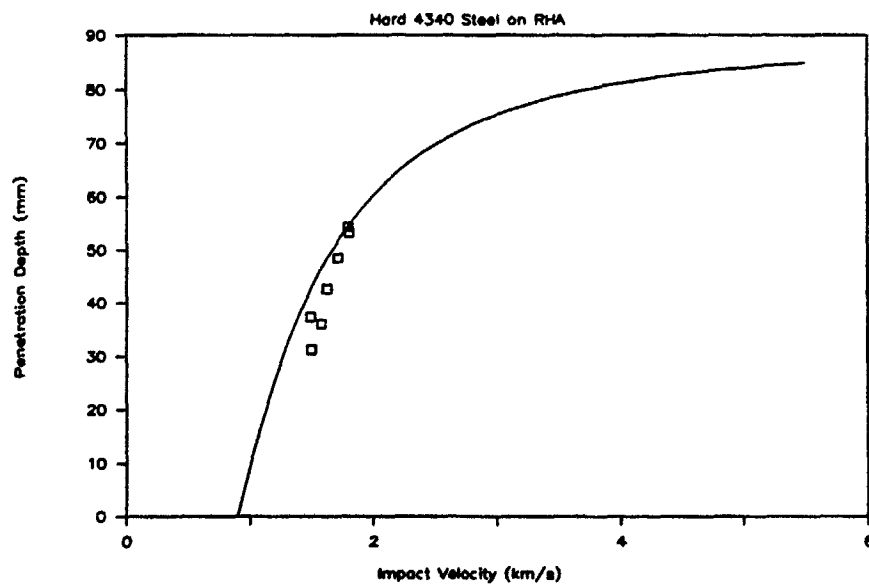


Figure 62e. Penetration Depth vs. Impact Velocity

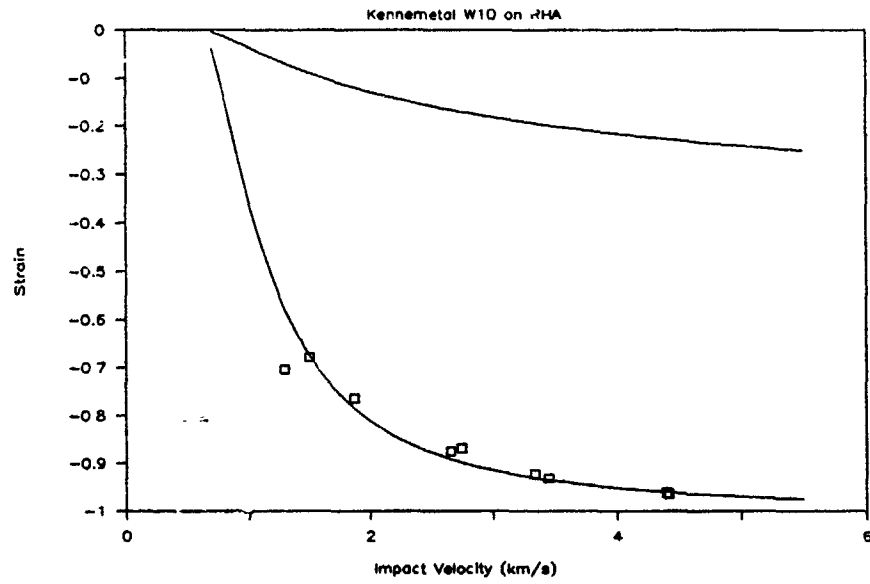


Figure 63a. Strain vs. Impact Velocity

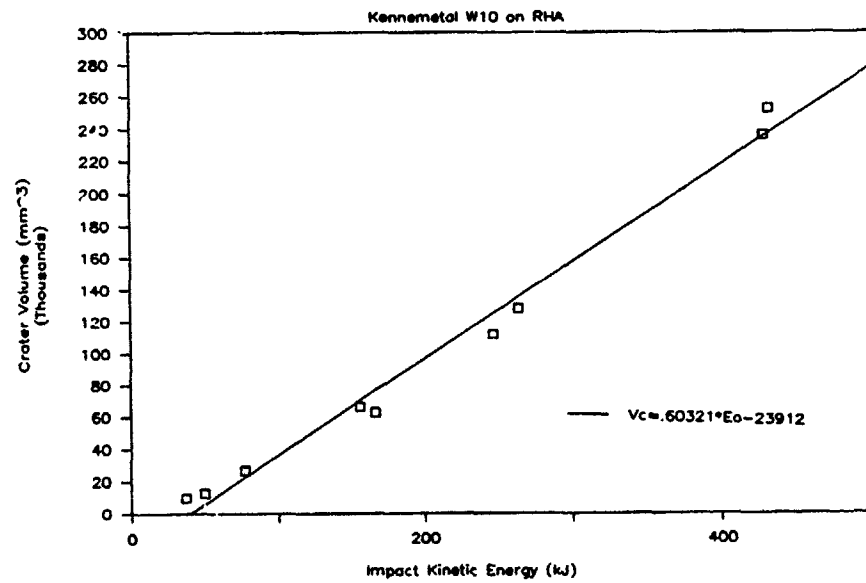


Figure 63b. Crater Volume vs. Impact Kinetic Energy

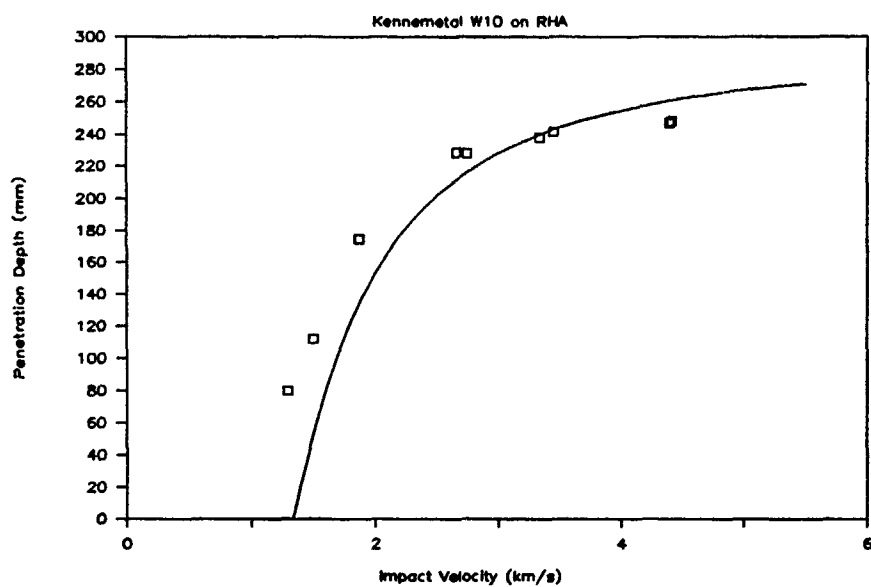


Figure 63c. Penetration Depth vs. Impact Velocity

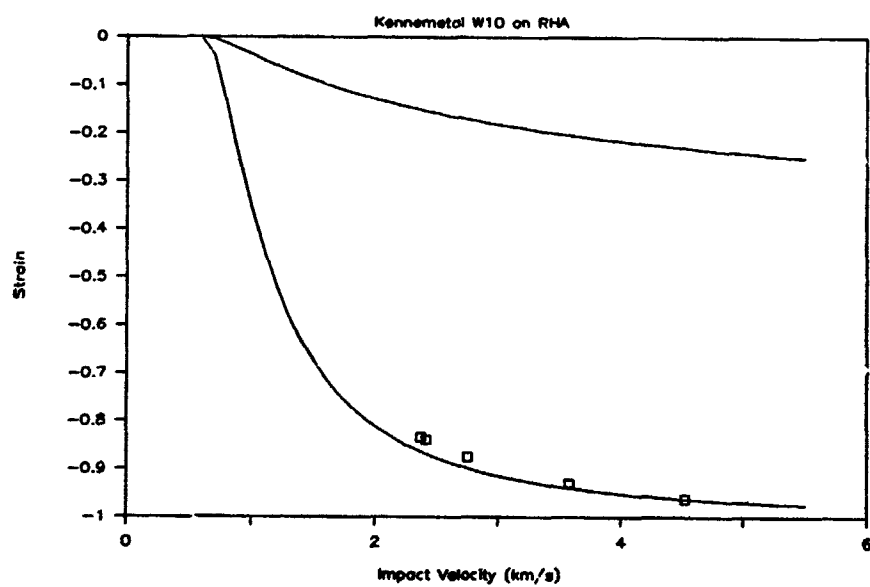


Figure 64a. Strain vs. Impact Velocity

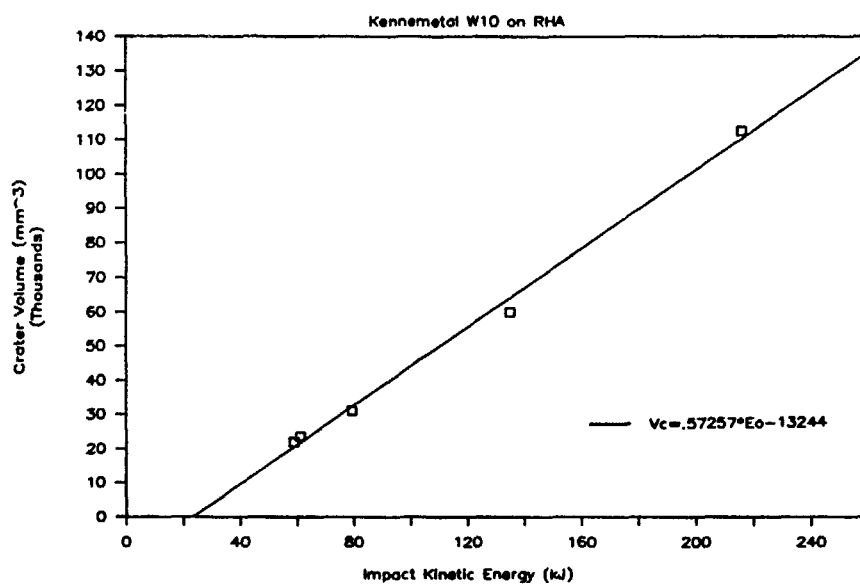


Figure 64b. Crater Volume vs. Impact Kinetic Energy

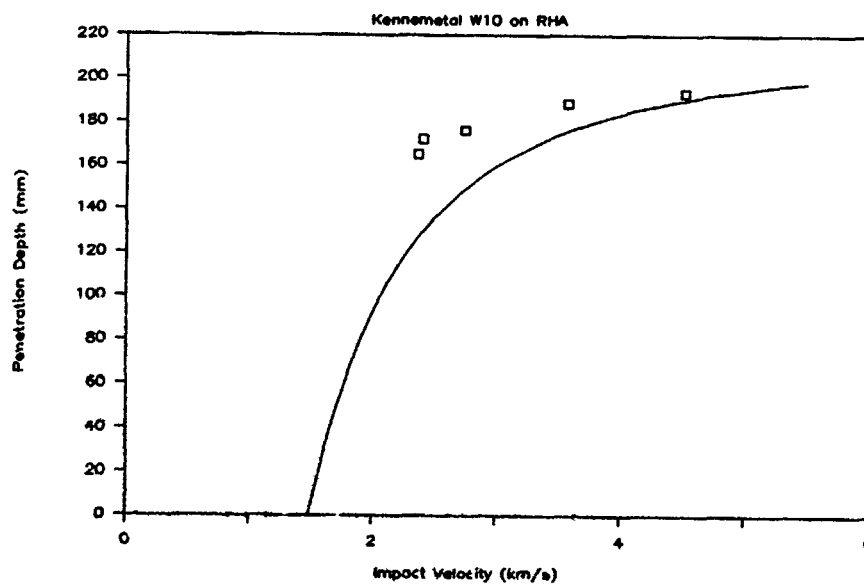


Figure 64c. Penetration Depth vs. Impact Velocity

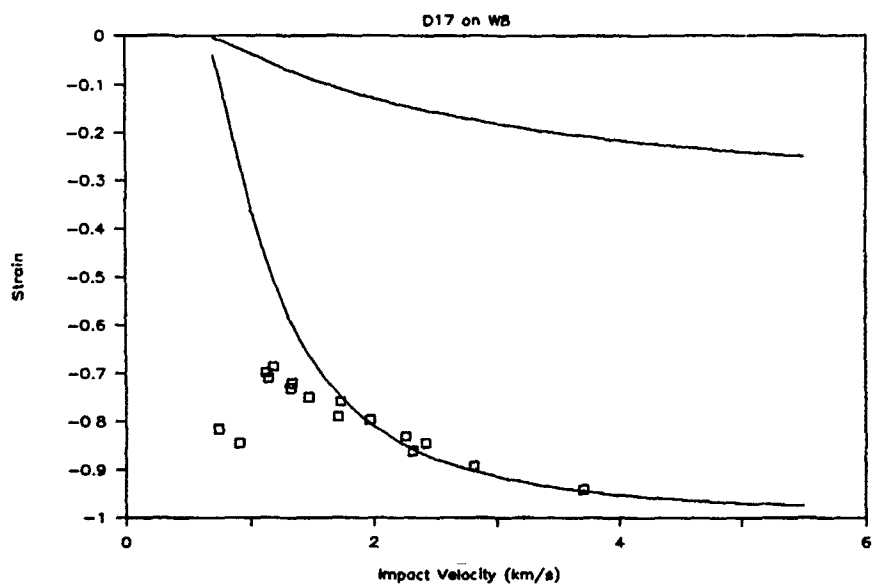


Figure 65a. Strain vs. Impact Velocity

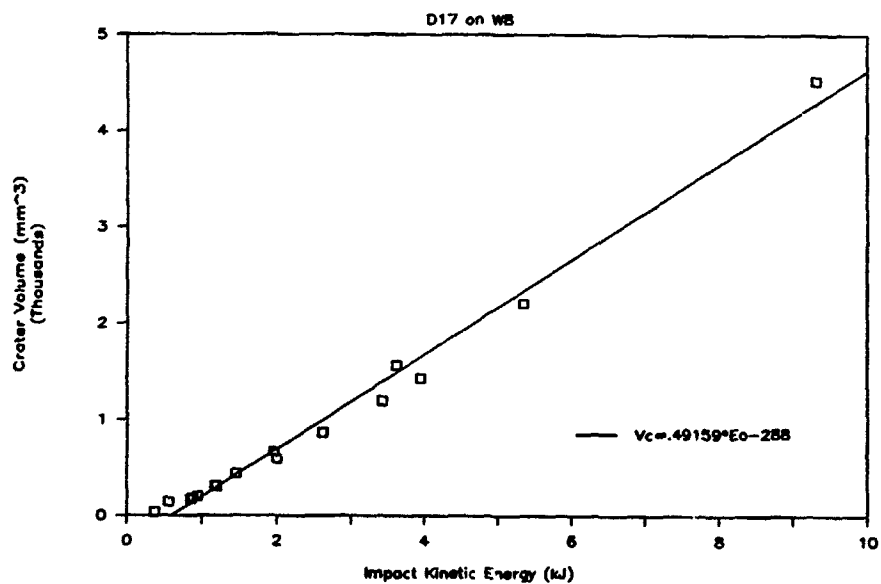


Figure 65b. Crater Volume vs. Impact Kinetic Energy

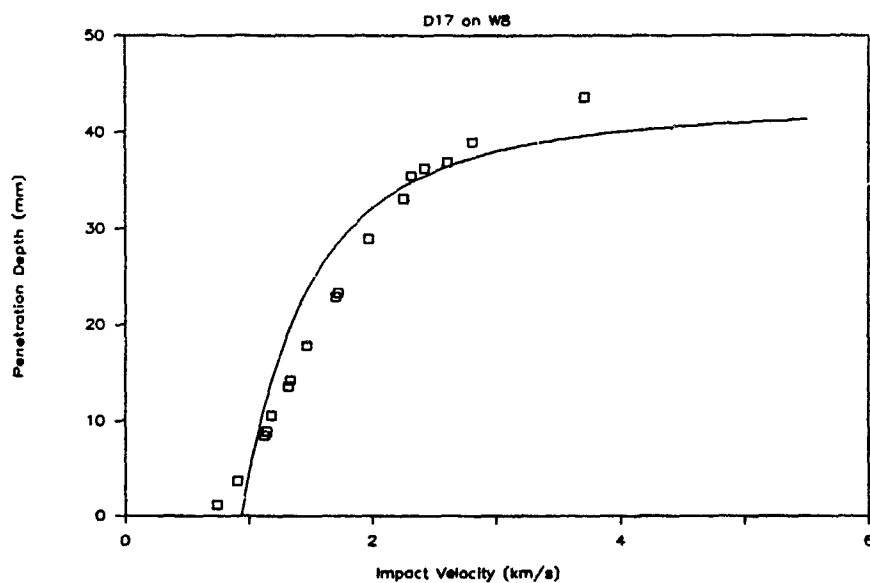


Figure 65c. Penetration Depth vs. Impact Velocity

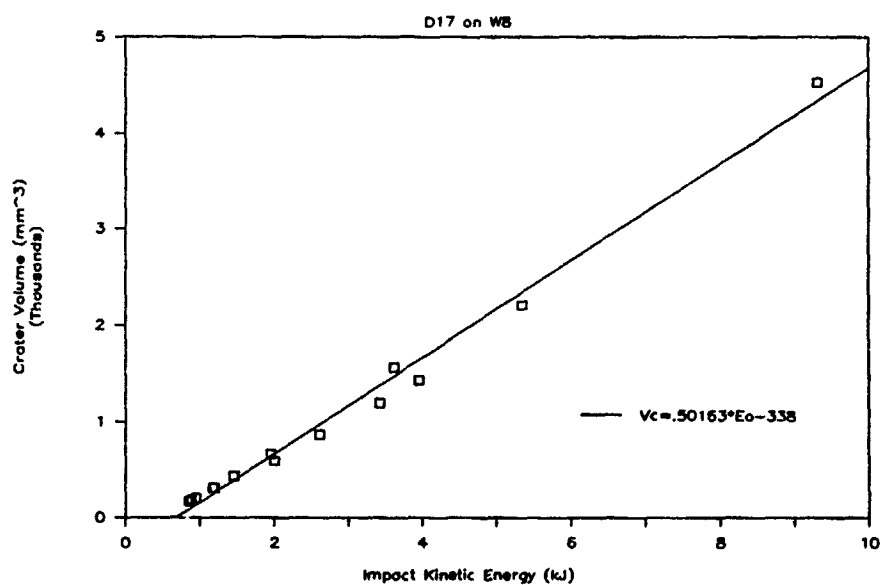


Figure 65d. Crater Volume vs. Impact Kinetic Energy

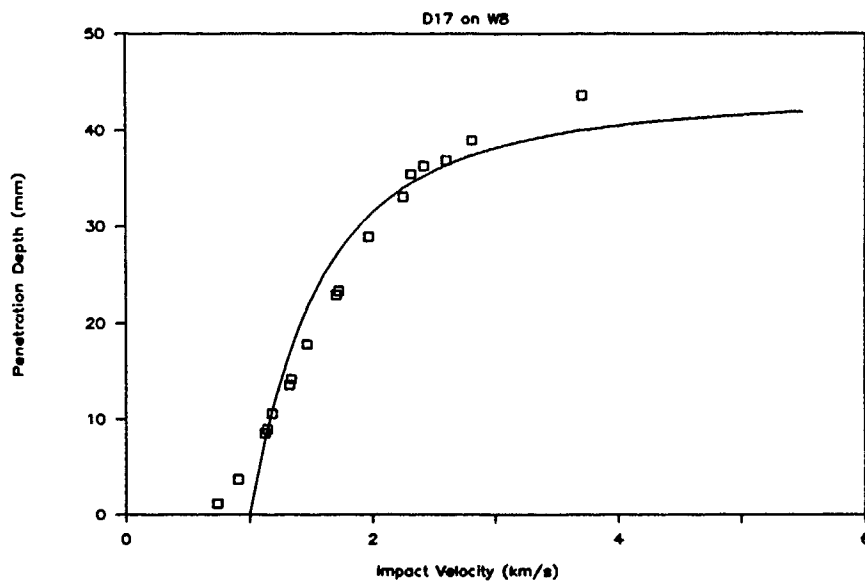


Figure 65e. Penetration Depth vs. Impact Velocity

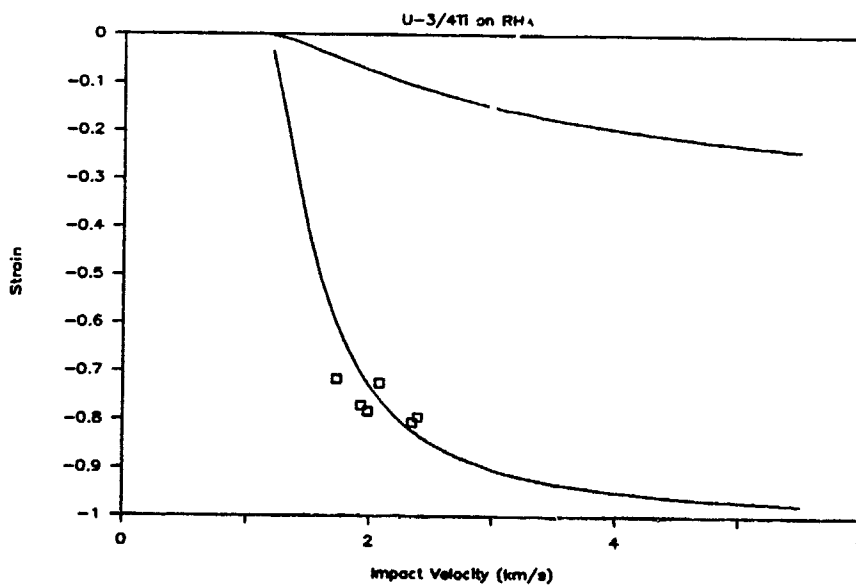


Figure 66a. Strain vs. Impact Velocity

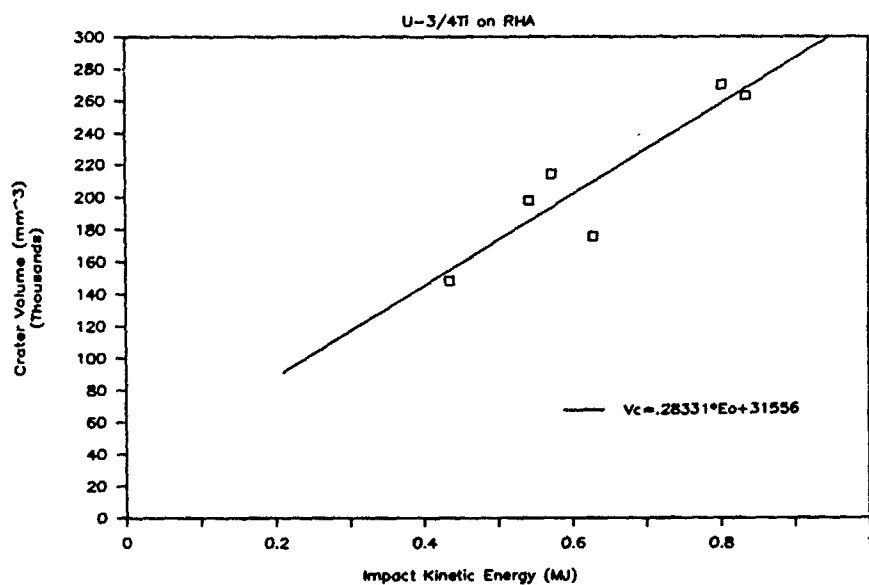


Figure 66b. Crater Volume vs. Impact Kinetic Energy

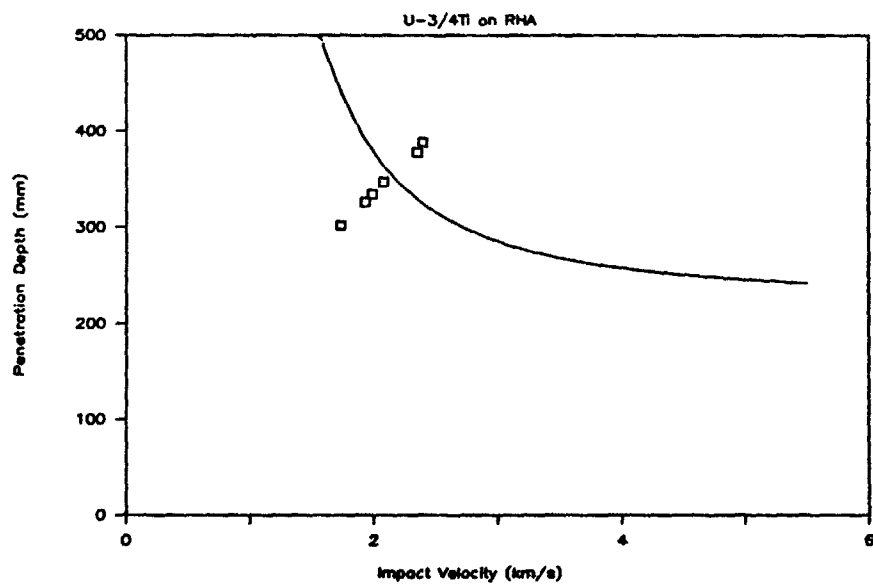


Figure 66c. Penetration Depth vs. Impact Velocity

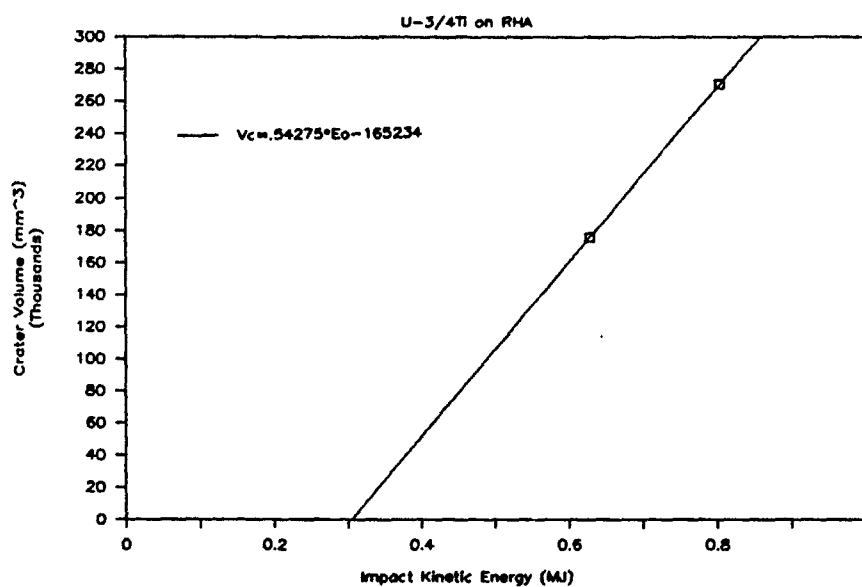


Figure 66d. Crater Volume vs. Impact Kinetic Energy

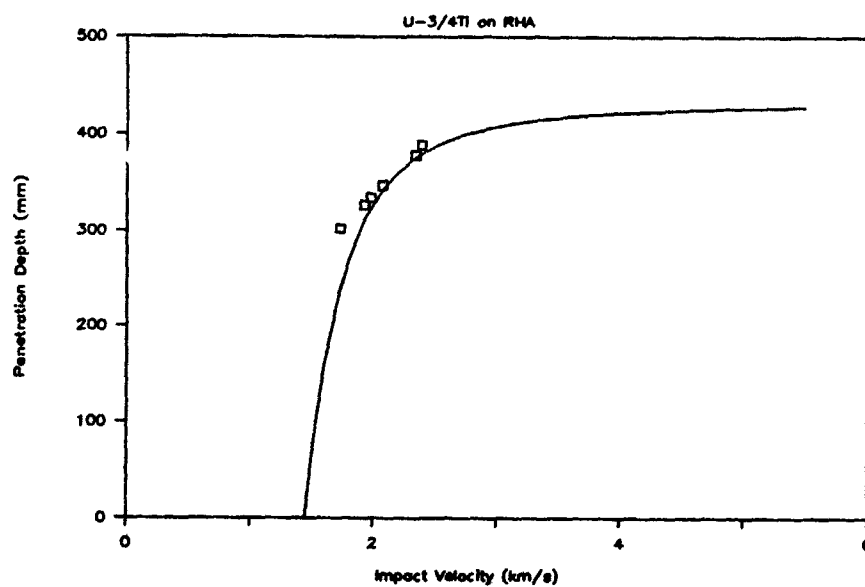


Figure 66e. Penetration Depth vs. Impact Velocity

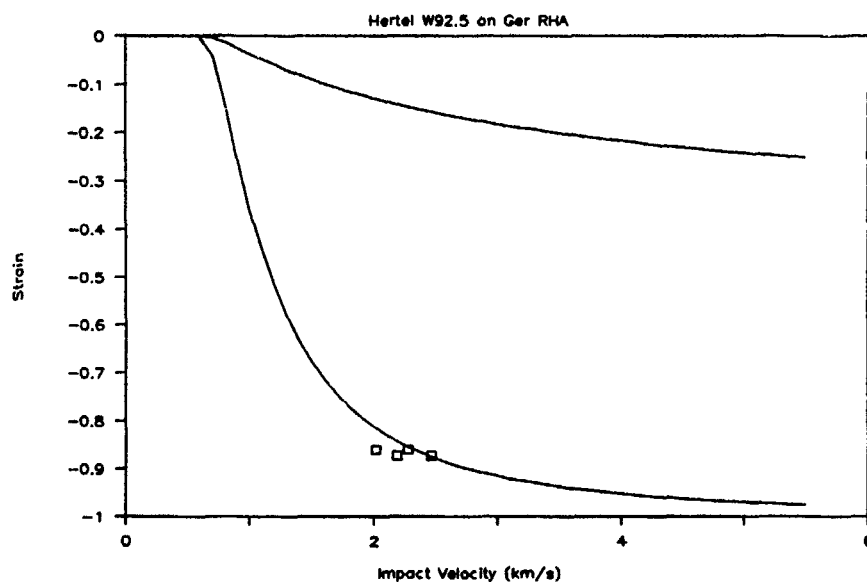


Figure 67a. Strain vs. Impact Velocity

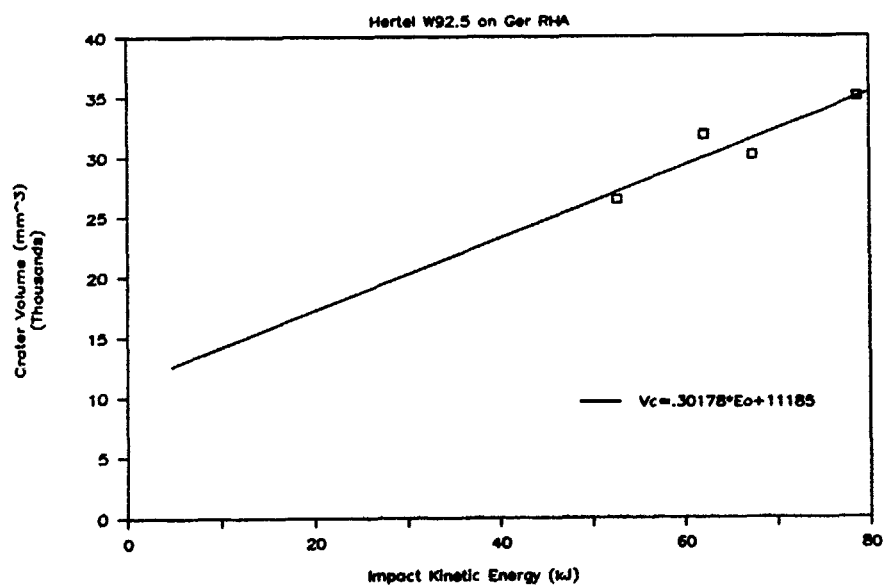


Figure 67b. Crater Volume vs. Impact Kinetic Energy

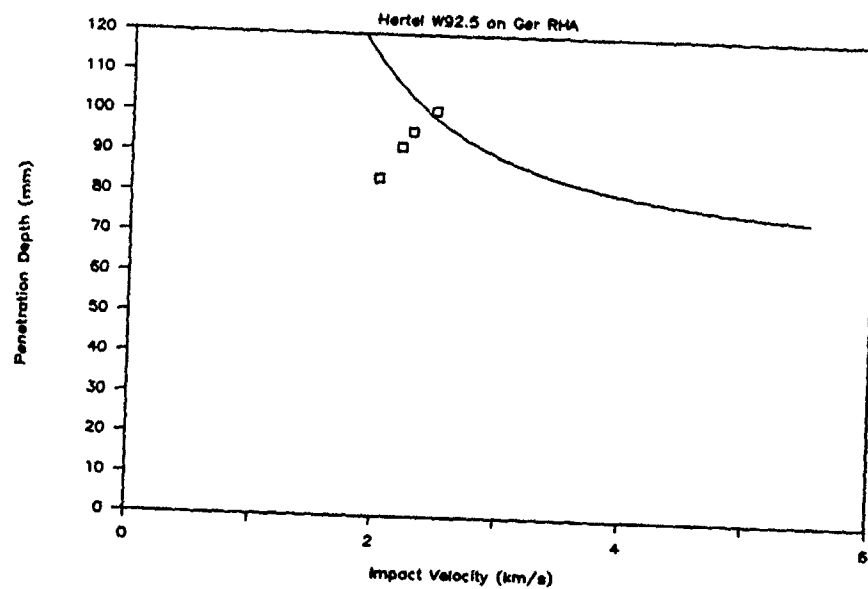


Figure 67c. Penetration Depth vs. Impact Velocity

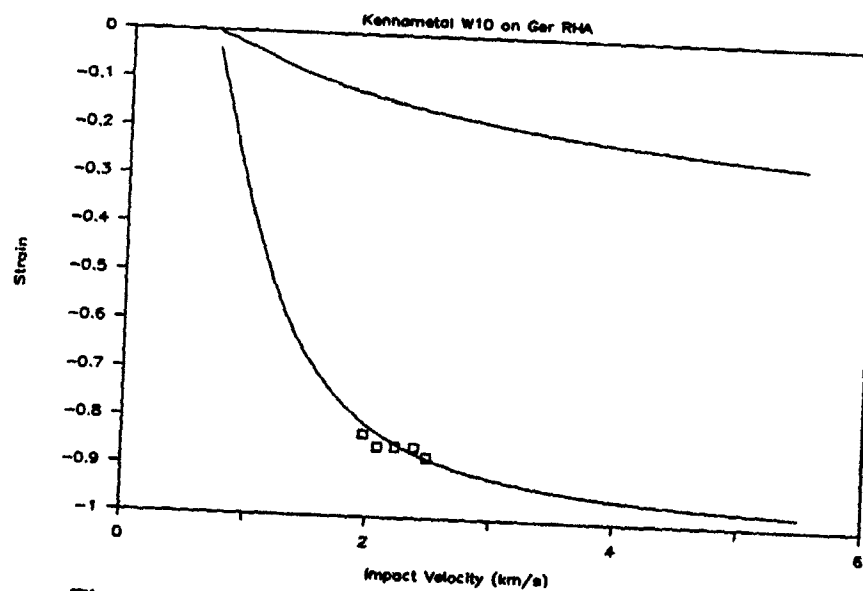


Figure 68a. Strain vs. Impact Velocity

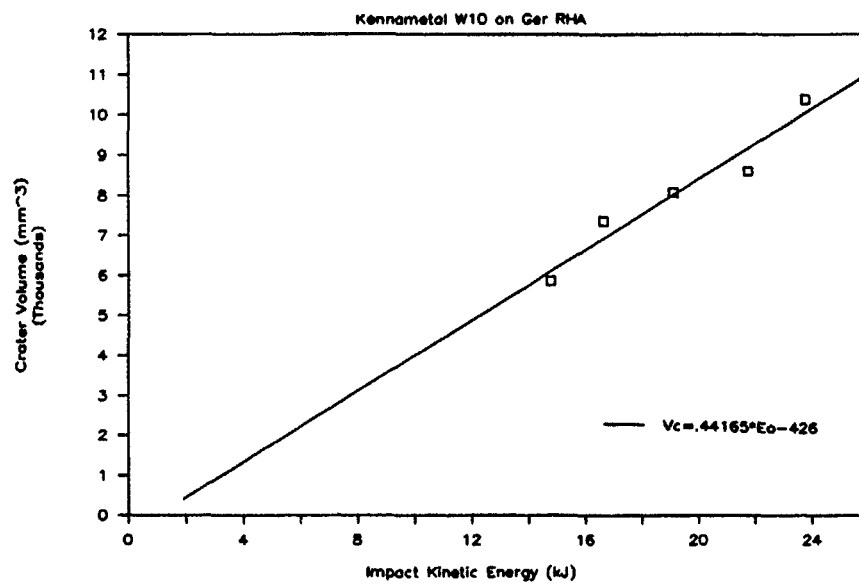


Figure 68b. Crater Volume vs. Impact Kinetic Energy

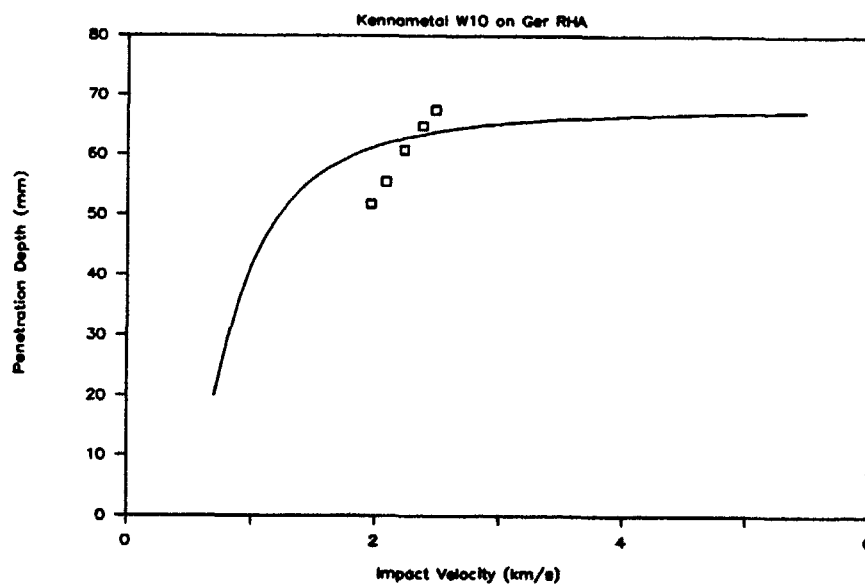


Figure 68c. Penetration Depth vs. Impact Velocity

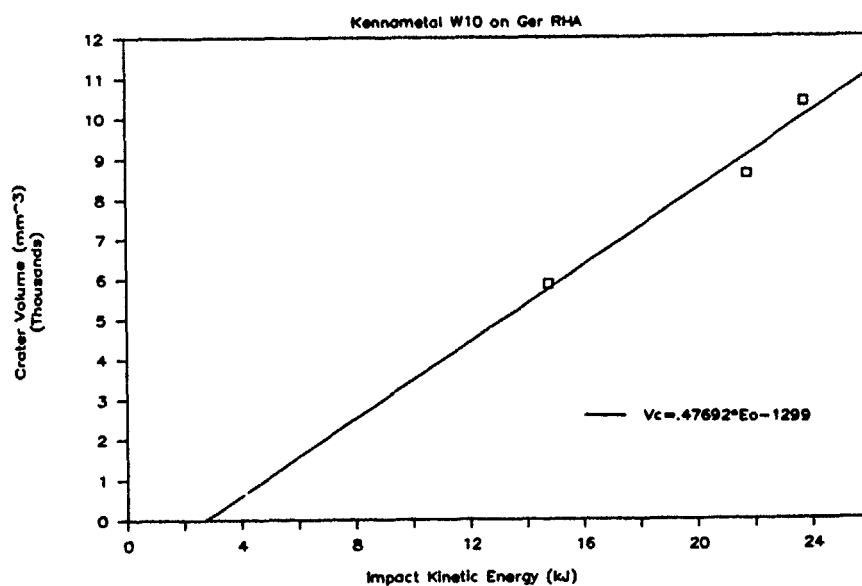


Figure 68d. Crater Volume vs. Impact Kinetic Energy

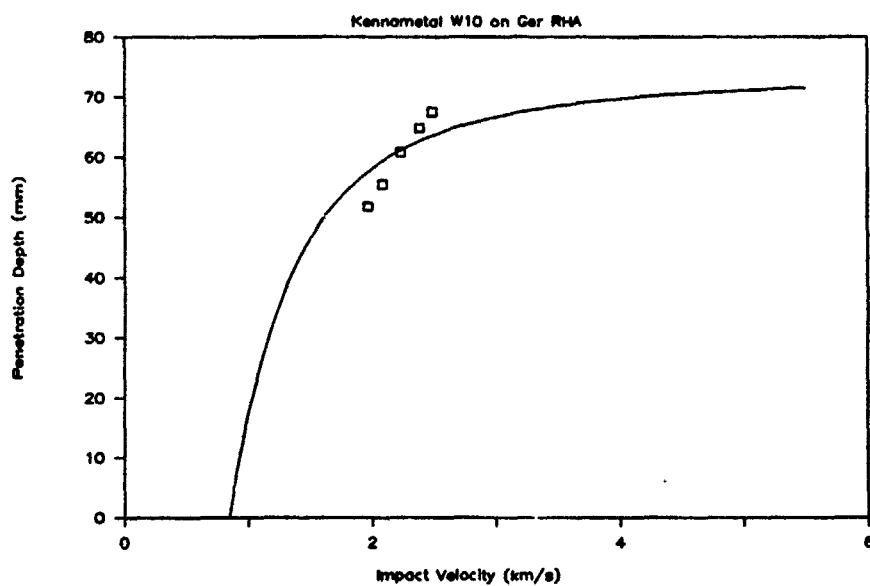


Figure 68e. Penetration Depth vs. Impact Velocity

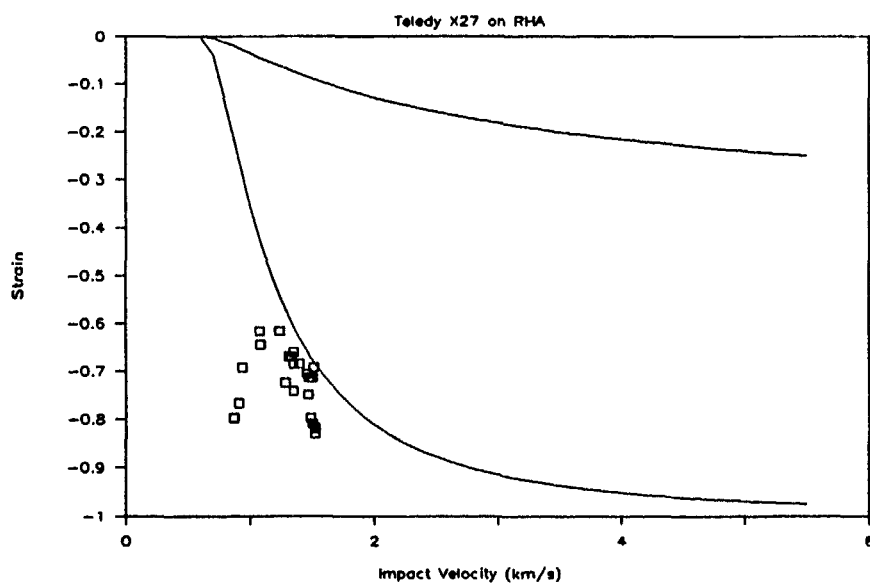


Figure 69a. Strain vs. Impact Velocity

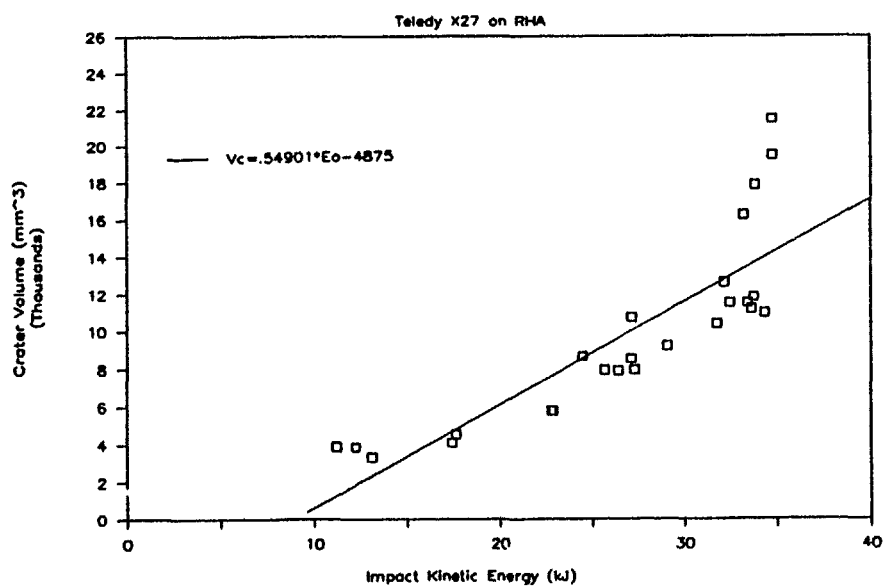


Figure 69b. Crater Volume vs. Impact Kinetic Energy

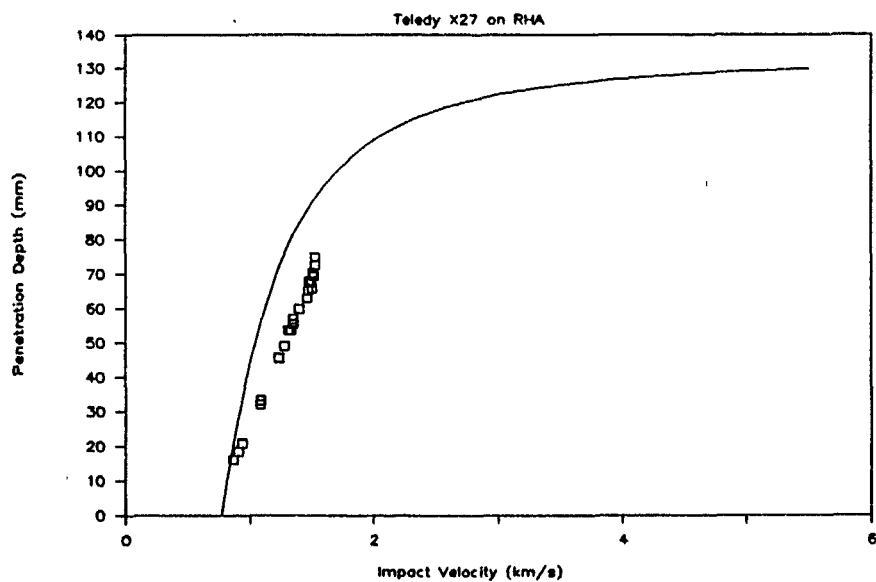


Figure 69c. Penetration Depth vs. Impact Velocity

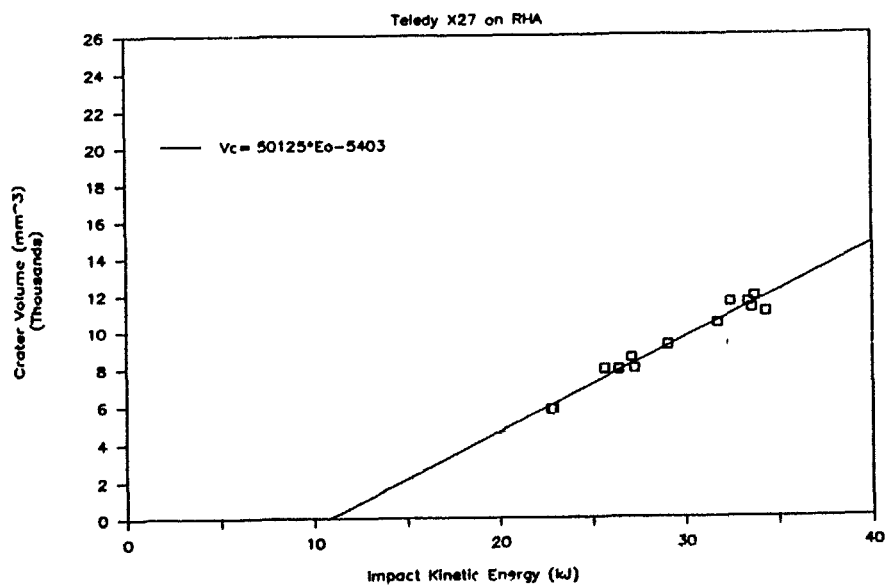


Figure 69d. Crater Volume vs. Impact Kinetic Energy

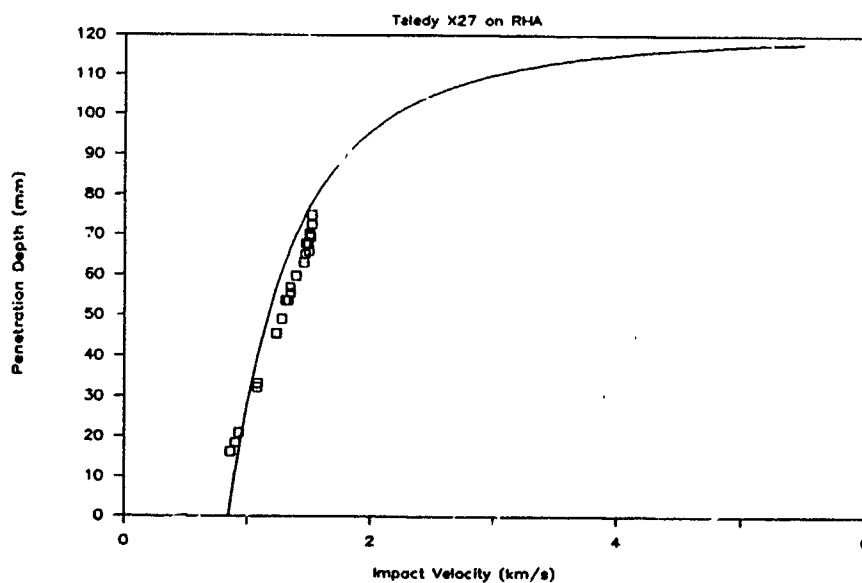


Figure 69e. Penetration Depth vs. Impact Velocity

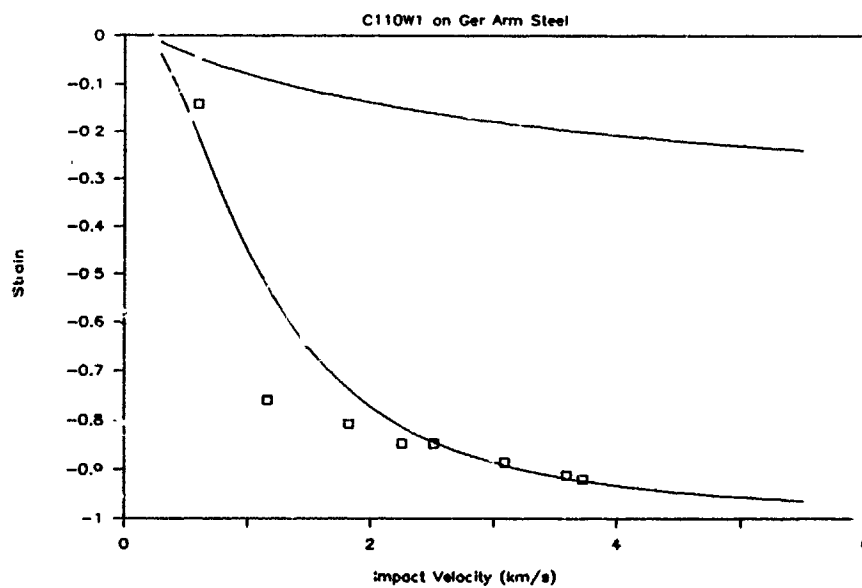


Figure 70a. Strain vs. Impact Velocity

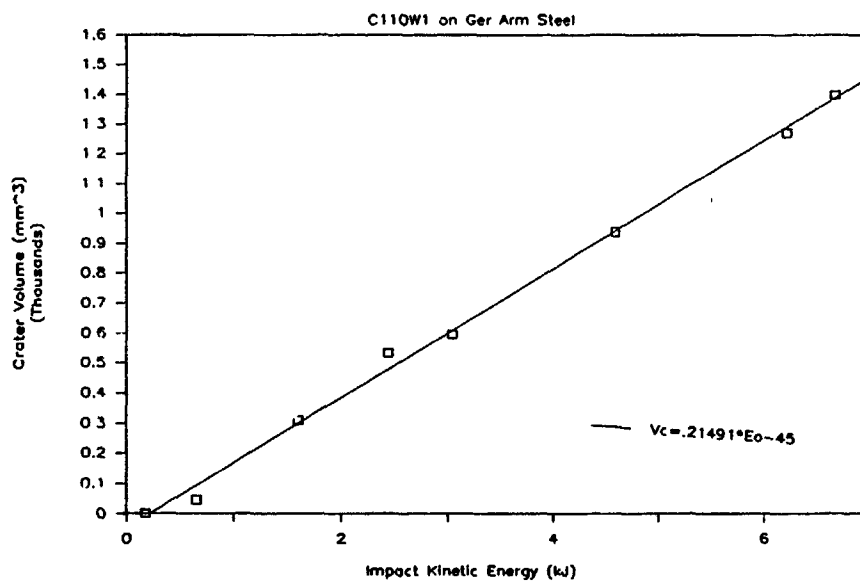


Figure 70b. Crater Volume vs. Impact Kinetic Energy

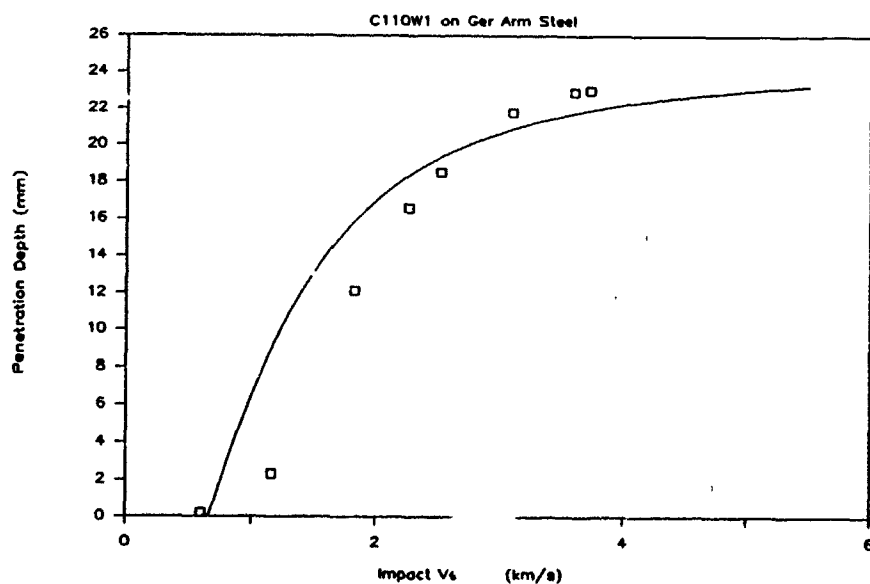


Figure 70c. Penetration Depth vs. Impact Velocity

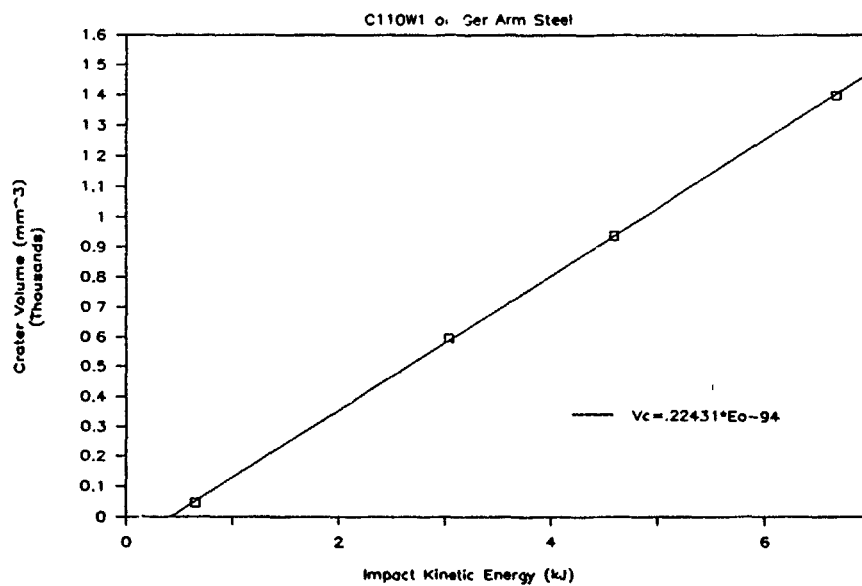


Figure 70d. Crater Volume vs. Impact Kinetic Energy

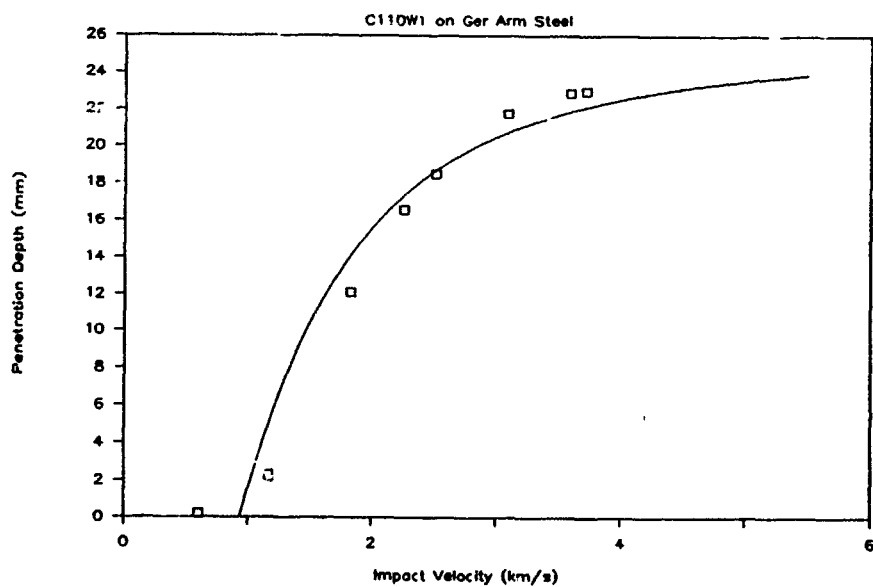


Figure 70e. Penetration Depth vs. Impact Velocity

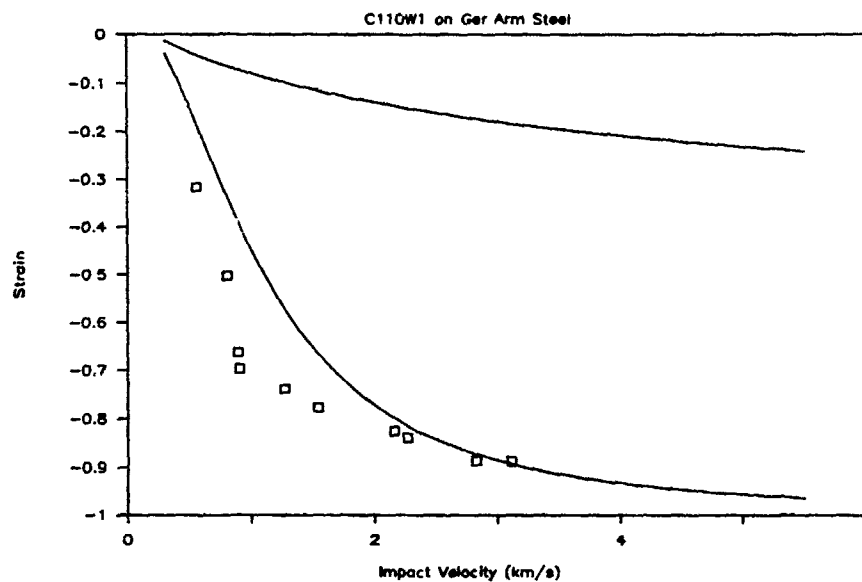


Figure 71a. Strain vs. Impact Velocity

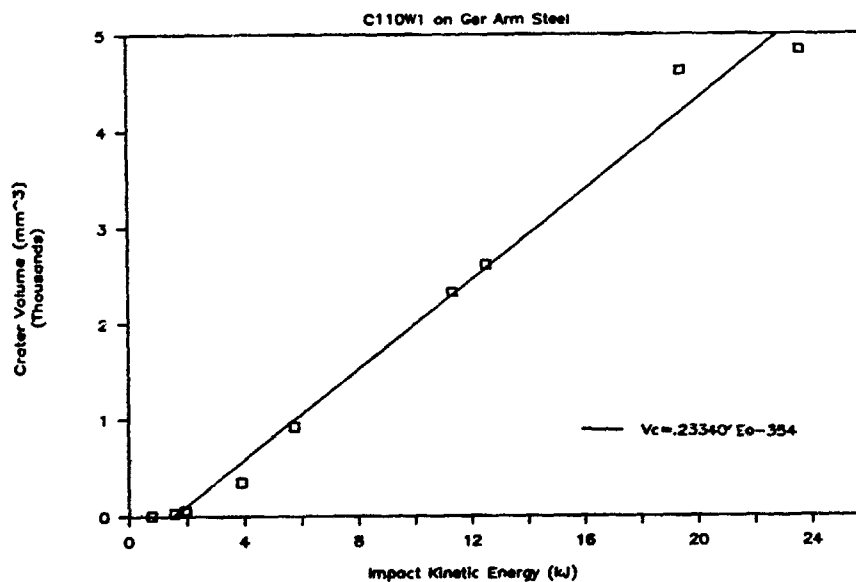


Figure 71b. Crater Volume vs. Impact Kinetic Energy

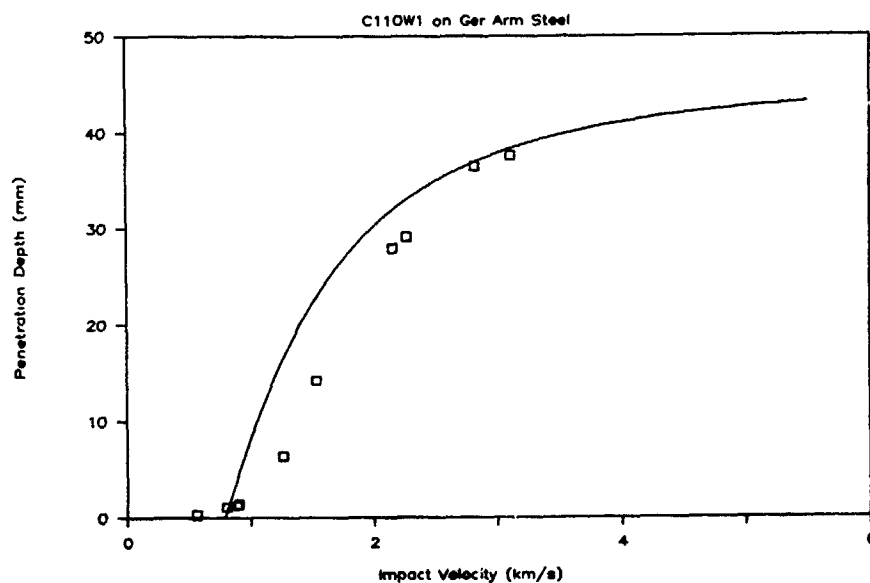


Figure 71c. Penetration Depth vs. Impact Velocity

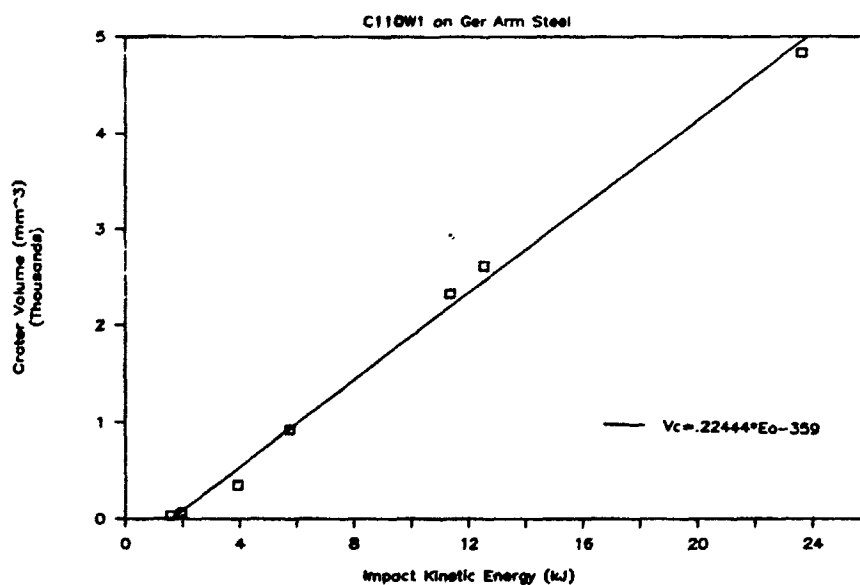


Figure 71d. Crater Volume vs. Impact Kinetic Energy

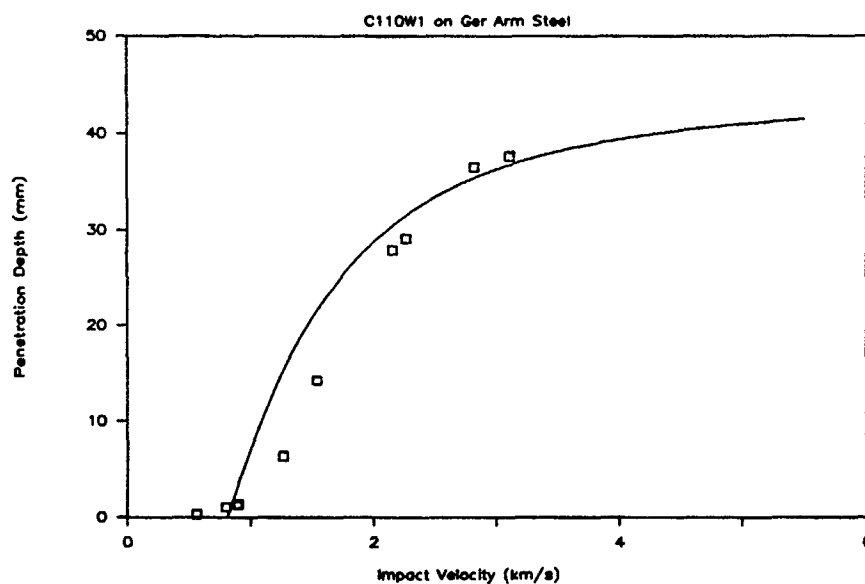


Figure 71e. Penetration Depth vs. Impact Velocity

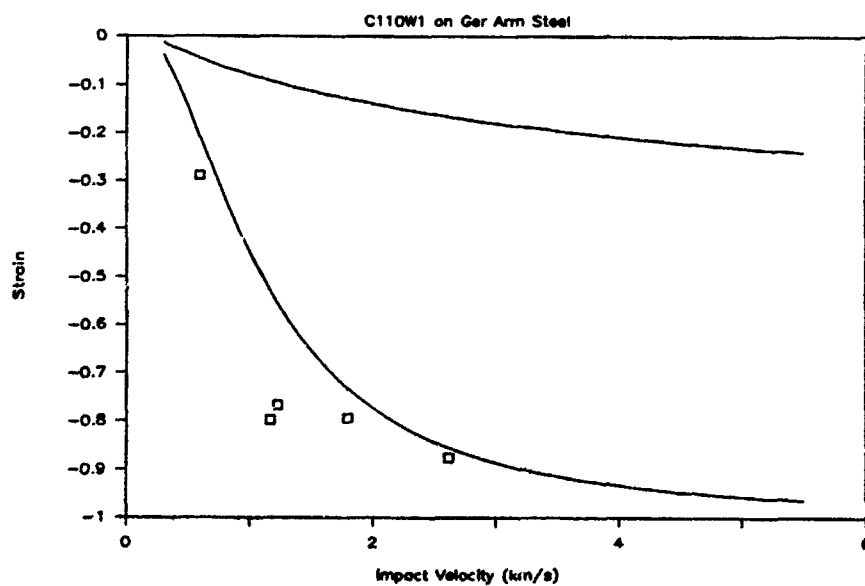


Figure 72a. Strain vs. Impact Velocity

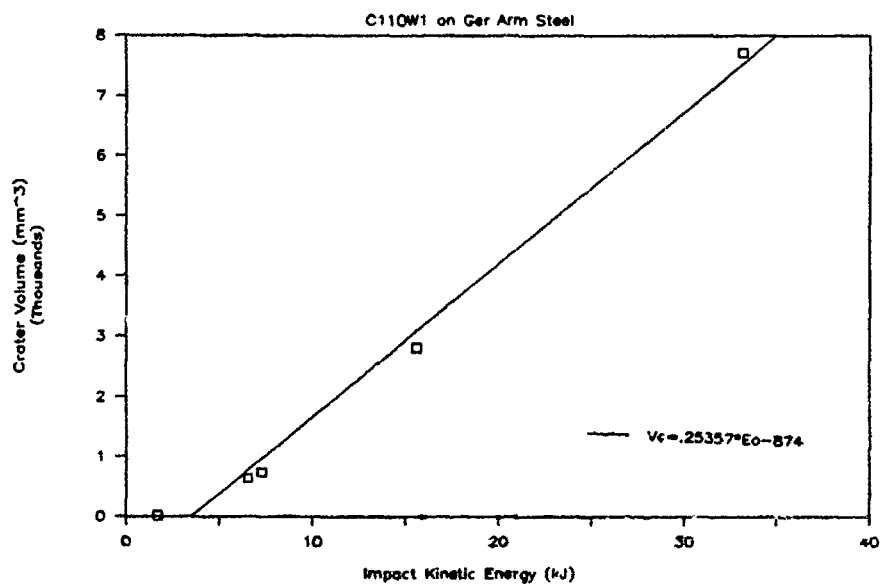


Figure 72b. Crater Volume vs. Impact Kinetic Energy

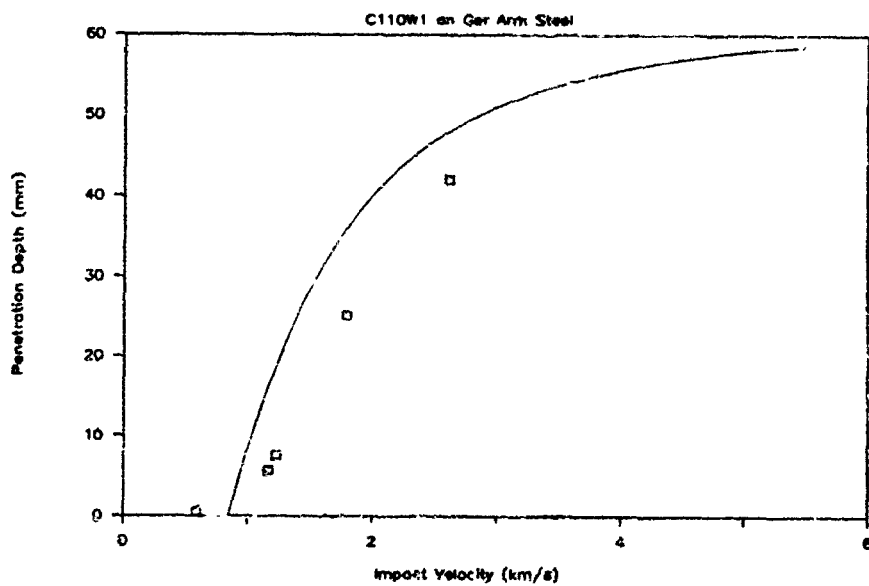


Figure 72c. Penetration Depth vs. Impact Velocity

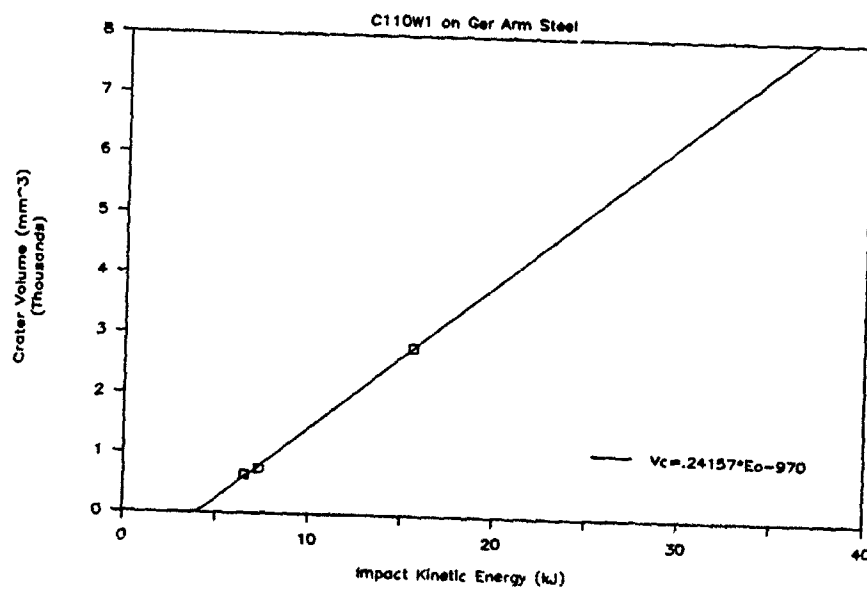


Figure 72d. Crater Volume vs. Impact Kinetic Energy

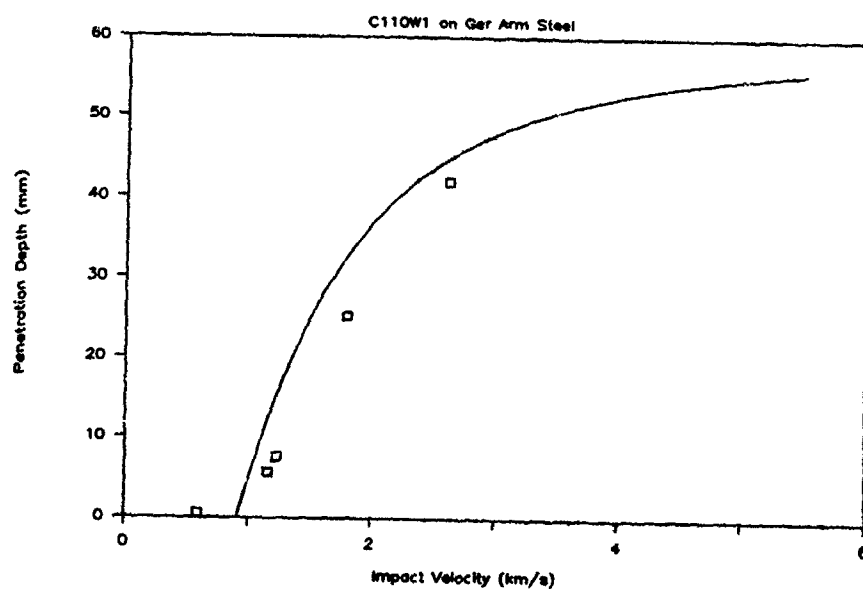


Figure 72e. Penetration Depth vs. Impact Velocity

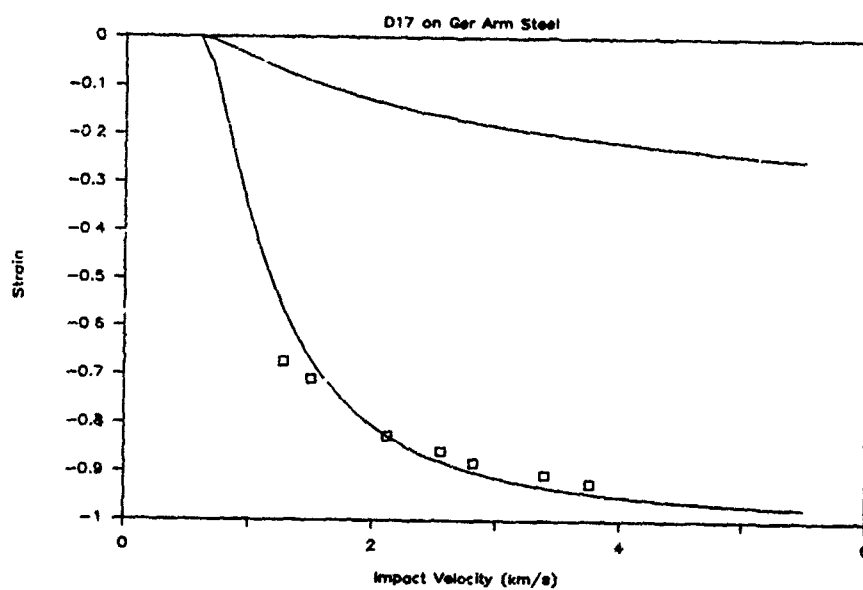


Figure 73a. Strain vs. Impact Velocity

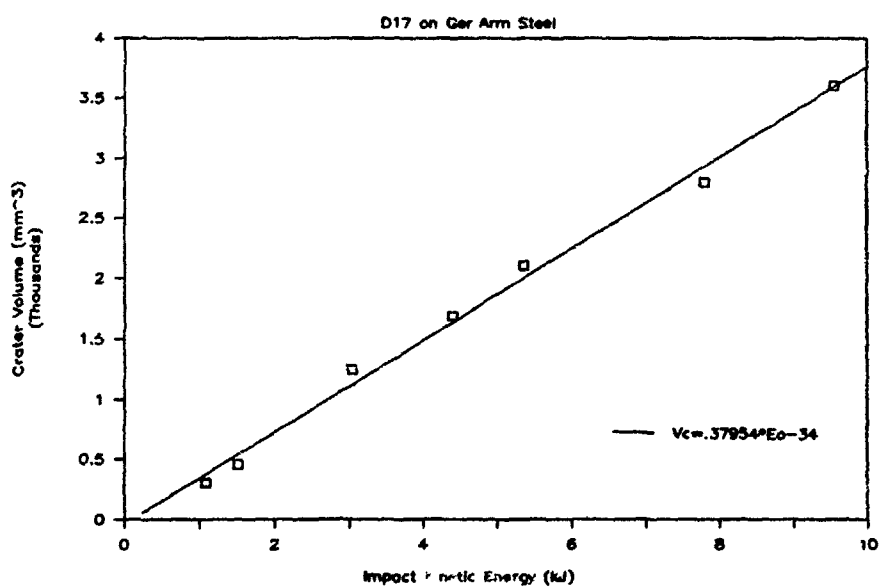


Figure 73b. Crater Volume vs. Impact Kinetic Energy

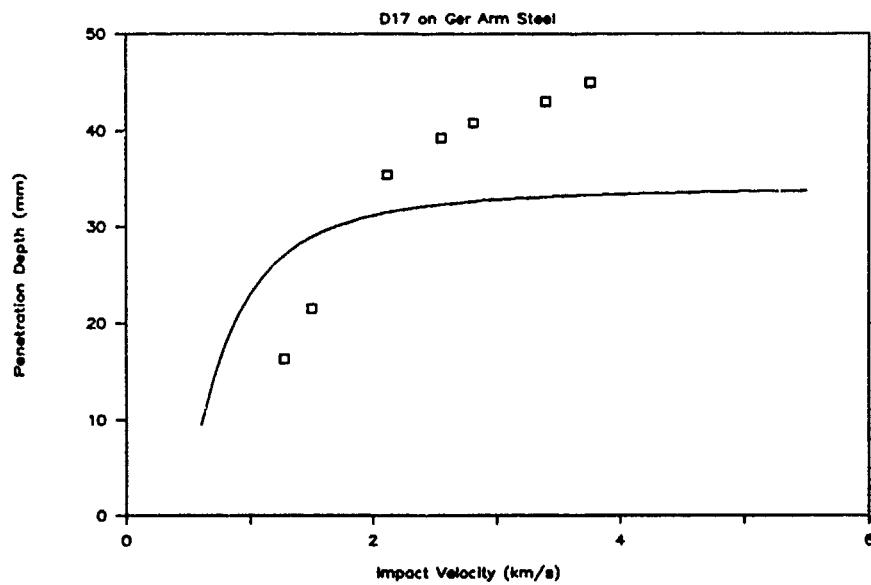


Figure 73c. Penetration Depth vs. Impact Velocity

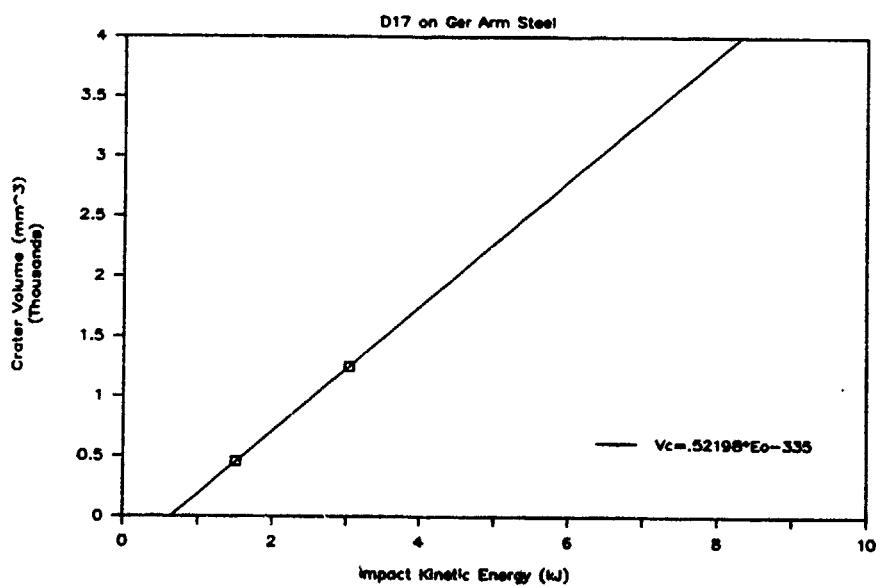


Figure 73d. Crater Volume vs. Impact Kinetic Energy

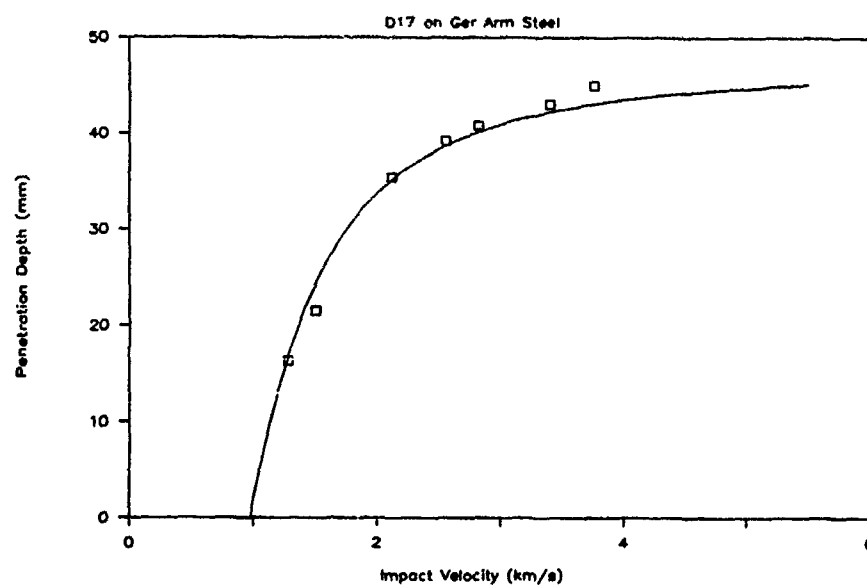


Figure 73e. Penetration Depth vs Impact Velocity

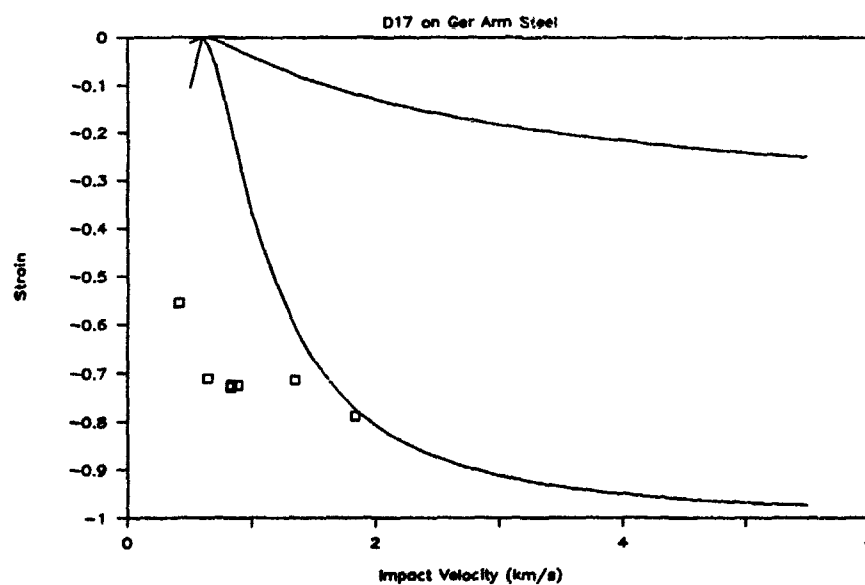


Figure 74a. Strain vs. Impact Velocity

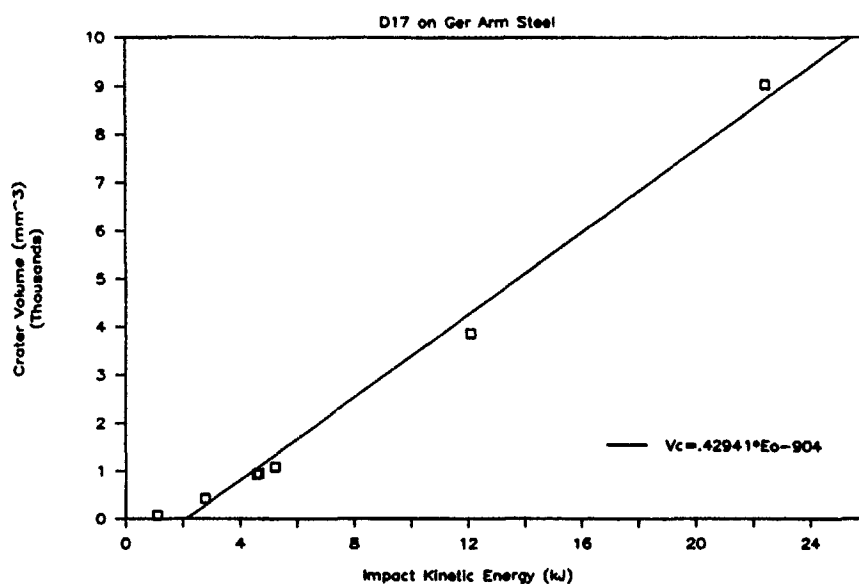


Figure 74b. Crater Volume vs. Impact Kinetic Energy

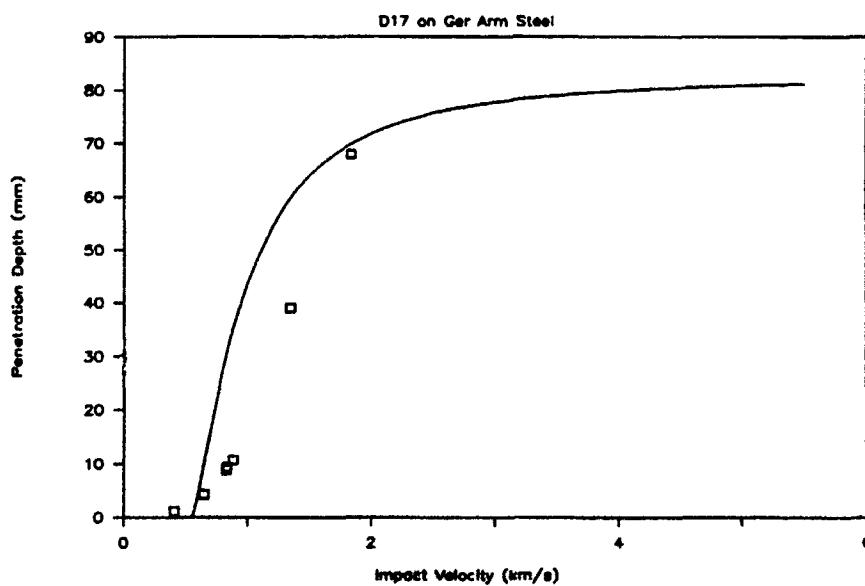


Figure 74c. Penetration Depth vs. Impact Velocity

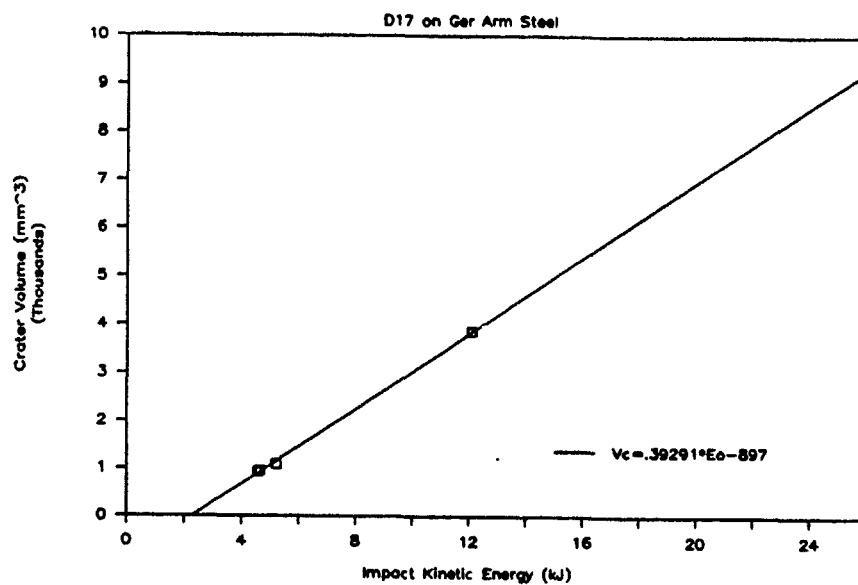


Figure 74d. Crater Volume vs. Impact Kinetic Energy

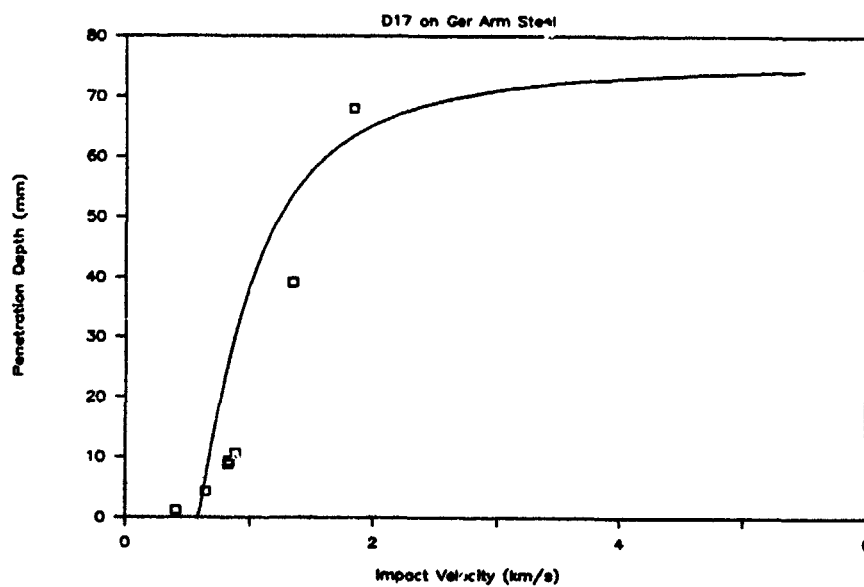


Figure 74e. Penetration Depth vs. Impact Velocity

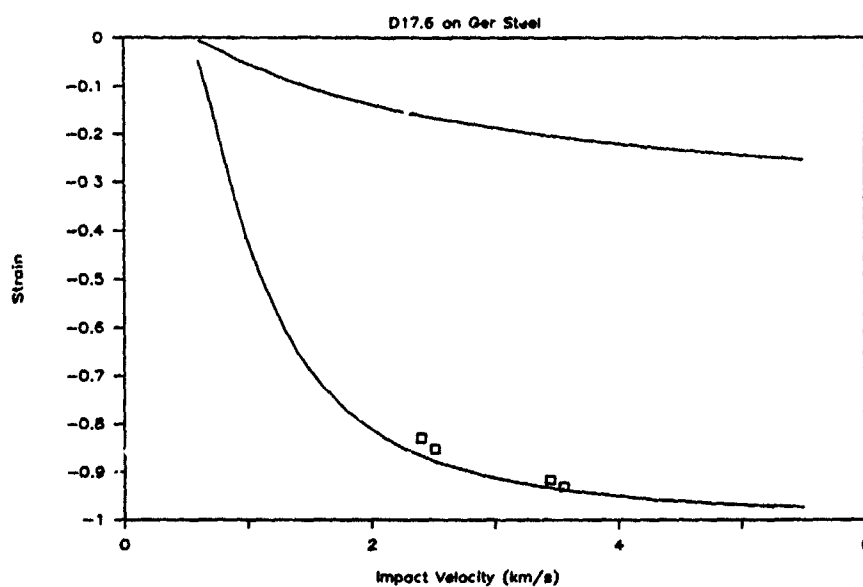


Figure 75a. Strain vs. Impact Velocity

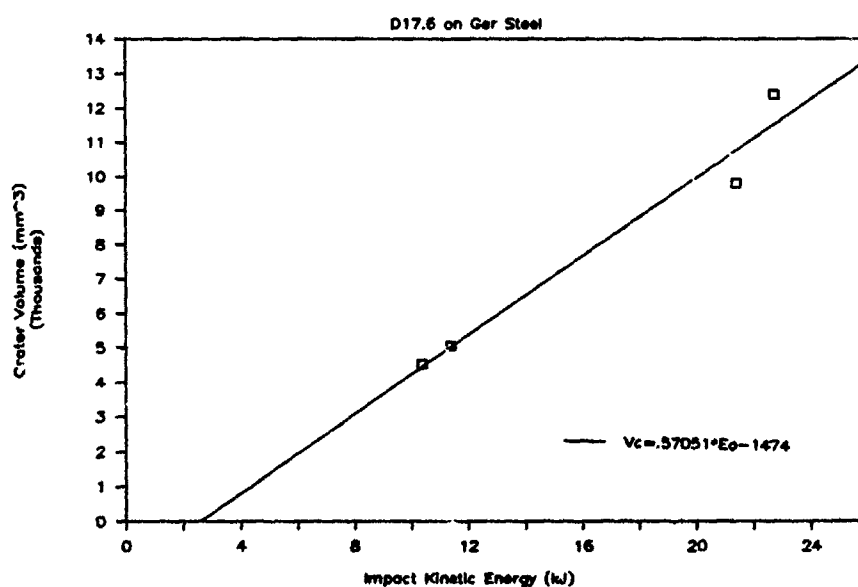


Figure 75b. Crater Volume vs. Impact Kinetic Energy

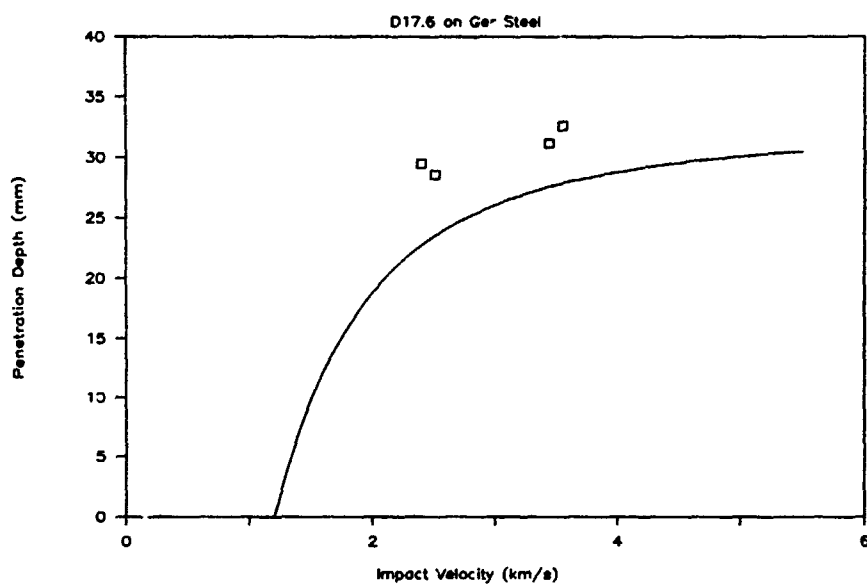


Figure 75c. Penetration Depth vs. Impact Velocity

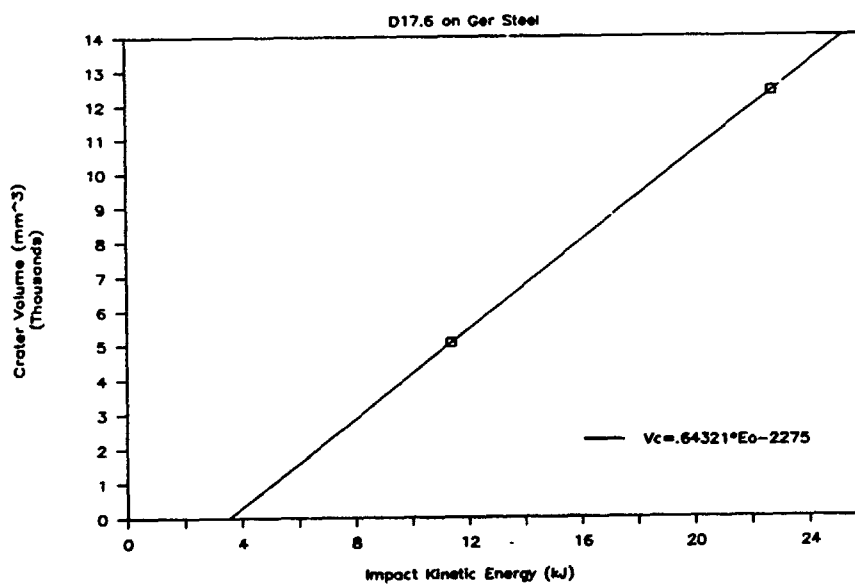


Figure 75d. Crater Volume vs. Impact Kinetic Energy

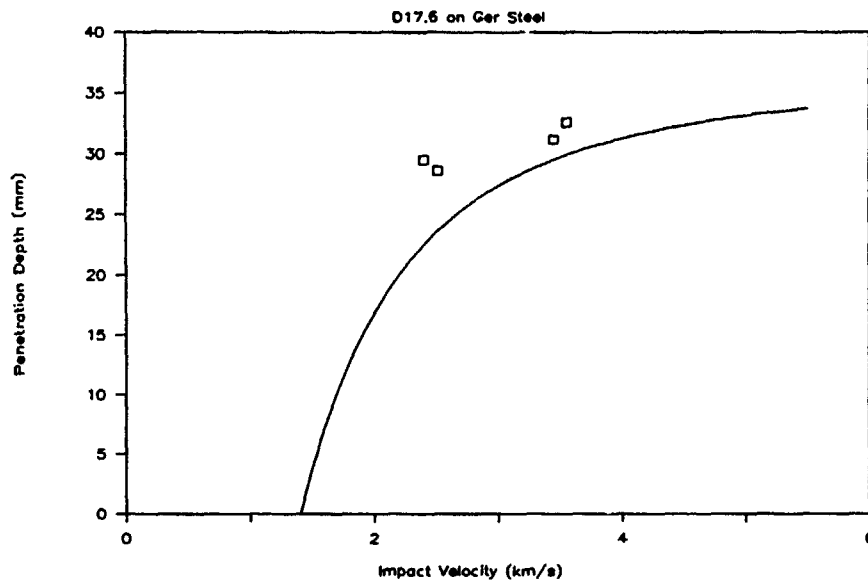


Figure 75e. Penetration Depth vs. Impact Velocity

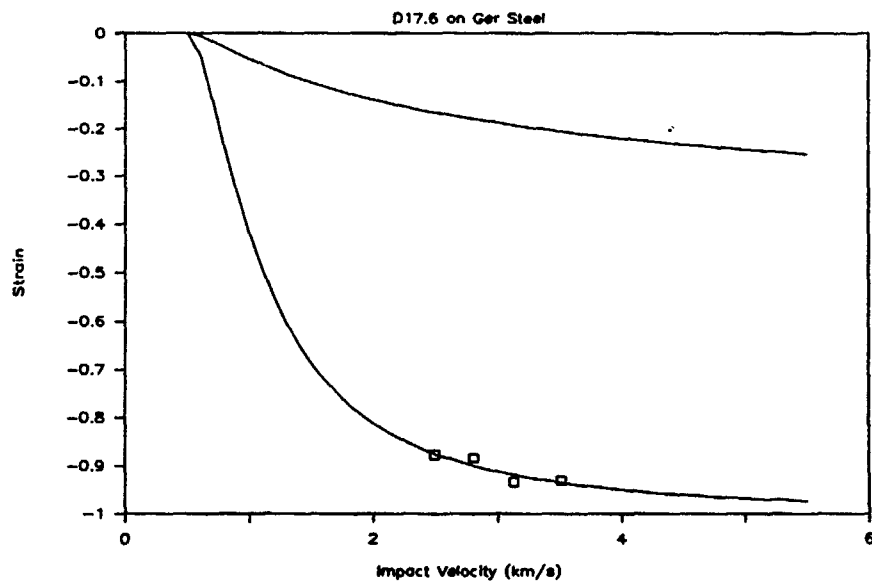


Figure 76a. Strain vs. Impact Velocity

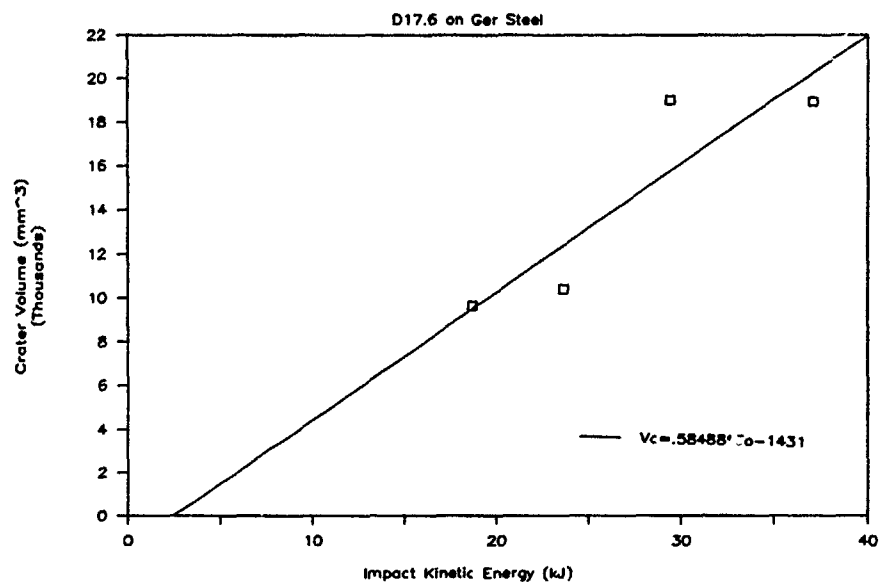


Figure 76b. Crater Volume vs. Impact Kinetic Energy

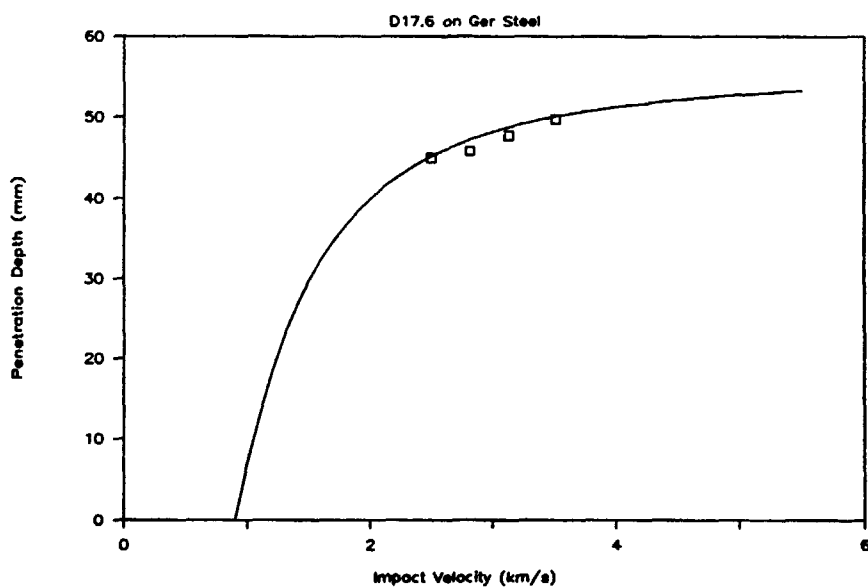


Figure 76c. Penetration Depth vs. Impact Velocity

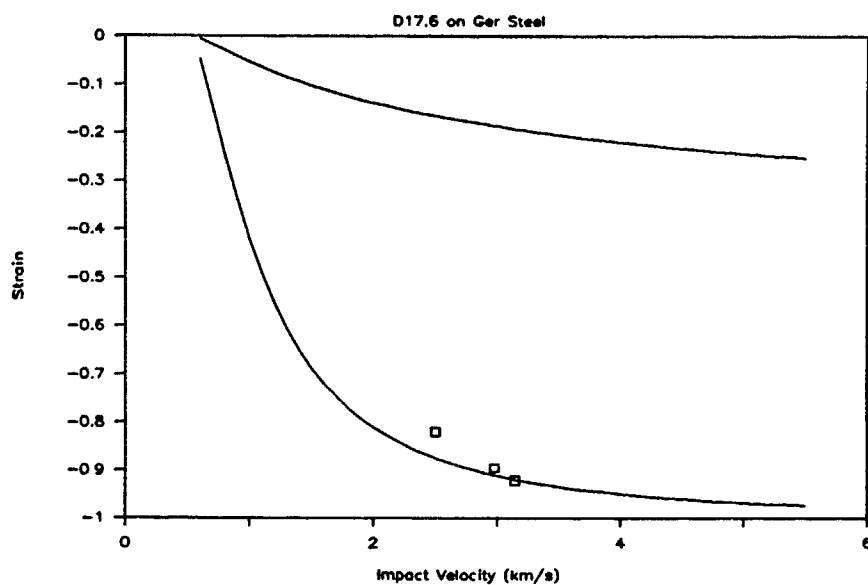


Figure 77a. Strain vs. Impact Velocity

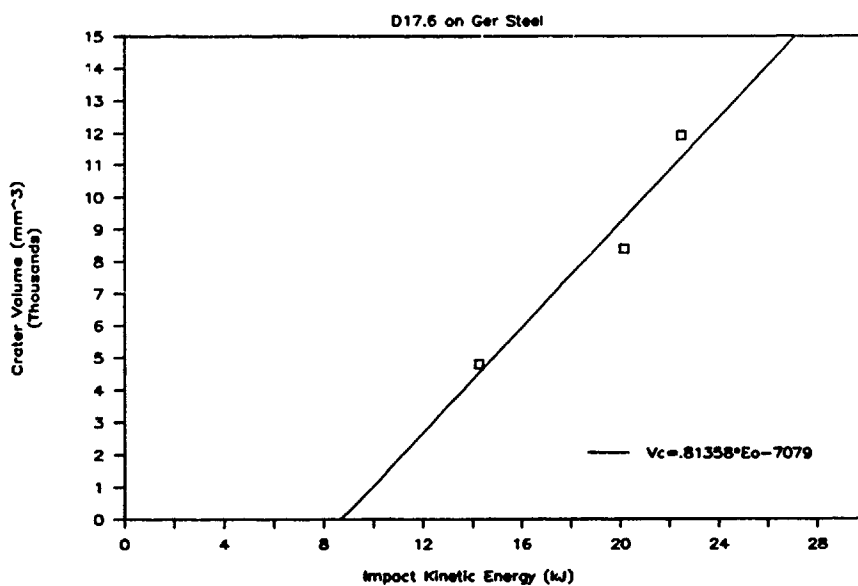


Figure 77b. Crater Volume vs. Impact Kinetic Energy

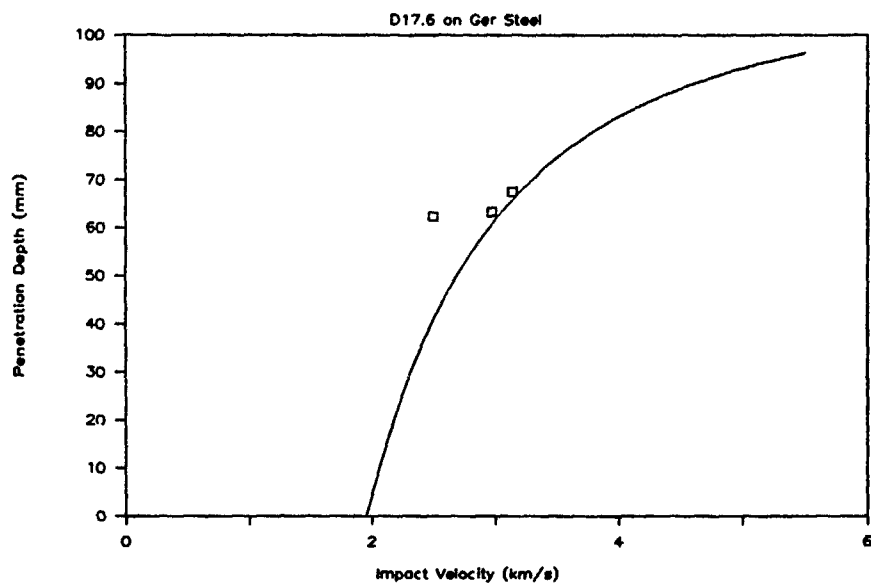


Figure 77c. Penetration Depth vs. Impact Velocity

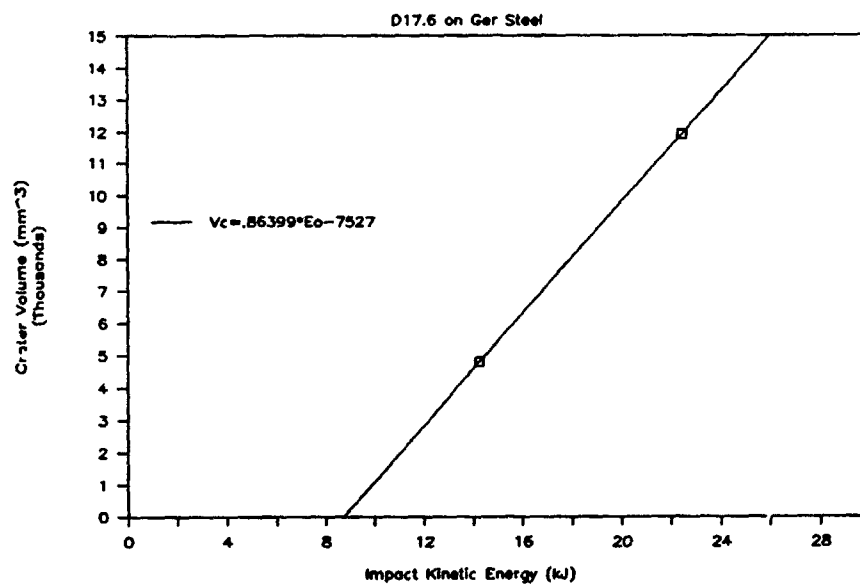


Figure 77d. Crater Volume vs. Impact Kinetic Energy

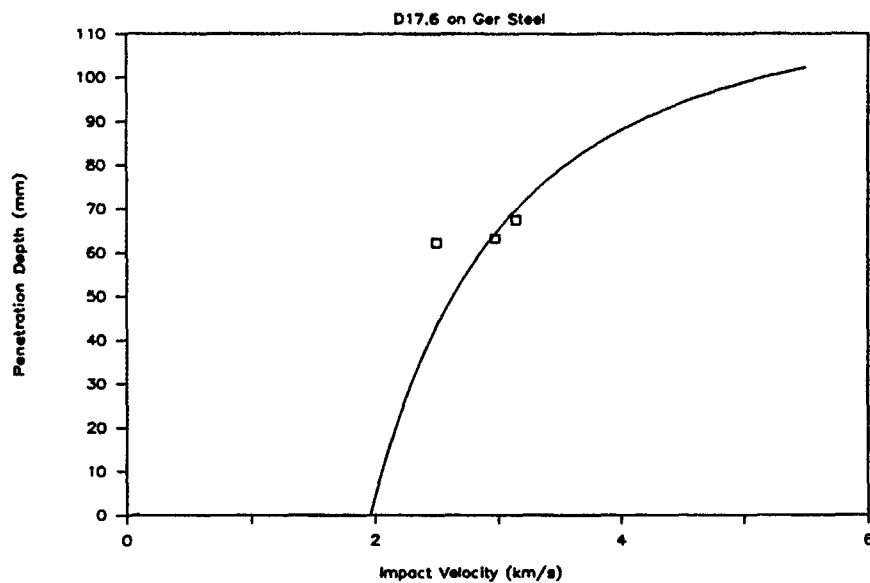


Figure 77e. Penetration Depth vs. Impact Velocity

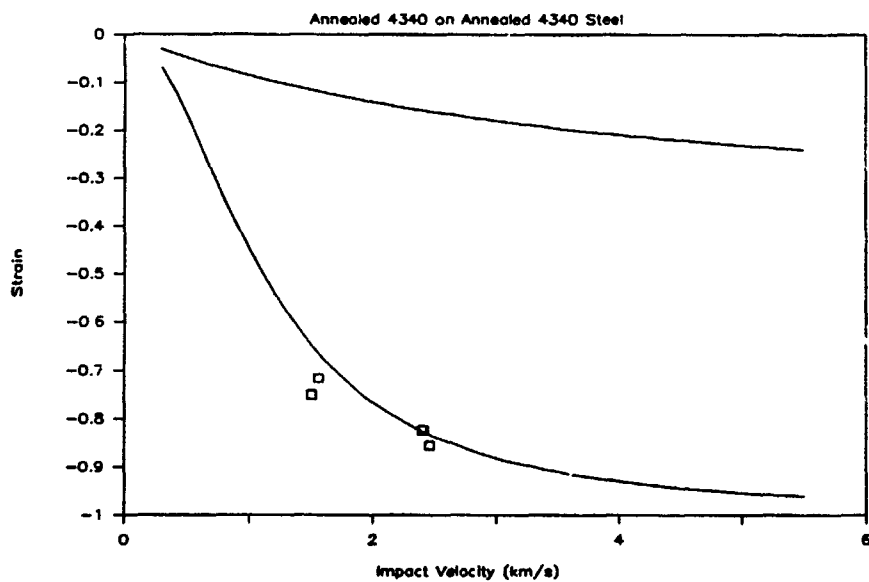


Figure 78a. Strain vs. Impact Velocity

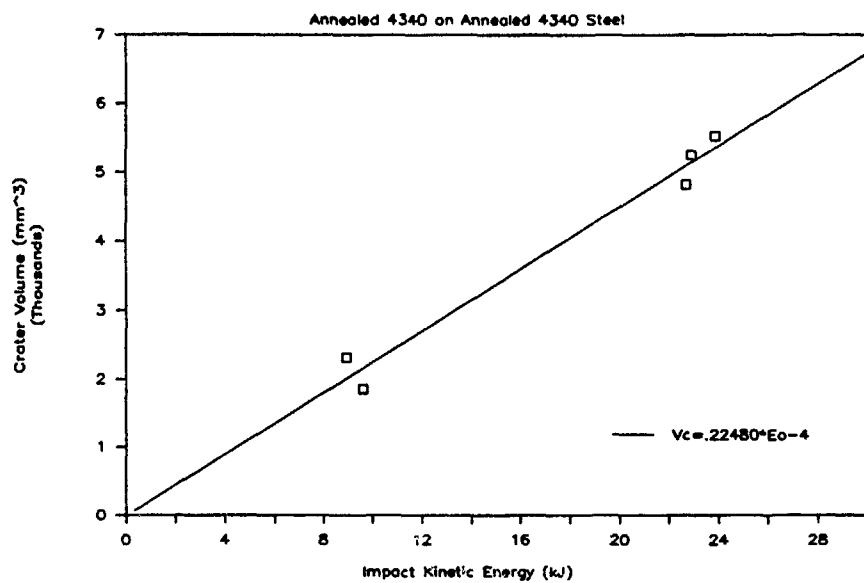


Figure 78b. Crater Volume vs. Impact Kinetic Energy

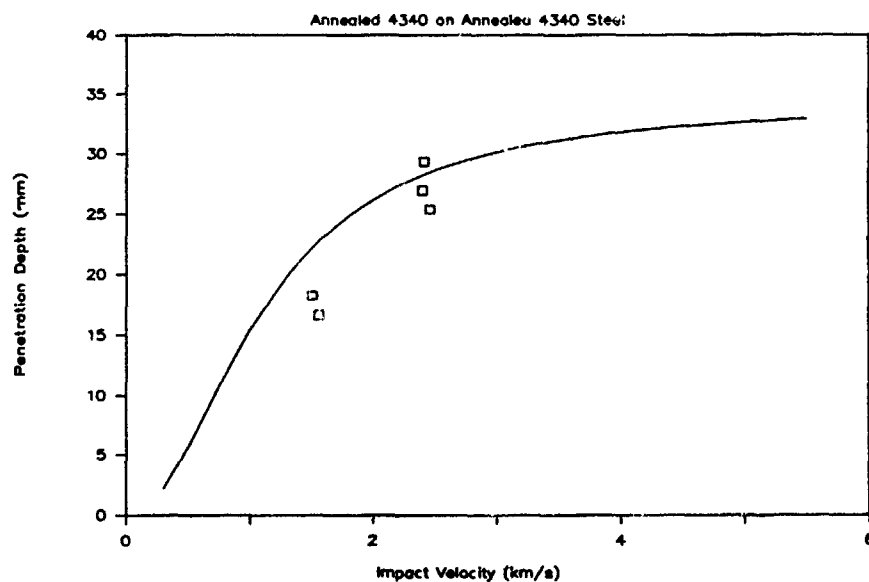


Figure 78c. Penetration Depth vs. Impact Velocity

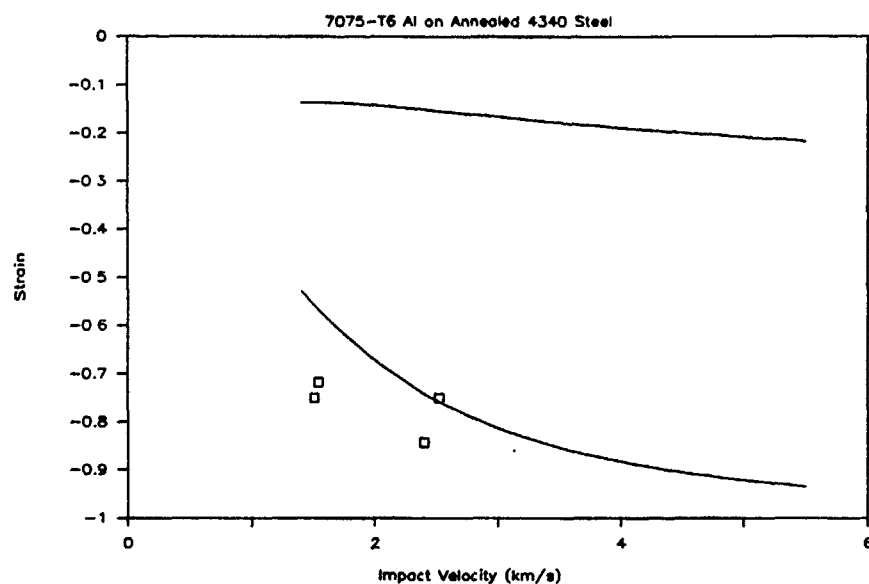


Figure 79a. Strain vs. Impact Velocity

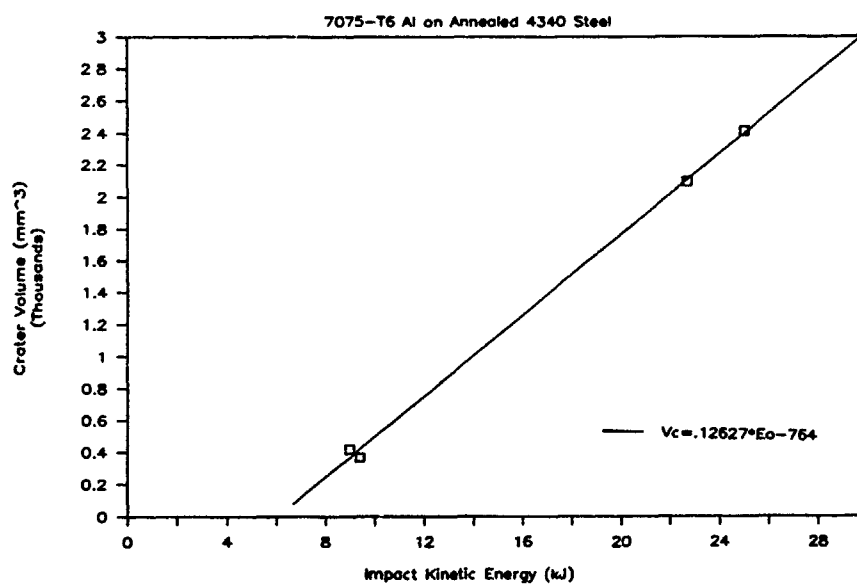


Figure 79b. Crater Volume vs. Impact Kinetic Energy

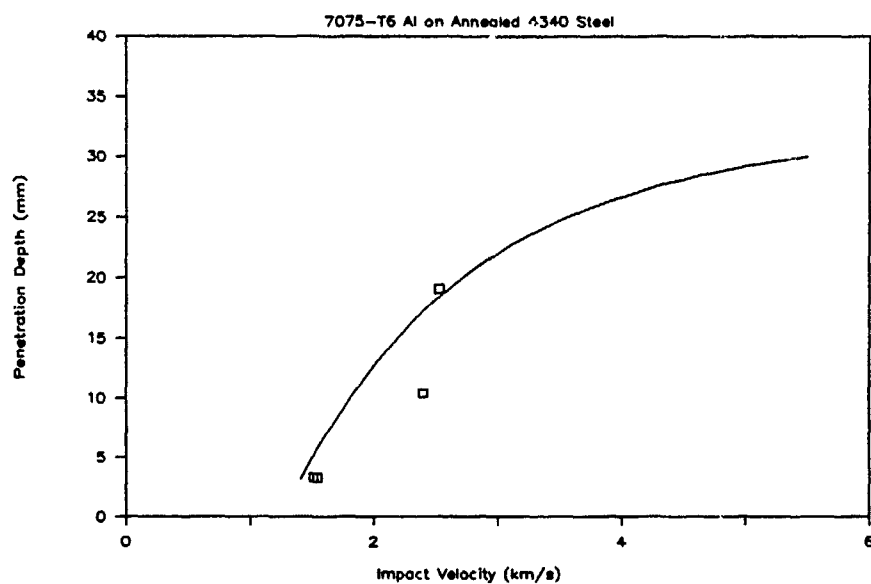


Figure 79c. Penetration Depth vs. Impact Velocity

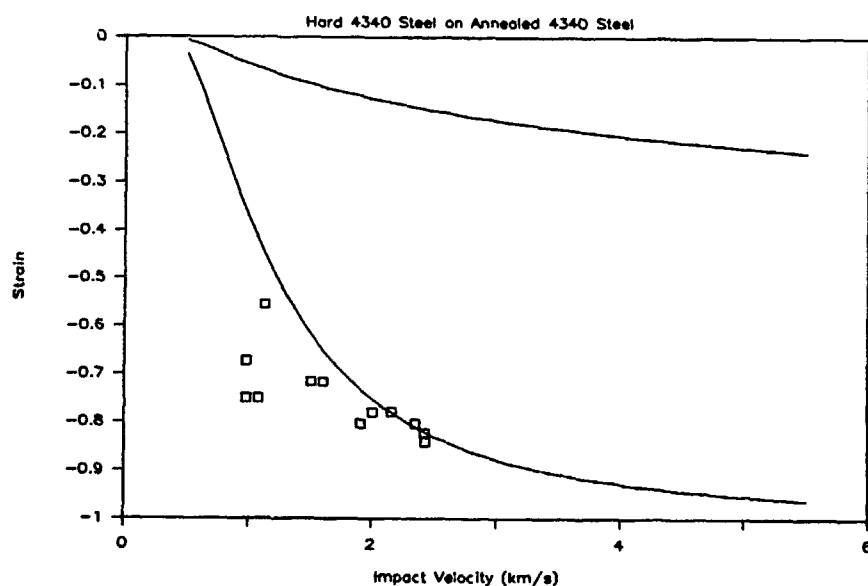


Figure 80a. Strain vs. Impact Velocity

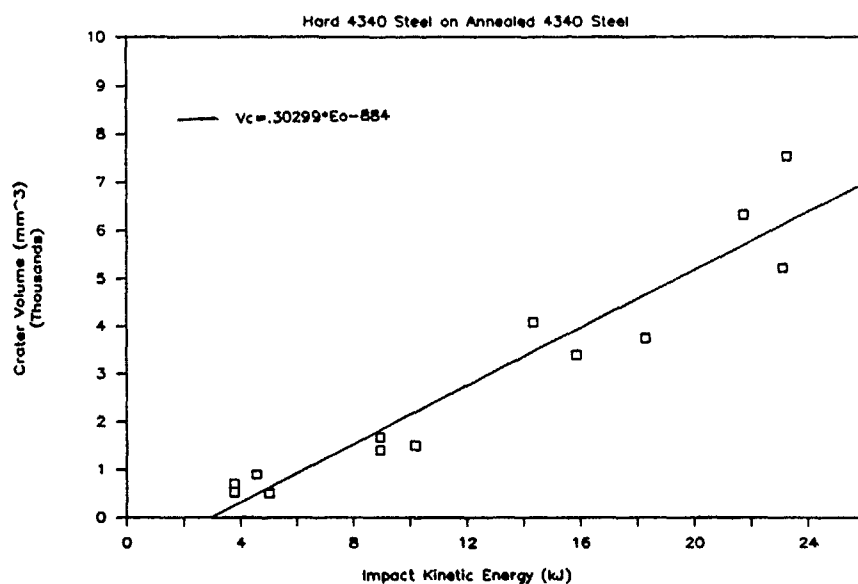


Figure 80b. Crater Volume vs. Impact Kinetic Energy

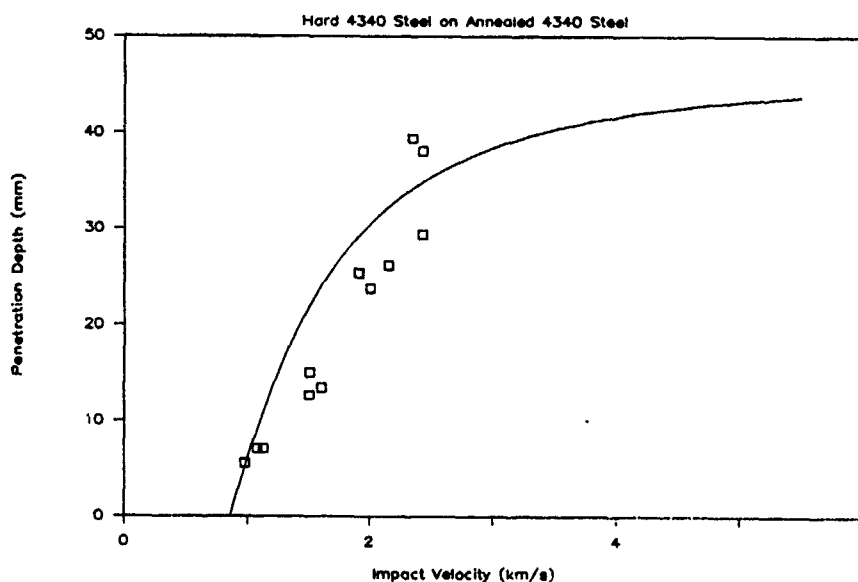


Figure 80c. Penetration Depth vs. Impact Velocity

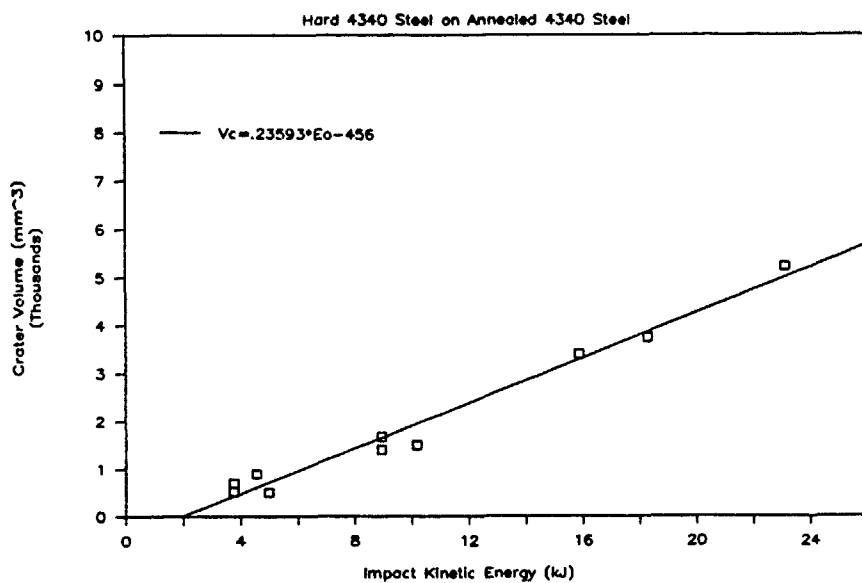


Figure 80d. Crater Volume vs. Impact Kinetic Energy

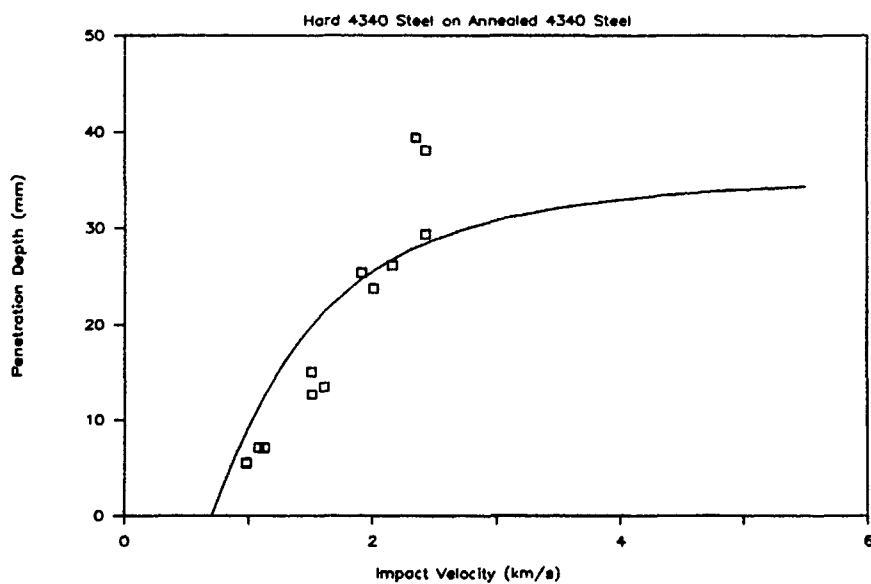


Figure 80e. Penetration Depth vs. Impact Velocity

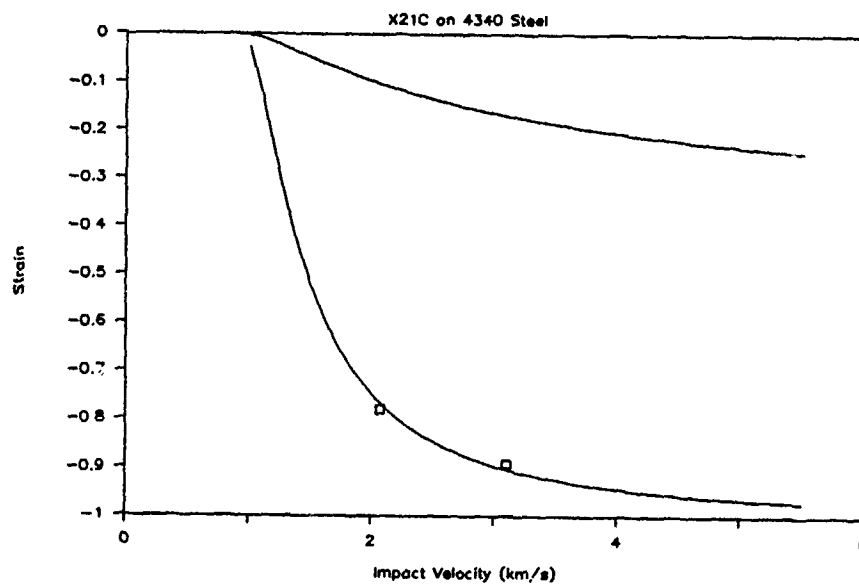


Figure 81a. Strain vs. Impact Velocity

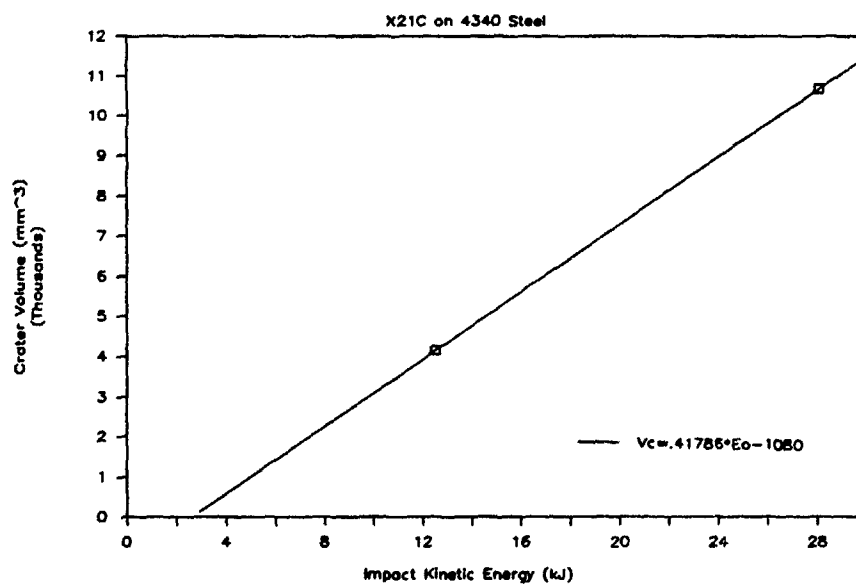


Figure 81b. Crater Volume vs. Impact Kinetic Energy

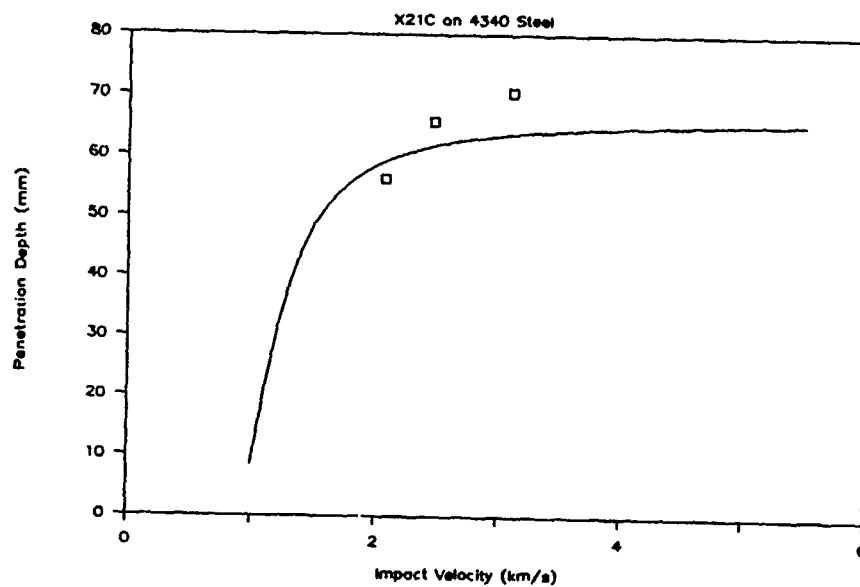


Figure 81c. Penetration Depth vs. Impact Velocity

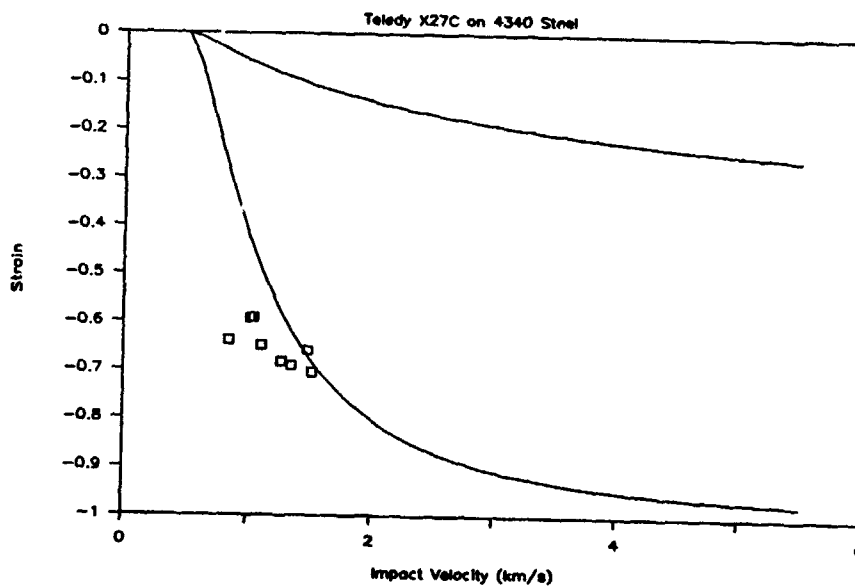


Figure 82a. Strain vs. Impact Velocity

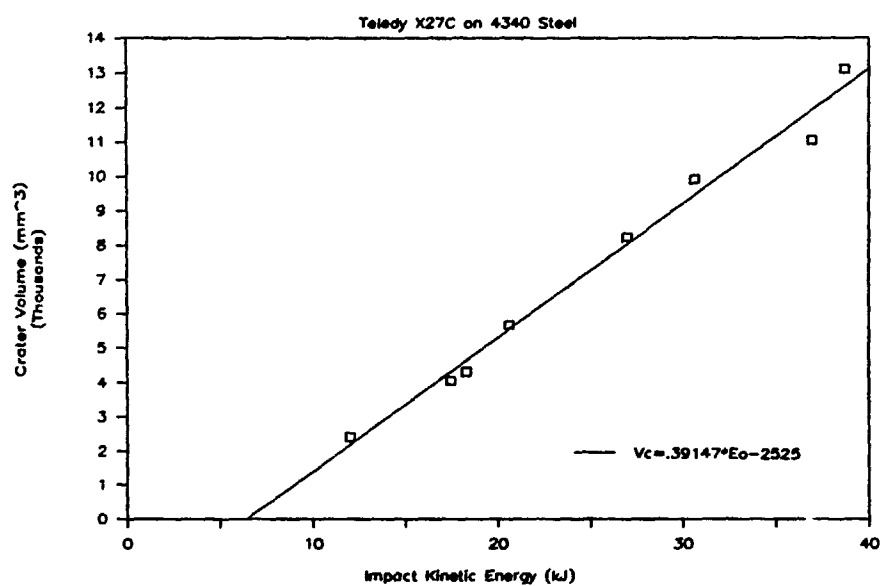


Figure 82b. Crater Volume vs. Impact Kinetic Energy

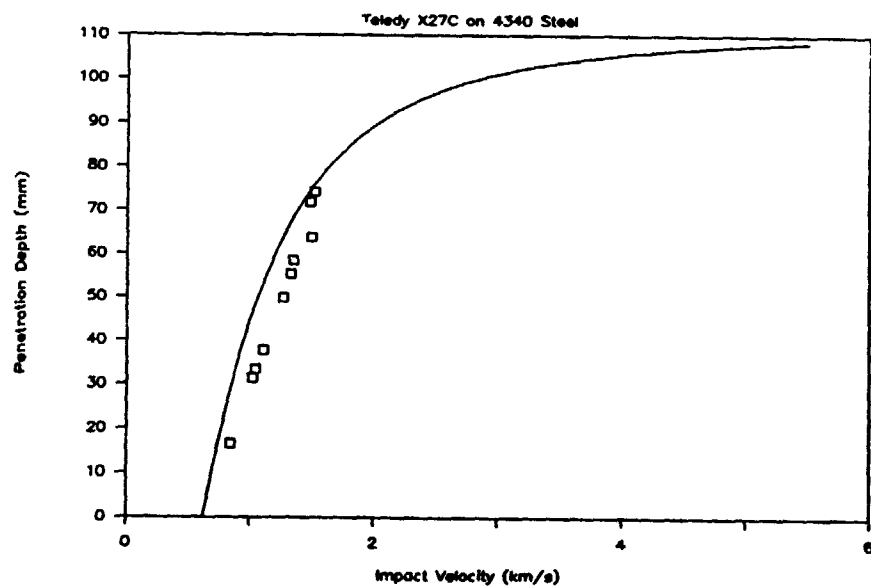


Figure 82c. Penetration Depth vs. Impact Velocity

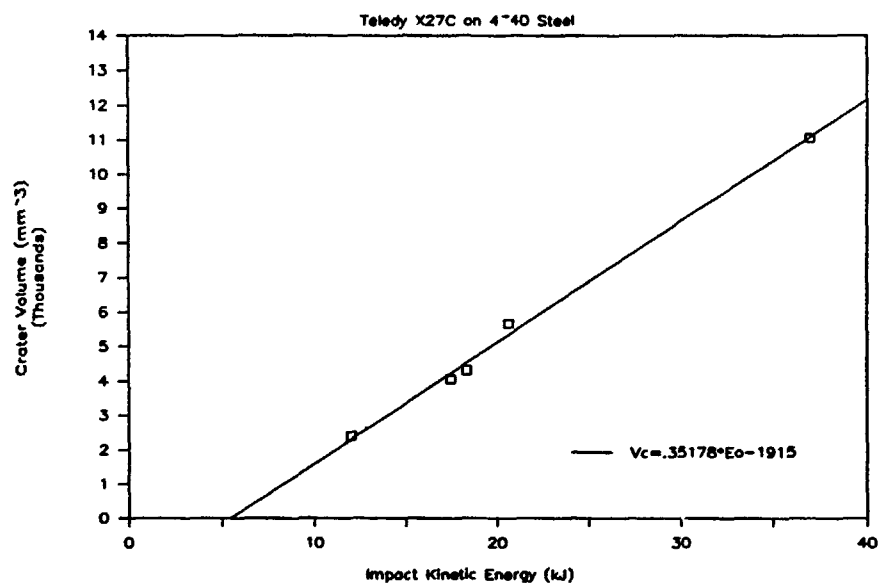


Figure 82d. Crater Volume vs. Impact Kinetic Energy

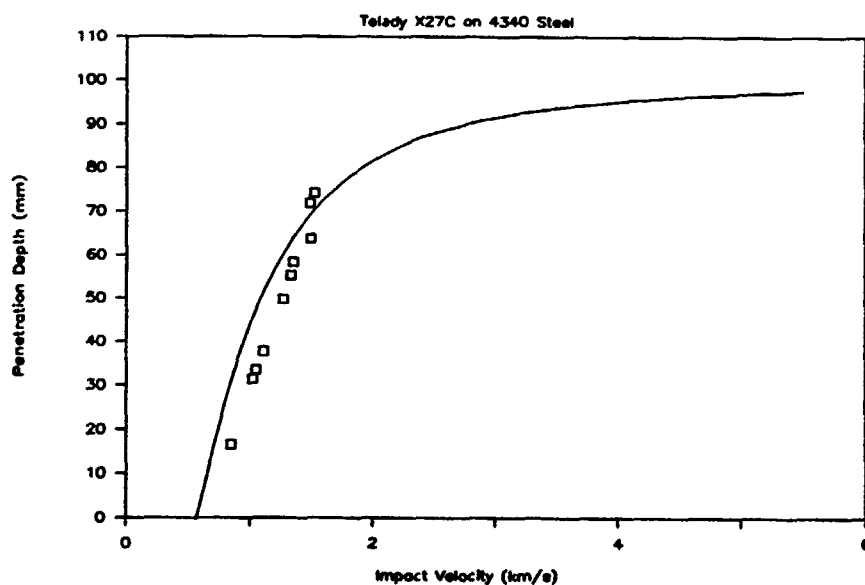


Figure 82e. Penetration Depth vs. Impact Velocity

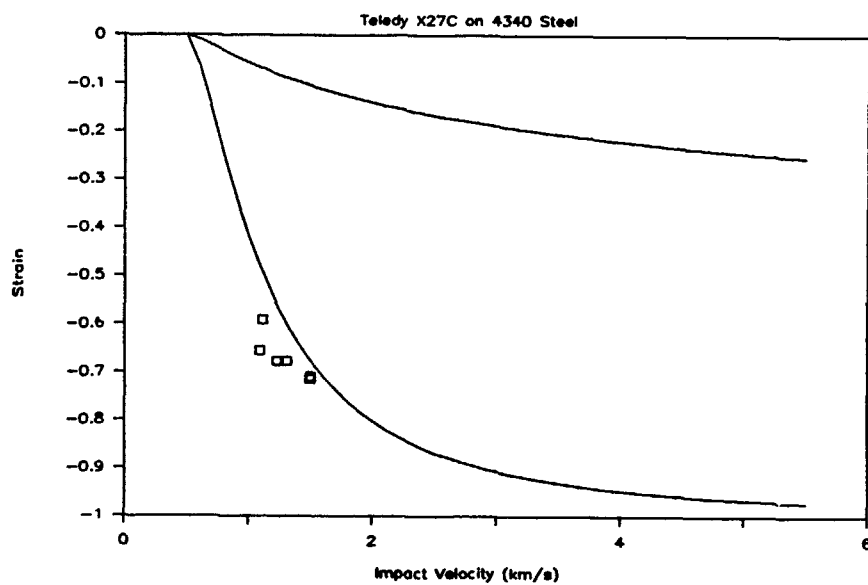


Figure 83a. Strain vs. Impact Velocity

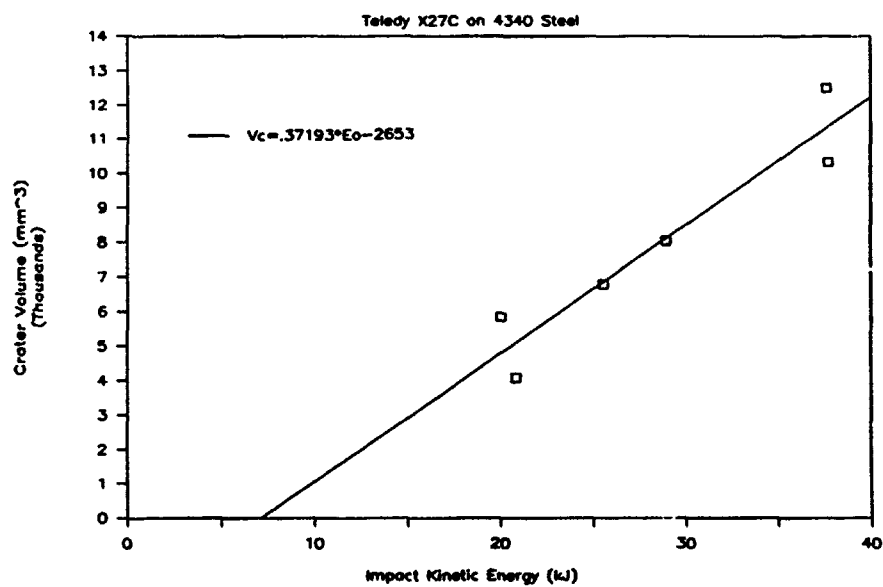


Figure 83b. Crater Volume vs. Impact Kinetic Energy

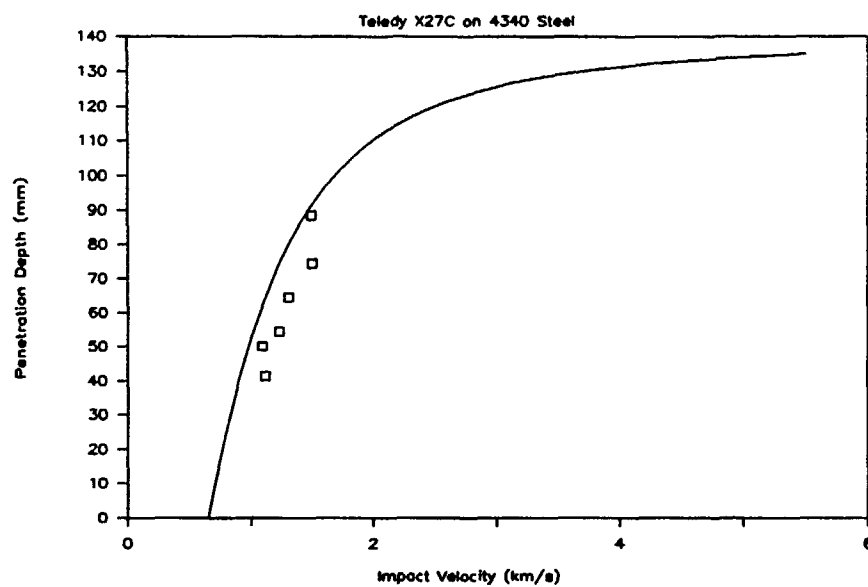


Figure 83c. Penetration Depth vs. Impact Velocity

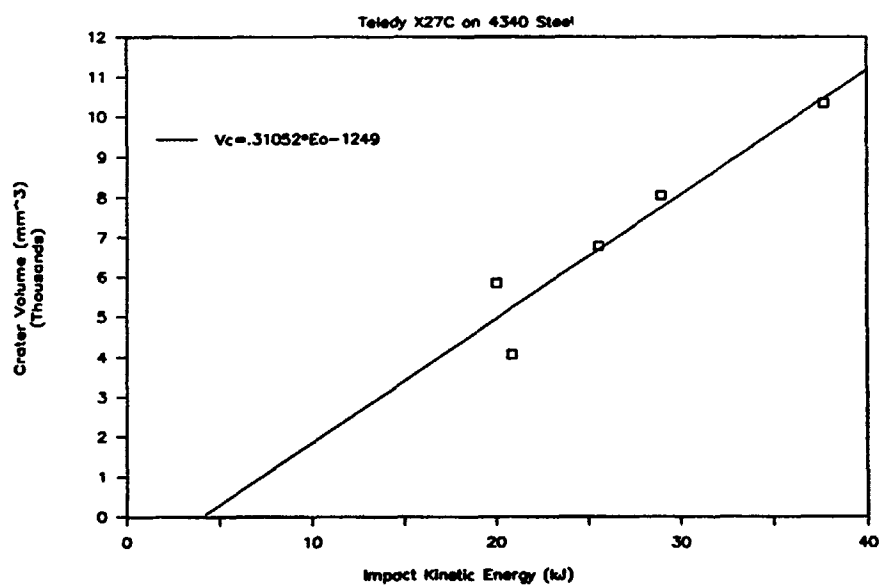


Figure 83d. Crater Volume vs. Impact Kinetic Energy

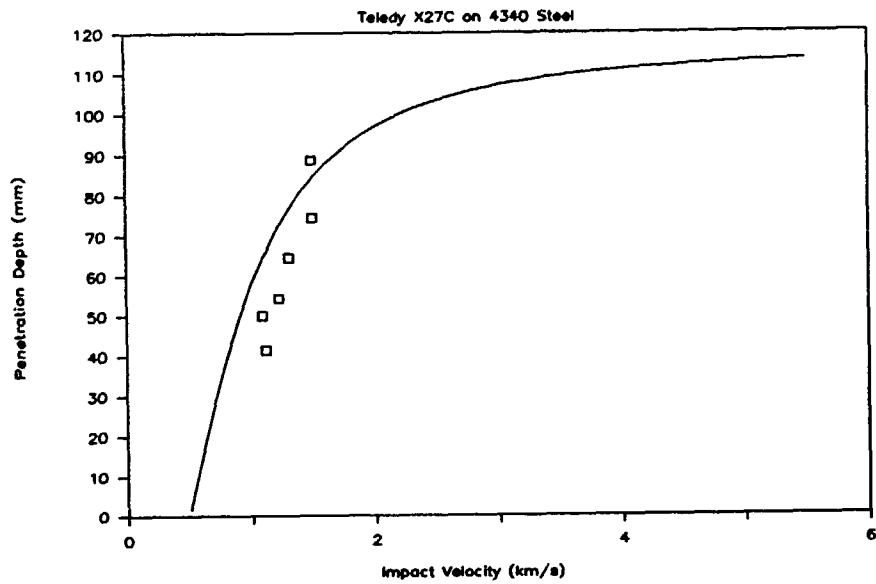


Figure 83e. Penetration Depth vs. Impact Velocity

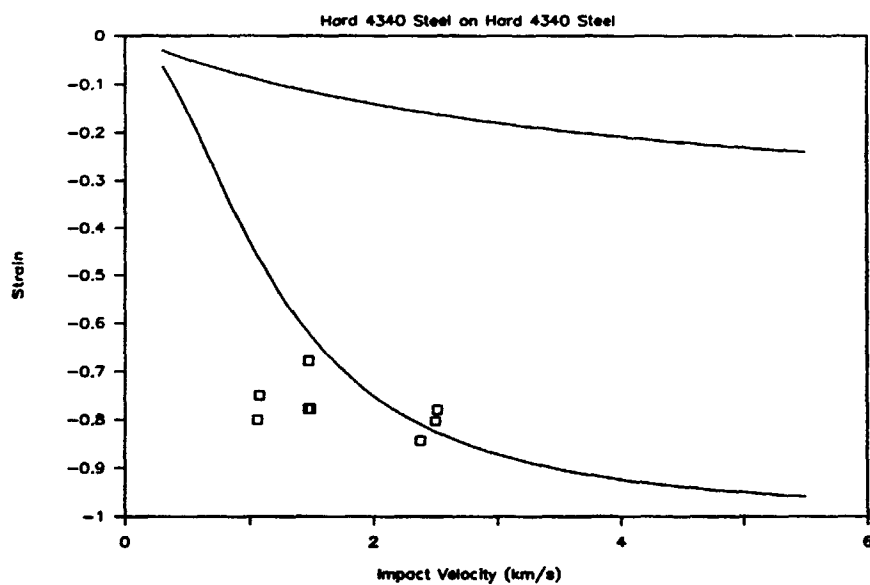


Figure 84a. Strain vs. Impact Velocity

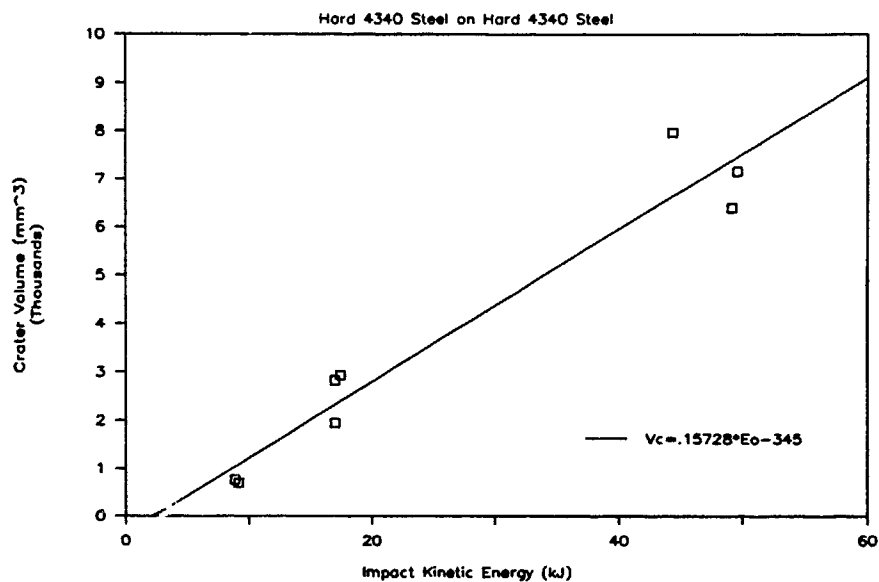


Figure 84b. Crater Volume vs. Impact Kinetic Energy

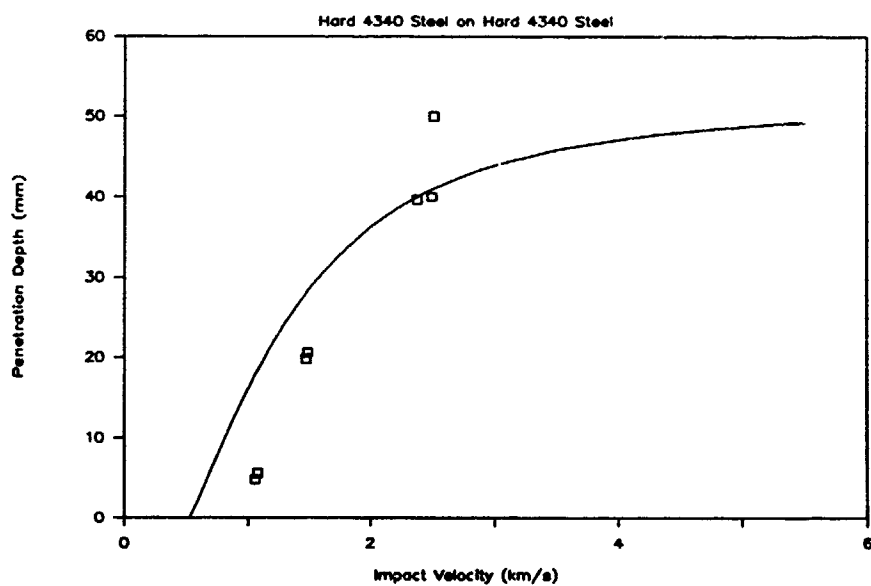


Figure 84c. Penetration Depth vs. Impact Velocity

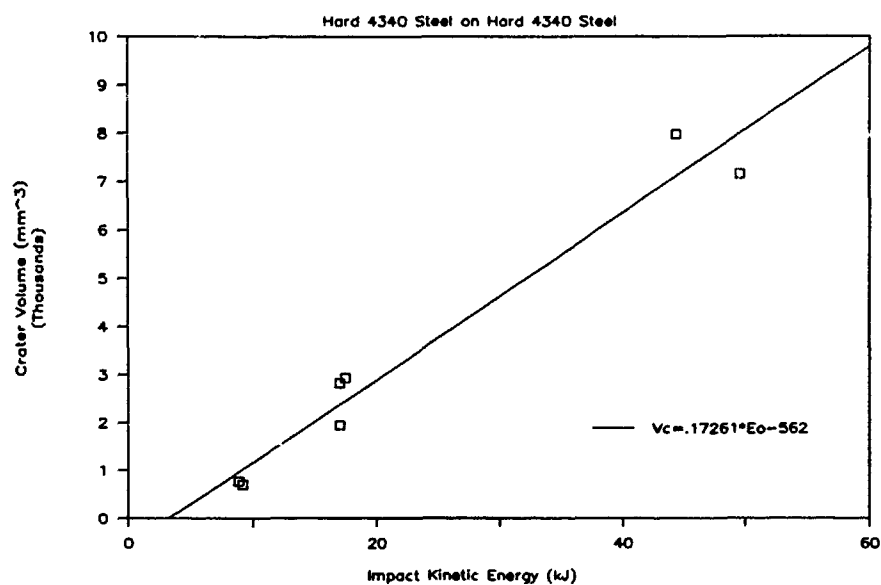


Figure 84d. Crater Volume vs. Impact Kinetic Energy

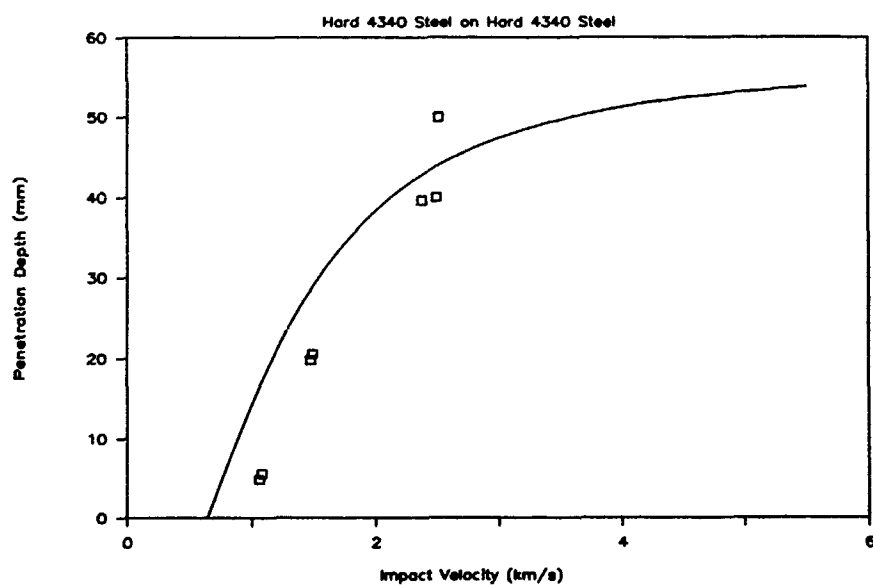


Figure 84e. Penetration Depth vs. Impact Velocity

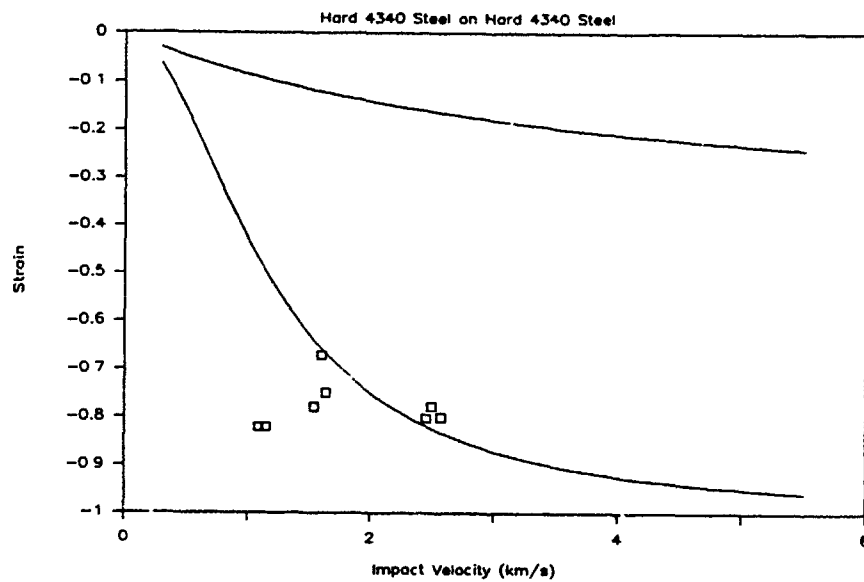


Figure 85a. Strain vs. Impact Velocity

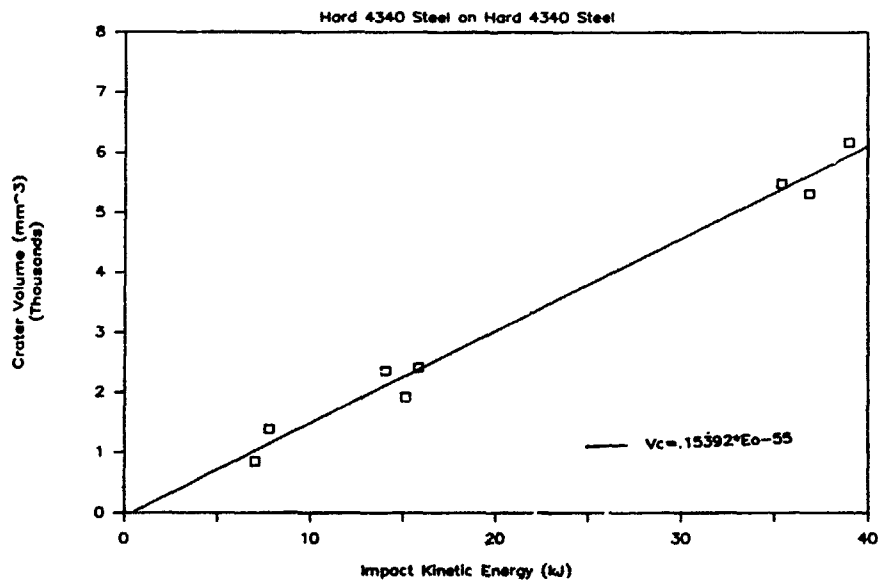


Figure 85b. Crater Volume vs. Impact Kinetic Energy

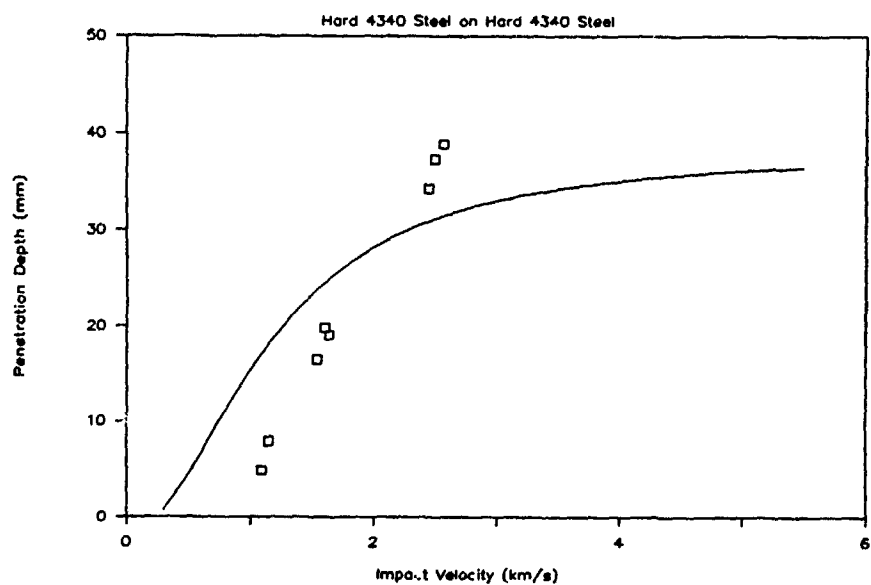


Figure 85c. Penetration Depth vs. Impact Velocity

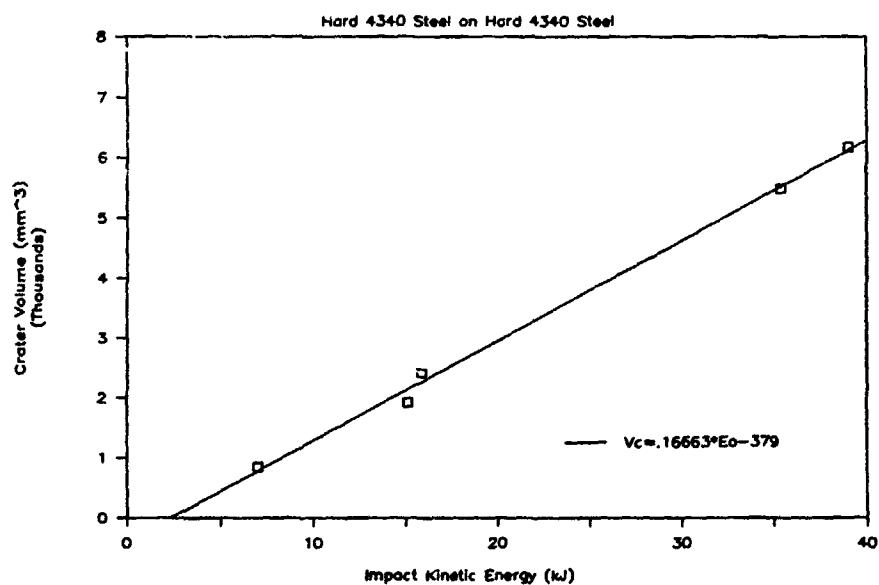


Figure 85d. Crater Volume vs. Impact Kinetic Energy

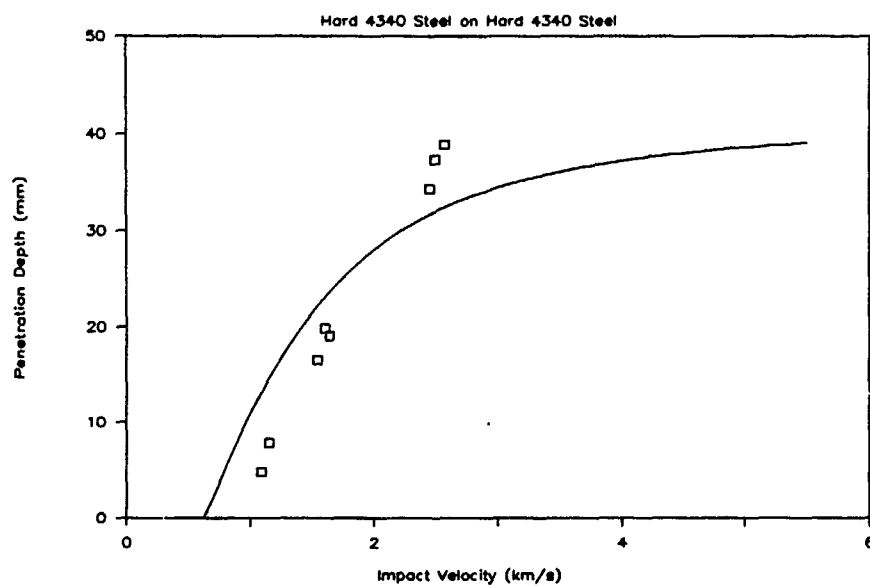


Figure 85e. Penetration Depth vs. Impact Velocity

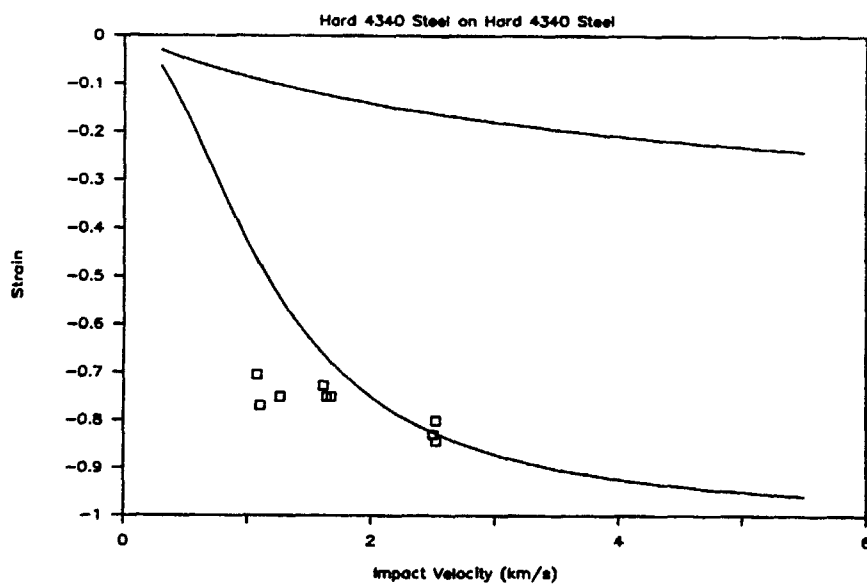


Figure 86a. Strain vs. Impact Velocity

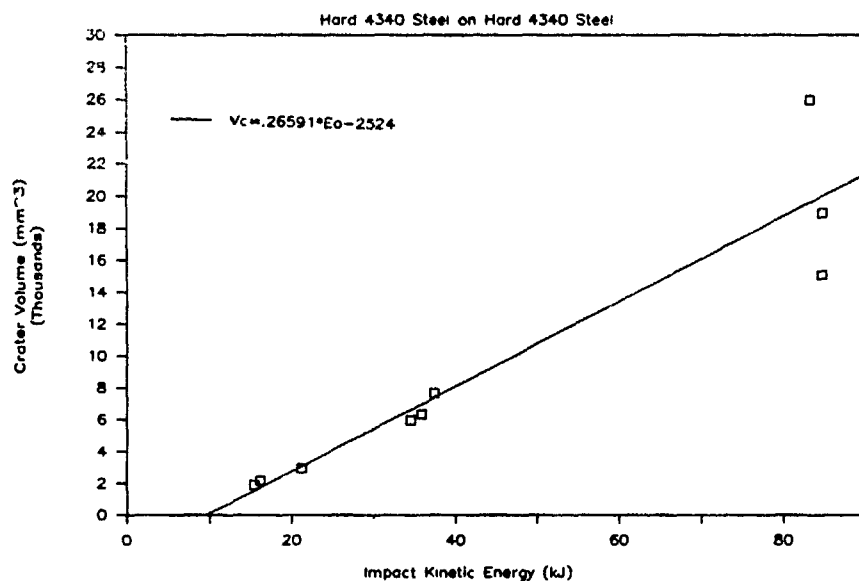


Figure 86b. Crater Volume vs. Impact Kinetic Energy

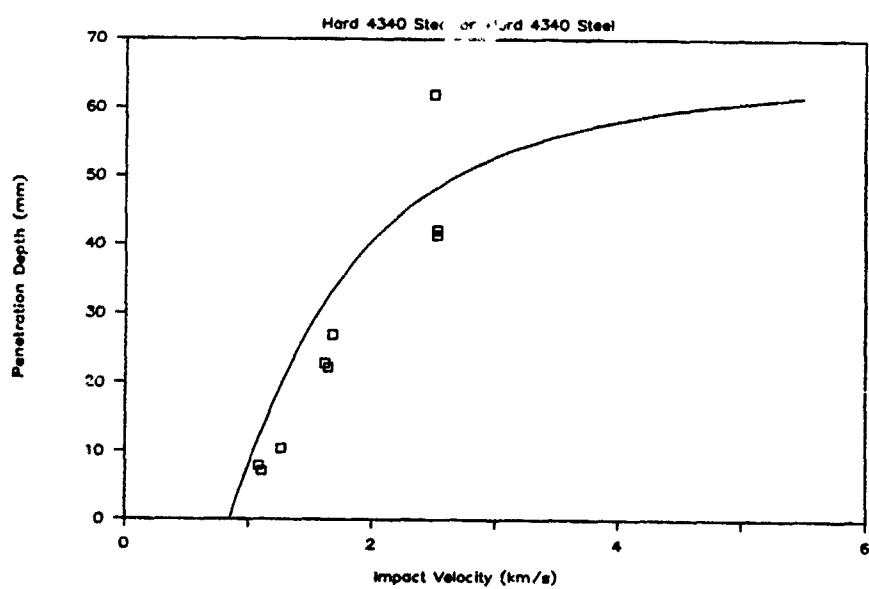


Figure 86c. Penetration Depth vs. Impact Velocity

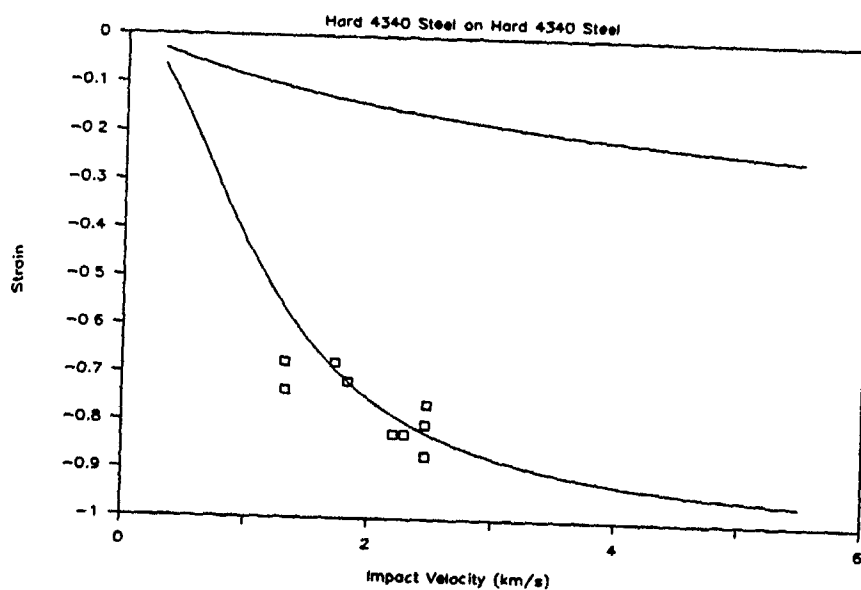


Figure 87a. Strain vs. Impact Velocity

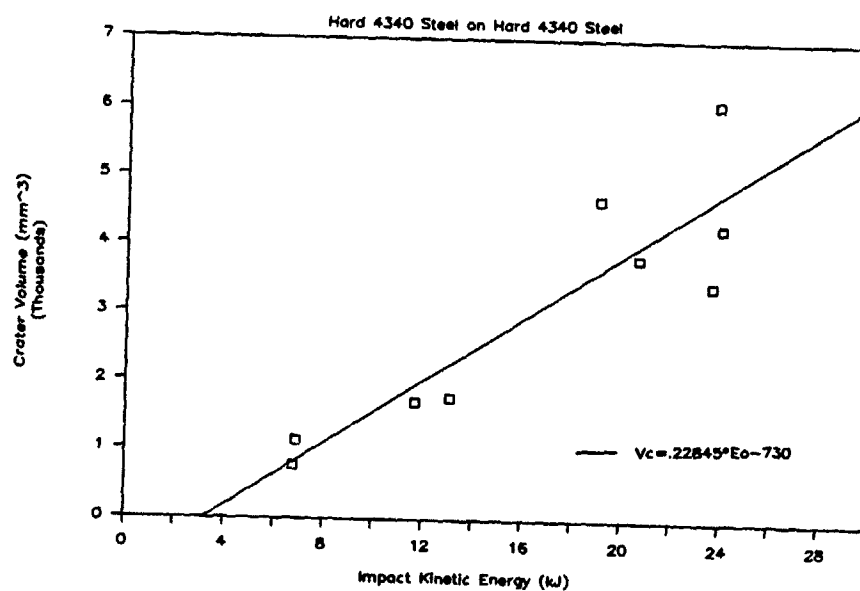


Figure 87b. Crater Volume vs. Impact Kinetic Energy

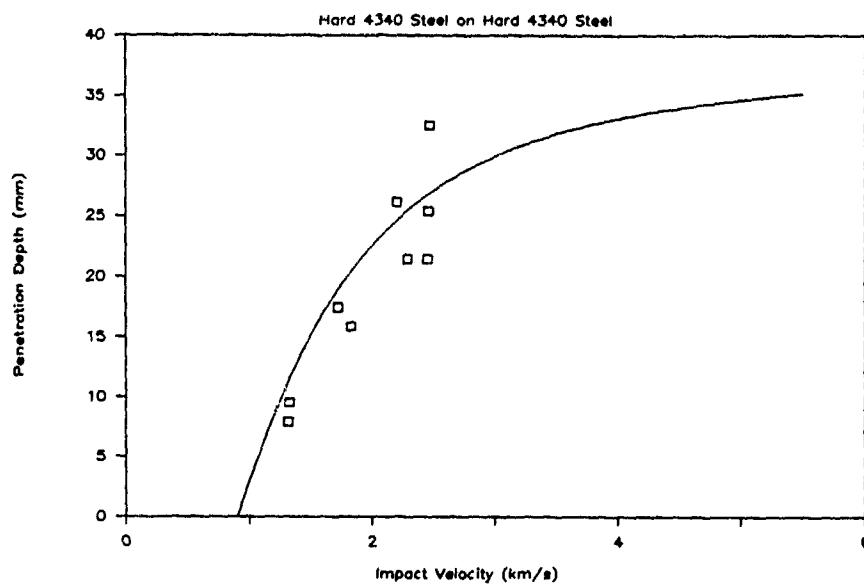


Figure 87c. Penetration Depth vs. Impact Velocity

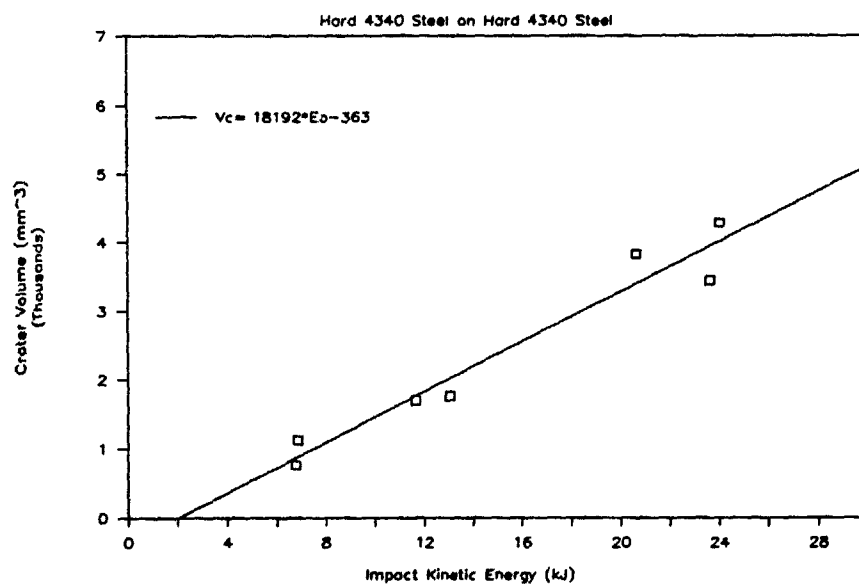


Figure 87d. Crater Volume vs. Impact Kinetic Energy

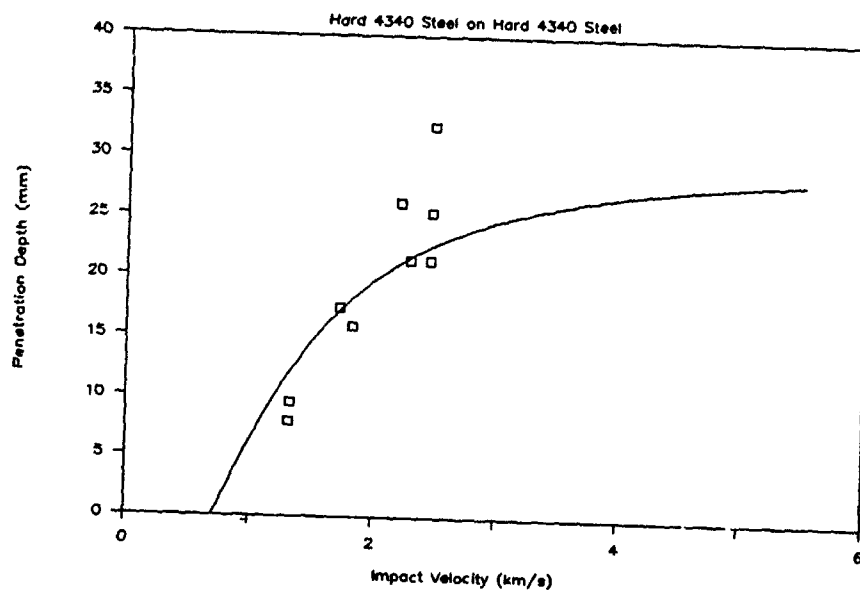


Figure 87e. Penetration Depth vs. Impact Velocity

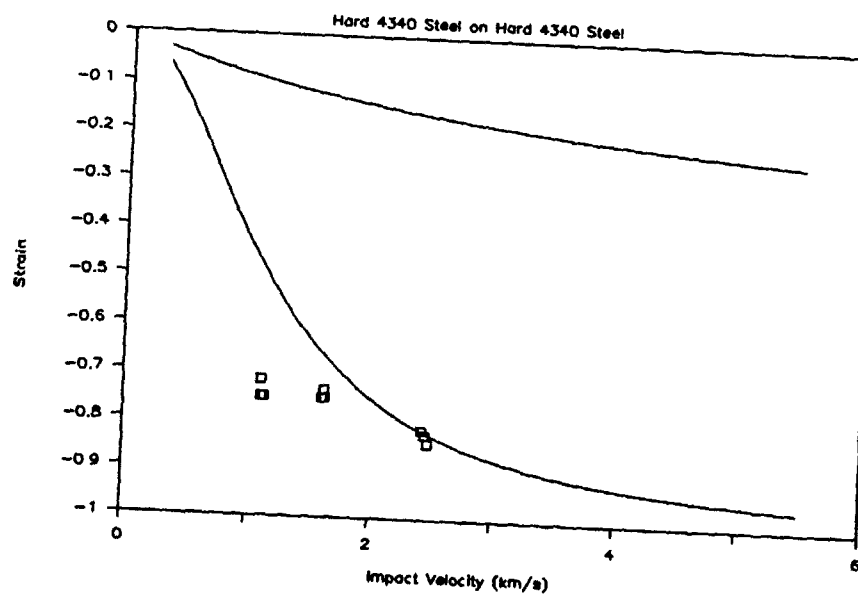


Figure 88a. Strain vs. Impact Velocity

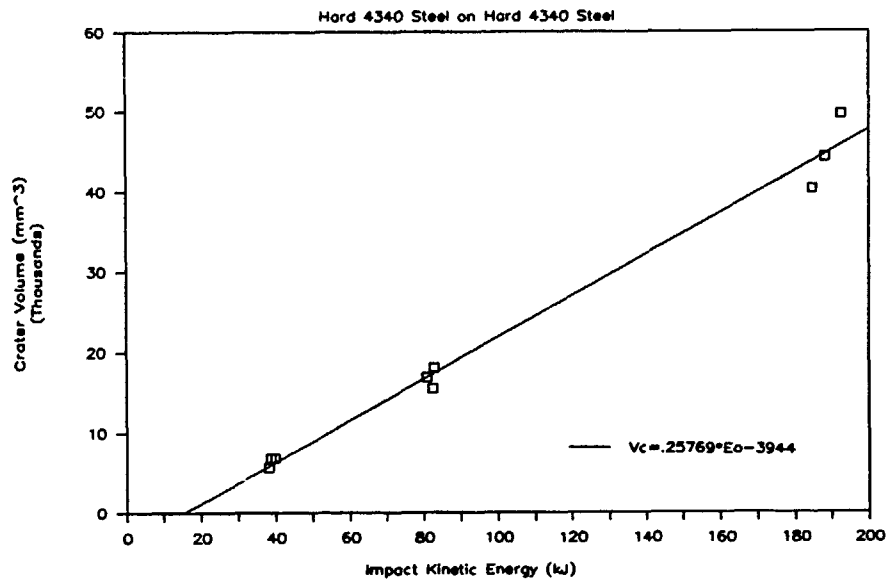


Figure 88b. Crater Volume vs. Impact Kinetic Energy

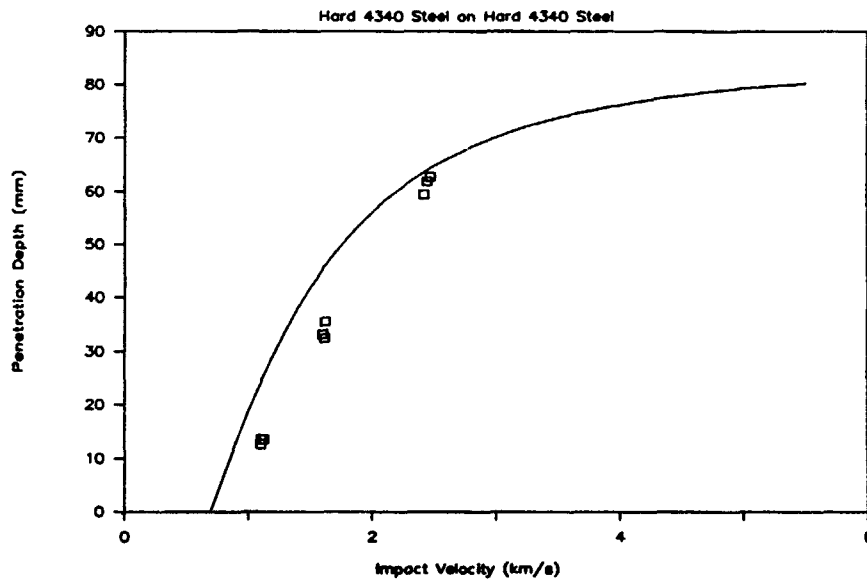


Figure 88c. Penetration Depth vs. Impact Velocity

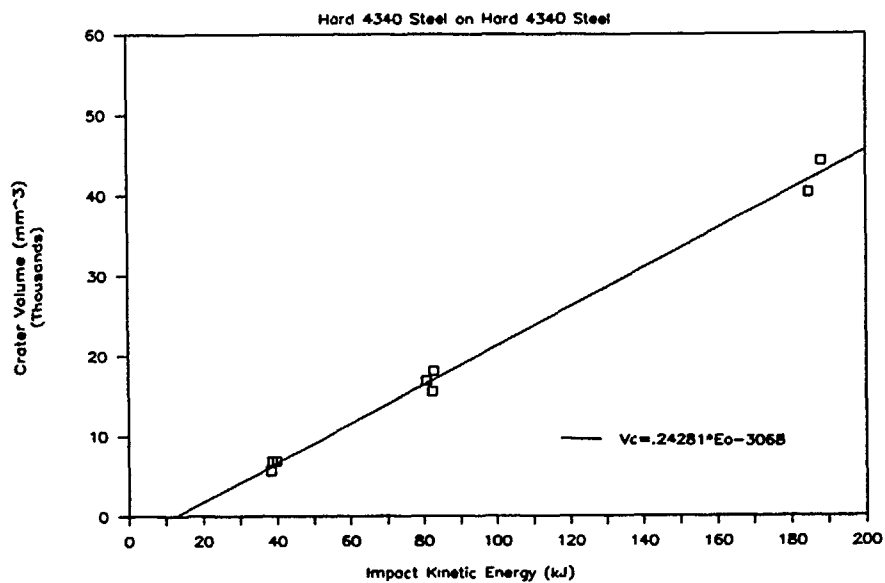


Figure 88d. Crater Volume vs. Impact Kinetic Energy

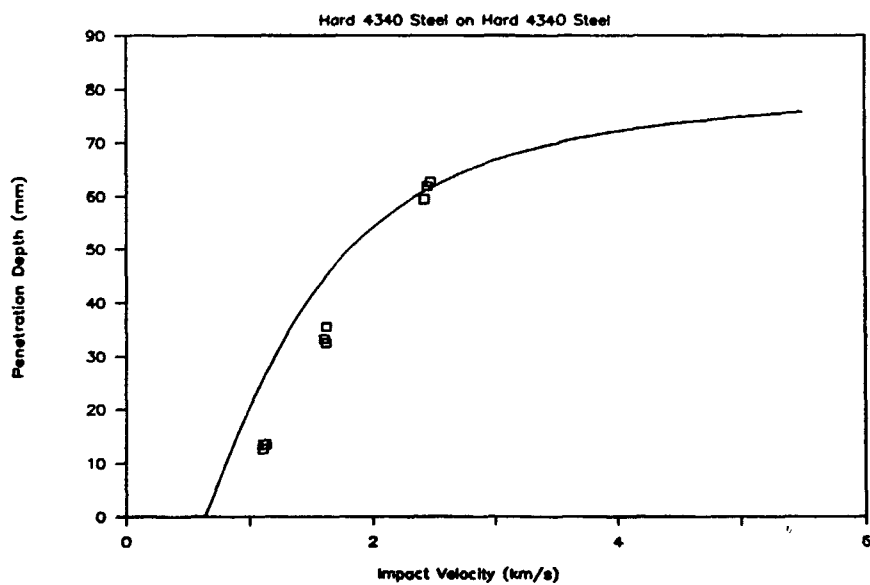


Figure 88e. Penetration Depth vs. Impact Velocity

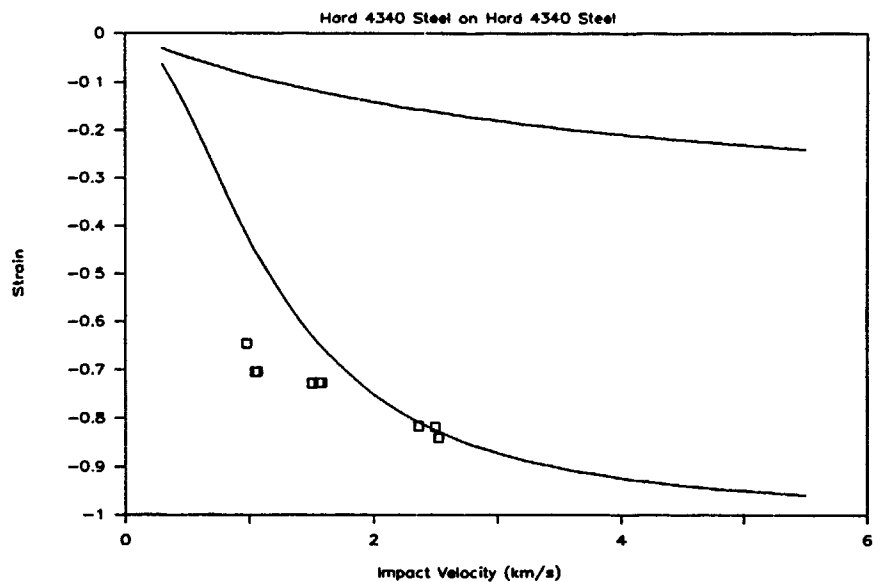


Figure 89a. Strain vs. Impact Velocity

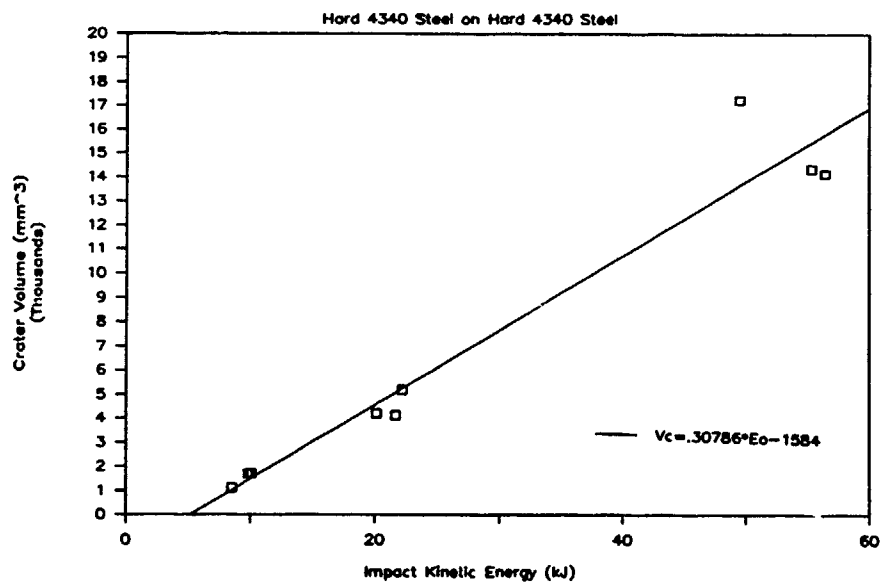


Figure 89b. Crater Volume vs. Impact Kinetic Energy

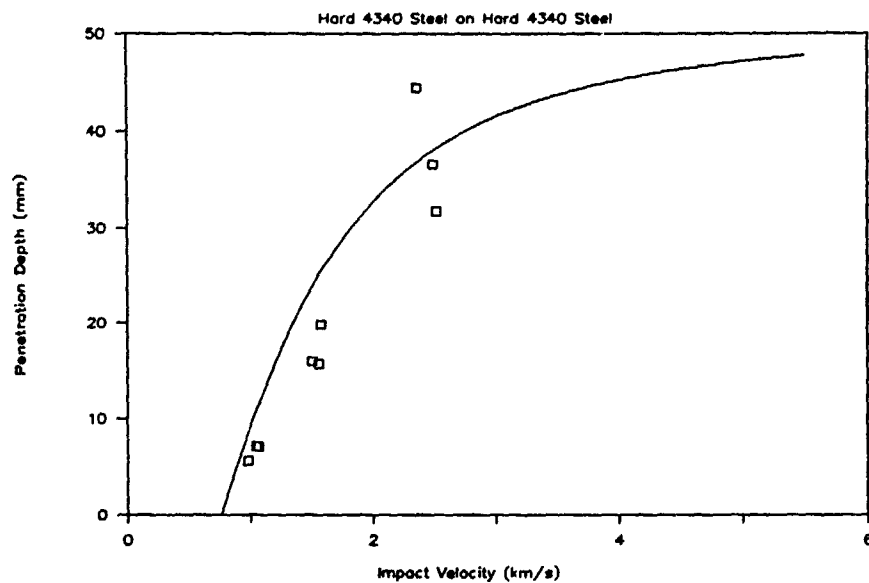


Figure 89c. Penetration Depth vs. Impact Velocity

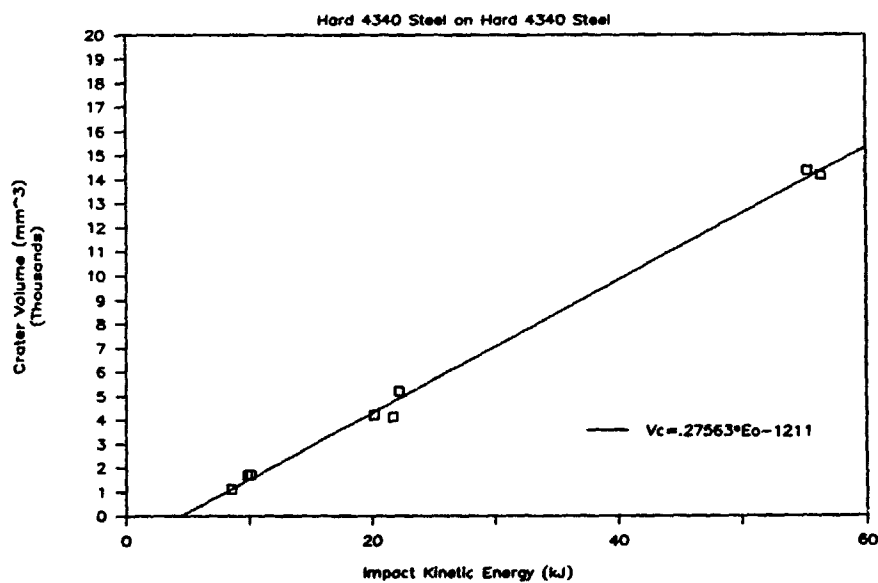


Figure 89d. Crater Volume vs. Impact Kinetic Energy

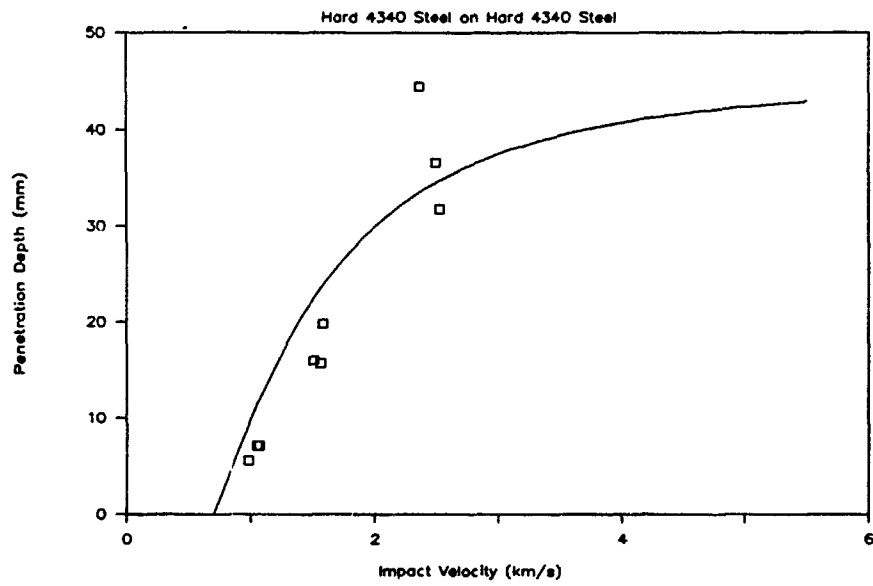


Figure 89e. Penetration Depth vs. Impact Velocity

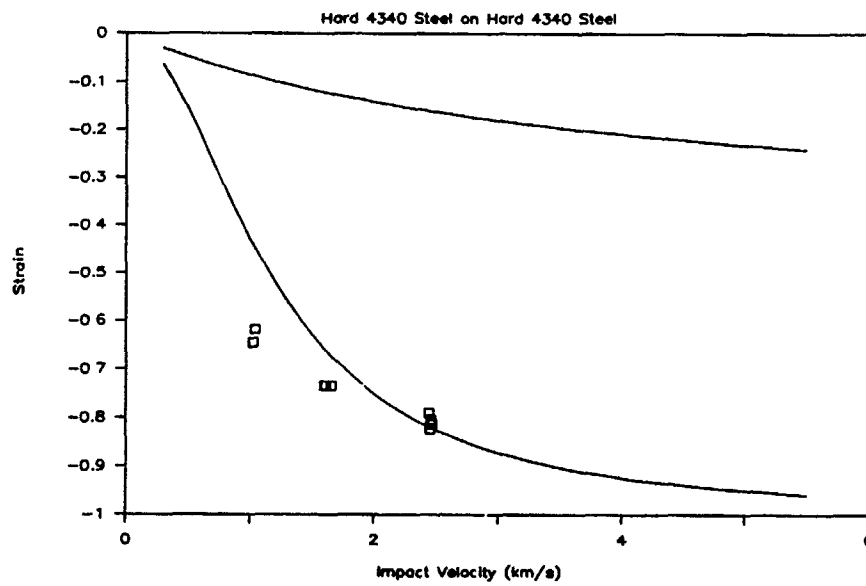


Figure 90a. Strain vs. Impact Velocity

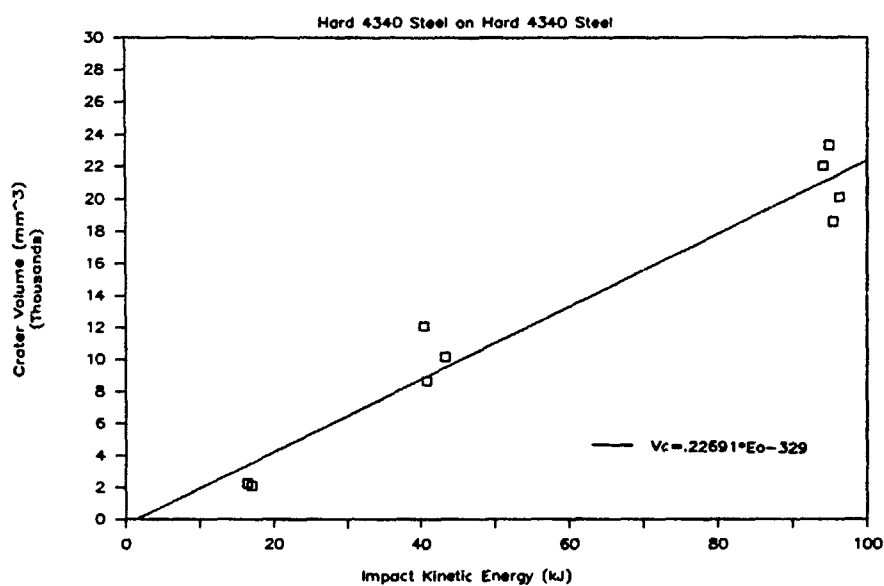


Figure 90b. Crater Volume vs. Impact Kinetic Energy

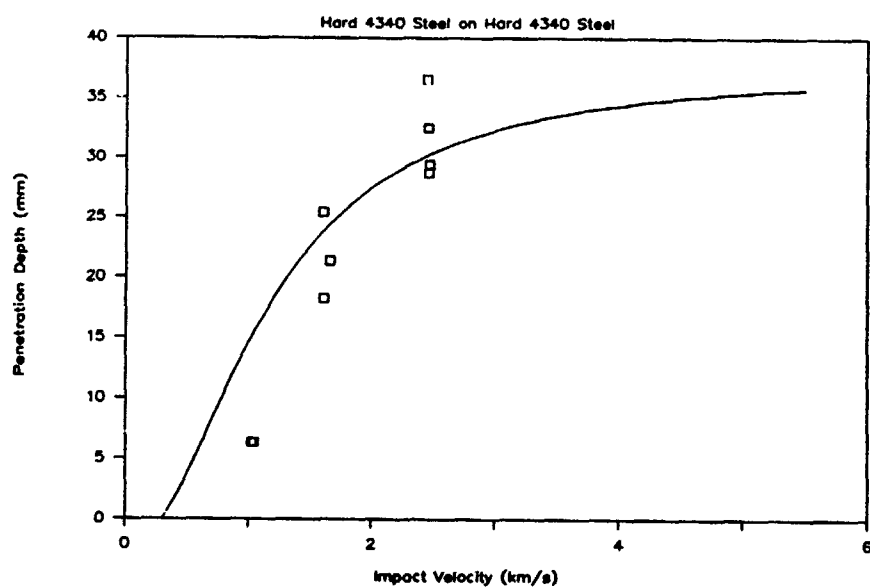


Figure 90c. Penetration Depth vs. Impact Velocity

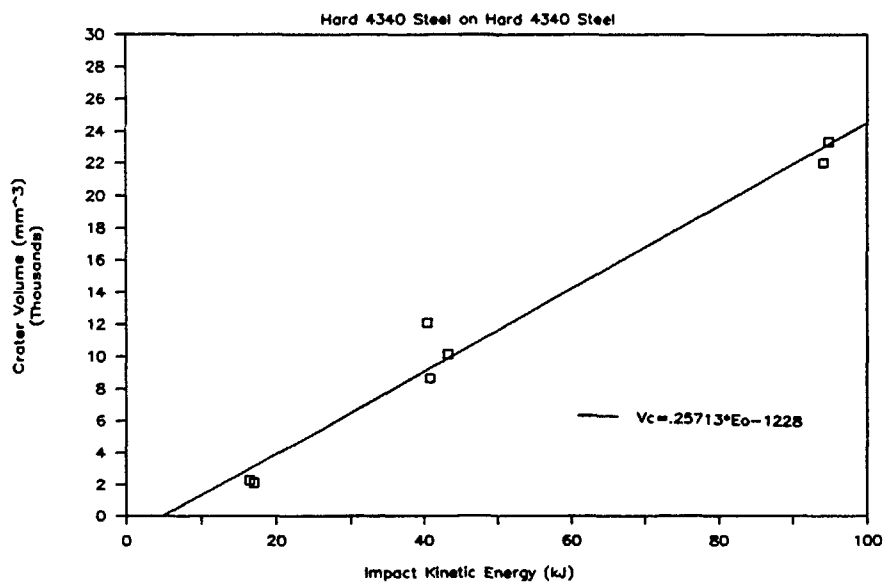


Figure 90d. Crater Volume vs. Impact Kinetic Energy

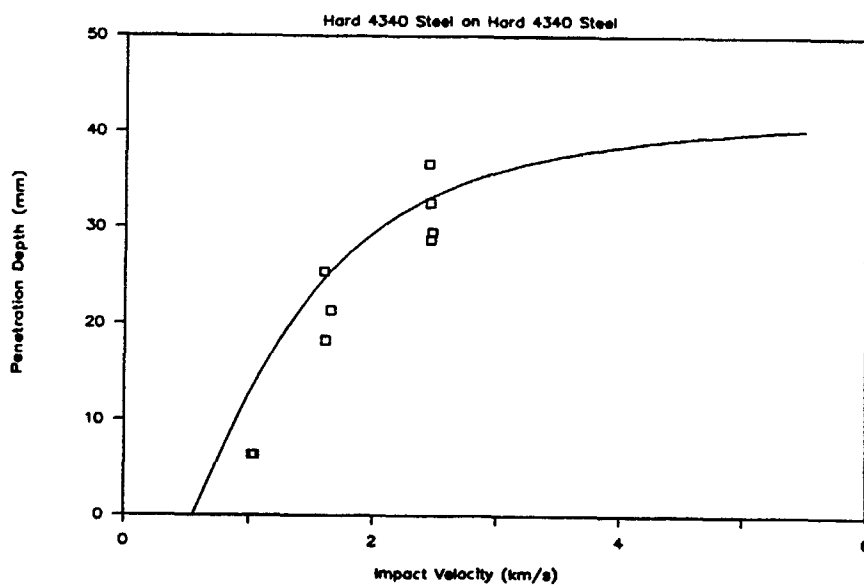


Figure 90e. Penetration Depth vs. Impact Velocity

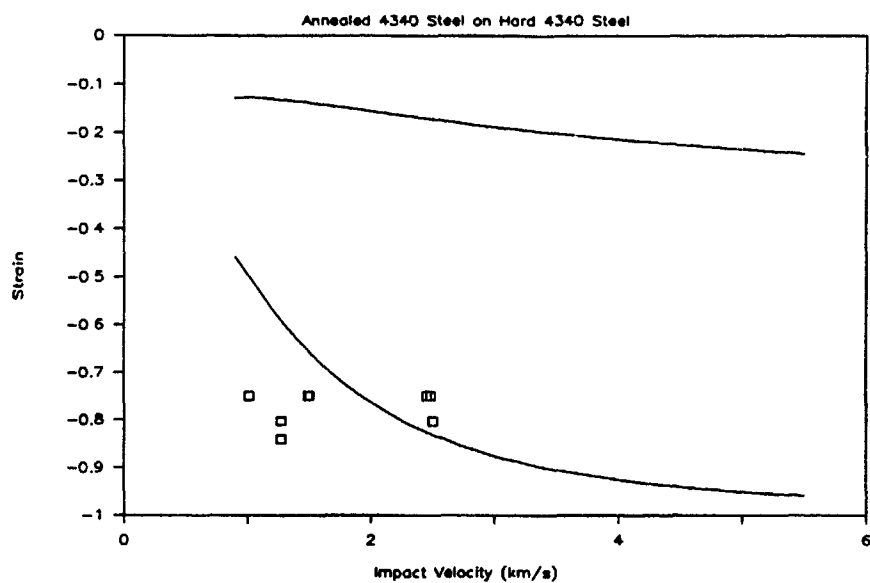


Figure 91a. Strain vs. Impact Velocity

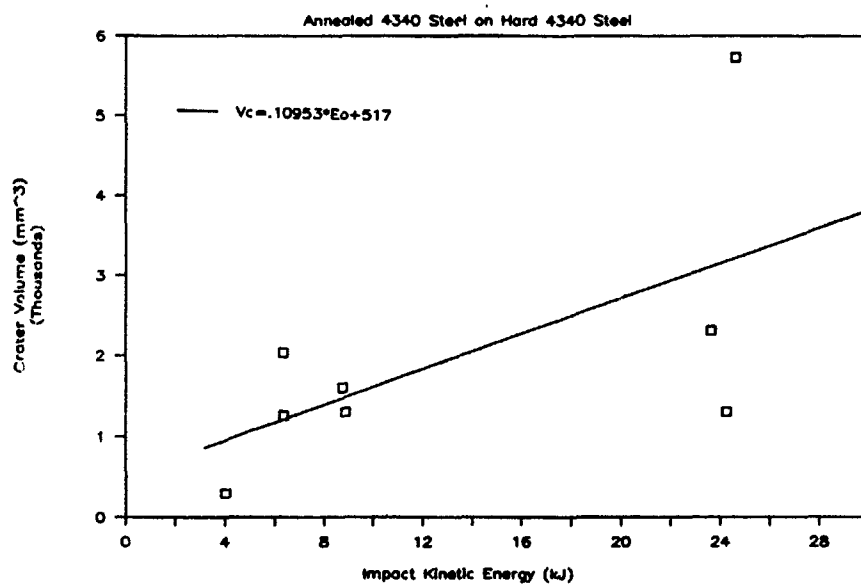


Figure 91b. Crater Volume vs. Impact Kinetic Energy

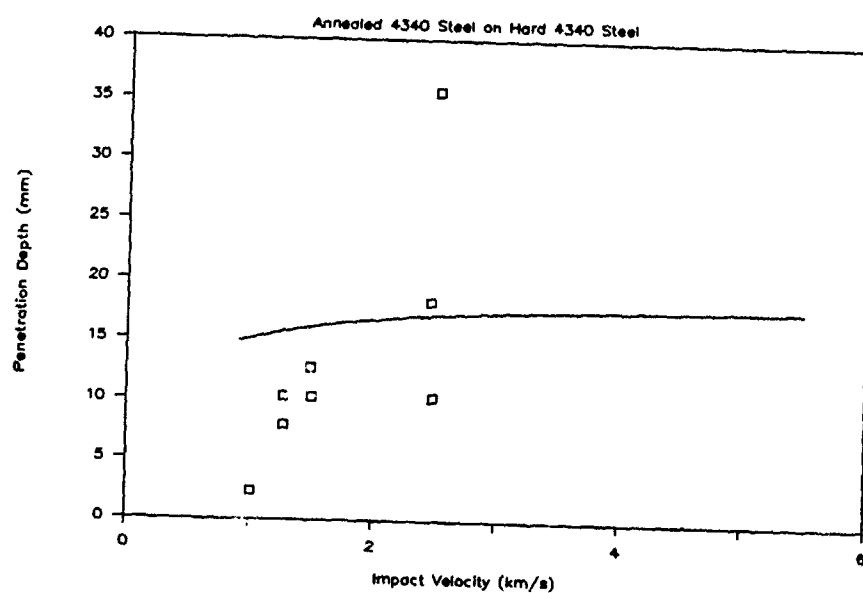


Figure 91c. Penetration Depth vs. Impact Velocity

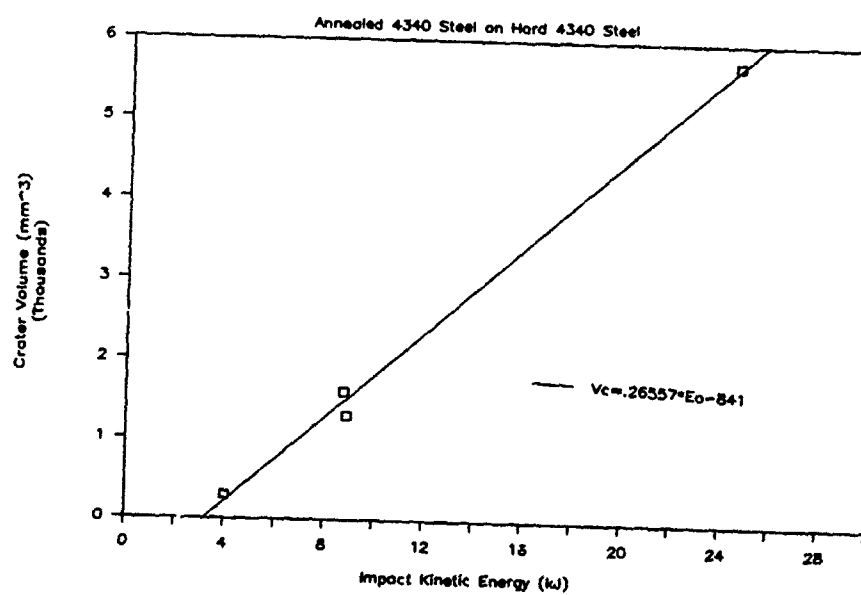


Figure 91d. Crater Volume vs. Impact Kinetic Energy

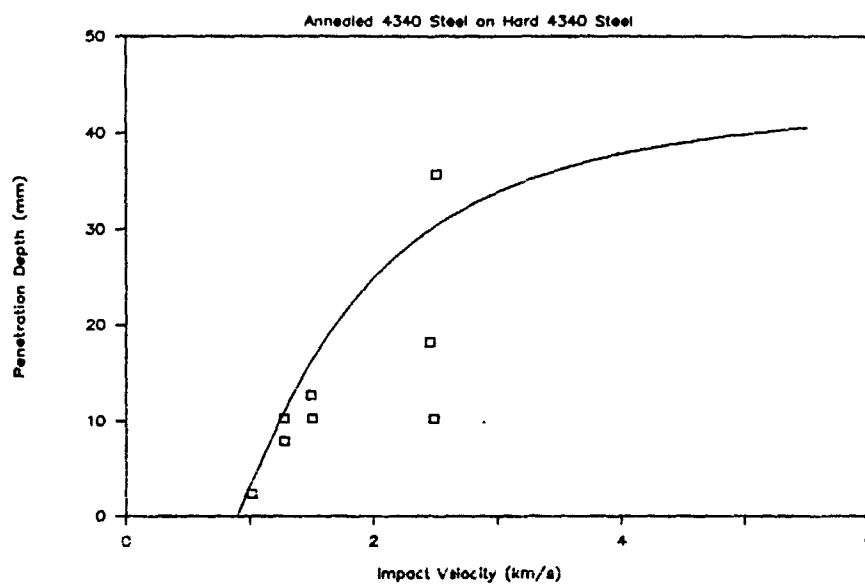


Figure 91e. Penetration Depth vs. Impact Velocity

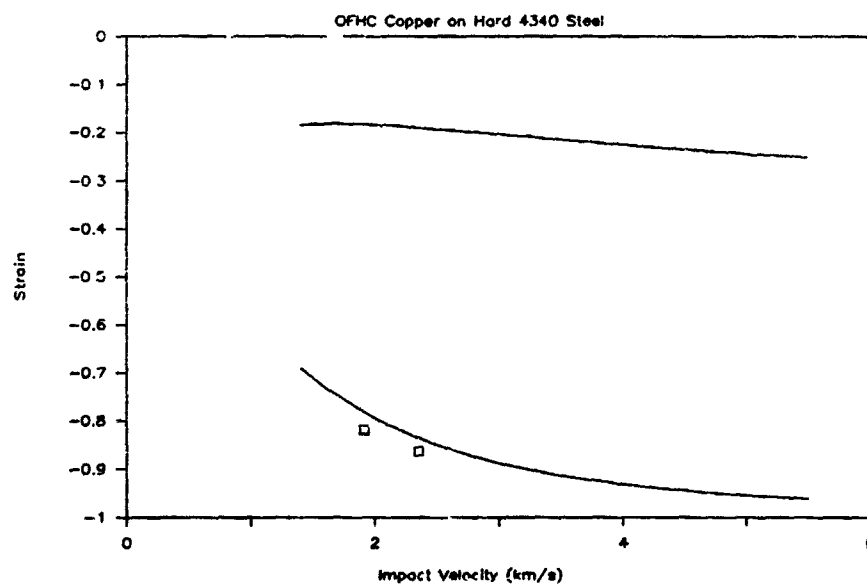


Figure 92a. Strain vs. Impact Velocity

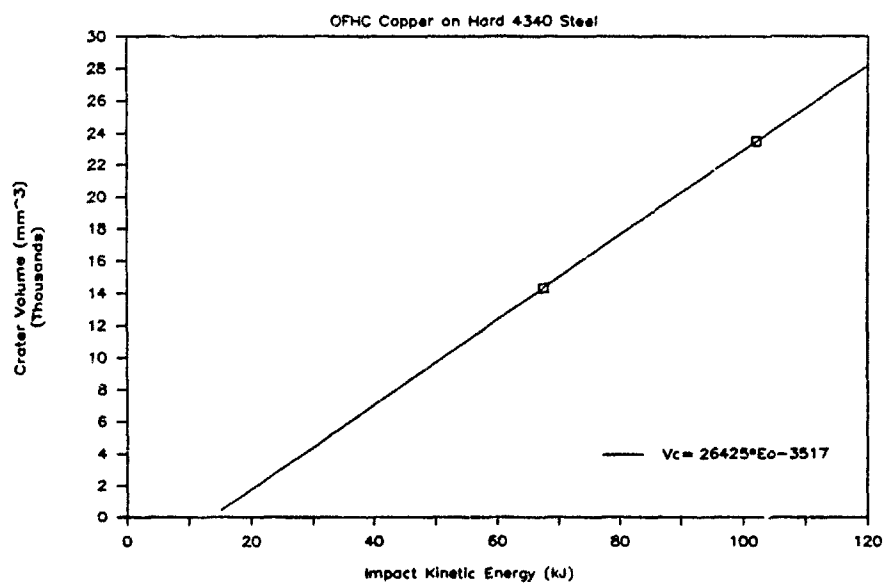


Figure 92b. Crater Volume vs. Impact Kinetic Energy

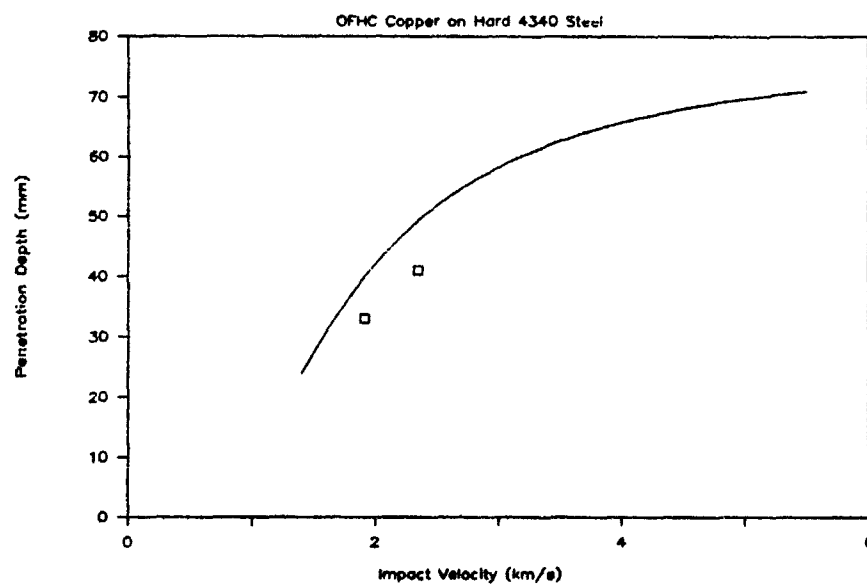


Figure 92c. Penetration Depth vs. Impact Velocity

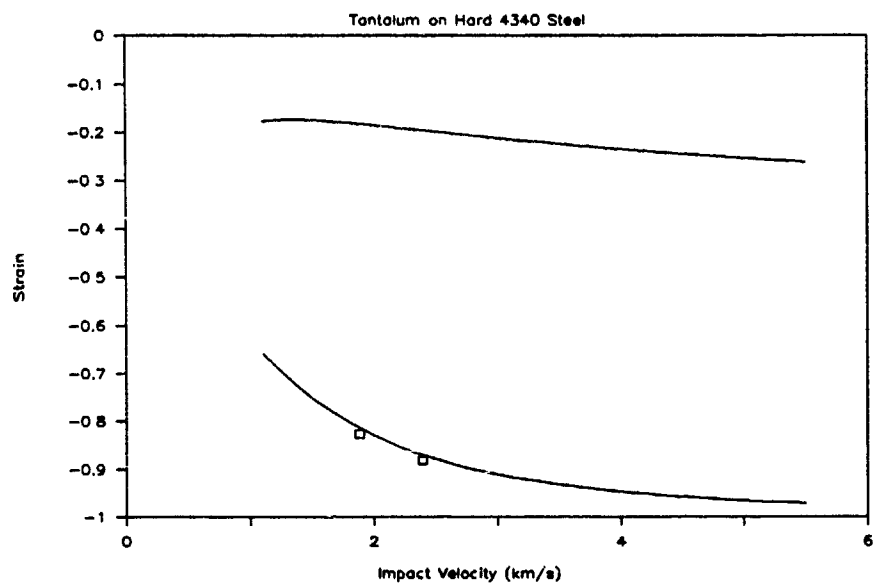


Figure 93a. Strain vs. Impact Velocity

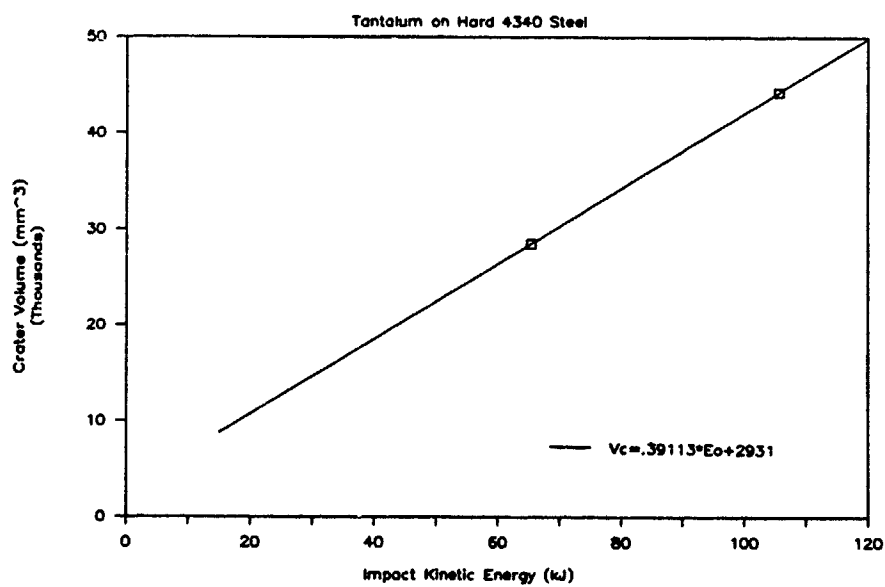


Figure 93b. Crater Volume vs. Impact Kinetic Energy

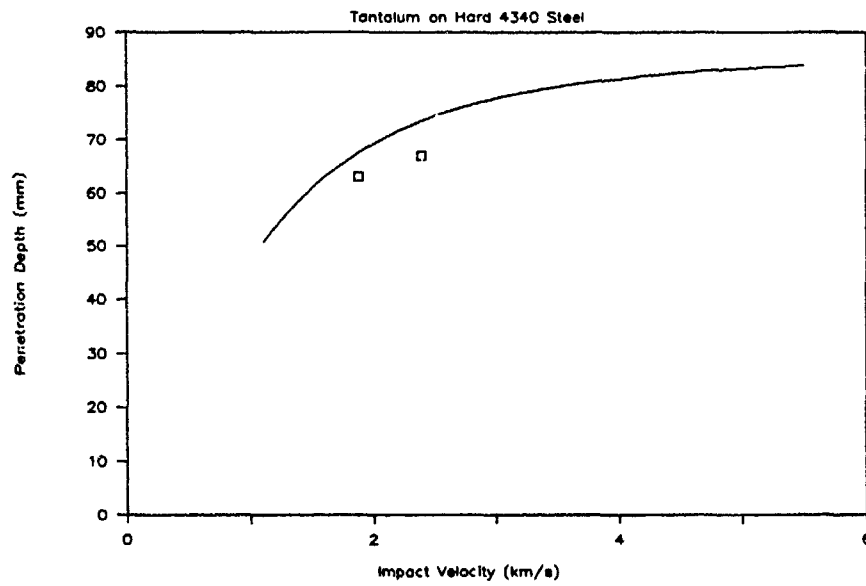


Figure 93c. Penetration Depth vs. Impact Velocity

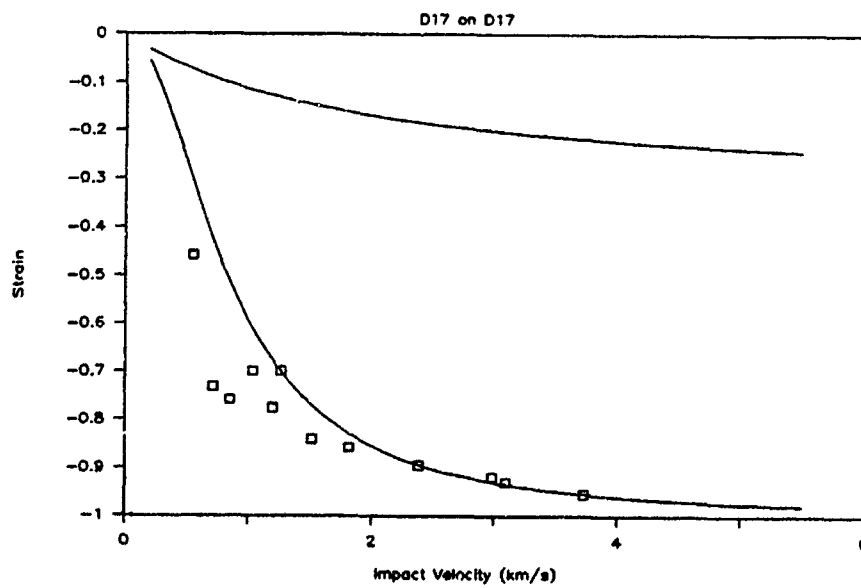


Figure 94a. Crater Volume vs. Impact Kinetic Energy

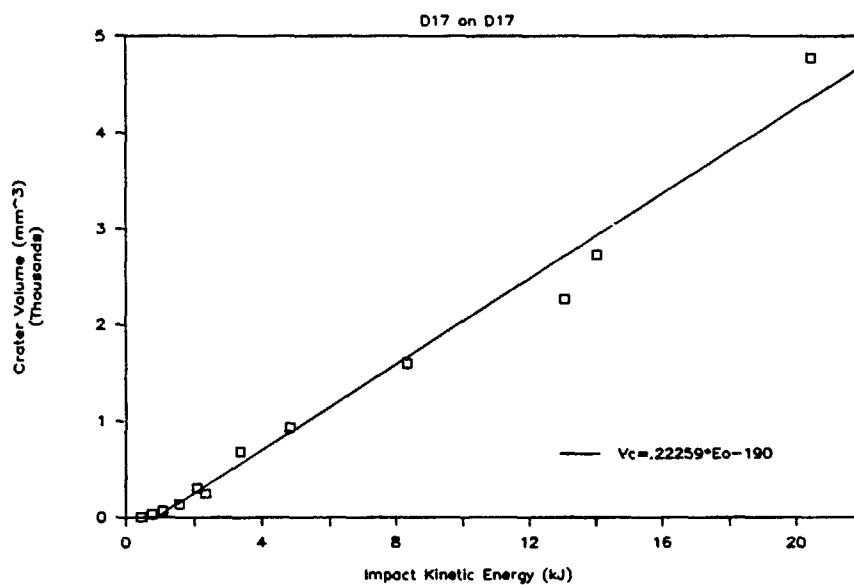


Figure 94b. Crater Volume vs. Impact Kinetic Energy

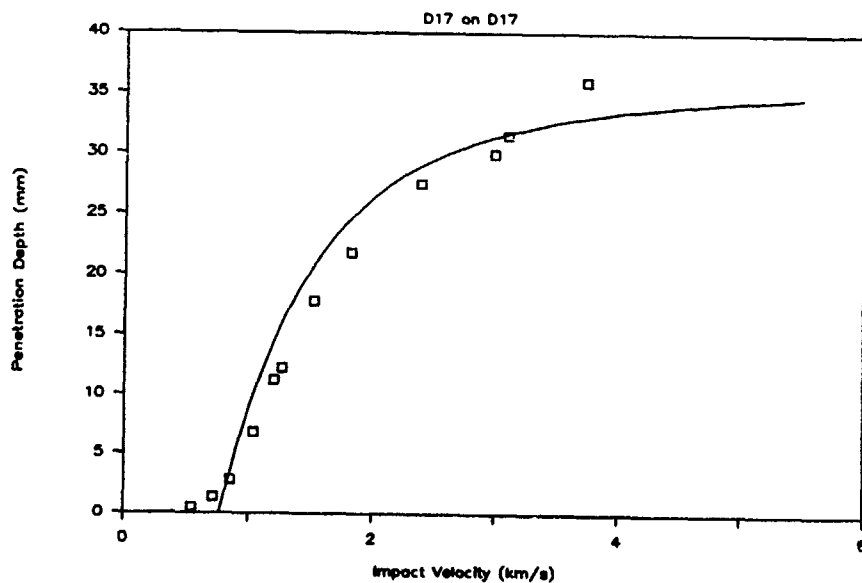


Figure 94c. Penetration Depth vs. Impact Velocity

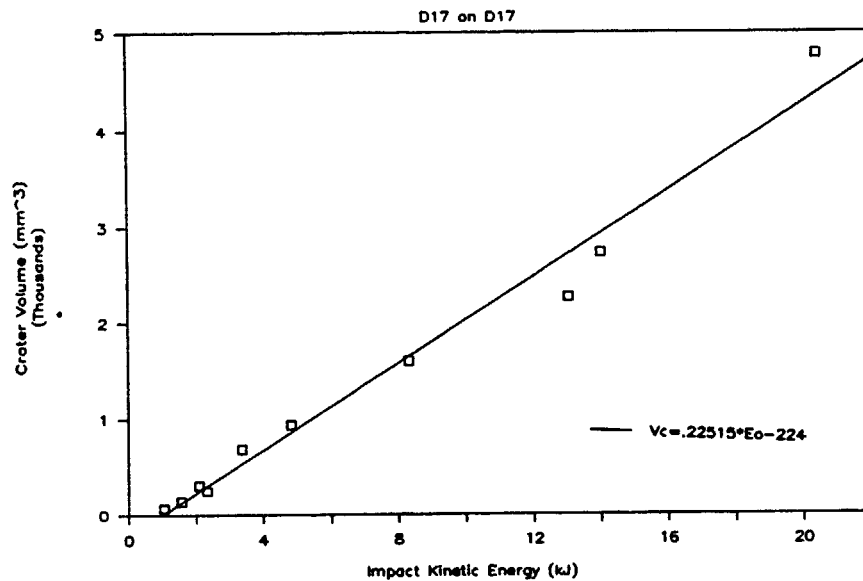


Figure 94d. Crater Volume vs. Impact Kinetic Energy

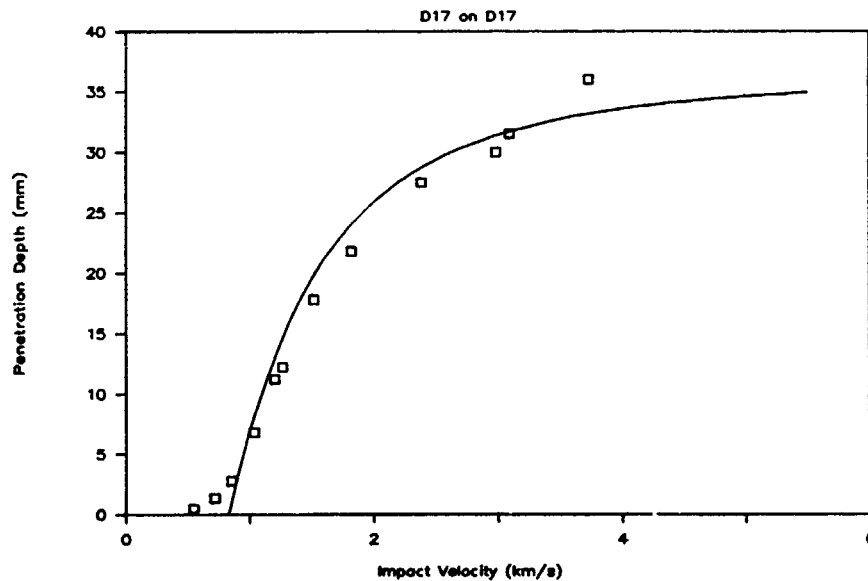


Figure 94e. Penetration Depth vs. Impact Velocity

6.0 REFERENCES

1. Tate, A. "A Theory for the Deceleration of Long Rods after Impact" J. Mech. Phys. Solids. 15, 387 (1967)
2. Alekseevskii, V. D. "Penetration of a Rod into a Target at High Velocity" In Combustion, Explosion, and Shock Waves. (1966)
3. Tate, A. "Further Results in the Theory of Long Rod Penetration" J. Mech. Phys. Solids. 17, 141 (1969)
4. Jones, S. E.; Gillis, P. P.; and Foster, J. C. Jr. "On the Penetration of Semi-infinite Targets by Long Rods" J. Mech. Phys. Solids. 35, 121 (1987)
5. Wilson, L. L.; Foster, J. C. Jr.; Jones, S. E.; and Gillis, P. P. "Experimental Rod Impact Results" Int. J. Impact Engng. 8, 15 (1989)
6. Gillis, P. P.; Jones, S. E.; Wilson, L. L.; and Foster, J. C. Jr. "An Analytical and Experimental Approach to the Penetration of Semi-infinite Targets by Long Rods" In Recent Advances in Impact Dynamics of Engineering Structures, ASME-AMD-Vol. 105 (D. Hui and N. Jones, eds.) (1989)
7. Kerber, M. W.; Jones, S. E.; Fisher, C. A.; and Wilson, L. L. "Penetration and Cratering of Semi-infinite Targets by Long Rods" Proceedings of the 12th International Symposium on Ballistics. Vol. 3, No. 77 (1990)

8. Murphy, M. J. "Survey of the Influence of Velocity and Material on the Projectile Energy/Target Hole Volume Relationship" Proceedings of the Tenth International Symposium on Ballistics. San Diego, CA (1987)
9. Cinnamon, J. D.; Jones, S. E.; Wilson, L. L.; and House, J. W. "Further Results in the One-Dimensional Analysis of Rod Penetration" Proceedings of the SECTAM XVI Conference. Nashville, Tennessee, 12-14 April (1992)
10. Cinnamon, J. D.; Jones, S. E.; House, J. W.; and Wilson, L. L. "A One-Dimensional Analysis of Rod Penetration" Int. J. Impact Engng. 12, 2 (1992)
11. Ravid, M.; Bodner, S. R.; and Holoman, I. "Analytical Investigation of the Initial Stage of Impact of Rods on Metallic and Ceramic Targets at Velocities of 1 to 9 km/s" Proceedings of the 12th International Symposium on Ballistics. Vol. 1, No. 401 (1990)
12. Gillis, P. P.; Jones, S. E.; Wilson, L. L.; and Foster, J. C. Jr. "Parabolic Penetration Pressures" Proceedings of the 19th Yugoslav Congress on Applied Mechanics. (1990)
13. Jones, S. E.; Gillis, P. P.; Foster, J. C. Jr.; and Wilson, L. L. "A One-Dimensional, Two-Phase Flow Model for Taylor Impact Specimens" In [6] and ASME Journal of Engineering Materials and Technology. Vol. 113, No. 228 (1991)

14. Jones, S. E.; Marlow, Rhett B.; House, J. W.; and Wilson, L. L. "A One-Dimensional Analysis of the Penetration of Semi-Infinite 1100-O Aluminum Targets" submitted for publication, Proceedings of the 1992 Hypervelocity Impact Symposium.
15. Anderson, Charles E.; Morris, Bruce L.; and Littlefield, David L. "A Penetration Mechanics Database" Southwest Research Institute. SwRI Report 3593/001. January (1992)
16. LASL Shock Hugoniot Data. Stanley P. Marsh, ed. Univ. of California Press: Berkeley.
17. Jones, S. E. University of Alabama. Private Communication. June (1992)
18. [3] as reported in [15]
19. Christman, D. R.; and Gehring, J. W. "Semiannual Report on Penetration Mechanisms of High-Velocity Projectile" Report No. TR63-250, prepared for Ballistic Research Laboratories under Contract No. DA-04-495-AMC-123(R), GM Defense Research Laboratories, Santa Barbara, CA (1963) as reported in [15]
20. [5], also reported in [15]
21. Luk, V. K.; and Piekutowski, A. J. "An Analytical Model on Penetration of Eroding Long Rods into Metallic Targets" Int. J. Impact Engng. 11(3), (1991) pp. 323-340 as reported in [15]

22. Hohler, V.; Schneider, E.; Stilp, A. J.; and Tham, R. "Length and Velocity Reduction of High Density Rods Perforating Mild Steel and Armor Steel Plates" Proceedings of the 4th International Symposium on Ballistics. Monterey, CA, 17-19 October (1978) as reported in [15]
Hohler, V.; and Stilp, A. J. "Penetration of Steel and High Density Rods in Semi-Infinite Steel Targets" Proceedings of the 3rd International Symposium on Ballistics. Karlsruhe, FRG, 23-25 March (1977) as reported in [15]
Hohler, V.; and Stilp A. "Influence of the Length-to-Diameter Ratio in the Range from 1 to 32 on the Penetration Performance of Rod Projectiles" Proceedings of the 8th International Symposium on Ballistics. Orlando, FL, 23-25 October (1984) as reported in [15]
Hohler, V.; and Stilp A. "Hypervelocity Impact of Rod Projectiles with L/D from 1 to 32" Int J. Impact Engng. 5(1-4), (1987) pp. 323-331 as reported in [15]
Hohler, V.; and Stilp, A. "Penetration Performance of Segmented Rods at Different Spacing - Comparison with Homogeneous Rods at 2.5 - 3.5 km/s" Proceedings of the 12th International Symposium on Ballistics. San Antonio, TX, 30 October - 1 November (1990) as reported in [15]
23. Experimental Data. Armament Directorate, USAF Wright Laboratories, Eglin AFB, FL.
24. reported in [9]

25. Silsby, G. F. "Penetration of Semi-Infinite Steel Targets by Tungsten Long Rods at 1.3 to 4.5 km/s" Proceedings of the 8th International Symposium on Ballistics. Orlando, FL, 23-25 October (1984) also reported in [15]
26. Keele, M.; Rapacki, E., Jr.; and Bruchey, W., Jr. "High Velocity Ballistic Performance of a Uranium Alloy Long Rod Penetrator" Proceedings of the 12th International Symposium on Ballistics. San Antonio, TX, 30 October - 1 November (1990) as reported in [15]
27. Wilkins, M.; Gibbons, J.; Hohler, V.; Stilp, A. J.; and Cozzi, M. "Ballistic Performance of AlN, SiC, and Al₂O₃ Ceramic Tiles Impacted by Tungsten Alloy Long Rod Projectiles" Proceedings of the U.S. Army TACOM Combat Survivability Symposium. 15-17 April (1991) Vol II, pp. 75-95 as reported in [15]
28. Woolsey, P.; Mariano, S.; and Kokidko, D. "Alternative Test Methodology for Ballistic Performance Ranking of Armor Ceramics" Proceedings of the Fifth Annual TACOM Armor Coordinating Conference. 7 March (1989) as reported in [15]
Woolsey, P.; Kokidko, D.; and Mariano, S. "Alternative Test Methodology for Ballistic Performance Ranking of Armor Ceramics" Report No. MTL TR89-43. U.S. Army Materials Technology Laboratory, Watertown, MA (1989) as reported in [15]
Woolsey, P.; Kokidko, D.; and Mariano, S. "Progress Report on Ballistic Test Methodology for Armor Ceramics" Proceedings of TACOM Combat Vehicle Survivability Symposium. Gaithersburg, MD, March (1990) as reported in [15]

29. Morris, B. L.; and Anderson, C. E., Jr. "The Ballistic Performance of Confined Ceramic Tiles" Proceedings of the 1991 TACOM Combat Vehicle Survivability Symposium. 15-17 April (1991) pp. 235-244 as reported in [15]

VITA

John Daniel Cinnamon was born in Seattle, Washington on April 2, 1969, the son of Irene JoAnn and Carl Davis Cinnamon. After completing secondary education at Kentridge Senior High School, Kent, Washington in 1987, John entered the United States Air Force Academy. He graduated with Academic Distinction and was awarded a Bachelor of Science degree in Engineering Sciences on May 29, 1991. In addition, John was commissioned into the U.S. Air Force as a Second Lieutenant. He subsequently received a graduate school scholarship to immediately attend the University of Texas at Austin. John has published several articles in the field of penetration mechanics and materials characterization during his undergraduate and graduate career. After completing his one year accelerated Master's program in Aerospace Engineering, he will continue his career in the U.S. Air Force.

Permanent Address: 18005 145th Ave SE
Renton, WA 98058

This report was typed by the author.